

T cell recognition of stress-induced post-translational modifications

A thesis submitted to the University of Nottingham for the degree of Doctor of Philosophy

Poonam Vaghela

July 2021

Funded by Scancell Ltd.

Acknowledgements

Firstly, I would like to thank my supervisor **Professor Lindy Durrant** for giving me the opportunity to complete my PhD. Thank you so much for believing in me way back in 2016. Your guidance and support has been invaluable throughout this experience and I really appreciate all the extra time and effort you have given. I also want to give a huge thank you to **Dr Rachael Metheringham** and **Mohammed Gijon** for your help, encouragement and friendship from when I first joined the group. I do miss our trio!

I would like to thank all my colleagues at Scancell Ltd and the Translational Medical Sciences department. Although our bubble at the City Hospital was small, the atmosphere was always friendly, and help was always available for those in need. A special acknowledgement for **Dr Jia Xin Chua, Maria Diez-Rodriguez, Christopher Nolan, Dr Katherine Cook, Dr Suha Atabani, Dr Elisa Marelli, Dr Sabaria Shah, Dr Ruhul Choudhury, Dr Ian Daniels** and **Peter Symonds** for all your help in the lab and for creating a fun environment. Those afternoon ice cream breaks were much needed after working in the tropical temperatures of Lab 7.

Thank you to Scancell Ltd who funded my PhD and in particular **Dr Samantha Paston, Dr Victoria Brentville** and **Dr Mireille Vankemmelbeke**, who have provided valuable support towards my project. This is very much appreciated.

Lastly, I would like to thank my husband, family and friends. Your love and encouragement has been the foundation of my will and strength to continue my PhD. Thank you all!

Publications

Victoria A Brentville, Peter Symonds, Katherine W Cook, Ian Daniels, Tracy Pitt, Mohamed Gijon, **Poonam Vaghela**, Wei Xue, Sabaria Shah, Rachael L Metheringham & Lindy G Durrant (2019) **T cell repertoire to citrullinated self-peptides in healthy humans is not confined to the HLA-DR SE alleles; Targeting of citrullinated self-peptides presented by HLA-DP4 for tumour therapy**, OncoImmunology, 8:5, DOI: 10.1080/2162402X.2019.1576490.

Brentville VA, Metheringham RL, Daniels I, Atabani S, Symonds P, Cook KW, Vankemmelbeke M, Choudhury R, **Vaghela P**, Gijon M, Meiners G, Krebber WJ, Melief CJM, Durrant LG. **Combination vaccine based on citrullinated vimentin and enolase peptides induces potent CD4-mediated anti-tumor responses**. J Immunother Cancer. 2020 Jun;8(1):e000560. doi: 10.1136/jitc-2020-000560.

Presentations

Medicine and Health Sciences Faculty Postgraduate Research Forum, poster presentation, University of Nottingham, June 2018.

Midland Research Festival, The Academy of Medical Sciences, poster presentation, Birmingham, March 2019.

British Association of Cancer Research (BACR) Tumour Microenvironment Conference, poster presentation, Nottingham, July 2019.

British Society of Immunology (BSI) Congress, poster presentation, Liverpool, December 2019.

Abstract

Background: Citrullination is the post-translational modification of arginine to citrulline mediated by peptidylarginine deiminases (PADs). We have previously shown that vaccination with citrullinated peptides from vimentin and α-enolase which are presented on HLA-DR4 or -DP4 in tumour cells mediate strong anti-tumour responses [1, 2]. This response is dependent upon autophagy and presentation of citrullinated peptides on MHC-II. Cytotoxic CD4 T cells can directly kill tumours expressing MHC-II and cognate peptide. As most tumours do not express MHC-II unless induced to do so by IFNγ we propose that citrullination is a normal stress response but that citrullinated epitopes are only presented on viable cells in the presence of inflammation.

Results: Exposure to nutrient starvation induced citrullinated vimentin expression in the murine melanoma cell line B16F1 grown *in vitro*, measured using the anti-Citrullinated vimentin rabbit polyclonal anti-serum GB17002 (ECV-1), but was also associated with apoptosis. Interestingly, up to 70% of low density plated cells expressed citrullinated vimentin which was mostly cytoplasmic with some cases showing punctate staining, increased phagosome associated LC3-II and increased proliferation marker Ki67 compared to high density cultures, suggesting actively growing cells undergo more autophagy and have greater potential to express citrullinated epitopes. The role the HIPPO pathway and Epithelial-to-Mesenchymal transition (EMT) plays in citrullination was investigated however results were inconclusive and require further work. Approximately 27-55% of human cancers were positive for MHC-II. The expression of MHC-II was associated with survival advantage in breast cancer patients (P=0.004), and positively correlated with citrullinated vimentin (P<0.001), PAD2 (P<0.001), IFNγ receptor (P=0.003) and Ambra1 (P=0.016) in ovarian cancer. In a panel of triple negative breast cancer

(TNBC) and ovarian cancer cell lines, 4/8 lines showed expression of MHC-II. This was enhanced following exposure to IFNγ which was dependent on activation of the Class II transactivator (CIITA) and is controlled by the pIV promoter. In addition, a strong correlation between IRF-1 and CIITA mRNA expression was found in 10 cancer types analysed from the TCGA database and in 4 cancer types CIITA expression alone correlated with good prognosis. Interestingly, IFNγ also increased citrullinated vimentin expression in the B16F1, suggesting this cytokine upregulates citrullination and MHC-II. Analysis of the human CD4 T cell repertoire responding to the citrullinated peptides, Vim28-49cit, Vim415-433cit and Eno241-260cit, showed oligoclonal proliferation of mainly T effector memory (Tem) cells but also an increase in the cytotoxic CD45RA expressing Tem population (TEMRA). In total, 28 high frequency TCRs were identified by RNA sequencing of proliferating CD4 T cells in response to Vim28cit (16), Eno241cit (4) and Vim415cit (8). These were transduced using lentiviral technology into Jurkat 76 and/or T cells and tested in antigen presentation assays to confirm their reactivity to citrullinated peptides by upregulation of the activation marker CD69 and the potent T cell stimulating cytokine, IFNγ. Despite numerous improvements to the lentiviral constructs, transfection/transduction methods and recognition assays, no positive responses were detected with any citrullinated peptide transduced TCRs. This suggests that the *in vitro* assays to detect citrulline specific T cell responses did not sufficiently expand the antigen specific T cells or that the TCR that did expand were of too low affinity for *in vitro* peptide recognition. Repeat stimulation assays to select for higher affinity more specific TCRs are required.

Summary: Lack of cell-to-cell contact induced the greatest levels of citrullination in viable cells which were also highly proliferative and had upregulated autophagy. For stress induced post-translational modifications (siPTMs) to be recognised by T cells, MHC-II expression is also required. This data shows MHC-II is present on human

tumour cells at low levels but can be further induced by the inflammatory cytokine IFNγ and is dependent on CIITA expression. Citrullinated peptides presented by MHC-II stimulated oligoclonal proliferation of CD4 T cells that expressed an effector phenotype. IFNγ released from these cells can induce MHC-II expression on tumours thus allowing presentation of siPTM epitopes. Citrullinated peptide vaccines have shown that siPTMs are good targets for immunotherapy but further results are required to determine if specific TCRs can be identified and used for adoptive T cell therapy.

Table of Contents

1 Introduction 1

1.1 Cancer – Hallmarks of Cancer 1

1.2 Immune Surveillance and Editing 2

1.3 T cells 4

1.3.1 MHC structure and function 6

1.3.2 Peptide processing and presentation 8

1.3.3 α/β T cell receptor structure and function 10

1.3.4 Gene rearrangement of the α/β TCR loci 13

1.4 Thymic selection 14

1.5 CD8 T cells 17

1.6 CD4 T cells 19

1.7 Checkpoint inhibitors 23

1.8 Adoptive T cell therapy 25

1.8.1 Tumour-Infiltrating Lymphocyte (TIL) therapy 26

1.8.2 Chimeric antigen receptor (CAR) T cell therapy 28

1.8.3 Engineered T cell receptor (TCR) therapy 28

1.9 Cancer vaccines 30

1.9.1 Tumour cell vaccines 31

1.9.2 Dendritic cell vaccines 32

1.9.3 Viral vaccines 33

1.9.4 Nucleic acid vaccines 34

1.9.5 Protein and Peptide vaccines 36

1.10 Citrullination 37

1.10.1 PADs 38

1.10.2 Apoptosis and Calcium 39

1.10.3 Citrullination and Antibodies in Rheumatoid Arthritis 40

1.10.4 Citrullination in Viable Cells 41

1.11 Autophagy 42

1.11.1 Autophagy 42

1.11.2 Autophagy and stress 44

1.11.3 Autophagy and cancer 45

1.12 Citrullination as a target for vaccines 46

1.13 Hypothesis and Aims 49

2 Materials and Methods 51

2.1 Cell lines 51

2.2 Antibodies 52

2.2.1 Cell lines and Tumour staining 52

2.2.2 PBMC staining 53

2.2.3 TCR experiments 54

2.2.4 Immunohistochemistry 55

2.3 Recombinant Proteins 55

2.4 Peptides 56

2.5 Inhibitors 56

2.6 Stress induction 56

2.7 MHC class II expression in tumour cell lines 57
2.8 Flow Cytometry 57
2.9 *In vitro* Deimination (Citrullination) 58
2.10 Western Blotting 58
2.11 Microarray 59
2.12 Confocal Microscopy 60
2.13 Murine Melanoma Tumours 61
2.13.1 Staining 61
2.13.2 Preparation of Murine Tumour Lysates and Mass Spectrometry 61
2.14 Epithelial-to-Mesenchymal Transition (EMT) experiments 62
2.15 Isolation of Peripheral Blood Mononuclear Cells (PBMCs) and Cell Proliferation Assays 62
2.16 RNA Sequencing Analysis 64
2.17 Lentivirus Construct Design 64
2.18 Lentivirus Production 65
2.18.1 Original method 65
2.18.2 Adapted method 66
2.19 Lentiviral Transduction 66
2.20 Generation of Monocyte Derived Dendritic Cells 68
2.21 B cell activation and expansion 68
2.22 Antigen Presentation Assay 69
2.22.1 CD69 marker expression 69
2.22.2 IFNγ secretion 69
2.23 ELISpot 70
2.24 ELISA 71
2.25 Tissue 71

2.25.1 Head and Neck 71
2.25.2 Sarcoma 72
2.25.3 Osteosarcoma 72
2.25.4 Renal 73
2.25.5 Ovarian 73
2.25.6 Lung 73
2.25.7 Breast 73
2.26 Immunohistochemistry 74
2.27 Statistical Analysis 75
3 Stress induced Citrullination 76
3.1 Introduction and Aims 76
3.1.1 Vimentin 76
3.1.2 Epithelial - to - Mesenchymal Transition (EMT) 76
3.1.3 Aims 78
3.2 Results 79
3.2.1 Characterisation of anti-citrullinated vimentin anti-serum 79
3.2.2 Upregulation of Citrullination by Starvation 84
3.2.3 Prolonged Stress results in Cellular Apoptosis 87
3.2.4 Increased Citrullination, Autophagy and Proliferation in Low Density Cells 91
3.2.5 Involvement of the HIPPO pathway in citrullinated protein expression 104
3.2.6 Citrullination in Murine Melanoma Tumours 111

3.2.7 Involvement of EMT in citrullinated protein expression 117

3.2.8 Citrullination and Autophagy in human cancers 123

3.2.9 Results summary 136

3.3 Discussion 137

4 The importance of MHC class II expression in tumours 149

4.1 Introduction 149

4.1.1 MHC regulation by CIITA 149

4.1.2 Aims 151

4.2 Results 152

4.2.1 MHC class II expression in human cancer cell lines 152

4.2.2 Gene expression of CIITA, IRF-1 and HLA-DPA1 in human cancers 155

4.2.3 MHC class II protein expression in human cancers 163

4.2.4 MHC class II correlations with citrullination and autophagy markers 169

4.2.5 IFNγ upregulates MHC class II and citrullination in B16F1 cell line 172

4.2.6 Results summary 174

4.3 Discussion 176

5 Identification of citrullinated protein specific T cell receptors 184

5.1 Introduction and Aims 184

5.1.1 T cell receptor repertoires; Public and Private T cell receptors 184

5.1.2 Aims 186

5.2 Results 187

5.2.1 Expression of MODI1 peptides in B16F1 tumours 187

5.2.2 MODI1-specific CD4 T cell repertoire in healthy individuals 190

5.2.3 Identification of MODI1 T cell receptors 196

5.2.4 TCR transductions of Jurkat 76 cell line 211

5.2.5 Improved T cell transduction efficiencies 220

5.2.6 Production of activated B cells for antigen presentation assays 234

5.2.7 Specificity of Transduced T cells 238

5.2.8 Results summary 246

5.3 Discussion 248

6 General Discussion 258

6.1 Citrullination in normal vs tumour cells 258

6.2 Citrullinated epitopes for immunotherapy 260

6.3 Importance of findings in other fields 263

6.4 Summary 264

6.5 Future work 266

6.5.1 Improvements to TCR selection process 266

6.5.2 Normal cells checked for citrullination 266

6.5.3 Confirmation of HIPPO pathway and EMT involvement in citrullination 267

6.5.4 Testing in outbred mouse strain 267

7 References 269

8 Appendix 299

1 Introduction

1.1 Cancer – Hallmarks of Cancer

Cancer is the abnormal growth of cells that accumulate to form tumours, that spread and invade neighbouring tissues, and quite often distant parts of the body by metastasis. Currently, over 100 different types of cancers have been identified, each with unique features depending on the tissue affected. However, as this is a genetic disease and therefore controlled by alterations to genes involved in cellular growth, division, proliferation and death, a range of hallmarks have been identified essential for cancer development. This was first suggested by Hanahan and Weinberg over 20 years ago, who stated six important traits essential for cancer physiology; self-sufficiency in growth signals such as cytokine expression oncogene activation, insensitivity to anti-growth signals that regulate cell cycle machinery, evading apoptosis by inactivation of p53 tumour suppressor gene or overexpressed oncogenes, limitless replication, sustained angiogenesis providing oxygen and nutrients to expanding tumours and tissue invasion/metastasis [3]. They later revisited this theory and added two more hallmarks, reprogramming cellular metabolism and avoiding immune destruction, and two essential characteristics that promote tumour formation, genomic instability allowing mutations and tumour promoting inflammation (Figure 1.1) [4].

Figure 1.1

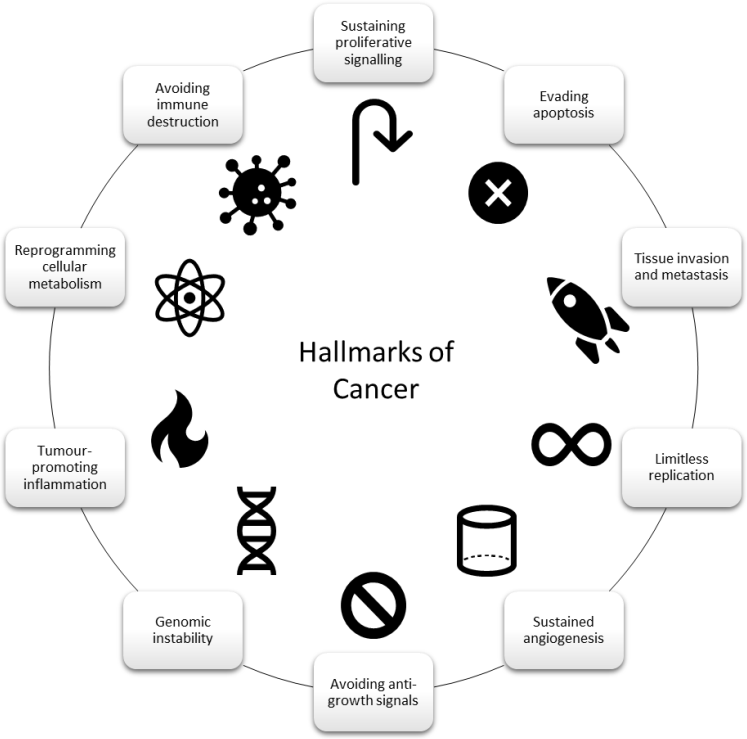


Figure 1.1 Hallmarks of cancer. The various factors that contribute to the establishment and progression of cancer.

1.2 Immune Surveillance and Editing

The immune system was hypothesised to combat developing tumours over 100 years ago by Paul Ehrlich but due to the lack of tools, scientific evidence to support this theory only emerged 50 years later. The general term used to describe this function is cancer immunosurveillance, where the immune system is capable of recognising and eliminating tumour cells. Interferon-γ (IFNγ) and perforin was shown to be an important mediator in anti-tumour responses. Both have been shown to protect against development of chemically induced tumours or spontaneous tumour formation [5, 6]. In addition, tumour rejection was reversed when mice were administered with an IFNγ neutralising antibody [7]. As major effectors of the immune

system that secrete high levels of IFNγ and lytic granules, T cells were studied for their specific anti-tumour activity. Their structure and functions will be discussed in more detail in sections 1.3, 1.5 and 1.6. Increased numbers of tumour-infiltrating lymphocytes (TILs) have also been associated with improved patient survival and better prognosis in many cancers further supporting the concept of immunosurveillance [8-10]. However, it became clear that not all individuals are able to prevent the spread of cancer and that tumours had found a way to avoid pressure from the immune system. In the early 2000's, Dunn and colleagues proposed the interaction between tumour and immune system which flipped the switch on tumour suppression involved three E's; elimination, equilibrium and escape [11]. Together they contributed to immunoediting within the cancer. At the first stage, elimination, immune cells are able to identify malignant cells and exert pro-inflammatory effects to destroy them. The initial recognition is most likely by cells of the innate immune system such as natural killer (NK) cells or macrophages that are summoned to the tumour site by chemokines produced through local tissue damage [12]. When stimulated these cells produce IFNγ and other pro-inflammatory cytokines as well as chemokines to attract lymphocytes to the area [13]. Both NK cells and T cells are then able to eliminate the target cells by release of lytic granules or engagement of the tumour necrosis factor receptor superfamily (TNFSF) members such as TRAIL [14, 15].

During the equilibrium phase, lymphocytes are able to exert enough pressure through pro-inflammatory mediators to maintain the tumour cells and prevent progression, but the response is not strong enough to fully eliminate the cells. This contributes to the longest period for a cancer patient and can span many years [11]. From the hallmarks of cancer, factors such as genetic instability, sustaining proliferative signals, avoiding anti-growth signals and regulating angiogenesis all contribute to this stage, enabling the tumour to resist immune pressure. In the final phase, escape, tumour cells are

able to grow unchecked by both, innate and adaptive, arms of the immune system. There are many mechanisms the tumour will utilise to overcome immunosurveillance such as secretion of suppressive cytokines and mediators such as TGF-β, IL-10 and IDO, expression of PD-L1 and CTLA-4 to block co-stimulation of T cells, and loss of antigen and major histocompatibility complex (MHC) molecules, in particular β2 microglobulin for MHC class I [16, 17]. Some of these will be discussed in more detail throughout this chapter. For the immune system to counterattack the tumour, it must overcome this tolerance and fight against the immunosuppressive environment.

1.3 T cells

T lymphocytes (cells) are a major component of the adaptive immune system and are responsible for the cell mediated immune response. They can directly kill cells but only when activated by protein fragments (peptides) presented by Major-Histocompatibility Complex (MHC) molecules on the surface of other cells. The structure, function and peptide processing methods are discussed in section 1.3.1 and 1.3.2. When presented with a MHC:peptide complex the T cell will recognise the antigen via the T cell receptor (TCR). TCR structure, function and diversity is discussed in section 1.3.3 and 1.3.4. Several types of T cells exist but can be divided into two main classes depending on their expression of the co-receptor; CD4 or CD8. The function and antigen recognition of these subsets is discussed later in section 1.5 and 1.6. T cells that have not yet recognised and been activated by antigen are called Naïve T cells [18]. These have a long-life span of 5-10 years and are commonly characterised by expression of CD45RA, C-C chemokine receptor 7 CCR7, lymph homing receptor CD62L (L-selectin) and CD27 [19]. CD62L facilitates T cell migration into lymphoid tissues where CCL21 and CCL19 is released to attract T cells by binding to CCR7. Mature naïve T cells express the early activation marker CD25. $CD25^{dim}$ cells have a lower expression of CD45RA, higher Ki-67 (cell cycling marker),

but a broader TCR Vβ repertoire than $CD25^{neg}$ cells, so are not completely differentiated [19].

Two main signals are required to fully activate naïve T cells and induce differentiation into effector T cells. Signal 1 is the presentation of peptide via MHC and binding to TCR. This process also requires the interaction of adhesion molecules CD2 and CD58 on the T cell surface with APC expressing lymphocyte function-associated antigen (LFA) 2 and 3 respectively to form the immunological synapse [20, 21]. In addition, LFA 1 is found on T cells and binds to ICAM-1 (CD54) on APCs. Signal 2 is facilitated by costimulatory molecule CD28 on naïve T cells which binds to B7.1 (CD80)/B7.2 (CD86) on APCs. Other costimulatory molecules such as CD40L on T cells also facilitate activation after binding to APC surface molecule CD40. T cell proliferation and function was inhibited in the absence of CD28 and CD40L where CD28 deficient T cells lacked IL-2 and IL-4 release and CD40L deficient T cells were defective in IFNγ production [22].

The effector population, characterised by the expression of CD45RO, can be further divided into 3 subsets; Cytotoxic T cells that can directly kill pathogens, infected cells or tumour cells, Helper T cells that provide cytokine support and other pro-inflammatory signals for other B and T cells and can also differentiate to cytotoxic cells, and Regulatory T cells that help to control the immune response by monitoring T cell activity. Some T cells will also differentiate into Memory T cells that contribute to long-lasting immunity against a particular pathogen or disease. CD62L and CD25 are downregulated on these cells, but when exposed to specific antigen, memory T cells will be quicker to recognise and activate, re-expressing CD25 and then differentiating into effector cells [18]. Memory T cells can be further divided into central memory T cells (Tcm, CD45RO+ve, CCR7 high), effector memory T cells (Tem, CD45RO+ve, CCR7low), effector memory T cells re-expressing CD45RA (Temra,

CD45RA+ve, CCR7low), tissue-resident memory T cells (Trm, CD45RO+ve, CCR7low) and follicular helper cells (Tfh, CD45RO+ve, CCR7high) depending on their receptor/ligand expressions [23, 24]. Naïve, effector and memory T cell subsets also have varying expressions of adhesion molecule CD44, activation markers CD127, CD25 and CD69, and homing ligand CD62L, showing a switch in expressions from naïve to effector phenotype (Table 1.1) [23-25].

Table 1.1

Marker		Naive	Effector	Memory				
				Tcm	Tem	Temra	Trm	Tfh
Tyrosine phosphatase	CD45	RA	RA/RO	RO	RO	RA	RO	RO
Adhesion	CD44	Low	High	High	High	-	High	High
Activation	CD127	High	Low	High	High	Low	-	-
	CD25	Low	High	High	High	Low	-	Low
	CD69	Low	High	Low	-	-	High	-
Lymph node homing	CD62L	High	Low	High	Low	Low	Low	High
	CCR7	High	Low	High	Low	Low	Low	High

Table 1.1 Summary of cell surface markers used to distinguish Naïve, Effector and Memory T cell subsets.

1.3.1 MHC structure and function

Two classes of MHC molecules are found, MHC class I and MHC class II, both differ in their structure and tissue expression. Their main purpose is to present a range of peptides broken down from extracellular foreign bodies or phagocytosed cells to T cells. MHC class I molecules are found the surface of all nucleated cells and present peptides that are recognised by CD8 T cells. Whereas MHC class II is constitutively expressed on specialised cells such as antigen presenting cells and only upregulated on other cells in response to interferons. Peptides presented by MHC class II molecules are recognised by CD4 T cells. The structure of both classes is similar and

are composed of four domains (Figure 1.2). The two paired domains adjacent to the cell surface membrane resemble immunoglobulin domain and the two outer domains fold to form a groove in which the peptide sits [18, 26].

Figure 1.2

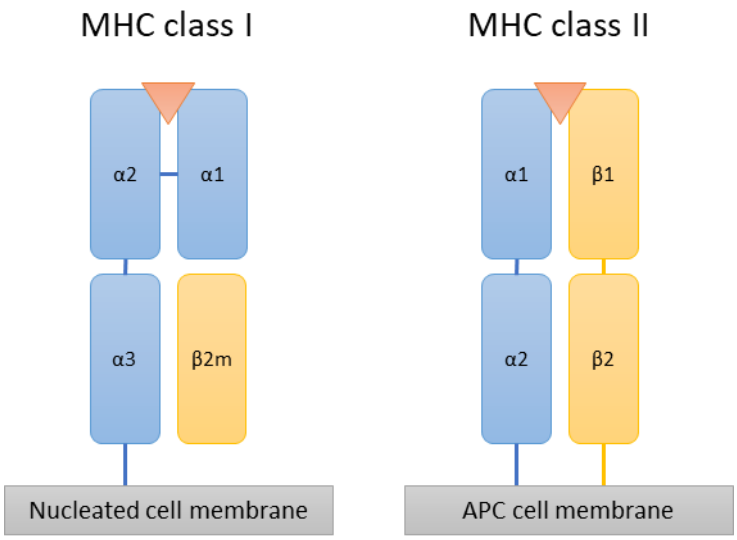


Figure 1.2 Structure of MHC class II and MHC class II molecules found on all nucleated cells and antigen presenting cells respectively. Both are made up of four domains however, MHC class I consists of 3 domains formed by an α chain (blue) noncovalently bound to β2-microglobulin (orange). MHC class II is composed of and α (blue) and β (orange) chain, each spanning two domains. Peptide (red) lies in the peptide-binding groove that is framed by α1 and α2 domains in MHC class II and α1 and β1 domains in MHC class II.

MHC class I molecules are composed of an α chain that spans three of the domains and β2-microglobulin that makes up the fourth domain. The folded α1 and α2 domains make up the peptide-binding groove which is closed at both ends by conserved tyrosine residues limiting the size of peptide it can accommodate to 8-10 amino acids. In contrast, MHC class II molecules are able to bind much longer peptides ranging from 13-25 amino acids in length [26]. This complex consists of two chains, α and β, both of which form two domains each. The peptide-binding groove is framed by one domain from each chain furthest from the membrane, α1 and β1 [26]. MHC molecules

are unstable, and the bound peptide helps to strengthen the structure allowing efficient interactions with the TCR.

Various allotypes of each MHC molecule can be found based on the expression of certain gene regions encoding human leukocyte antigens (HLAs). Both MHC class I and II can be divided into 3 HLA groups; A, B and C for MHC class I, and DR, DP, DQ for MHC class II. MHC molecules are highly polymorphic with multiple alleles within each HLA group. These variations affect the composition of the peptide binding groove therefore further defining the peptide repertoire the molecule can present [26, 27].

1.3.2 Peptide processing and presentation

Peptides are produced after proteolytic cleavage of proteins for presentation to T cells via MHC molecules. In general, endogenous proteins degraded within proteasomes result in peptides bound to MHC class I which will be recognised by CD8 T cells (Figure 1.3a). Whereas, both endogenous and exogenous proteins degraded by the lysosomal pathway will produce peptides for MHC class II binding and recognition by CD4 T cells (Figure 1.3b) [18]. However, cross-presentation can occur where MHC class I will bind exogenous peptides internalised by phagocytosis. Dendritic cells exhibit this mechanism which allows the cross-priming of naïve CD8 T cells [28].

MHC class I molecules are folded, and chains are assembled in the endoplasmic reticulum (ER) (Figure 1.3a). Meanwhile, proteins in the cytosol are ubiquitinated and subsequently tagged for degradation into short peptides. The newly formed peptides are transported to the ER by proteins called transporter associated with antigen processing 1 and 2 (TAP1 and TAP2). TAP proteins preferentially transport peptides of shorter length, 8-16 amino acids, which contributes to the difference in peptides presented via MHC class I vs MHC class II [29]. The MHC class I α chain enters the

ER bound to calnexin. When it encounters and binds to β2-microglobulin, the partially folded MHC heterodimer is incorporated into the peptide-loading complex (PLC) where Tapasin catalyses the loading of high-affinity peptides [18, 27]. Some MHC allotypes are tapasin-dependent and so are retained in the ER in its absence. These allotypes are still able to bind peptide but only with low affinity [27]. Tapasin-independent allotypes are still able to bind peptide and translocate to the surface [26]. A process called peptide editing occurs where the PLC retains the MHC class I complex in a state that allows exchange of low affinity peptides for high affinity peptides. Eventually, binding of a peptide will release the MHC molecule from PLC, and then transported to the cell surface [18]. Conformational differences in the peptide-binding groove due to allotype expression is also thought to alter the flexibility of the groove therefore binding peptides of various affinities [27].

Figure 1.3

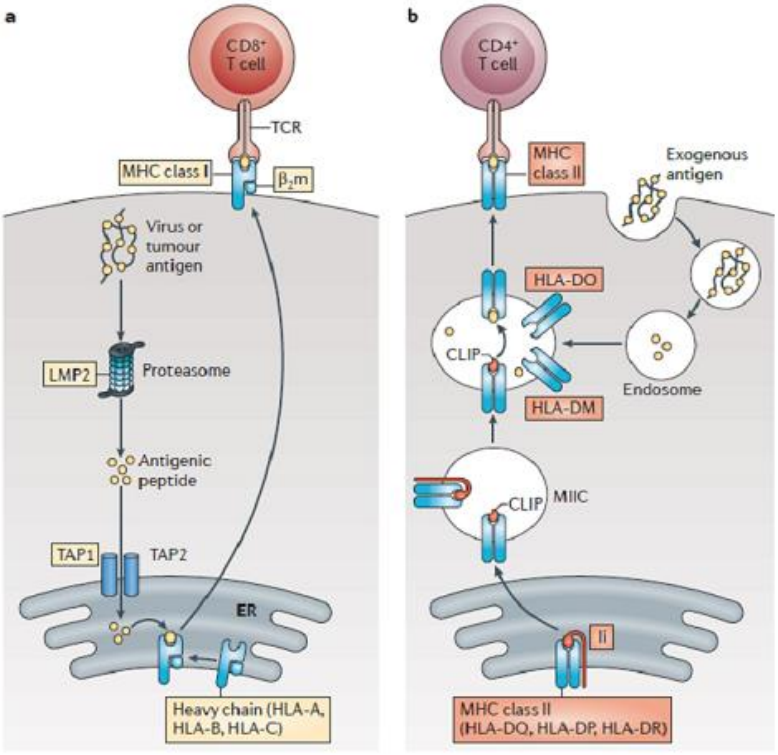


Figure 1.3 Overview of proteasomal (a) and lysosomal (b) protein processing pathways. Endogenous peptides are processed by the proteasomal pathway and transported to the endoplasmic reticulum (ER) by TAP molecules for loading onto MHC-I. The peptide:MHC-1 complex is transported to the surface for presentation to CD8 T cells (a). MHC-II molecules bound to invariant chain (Ii) are released from the ER into to MHC-II containing compartments. Ii is cleaved to form CLIP which is later displaced with the help of HLA-DM/DO by endocytosed peptides. The peptide-MHC-II complex then presents to CD4 T cells (b)[30].

MHC class II molecules are also assembled within the ER into endosomes or MHC class II containing compartments (MIICs), and associate with the invariant chain (Ii) also known as CD74 (Figure 1.3b). This chaperone blocks the MHC class II peptide-binding groove to prevent premature peptide loading, until the molecule enters the endosome and is cleaved by proteolysis to form a short class II associated invariant chain peptide called CLIP (~20 residues) remaining in the binding groove. Meanwhile, extracellular proteins are captured in endosomes and are cut into smaller antigen fragments by proteolytic enzymes before attaching to available MHC class II molecules [31]. Another MHC-associated protein termed DM (HLA-DM in humans) is responsible for releasing CLIP by binding to the class II molecule and promoting a conformational change. The peptide binding groove is now free to accept antigenic peptides. DM can also block low affinity peptides from binding to MHC class II therefore only high affinity peptides will be presented to CD4 T cells. This greatly influences the CD4 T cell repertoire [18, 28]. The MHC class II presentation pathway is further regulated by another MHC-associated molecule known as DO (HLA-DO in humans). DO inhibits DM by binding to the same sites on DM that interact with MHC class II [32].

1.3.3 α/β T cell receptor structure and function

TCRs are heterodimers and two classes exist; TCR-αβ and TCR-γδ. In the following chapters only α/β TCRs will be discussed, however others are investigating the use

of TCR-γδ T cells for cancer immunotherapy [33, 34]. TCRs are located on the surface of T cell membranes and consist of an extracellular domain, a transmembrane region and a short cytoplasmic tail (Figure 1.4). Both α and β chains make up the extracellular domain with a constant region adjacent to the membrane and a variable region furthest from the membrane. Like the BCR, the variable region is involved in peptide recognition. A CD3 molecule associates with the TCR, and is important for stabilising and eliciting T cell signals through the cytoplasmic tails of CD3 -ε,-δ, -γ and – ζ, that contain Immune-receptor Tyrosine-based Activation Motifs (ITAMs) as shown in Figure 1.4 [35-37].

The genes that encode TCRs are divided into Variable (V), Joining (J) and Constant (C) regions, that make up the α and γ chains. The additional region, Diversity (D) determines the structure of the β and δ chains. In the TCRα locus, the V and J regions consists of 70-80 and 61 gene segments respectively. The TCRβ locus contains 52 functional segments in the V region followed by two clusters of a single D segment and either 6 or 7 J region segments. A single C region follows each J region in both alpha and beta chains [18, 38]. TCR diversity arises from the random recombination events such as nucleotide additions, deletions and substitutions of a single segment from each region and can potential create between 10^{15} and 10^{20} TCR clonotypes (a population of T cells with identical TCRs) [38].

Figure 1.4

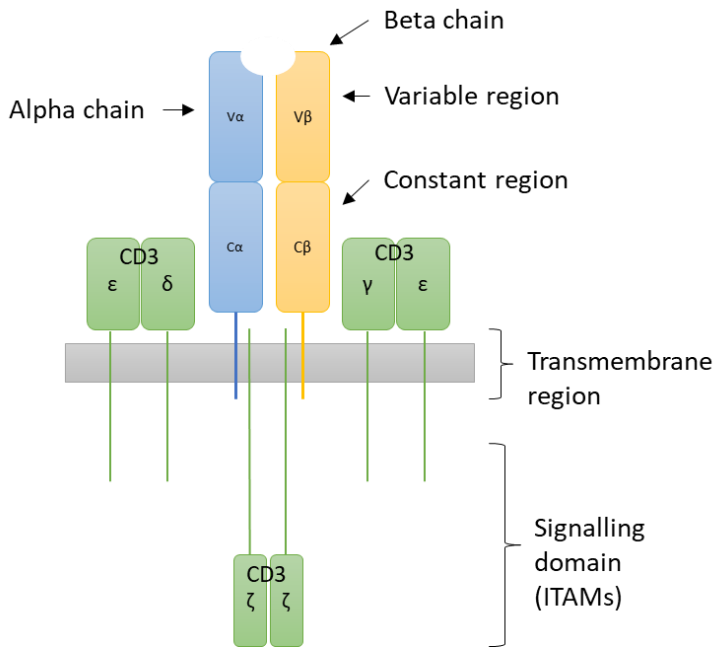


Figure 1.4 Structure of T cell receptor (TCR). The TCR is composed of two chains; alpha (α) and beta (β) which are form by a constant (C) region adjacent to the cell surface and variable (V) region that recognises the peptide-MHC complex. CD3 molecules surround the TCR with ε/δ and γ/ε on the cell surface and intracellular zeta (ζ) chains involved in TCR signalling.

A TCR's main purpose is to recognise and interact with antigen presented to a T cell via major-histocompatibility complex (MHC) molecules on the surface of antigen-presenting cells (APCs). The ability of a T cell to respond to a wide range of antigens stems from the high degree of variability in the TCR antigen-binding site. This part of the TCR structure is known as the third hypervariable loop (CDR3) and is formed by the D and J segments of both the α and β chains. The periphery of the antigen-binding site, which mostly interacts with MHC, is encoded by the V gene segments forming the CDR1 and CDR2 loops [18, 39]. The numerous combinations of α:β (or γ:δ) chains further increase TCR diversity.

1.3.4 Gene rearrangement of the α/β TCR loci

Various factors are involved in the development of T cells from maturation and selection in the thymus to stimulation, differentiation and proliferation in the periphery, contributing to numerous phenotypes each with their own specific function. The first stage of T cell development occurs at the gene level and results in the acquisition of a functional T cell receptor (TCR). T cell progenitors, known as thymocytes, in the thymus are negative for TCR until they undergo rearrangement of the antigen-receptor genes and become CD4+CD8+ double positive thymocytes.

Rearrangements are mediated by recombination activating genes RAG1 and RAG2 and the enzyme terminal deoxynucleotidyl transferase (TdT). Studies have shown that these genes can also alter TCRs post-selection in peripheral and tumour-infiltrating T cells, suggesting a later stage role RAG1/2 plays in shaping the TCR repertoire [40, 41]. In the beta chain, D-J rearrangement occurs first, followed by the addition of a V gene (Figure 1.5). As D genes are not present in the alpha chain loci, only V-J rearrangement occurs [39]. Although V(D)J rearrangement is considered to be a random event, some clonotypes are more common than others and are shared between individuals. This is believed to be due to the generation of certain amino acid sequences by a greater number of nucleotide triplets resulting in a higher chance of occurrence, also known as convergent recombination [42].

Figure 1.5

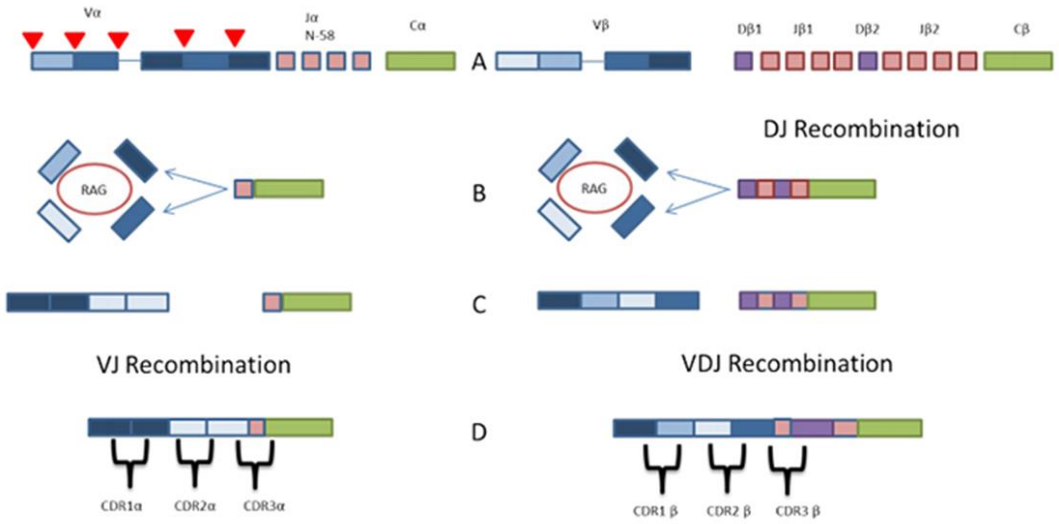


Figure 1.5 Recombination of the TCR alpha (left) and beta (right) chain genes. Gene locus composed on Variable [V], Diversity [D], Joining [J] and Constant [C] regions. D region only found in beta chain locus (a). DJ rearrangements occur first for the beta chain (b), followed by the addition of a V gene in both alpha and beta chains (c). The Constant region is then spliced and rearranged with the VDJ segment [43].

1.4 Thymic selection

A unique microenvironment exists in the thymus that aids T cell development. It consists of numerous lobules separated into an outer cortical region, the thymic cortex and the inner medulla. In young individuals, high numbers of new T cells are produced in the thymus to build a repertoire of antigen specific lymphocytes. Many hematopoietic cells are attracted to this area giving rise to high numbers of thymocytes (T cell precursors) that are differentially distributed [44]. Immature thymocytes will interact with thymic epithelial cells (TECs), initiating Notch signalling which switches on T-cell development specific genes and induces the initial phase of differentiation [45]. These early thymic progenitors (ETPs) are double negative (DN) for co-receptors CD4 and CD8 and do not express a T cell receptor. ETPs pass four

double negative stages before gaining a co-receptor; DN1, DN2, DN3 and DN4. In the first stage, DN1, thymocytes express CD44 and Kit, and gain CD25 expression by DN2. CD44 and Kit is lost at the DN3 stage but cells undergo TCR β chain selection [18, 46]. After β-selection, thymocytes in DN4 lose both CD25 and CD44 but express TCR-β chain and upregulate CD28 before proliferating in a Notch-dependent manner [18, 47]. An intermediate stage exists where the cells gain CD8 and are termed intermediate single positives (ISP) before becoming double positive (DP) by acquiring CD4 [18, 46, 48, 49]. There are two thymocyte populations negative for CD4 and CD8 that are considered as matured; thymocytes expressing γ:δ TCRs and thymocytes expressing the NK1.1 receptor (found on NK cells) as well as an α:β TCR with little diversity [44]. NK1.1+ T cells act as an early response to infections, they have an effector memory phenotype (CD62Lneg), differentiating in the presence of IL-15 and rapidly producing IFNγ in response to pathogen [50].

TECs show morphological differences depending on their location in the cortex or the medulla, contributing to T cell receptor diversity. Cortical thymic epithelial cells (cTECs) express high levels of MHC class II and undergo constitutive autophagy allowing presentation of self-peptides, favouring CD4 T cell differentiation. High abundance of the lysosomal proteases Cathepsin L and thymus-specific serine protease (TSSP) proteins are found in cTECs [51]. Autophagic activity has been found to decrease in these cells with age which may contribute to the low levels of T cells found in older individuals [52]. In addition to the ability of presenting self-peptides through autophagy, cTECs express the unique subunit, β5t, of the proteosome are known as the thymoproteosome which aids the degradation of cytoplasmic proteins for presentation via MHC class I and subsequent induction of CD8 T cells [48, 51, 53].

Thymocytes can be engulfed by the cTECs forming multicellular complexes known as thymic nurse cells (TNCs) [51]. Within the TNCs, DP thymocytes begin α chain rearrangement [49]. Once complete, low levels of an α:β T cell receptor will associate with CD3 on the cell surface. Receptors that fail to recognise self-peptide:MHC complexes presented by the cTECs will die. However, double positive cells that do recognise self-peptide:MHC are positively selected to mature and express high levels of that α:β TCR [44, 48, 49]. This is termed positive selection. At this stage the thymocytes will lose expression of either CD4 or CD8 depending on the class of MHC it recognises, eventually becoming single positive [18, 46].

Before the single positive thymocytes can leave the thymus and enter the periphery, they undergo one final test within the thymic medulla known as negative selection. Medulla thymic epithelial cells (mTECs) and dendritic cells in this area present various self-antigens to the newly single positive thymocytes [48]. These specialised mTECs express high levels of Cathepsin S, CD40 and AIRE; a nuclear protein that regulates promiscuous gene expression where up to 90% of genes including the tissue-restricted antigens are expressed [49, 51]. This process eliminates self-reactive T cells in circulation and therefore reduces the chances of autoimmune diseases, monitoring T cell tolerance. However, not all self-proteins are expressed in the thymus allowing mature T cells to recognise these antigens and produce a response.

The process of positive selection and negative selection appear to be counterproductive, as any cell that recognises self-peptide:MHC complexes are destined to mature during positive selection but are then eliminated during negative selection. The survival of a diverse T cell repertoire must therefore depend on the specificity and affinity of the TCRs to recognise self-peptide:MHC complexes. The affinity hypothesis states that thymocytes that weakly recognise self-peptide:MHC will survive but a strong interaction against self-antigen will drive the cell to apoptosis [18].

Two proposed models show how the TCR signal strength contributes to this outcome (Figure 1.4). In the first model, a TCR with moderate affinity for self-peptide will pass the positive selection threshold but avoid elimination by apoptosis. A high affinity TCR will pass both of these thresholds and will be destroyed (Figure 1.4a). The second model suggests lower affinity TCRs can sustain signalling over a long period of time avoiding negative selection, but high affinity TCRs peak in signalling faster, passing the apoptosis threshold (Figure 1.4b). Any high affinity TCRs that do not reach the apoptosis threshold would still be removed as signalling is not sustained [54].

Figure 1.6

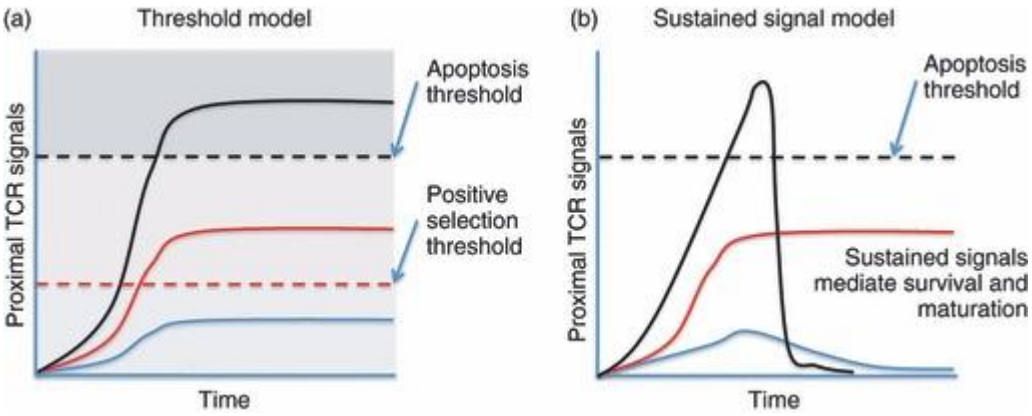


Figure 1.6 Affinity based TCR signalling contributes to positive and negative selection. Threshold model shows moderate affinity TCRs pass positive selection and avoid death, whereas strong signalling passes threshold for apoptosis (a). The sustained signal model is based on the length of signalling, showing low affinity TCRs survive positive and negative selection due to longer signalling period. High affinity TCR peak pass the apoptosis threshold and are eliminated and/or can not sustain signal for as long (b) [54].

1.5 CD8 T cells

CD8 T cells have long been considered the main mediators against infectious disease and cancer. When activated by antigen, they will differentiate into effector T (Teff) cells, secreting pro-inflammatory cytokines IFNγ, TNF-α and IL-2 to aid activation and

proliferation of neighbouring T cells, and release cytotoxic granules such as perforin and granzyme to directly kill the target cell. Many researchers measure immune responses to cancer via increased proliferation, IFNγ production and lytic activity of CD8 T cells. These cells express a range of phenotypes after differentiation known as central memory (Tcm), effector memory (Tem) and stem cell memory (Tscm), which can be distinguished by varied expressions of cell surface molecules CCR7, CD62L, CD27, and CD127 [55]. Some effector cells can also re-express the naïve T cell marker CD45RA. These highly cytotoxic cells are known as Temra and are often considered terminally differentiated, however some CD57-ve Temra cells still retain function [55-57]. CD8 T cells localised in tissues, termed tissue resident memory (Trm) will also express a slightly different phenotype with higher levels of activation marker CD69, E-cadherin ligand CD103, collagen binding integrin CD49a and extracellular matrix HUA receptor CD44 [58]. Although the role of these cells is still under investigation, the cell surface marker expression highlights the adaptation of the CD8 T cell subset to its surroundings.

As discussed in section 1.3.2, CD8 T cells recognise endogenous peptides presented via MHC-I. Due to the expression of this molecule on both APCs and epithelial cells, a wide range of epitopes can be presented and stimulate CD8 T cells. This is especially important as every nucleated cell has the potential to be infected by a virus, therefore CD8 T cells are able to scan MHC-I molecules for any foreign peptides. Due to the TAP loading restrictions and the closed end on the MHC-I peptide binding groove, only peptides of approximately 8-16 amino acids are presented by MHC-I and therefore available for recognition by CD8 T cells [26, 29]. The CD8 co-receptor is proposed to have two main roles in antigen recognition; firstly binding to MHC-I in synergy with the TCR and secondly signalling through recruitment of intracellular kinase Lck to the TCR/CD3 complex. Although TCR can bind MHC-I without CD8 help, the synergy of CD8 with the TCR allows stabilisation of the peptide-MHC-TCR

complex and induction of cytotoxic activity in the T cells with low TCR affinities [59, 60]. This synergy diminishes as the TCR affinity increases [60]. CD8 synergy is particularly important in the context of cancer, as T cells that bind self-peptide-MHC with high affinity are usually deleted during thymic selection. But this characteristic allows the recognition of TAAs which are usually recognised with low affinity. After recognition of peptide, the co-receptor helps to ensure successful activation of the CD8 T cell. Initially by binding to MHC-I. This occurs at relatively low affinity (Kd ~100-200μM) depending on the allele, however this interaction can increase sensitivity and activity of the T cell to MHC-I and cognate peptide by a million-fold [61-63]. More importantly, CD8-MHC binding ensures specific antigen recognition [64]. TCR signalling through Lck initially occurs without coordination of CD8 but the CD8/Lck interaction stabilises this signalling allowing full activation [65]. This CD8-Lck coupling increases upon T cell maturation; 13-fold increase in coupling in peripheral CD8 T cells compared to DP thymocytes, highlighting this enhancement as another contributing factor to their ability to recognise self-peptides with low affinity TCRs [66]. Due to these characteristics CD8 T cells have been of great interest in cancer immunotherapy techniques and TAA's recognised by them have been studied intensely for over 20 years.

1.6 CD4 T cells

Like CD8 T cells, when activated CD4 T cells will differentiate into effector and memory T cells. Traditionally effector CD4 T cells were considered solely as helper cells, supporting B cells in antibody production and cytotoxic activity of CD8 T cells. However, accumulating evidence indicates these cells are capable of exhibiting cytotoxic phenotypes and can kill target cells through indirect and direct methods (discussed later). CD4 T cells have a great degree of plasticity and various subsets exist; Th1, Th2, Th17, follicular helper T cells (Tfh), regulatory T cells (Treg), Th9,

Th22 [18]. Each portray distinct functions however all except Tregs aim to defend against pathogens and parasites (Figure 1.10). Newly differentiated effector CD4+ T cells (Th0) will secrete IL-2 to stimulate their own proliferation which will then differentiate into the various Th subsets when activated by a cocktail of cytokines. IL-12 and IFNγ are considered pro-inflammatory cytokines as they aid differentiation of Th0 cells into Th1 (T helper 1). These secrete IFNγ and TNFα to activate macrophages and increase toll-like receptor (TLR) expression. Th2 cells are produced in response to IL-4 which this subtype also secretes, in addition to IL-5 and IL-13, to activate B cells for antibody-mediated inflammation and target parasitic infections [67, 68]. Th1 and Th2 have traditionally been known as the major CD4 effector subsets however research has allowed more subsets to be distinguished. Th17 cells, so called for their expression of IL-17, can be differentiated by a combination of IL-21, IL-6, IL-23 and TGF-β. These cells also secrete IL-21, IL-22, IL-25 and IL-26 for neutrophil activation and protection against extracellular pathogens. Other subsets include Th9 (stimulated by IL-2, IL-4 and TGF-β, release IL-9 and IL-10), Th22 (stimulated by IL-6 and TNF-α, release IL-22), and Tfh (stimulated by IL-6 and IL-21, release IL-6 and IL-21) [67, 69].

Figure 1.10

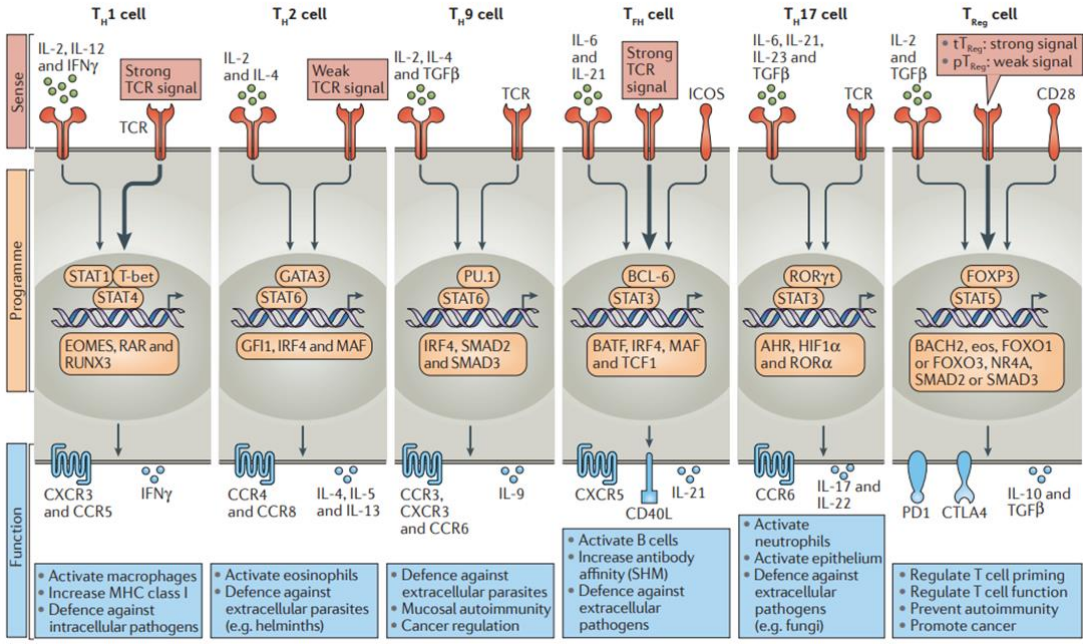


Figure 1.10 CD4 T cell subsets induced by various cytokines (Red) which activate different pathways (Orange) and promote secretion of cytokines and chemokines to elicit unique functions (Blue) [69].

Th1 cells are the main focus of anti-tumour activity. The other subtypes, Th2, Th9, and Tfh and Th17 have shown both tumour suppressive and promoting effects so their contribution to anti-tumour response still needs to be defined [68]. Subtype differentiation depends on a multitude of extracellular signals that initiate signalling pathways followed by new gene expression within the cells. These extracellular signals include cytokines, TCR and co-stimulatory binding strength [69]. Strong TCR signalling preferentially polarises toward a Th1 rather than Th2 phenotype. In contrast, weak signalling promotes FOXP3 expression and therefore Treg differentiation. However, in the presence of abundant antigen or high TCR affinities, very strong TCR signalling can occur and induce an Th2 phenotype [69]. All subtypes differ in their cell surface protein expression and cytokine secretion patterns, however there is a degree of plasticity between the subpopulations allowing switching from

one phenotype to another when induced by cytokines. For example, TGF-β caused Th2 switching to Th9 and IL-12 converted Th17 cells to Th1 [70]. In cancer immunity, the Th1 phenotype is most desirable due to the secretion of pro-inflammatory cytokines that drive macrophage, T cell and NK cell activation [71-73]. By this mechanism, CD4 T cells can indirectly induce killing of tumour cells [74]. This phenotype was also associated with apoptosis of tumour cells in ovarian cancer [75]. In addition, CD8 T cells require help from Th1 for naïve T cell proliferation, survival, optimal IFNγ production, memory CD8 T cell development [73, 76].

Current research shows CD4 T cells can also express a cytotoxic phenotype [1, 77], due to the expression of the termination of transcription factor thPOK [78]. Like CD8 T cells, memory CD4 T cells can be distinguished from naïve cells and divided into 3 groups depending on their expression of CD45RA and CCR7; Tcm, Tem and Terma. This highly cytotoxic Temra population expressed increased granzyme B and perforin compared to the other groups [79]. As discussed previously these lytic granules induce apoptosis of target cells, therefore CD4 T cells are able to upregulate similar cytotoxic mechanisms directly killing tumour cells expressing peptide-MHC-II, independently of CD8 T cells [80-83].

CD4 T cells recognise peptide presented via MHC-II molecules. As MHC-II is primarily found on professional APCs, it is thought a smaller range of target antigens are available for sampling. However, evidence has shown MHC-II can be induced in non-professional APCs including tumour cells, and unlike MHC-I this molecule is capable of presenting peptides longer than 16 amino acids, allowing the recognition of endogenous TAAs not normally exposed to the adaptive immune system. This is very beneficial when selecting TAA as targets to avoid toxicity effects on normal cells and non-cancerous tissues. Mass spectrometry analysis of MHC-II bound peptides in DCs and B cells show they originate from all cellular compartments; membrane, nucleus,

endo/lysosomes, and cytoplasm, with only 11-25% detected from extracellular proteins [84]. As a large range of peptides are presented, a mechanism must exist to select specific T cell recognition and activation of antigenic peptides. Again, the co-receptor CD4 contributes to this, in similarity to CD8, it regulates signalling by recruiting Lck. Like the CD8 co-receptor, CD4 aids T cell signalling through interactions with Lck and CD4-Lck coupling events were also found to increase from the thymus to the periphery [64, 66]. But this elevation was to a lesser extent, only 2-fold, compared to the 13-fold increase seen in CD8 T cells [66]. Nevertheless, the CD4-Lck coupling does alleviate T cell activation as seen by increased CD69 levels and proliferation in CD4-Lck compared to Lck deficient T cells [64]. CD4 binds to MHC-II with very low affinity, >2000μM Kd, and does not stabilise the peptide-MHC-TCR complex but its main function is to enhance Lck recruitment and elicit TCR phosphorylation [59, 63]. Interestingly, CD4 was shown to accumulate on the cell surface of unstimulated cells and interact with MHC-II in the absence of TCR. This was suggested to facilitate adhesion to MHC-II expressing cells increasing the chances of peptide recognition. As CD4-MHC interactions are of low affinity, it is possible CD4 multimerization induced by Lck, increases the avidity of TCR-MHC interactions thereby stabilising this complex [85, 86].

1.7 Checkpoint inhibitors

Immune checkpoints are necessary to avoid over stimulation of an immune response and subsequent destruction of healthy cells. However, in cancer where responses are often suppressed, these checkpoints can be blocked to stimulate T cells. There are many stimulatory and inhibitory molecules found on the surface of T cells but two major targets utilised for checkpoint blockade are the cytotoxic T-lymphocyte antigen-4 (CTLA-4) and programmed cell death protein-1 (PD-1) (Figure 1.11) [87]. Both of these have substantially changed the forefront of cancer immunotherapy. CTLA-4 is

upregulated when the T cell is activated and competes for CD80/CD86 on APCs, inhibiting binding to CD28 [88]. When CTLA-4 is bound to CD28, the TCR induced signalling is blocked, putting the brakes on T cell activation. This self-induced antagonism has been a target for cancer immunotherapy for over a decade with anti-CTLA-4 antibody Ipilimumab at the frontline [89]. Ipilimumab blocks CTLA-4 interactions with CD80/CD86 allowing the co-stimulatory molecules CD28 to bind, therefore removing the brake. It has also been used in combination with other therapeutics such as radiotherapy which reduced tumour volume and increased TIL clonality compared to radiotherapy alone [90, 91]. The second immunosuppressive molecule, PD-1, blocks CD3/CD28 mediated activation, by binding to it ligand PD-L1 on APCs [92]. In both viral infections and tumours, PD-1 was expressed on T cells (or TILs) with an effector memory phenotype exhibiting reduced proliferation and lower IL-2/IFNγ expression compared to PD-1 negative cells [93, 94]. PD-1+ TILs isolated from melanoma patients also expressed higher levels of CTLA-4 compared to in normal tissue and blood [94]. Taken together, cells expressing one or both of these receptors represents an exhausted phenotype with altered effector functions. Blocking PD-1 allowed activation of CD8 T cells via CD3/CD28 as seen by increased phosphorylated ZAP70, AKT and SHP2 signalling molecules [95]. In addition, non-small cell lung cancer (NSCLC) and gastric cancer patients that responded to PD-1 blockade (complete/partial response or stable disease for >6 months), showed increased tumour infiltration of PD-1+ CD8 T cells with a greater ratio compared to PD-1+ CD8 T regulatory cells [95]. This suggests PD-1 blockade restored the effector function of TILs. Combination therapies targeting both CTLA-4 (Ipilimumab) and PD-1 (Nivolumab or Pembrolizumab) termed immune checkpoint blockade, gained popularity for a number of different cancers showing decreased disease progression and overall survival [96]. However this combination has a high incidence of treatment related adverse events that has led to the discontinuation of treatment in some

patients [97]. Individual use of checkpoint inhibitors or in combination with other therapeutics is now more common [98-100].

Figure 1.11

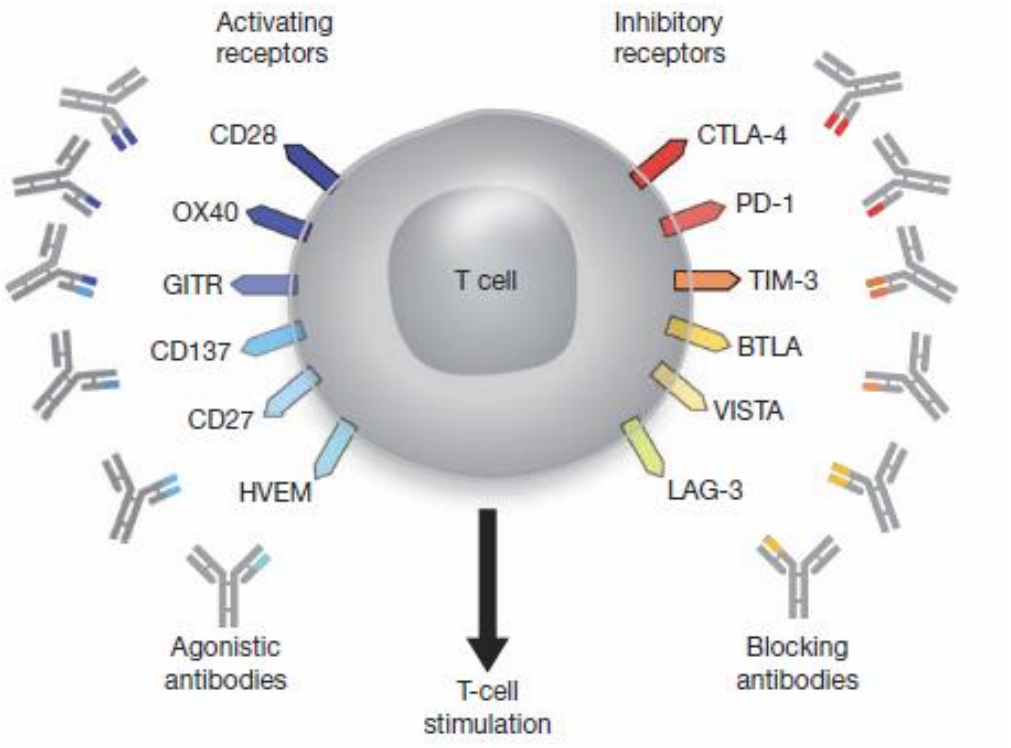


Figure 1.11 Co-stimulatory and co-inhibitory molecules regulating activation or inhibition of T cell responses. Therapeutic antibodies targeting inhibitory receptors will block T cell signalling whereas those that bind activation receptors will stimulate a T cell response [87].

1.8 Adoptive T cell therapy

For some cancer patients therapies such as target antibodies and immunomodulators that focus on immune checkpoint blockade, agonists and cytokine treatment, work efficiently to recognise and eliminate tumours. However, the efficacy of these treatments can be low due to poor T cell infiltration to the tumour, lack of target recognition and ablated responses by the patients T cells, creating ‘cold’ tumours. Adoptive T cell therapy (ACT) addresses these challenges and can be divided into

multiple groups; tumour-infiltrating lymphocyte (TIL) therapy, engineered T cell receptor (TCR) therapy, chimeric antigen receptor (CAR) T cell therapy, and natural killer (NK) cell therapy. These therapies have been shown to induce robust T cell responses however the technologies and targets involved differ greatly.

1.8.1 Tumour-Infiltrating Lymphocyte (TIL) therapy

Naturally occurring T cells with the ability to recognise cancer antigens exist within the tumour. These lymphocytes can be harvested from an excised tumour, activated and expanded *in vitro*, and administered back to the same patient as a method of ACT. One of the first TIL therapy trials conducted by Rosenberg and colleagues was performed in metastatic melanoma patients who received two cycles of autologous TILs alongside high dose bolus IL-2. TILs were generated from enzymatic digestion of the entire tumour and expanded using high concentrations of IL-2. Unfortunately, the overall response rate was low at 34%, only slightly greater than treatment with high dose IL-2 alone (31%) [101]. Some toxicity has been found when using high dose IL-2 and reducing this to 125000 IU/kg/day alongside TIL therapy in metastatic melanoma patients still produced comparable results with limited adverse effects [102]. Lymphodepletion prior to administration of TIL therapy resulted in better clinical response rates; 51% of metastatic melanoma patients exhibited complete (3/35) or partial (15/35) responses [103].

Advancements to this technique involved the selection of tumour antigen specific TILs prior to expansion and use for treatment. Generated TILs are co-cultured with autologous melanoma cells or HLA-matched melanoma cell lines, and recognition is measured by IFNγ responses [104, 105]. Positively responding cultures are then selected for expansion using anti-CD3 antibodies, irradiated PBMC feeder cells and IL-2 [105]. Selected TIL therapy, after a lymphodepleting nonmyeloablative condition

regimen, resulted in clinical responses (complete and partial) in 46% of metastatic melanoma patients, with clonal expansion of CD8 T cells, increased CD8 tumour infiltration and elevated MHC class I and II expression compared to pre-treatment [106]. However, one major drawback of this method is the requirement of autologous or HLA-matched melanoma cells for specific TIL selection which is not always available for each patient. This resulted in the exclusion of many patients from receiving this treatment [104].

Better response rates were reported in patients treated with TILs from 'young' cultures [101, 104]. In contrast to the selected TIL protocol, these cultures are produced from a single cell suspension of the excised tumour, rather than from multiple small tumour fragments. Due to the initial high cell recovery, young TILs are considered fully expanded after ~2 weeks when all melanoma cells have been removed. A higher percentage of young TILs (44%) displayed tumour specific IFNγ responses compared to standard TILs (38%), and contained a greater frequency of CD4 T cells [107]. CD8 T cells in young TIL cultures also expressed higher levels of co-stimulatory molecules CD27 and CD28 [107, 108]. In metastatic melanoma patients, treatment with young TILs results in complete or partial responses in 50% of the population and specific IFNγ production was observed in 5 out of 6 responding patients tested [109]. Long term follow up of a young TIL trial also showed clinical responses in 50% of patients and CD8 T cell reactivity to neoantigens in TIL products which was elevated in peripheral bloods after treatment [110]. The phenotype of these neoantigen specific CD8 T cells were of an effector and effector memory phenotype, however greater clinical success has been reported with stem-like CD8 (CD39-ve CD69-ve) TILs. The frequency of these stem-like TILs was higher in complete responders compared to non-responders, correlated with reduced tumour volume and percentage survival in mouse models, were capable of persisting for up to 75 months and could differentiate

into other subsets after TCR stimulation *in vitro* [111]. Together this highlights the importance of using non-differentiated T cell subsets for TIL infusion products.

1.8.2 Chimeric antigen receptor (CAR) T cell therapy

CARs are made up of three parts; a single chain fragment variant (scFv) in the extracellular domain that recognises the antigen and is followed by a spacer that connects to the transmembrane domain and then an intracellular domain that is involved in T cell signalling. Over time the structure and components of CARs have evolved to improve proliferation and effector functions. The first generation of CAR-Ts used CD3ζ with three immunoreceptor tyrosine-based activation motifs (ITAMs) to elicit activation signals however efficacy was only achieved by administering exogenous cytokines such as IL-2 [112]. Second generation CAR-Ts included additional signalling domains such as CD28, 4-1BB, OX40 or ICOS to enhance proliferation and cytokine responses. These molecules were added individually with pros and cons for each receptor. Third generation CAR-Ts better represented a natural T cell as multiple co-stimulatory molecule signals were added to the intracellular domain enhancing pro-inflammatory cytokine expression, anti-tumour activity and T cell persistence [113]. These have been successful in combating B-cell malignancies such as lymphoma and leukaemia however increased survival was linked to the expression of myeloid activation markers IL-12 and DC-Lamp [114]. The fourth generation also termed TRUCKs (T cells redirected for universal cytokine-mediated killing) involved adding IL-12 (or other effector cytokines) to the structure of second generation CARs to promote pro-inflammatory responses [115-117].

1.8.3 Engineered T cell receptor (TCR) therapy

Engineered T cell therapy involves equipping a patients T cells with a TCR directed against a specific epitope before administrating back to the patient. As TCRs

recognise specific peptides presented by MHC, this therapy method allows detection of intracellular proteins and increases the pool of suitable targets available compared to CAR-T technology which relies on detection of cell surface molecules only. In addition, TCRs require fewer peptide:MHC targets on the cell surface to be activated compared to the higher extracellular antigens needed to stimulate CAR-Ts. However, all identified peptide targets are subject to HLA-restrictions limiting the population available for treatment. As discussed earlier, peptides from self-antigens are recognised by TCR with low affinity compared to foreign antigens. Researchers sort to overcome this problem by generating high-affinity TCRs specific to cancer peptides for ACT however in some cases this led to unexpected cross-reactivity and toxicity. For example, the HLA-A2 restricted MAGE A3 TCR also recognised a HLA-A2 restricted MAGE-A12 epitope in the brain causing neurological toxicity and was fatal for two patients [118]. Another MAGE A3 TCR, restricted by HLA-A1, also showed severe adverse effects when it cross-reacted with titin expressed in beating cardiac tissue [119]. Both of these TCRs had been modified to enhance TCR affinity but not all enhanced TCRs display serious off-target toxicity. Partial responses and 38% survival (3 years) rates were observed in sarcoma and melanoma patients given adoptive transfer of HLA-A2 restricted NY-ESO-1 TCR transduced T cells, with no off-target effects [120]. The HLA-A2 restricted MAGE A4 TCR known as ADP-A2M4 has shown promising anti-tumour activity with no major cross-reactivity but some response to an antigen negative melanoma cell line and a small airway epithelial line were detected, as well as recognition of MAGE-A8 and MAGE-B2 peptides [121]. So far phase I clinical studies with ADP-A2M4 have not reported any off-target effects [122].

The majority of clinical ACT trials have looked at cancer testis antigens (NY-ESO, MAGE), melanoma antigens (gp100) and some myeloid malignancies (WT-1) with most restricted by MHC class I HLA alleles [123]. Only one MHC class II restricted

(HLA-DPB1*04:01) TCR against MAGE A3 has entered clinical trials but only showed responses in 3/9 patients who received a high cell number dose, with no correlation to serum cytokine levels [124]. In preclinical studies, adoptively transferred CD4 T cells have proved to be successful in inducing tumour regression, maintaining anti-tumour immunity and directly killing tumour cells [80, 125]. In the case of CD4 T cells transduced with a HLA-DPB1*05:01 restricted $WT1^{332}$ specific TCR and $TRP1^{113\text{-}127}$ specific CD4 T cells, WT-1 and TRP1 expressing target cells were eliminated through granzyme B and perforin release [80, 126]. In addition, responses were HLA-DQA1*03:01/HLA-DQB1*03:02 restricted in TILs from a melanoma patient with mutated $BRAF^{V600E}$ and the CD4 $BRAF^{V600E}$ specific cells displayed an effector memory phenotype producing IFNγ, TNF-α, IL-4 and IL-21 [127]. An alternative approach equipped CD4 T cells with a HLA-A2 restricted TCR specific for STEAP1, a TAA that is overexpressed in sarcoma. Anti-tumour activity of the TCR transduced CD4 cells increased over a 46 day period and showed comparable effects to TCR transduced CD8 cells [128]. Similar survival rates and T cell persistence was observed with MHC class I restricted high affinity m33 TCR transduced CD4 T cells [129]. The only flaw was a lack of anti-tumour response in metastatic tumours compared to TCR transduced CD8 T cells [126, 128]. However, adoptively transferred CD4 T cells were also capable of inducing antigen specific CTL activation [126]. Taken together, this evidence highlights the potential for CD4 TCR targets in adoptive cell therapy.

1.9 Cancer vaccines

A vaccine stimulates the immune system to protect against disease. In the context of cancer, these vaccines are a form of immunotherapy allowing immune cells to recognise and kill tumour cells. Some vaccines, prophylactic vaccines, can prevent the development of cancer such as protection against human papillomavirus (HPV)

dependent cervical cancer development. However, this vaccine is only effective if given prior to infection with the virus. The majority cancer vaccines are given to patients as a treatment method for cancer, and the various types of vaccines will be discussed below.

1.9.1 Tumour cell vaccines

Tumour cell vaccines, also referred to as whole cell vaccines, utilise the entire TAA repertoire of the cancer without the need to identify specific epitopes to generate an immune response. Tumour cells from the patient are treated *in vitro*, prior to administration, to ensure proliferation is blocked by freeze-thaw, heat shock, irradiation or lysis. Vaccination of a patient with their own cancer cells, known as an autologous cell vaccine, were associated with better survival in patients that mounted an immune response to their own tumour cells. In some cases, the tumour cell is engineered to express other pro-inflammatory mediators to further boost the immune response. The addition of GM-CSF and knockdown of TGF-β in an autologous ovarian cell vaccine significantly increased survival and maintained T cell activity (IFNγ responses) up to 20 months after the last treatment [130]. They can also be given in combination with foreign organisms such as Bacilli Calmette-Guerin (BCG) as an adjuvant as shown for colon, breast and bladder cancer [131-133]. These results are promising however live tumour cells can produce immunosuppressive cytokines such as IL-10 and TGF-β downregulating dendritic cell and T cell responses, therefore vaccine preparations that result in tumour cell death such as freeze-thaw and lysis are more desirable.

There are currently no approved tumour cell vaccines as most tumours will express self-antigens for which the corresponding T cell has been deleted in the thymus. The only antigens that can be utilised as TAAs are neo-epitopes. Due to the genetic

instability of cancers resulting in somatic mutations, most tumours express distinctly different peptide sequences that are absent in normal tissues [134]. These are created by codon alterations and antigen processing allows the presentation of these novel, tumour specific antigens on MHC. As T cells will not have experienced these antigens during thymic selection, a robust response is often generated highlighting neo-epitopes as a favourable target for T cell immunotherapies. As melanoma and lung cancers are more prone to high levels of somatic mutations, they have a greater chance of expressing of neo-epitopes, majority of which are recognised by CD4 T cells, therefore in these cancers tumour cell vaccines would be more successful [134].

1.9.2 Dendritic cell vaccines

Dendritic cells (DCs) are specialised immune cells that can engulf and digest cells and proteins, presenting a variety of antigens on its cell surface to activate T cells. As professional APCs, DCs are able to initiate naïve T cells and boost memory T cell responses. They also release a variety of cytokines regulating the responding T cell phenotype. Three main subsets of DCs are found in the blood; cDC1s, cDC2s and plasmacytoid DCs (pDCs) [135]. The formation of DCs can also be induced by exposure of CD14+ve monocytes to GM-CSF and IL-4 and many utilise this method to study DC kinetics *in vitro*. Due to their easy culture and expansion, the earliest DC vaccines involved immunisation of melanoma patients with monocyte-derived DCs pulsed with a range of TAA peptides or tumour lysate. Potent cytotoxic T cell responses to Melan-A and gp100 were found, however most patients had a low complete/partial responses and increased disease progression [136]. In more recent studies, the use of autologous patient DCs and specific selection of TAAs contributed to greater success with these vaccines. Higher complete response rates correlated with antigen specific CD8 T cell responses [137, 138]. In addition, immunisation with the MART-1 (a melanoma antigen) pulsed DCs increased T cell responses to two

other melanoma TAAs, gp100 and tyrosinase in a patient who exhibited a complete response, suggesting epitope spreading [139]. No severe adverse effects were reported with the most common side effect being erythema at the site of injection [138]. The low levels of myeloid and plasmacytoid DCs in peripheral blood make them poor targets for DC vaccines. However, the establishment of a plasmacytoid DC line has allowed the use of this DC subset for a cancer vaccine against melanoma [140]. To date, the majority of DC vaccines in clinical trials have been tested in melanoma patients with some in acute myeloid leukaemia (AML), multiple myeloma and prostate cancer [141-143]. This method has shown promising results however, it can be expensive and laborious, especially when using autologous DCs that require leukapheresis products from the patients. This also increases the risk of side effects such as vascular injury and electrolyte imbalance.

1.9.3 Viral vaccines

As viruses naturally induce an immune response, they can be utilised as vectors for stimulating anti-tumour immunity in cancer patients. The simplest method is by inserting the genes that encode TAAs into the viral genome and advancements to this technique include the addition of immune mediators such as CD80, the ligand for T cell surface activation protein CD28 [144]. There are several potential viruses for vaccine development with examples of genetically engineered poxviruses, adenoviruses, herpesviruses, retroviruses and lentivirus under investigation. However, each vector comes with a range of advantages and disadvantages. Expression of large gene inserts, strong immune response induction, and infection of both proliferating and quiescent cells are common positives among these viral vectors. But disadvantages include toxicity in immunocompromised hosts and the development of neutralising antibodies limiting efficacy of booster vaccinations [145]. In addition, viral vaccines produce substantially lower immune responses to the

tumour compared to the virus from which the vector was produced. However, oncolytic viral vaccines have shown more success. This technique involves intra-tumoral administration ensuring the vaccine is delivered to the specific site. The virus then replicates and kills the tumour cell it has infected. This inflammation recruits other immune cells directing the immune response against the tumour [146]. An oncolytic viral vaccine for treatment of advanced melanoma has gained FDA approval. The herpes simplex virus (HSV) Talimogene laherparepvec (T-VEC) reduced tumour size by 50% in 60% of treated patients, with an overall response rate of 26% compared to responses observed in un-injected lesions [147, 148].

1.9.4 Nucleic acid vaccines

This form of vaccine consists of genetically engineered RNA or DNA encoding a TAA and/or immunostimulatory molecules such as cytokines and immune checkpoint inhibitors [149, 150]. In addition to stimulating the adaptive immune response, DNA vaccines can elicit ‘danger signals’ that promote DNA-sensing pathways of the innate immune system. To ensure these nucleic acid vaccines are able to enter the nucleus of cells they need to be administered using physical methods such as electroporation, biojector, microneedle array, gene gun, needle free devices, and chemical methods liposomes and nanoparticles, some of which are fairly expensive and can cause discomfort to the recipient. These methods are under continuous development to improve uptake and immunogenicity of these vaccines [151]. In addition, mRNA vaccines require storage at low temperatures due to their stability, limiting their distribution to unequipped sites. One major advantage of the nucleic acids vaccines is that multiple TAAs can be encoded in one vaccine which allows targeting of both CD4 and CD8 T cells depending on the antigen selected. For example, a DNA vaccine encoding the CD8 TRP2 and CD4 gp100 epitopes, or multiple NY-ESO-1 epitopes with various HLA-restrictions, increased tumour infiltration of both CD8 and

CD4 T cells, stimulated antigen specific IFNγ responses and correlated with tumour growth reduction and increased survival in mouse models [152, 153]. Many DNA vaccines have entered clinical trials and target a range of cancers including breast, prostate, cervical, ovarian, pancreatic, renal, melanoma, and glioblastoma [154]. Most of these trials are still ongoing but treated prostate cancer patients have shown significantly increased metastasis-free survival up to 2 years, and increased antigen specific antibody titres from 6 weeks up to 1 year [155, 156]. In addition, the phase I/II clinical trial of DNA vaccine SCIB1 Immunobody targeting a mix of HLA-A2, HLA-DR4/DR7/DR53 and HLA-DQ6 restricted epitopes in melanoma patients has shown promising T cell responses through IFNγ expression and proliferation [157]. DNA and mRNA vaccines against neo-epitopes are also gaining interest. A DNA vaccine targeting mutation-inactivated E6 and E7 proteins from human papilloma virus type 16 (HVP16) is currently in phase II clinical trials for patients with HPV16 positive melanoma, non-small cell lung cancer, renal clear cell carcinoma, urothelial cancer and squamous cell head and neck cancer. Strong immune responses were found in all patients which was greater in those with high frequency of neo-epitopes [158]. The mRNA-4650 vaccine encoding 20 different neo-epitope targets, stimulated both CD4 and CD8 antigen specific T cells after 4 rounds of vaccinations in gastrointestinal cancer patients [159]. Personalised neo-epitope RNA vaccines have also shown great efficacy against tumour metastasis resulting in elevated progression free survival. Tumours from stage III and IV melanoma patients were resected and comparative exome RNA sequencing was performed to identify neo-epitopes. Majority were found to be immunogenic and stimulate CD4 responses [160]. Together, this highlights the potential of nucleic acid vaccines against neo-epitopes.

1.9.5 Protein and Peptide vaccines

As discussed earlier, cancer cells will express a range of unique proteins that are not present (or found at low levels) on normal cells. Patients can be immunised directly with these TAAs as whole proteins or a specific epitope (peptide) to trigger T cell responses. Peptide vaccines have shown great anti-tumour responses. Immunisation of breast, ovarian and non-small cell lung cancer patients with a mixture of HER2/neu peptides induced T cell responses in 92% of patients and epitope spreading with antibody responses to p53 [161, 162]. Various immunogenic peptide sequences within this protein have since been identified and induce tumour regression, increased survival and T cell activity in mouse models [163-165]. However, as this form of vaccine does not stimulate innate immune responses and is usually composed of self-proteins that elicit weaker responses compared to foreign antigens, they are administered with adjuvants such as cytokines, incomplete Freunds (IFA), aluminium and toll-like receptor (TLR) agonists [166]. The covalent attachment of TLRs to antigenic peptides are known to enhance cytotoxic T cell responses [167]. In some cases, TAAs can be linked to natural molecular chaperones, heat shock proteins (HSP) HSP110 or Grp170, to direct the antigen for processing and presentation in APCs [168]. The use of nanoparticles for delivery of peptide vaccines has also gained popularity due to the adaptability of particle coating to enhance APC uptake and activation. Liposomes and Polymeric nanoparticles have already gained FDA approval and including nanogels and micelles are biodegradable. Other options include inorganic nanoparticles like Gold, Iron Oxide, Alum and Calcium Phosphate, or silicas and virus-like particles [169].

Peptide vaccines can also be combined with other therapeutics to enhance immunity. For example, the common TAA gp100 was given in combination with CTLA-4 checkpoint inhibitor Ipilimumab to HLA-A2 stage III and IV melanoma patients. Overall

survival rates with combined treatment was double compared to the single treatment (gp100 only immunised) group at 12 and 18 months, however levels matched that of checkpoint blockade alone [170]. One limiting factor of peptide vaccines is the HLA-restriction of certain TAA sequences. However, as a mixture of peptides can be administered together, a wider range of HLAs can be covered. Successful identification of cancer peptides on tumour cells is critical to select the correct peptide for inclusion in vaccines. Protein vaccines have also shown promising results. Better overall survival was observed in patients with metastatic melanoma and a predictive responder gene signature compared to predicted non-responders, when immunised with recombinant MAGE A3 and adjuvant [171]. Oral administration of recombinant Wilm's tumour 1 (WT1) protein reduced tumour volume and increase tumour T cell infiltration and survival in mouse models [172]. This vaccine also induced better survival compared to a WT1 peptide amino acids 117-419 [173]. These vaccines can also be used to target neo-epitopes formed by post-translational modifications such as phosphorylation. A HLA-A2 restricted phosphorylated peptide from breast cancer anti-estrogen receptor 3 (BRCA3) was administered to stage III and IV melanoma patients with either IFA or TLR ligand Poly I:C. No severe adverse effects were measured and CD8 IFNγ responses were found in 40% of patients from 3-12 weeks post treatment [174]. Another common stress induced post-translational modification is citrullination.

1.10 Citrullination

Post-translational modifications have been shown to play an important role in autoimmunity and tumourigenicity. One of these mechanisms is citrullination; the deimination of arginine to citrulline. A positively charged aldimine group is replaced with a neutrally charged ketone resulting in a 1Da decrease in size (Figure 1.12). This

process is catalysed by a family of calcium dependent enzymes called peptidyl-arginine deiminases (PADs).

Figure 1.12

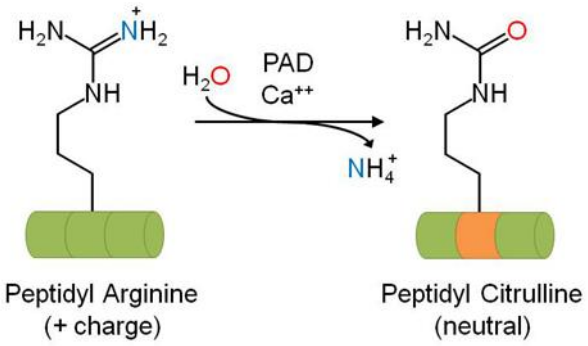


Figure 1.12 Deimination (also known as citrullination) of a positively charged arginine to a neutral citrulline by the calcium dependent enzyme peptidyl arginine deiminases (PADs) [175].

1.10.1 PADs

Five isozymes of PADs exist in humans; PAD 1-4 and 6 with variable distribution in cells and tissue types. All PADs are located in the cytoplasm but PAD4 has been identified in the nucleus and granules and PAD2 in mitochondria [176]. Target substrates differ between the 5 PAD enzymes and not all arginine residues are always citrullinated in a protein. The secondary structure of a protein will block some arginine residues whilst exposing others with the potential for deimination. Neighbouring amino acids can also influence the success of citrullination. Arginines followed by aspartic acid residues were more frequently citrullinated compared to those next to glutamic acid residues or surrounded by two proline residues [177]. The location of each isozyme contributes to its main target substrates. PAD1 is found in the epidermis, hair follicles and uterus and therefore binds keratin and filaggrin. PAD3 is also located in the epidermis and hair follicles and has been shown to bind filaggrin,

trichohyalin, apoptosis-inducting factor and vimentin [176]. PAD6 is found in the eggs, ovary and early embryo but there are no known targets. In addition, literature suggests this isozyme lacks enzymatic activity [178].

PAD2 and PAD4 are the most studied due to their links with autoimmune diseases and cancers. They are located in the central nervous system, spleen, skeletal muscle and leukocyte (PAD2) and in inflammatory cells such as macrophages, granulocytes and neutrophils (PAD4) [179]. Both have also been identified in various tumours including lung cancer, breast carcinomas, cervical squamous cell carcinomas, hepatocellular carcinomas, thyroid adenocarcinoma and ovarian adenocarcinomas [180-182]. PAD enzymes, and by extension citrullination, are important for the migration, proliferation and survival of tumour cells [182]. PAD2 targets myelin basic protein, vimentin and actin whereas PAD4 substrates include ING4, p300, p21, Nucleophosmin and nuclear lamin C [177]. Both isozymes also bind histones indicating their involvement in gene regulation.

1.10.2 Apoptosis and Calcium

Calcium (Ca^{2+}) is known to regulate many cellular mechanisms such as secretion of insulin by β cells and contraction of cardiac myofilaments [183, 184]. This ion is also required to activate PAD enzymes as discussed earlier. B cell lymphoma 2 (Bcl-2), a family of proteins greatly involved in the apoptotic pathway, are commonly localised within the mitochondrial membrane and ER. Overexpression of Bcl-2 and related family member Bcl-xL, was associated with reduced ER Ca^{2+} stores and increased leakage [185, 186]. Additionally, inactivation of Bcl-2, reduced Ca^{2+} release from the ER and restored levels within the ER [187]. This indicates increased cytosolic Ca^{2+} is involved in apoptosis induction. Intracellular Ca^{2+} released from the ER is thought to be taken up by the mitochondria to stimulate the release cytochrome c, a major

regulator of the apoptosis pathway [188]. Excessive cell death is found to exacerbate inflammation in the synovial fluid of Rheumatoid Arthritis (RA) patients and calcium deposits in osteoarthritis and RA patient synovial fluids have been document. Crystallisation of basic calcium phosphate (BCP) and calcium pyrophosphate dihydrate (CPPD) in these joints is found at the later stages of these autoimmune diseases and in the older population [189, 190]. The correlation between RA and CCP is yet to be determined but injection of BCP crystals into the mouse knee joints induced macrophage infiltration and cartilage damage [191]. This suggests not only does the continuous localised inflammation promote formation of BCP and CDDP but that the presence of the calcium deposits further induces cell death and damage.

1.10.3 Citrullination and Antibodies in Rheumatoid Arthritis

Elevated levels of PAD enzymes have been linked to many diseases including rheumatoid arthritis (RA), multiple sclerosis (MS), Alzheimer's disease (AD) and cancer [192, 193]. RA is a chronic autoimmune disease marked by excessive inflammation of the joints due to immune cell activation and the generation of autoantibodies [194]. One of the first autoantibodies to be identified in RA was specific for the Fc region of IgG and known as the Rheumatoid Factor. Since its discovery in RA patients (and absence in healthy individuals) it has become an important diagnostic marker [195]. The presence of citrullinated proteins in RA results in a more recently identified group of autoantibodies called anti-citrullinated protein antibodies (ACPAs). Due to their early detection in the disease and their correlation with disease severity, ACPAs have taken over as the main diagnostic and prognostic marker in identifying RA. Synovial fluid from patients containing anti-APCAs are often used to determine the presence of specific citrullinated proteins. Commonly identified citrullinated proteins in RA synovial fluid include vimentin, fibrinogen, α-enolase and histone H3 [196-200]. Immune complexes of citrullinated peptides and ACPAs form

in the synovial fluid promoting an inflammatory environment. Infiltrating neutrophils, macrophages and lymphocytes will be activated and form extracellular DNA traps resulting in cell death. Impaired clearance of the dead cells is followed by PAD activation and hence increased citrullination and production of ACPAs [201].

Specific alleles have been identified as risk factors for many autoimmune diseases and some forms of cancers. The association of specific HLA alleles with 'shared epitopes' (SE); a 5 amino acid sequence in the DRβ chain in residues 70-74, in RA has long been known. These SE alleles correlate with higher risk of RA and the development of ACPAs. The more SE alleles expressed by one individual, the greater the risk factor and disease severity. The distribution of dominant HLA SE alleles varies depending on geographical region. HLA DRB1*04 is the most common allele in association with RA risk however in Europe alleles DRB1*01 and *10 are also at a higher frequency in RA patients [202]. In the East Asian population DRB1*04 also appears as the major risk allele but in the Middle East the DRB1*10 allele is more predominant. Interestingly in this population, the frequency of HLA-DRB1*03 was lower in RA patients compared to healthy individuals suggesting this allele reduces the risk of RA development [203].

1.10.4 Citrullination in Viable Cells

Previously, the majority of documented events on citrullination was related to RA and other autoimmune diseases where excessive cell death induced inflammation. This suggests citrullination was associated with dying cells. However, Ireland et al (2011) found APCs in transgenic mice presented a citrullinated peptide from hen egg white lysozyme (HEL) protein which also stimulated CD4 T cell proliferation. The modified peptide was naturally presented by DCs and macrophages but not B cells unless stimulated by serum starvation [204]. This method of cellular stress is known to induce

a survival mechanism called autophagy, which is discussed in more detail in section 1.11. In addition PAD activation was found within autophagosomes, experiments using autophagy inhibitor 3MA and knockdown of Atg5 (an essential protein in this pathway) reduced presentation of the HEL 48-62cit peptide in serum starved B lymphoma cells and proliferation of responders [204]. Together this indicates the involvement the autophagy pathway for presentation of citrullinated epitopes to CD4 T cells.

1.11 Autophagy

Under stressful conditions cells will degrade damaged or unwanted organelles and proteins in a process termed autophagy. These degraded proteins can be processed via the MHC presentation pathways and therefore can be recognised on the cell surface by T cells.

1.11.1 Autophagy

There are three types of autophagy; macro-autophagy, micro-autophagy and chaperone-mediated autophagy. All involve the proteolytic degradation of cytosolic proteins within a double-membraned vesicle called an autophagosome, however literature suggests macro-autophagy is the main pathway that allows the presentation of proteins on MHC. In macro-autophagy (further stated as autophagy), a phagophore is formed from the lipid bilayer of the endoplasmic reticulum (ER) and/or Golgi and endosomes, which then expands to form an autophagosome whilst engulfing target substrates, and finally fuses with the lysosome to begin proteolytic degradation [205]. Micro-autophagy and chaperone-mediated autophagy, which may also contribute to presentation via MHC, use HSP70 chaperones for target protein recognition and binding and later fuse with lysosome for protein degradation.

Initially, the selection of protein substrates for autophagy was thought to be a random process but an order of degradation has been identified, even under stress conditions such as nutrient starvation. The first targets are proteasomes and protein aggregates followed by ribosomes and after prolonged starvation, mitochondria are degraded [206]. The microtubule-associated protein light chain 3 (LC3) and GABARAP are both mammalian homologs of the autophagy related gene (atg) product Atg8 and aid the recruitment of cargo for autophagy. LC3 is located in the cytoplasm and is cleaved by Atg4, a cysteine protease, to generate LC3-I. Once activated in an ATP-dependent manner and further processing to form LC3-II, the molecule is integrated onto the inner and outer surfaces of the autophagosome [205]. Both LC3 and GABARAP are also involved in recruitment of the cargo to autophagosomes. Many studies utilise the upregulation of LC3-II to determine the level of autophagy in cells.

Figure 1.13

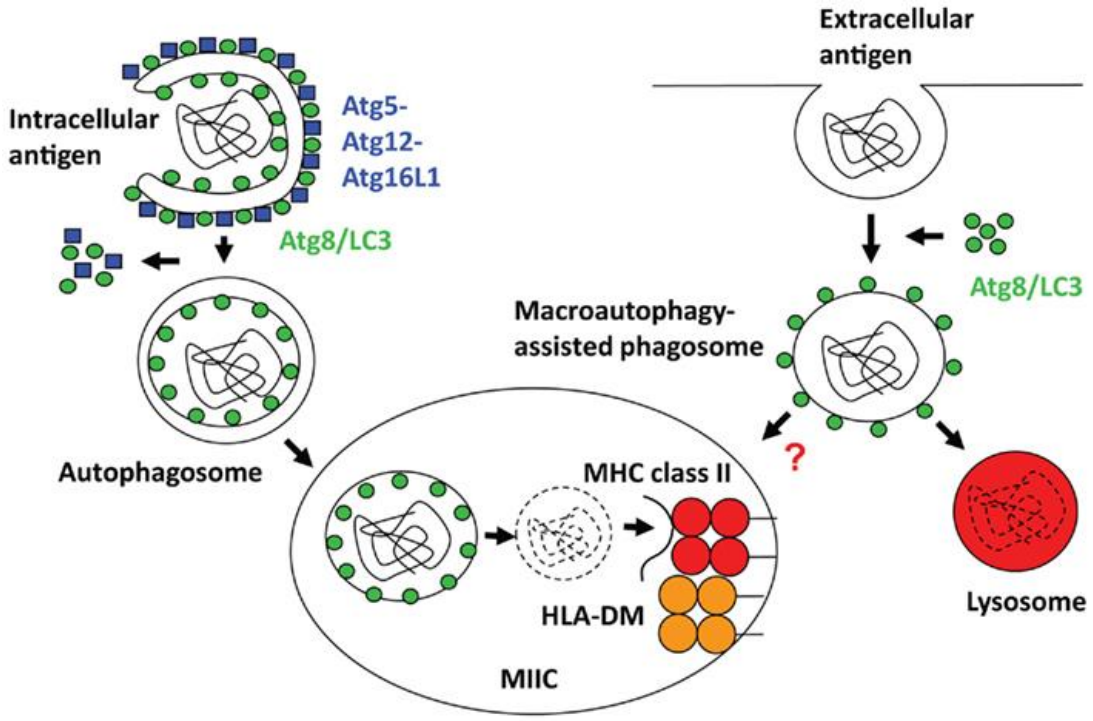


Figure 1.13 Pathways involved in endogenous and exogenous antigen processing for presentation by MHC class II via autophagy. LC3 coated autophagosomes will recruit cargo and fuse with MHC class II containing compartments (MIICs) [207].

The crossover of autophagy and MHC class II presentation occurs when the autophagosome fuses with MIICs for lysosomal proteolysis forming multivesicular bodies (MVBs) that contain MHC class II as well as LC3 (Figure 1.13). Self-peptides processed during autophagy can now be presented via MHC class II. This concept is particularly important during thymic maturation of CD4 T cells [207]. Thymic epithelial cells will utilise this mechanism to present self-peptides for positive and negative selection.

1.11.2 Autophagy and stress

Many stresses act upon tumour cells including nutrient deprivation, hypoxia, uncontrollable proliferation, and in cases of treatment, radiation and chemotherapy. Despite these stress factors, tumour cells are still able to survive, proliferate and metastasise utilising autophagy as their defence mechanism. Autophagy is controlled by the serine/threonine protein kinase termed the mammalian target of rapamycin (mTOR). This protein is composed of two subunits, mTORC1 and mTORC2, and the first is directly involved in autophagy regulation in response to stress. Under normal conditions, mTORC1 associates and phosphorylates the ULK1 complex, inhibiting its activity, suppressing autophagy. During starvation, ULK1 localises to the endoplasmic reticulum (ER) where it phosphorylates Ambra1, allowing it to bind and stabilise the Beclin1/Vps34 complex promoting autophagosome formation [208]. In addition to LC3, the expressions of ULK1, Beclin1 and Ambra1 are often assessed to measure the level of autophagy in cells.

One heavily affected organelle that upregulates a stringent stress response under non-permissive growth conditions is the ER. In addition to autophagosome membrane formation, the ER is involved in a multitude of functions including protein folding and transport through chaperones, lipid biosynthesis and intracellular calcium (Ca2+) homeostasis [209]. During ER stress, homeostasis is disrupted resulting in the aggregation of misfolded proteins and the activation of the unfolded protein response (UPR). The UPR consists of three main signalling pathways initiated by the dissociation of ER membrane proteins, PERK, ATF6 and IRE1α from the ER chaperone protein GRP78/BiP [210]. These ER stress transducers act to lessen protein translation and increase protein degradation through processes such as autophagy [209]. The UPR is thought to regulate the autophagy pathway at various stages. Within the ER stress induced PERK signalling pathway, ATF4 was activated and switched on the downstream gene CHOP that aided cell survival under stress induced autophagy [211]. In addition, ATF4 was upregulated by serum starvation and bound to gene MAP1LC3B that codes for LC3 molecules whilst CHOP activated Atg5 transcription, two important proteins required for autophagosome elongation and maturation [119, 212].

1.11.3 Autophagy and cancer

Autophagy has been found to promote tumorigenesis in many cancers including breast, prostate, pancreatic and melanoma [213-216]. Conflicting evidence suggests that autophagy does not only play a tumour survival role but instead can promote tumour cell death. The idea that autophagy plays a tumour suppressive role stems from the increased levels of class I PI 3-kinase pathway in tumour cells which activates the autophagy inhibitor mTOR [217]. In addition, Beclin-1 (mammalian homolog of Atg6) which initiates autophagosome formation and is required for starvation induced autophagy [214], and Atg5 involved in the extension of the

phagophore membrane, is often found deleted or downregulated in breast, ovarian and prostate tumours [218]. Furthermore, silencing of Beclin-1 resulted in increased tumour volume and size in breast tumour mouse models [214]. The loss of Atg6 (Beclin 1) and Atg5 in autophagy deficient tumour cells results in DNA damage and therefore chromosomal instability. These autophagy-deficient cells are unable to degrade mitochondria and peroxisomes which produce reactive oxygen species that could contribute to further DNA damage [217]. The regulation of chromosomal instability by autophagy is advantageous for tumour cell survival.

1.12 Citrullination as a target for vaccines

The recognition of citrullinated epitopes in autoimmune disease have long been known however Ireland et al (2011) have shown these post-translational modifications can also be presented by APCs in an autophagy dependent manner [204]. Autophagy is constitutive in APCs but is only upregulated in other cells when exposed to cellular stress factors such as nutrient starvation [219]. As tumour cells are subjected to multiple stress factors and yet are viable it was proposed that autophagy promoted survival in these cells and that citrullinated epitopes could be presented on the surface. In addition, these epitopes would be greatly expressed on tumour cells compared to normal cells and therefore are ideal targets for immunotherapy. Earlier experiments showed that immunisation with two vimentin citrullinated peptides (Vimentin28-49cit and Vimentin415-433cit) in B16F1 tumour bearing HLA-DR transgenic mice reduced tumour growth and increased survival by ~60% compared to unimmunised controls. This also correlated with significant T cell responses measured by IFNγ production which were not seen when immunised with the wildtype (non-citrullinated) peptide. These responses were dependent on MHC class II presentation to CD4 T cells and autophagy (Figure 1.14a and b) [1]. A citrullinated epitope from alpha-enolase (Eno241-260cit) was also identified and

promoted ~90% survival after immunisation in transgenic mice bearing B16F1 tumour cells expressing HLA-DR4 under the control of an IFNγ promotor, which was also CD4 dependent [2]. Together, these three citrullinated peptides form the MODI1 vaccine. Later experiments showed these peptides could also be presented by HLA-DP4 inducing >90% survival in mouse models when administered as single peptides or in combination (Figures 1.14c and d). The MODI1 peptides also stimulated proliferation of CD4 T cells in PBMCs isolated from healthy human individuals suggesting a repertoire of T cells that can recognise these citrullinated epitopes (Figure 1.14e) [77]. Lastly, CD4 T cell proliferation responses were similar in ovarian cancer patients compared to healthy individuals and these proliferating cells expressed a cytotoxic phenotype measured by levels of IFNγ, Granzyme B and co-stimulatory molecule CD134 (OX40) [220]. In summary, this data shows citrullinated peptides are presented by tumour cells through autophagy and MHC-II. They are recognised by CD4 T cells in both tumour bearing mice, promoting survival, and in humans, expressing cytotoxic molecules.

Figure 1.14

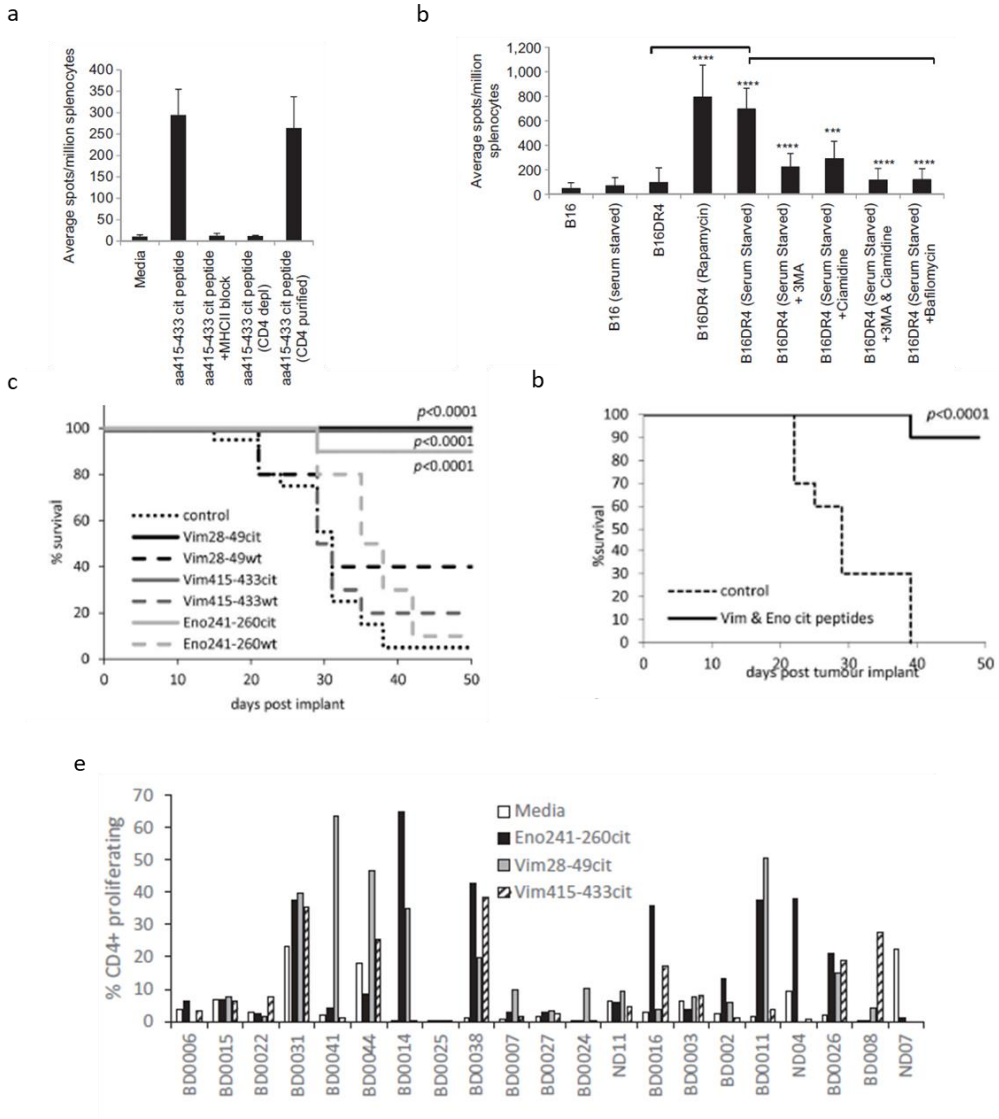


Figure 1.14 Splenocytes from mice bearing B16F1 tumours constitutively expressing HLA-DR4 immunised with citrullinated Vimentin peptides, cultured *ex vivo* with citrullinated or wildtype peptides and checked for specific IFNγ responses with and without MHC class II blocking and CD4 T cell depletion (a). Recognition of nutrient-starved tumour cells by splenocytes (mentioned previously) with and without autophagy inducer (Rapamycin), autophagy inhibitors (3MA and Bafilomycin) and PAD inhibitor (Cl-amidine) (b) [1]. Survival of mice bearing B16F1 tumours expressing HLA-DP4 under an inducible-IFNγ promotor, and immunised with MODI1 as single peptides (c) or combined (d). Proliferation of CD4 T cells in PBMCs isolated from healthy human individuals after culture with MODI1 peptides for 7 days (e) [77].

1.13 Hypothesis and Aims

The hypothesis is that cellular stress can induce citrullination of proteins which are presented by inflammation induced MHC-II on the surface of tumour cells and are therefore good targets for cancer immunotherapy.

Aims:

1. To investigate the environmental conditions/stresses that promote citrullination and autophagy in tumour cells.

This will be addressed through the *in vitro* study of human/mouse tumour cell lines that are subject to various cellular stresses and the *ex vivo* analysis of B16F1 tumours. The involvement of tumour survival signalling pathways will also be assessed in relation to citrullination.

2. To observe the upregulation of MHC-II by inflammation and the subsequent presentation of citrullinated peptides.

The expression and inducibility of MHC-II on tumour cell lines and tumour tissues will be assessed by flow cytometry in human/mouse cell lines treated with or without inflammatory cytokines. Upregulation of MHC class II in tumour under these conditions will be examined. The expression of MHC class II and related proteins in human cancers will be investigated by immunohistochemistry and data analysis of The Cancer Genome Atlas program (TCGA).

3. To assess the CD4 T cell repertoire that recognise siPTMs and identify a citrullinated protein specific TCR.

Blood will be collected under ethical approval from healthy donors. Peripheral blood monocytes (PBMC) will be isolated and labelled with CFSE before incubating with the citrullinated peptides. Proliferating CD4 T cells will be sorted as single cells into 96 well plates and sent for TCR sequencing. The specificity of the TCRs will be confirmed by cloning the TCR genes into an expression vector, transducing Jurkats/T cells and looking for induced activation and/or cytokine secretion in response to peptide pulsed target cells or stressed tumour cells.

2 Materials and Methods

2.1 Cell lines

The murine melanoma cell line B16F1, ovarian cell lines SKOV-3, OVCAR 3, OVCAR 8 and OAW42, and the triple negative breast cancer cell line DU4475 were obtained from ATCC and cultured in complete media; RPMI medium 1640 (GIBCO/BRL) supplemented with 10% FBS. HEK293T cell line was also purchased from ATCC but was cultured in DMEM with 4.5g/L glucose (Sigma D6429) supplemented with 10% FBS and 2mM L-Glutamine. NIH3T3 purchased from ECACC and transfected to express CD40 ligand by Scancell Ltd produced NIH373 CD40L clone 18.2. Cultured in DMEM with 4.5g/L glucose (Sigma D6429) supplemented with 10% FBS and 750µg/mL G418. Jurkat 76 cell line was kindly gifted by Dr Heemskerk, Leiden University Medical Center, and cultured in IMDM (Gibco 12440-053) supplemented with 10% FBS. Triple negative breast cancer cell lines MDA-MB-231, BT549 and MDA-MB-468 were kindly gifted by the Nottingham Breast Cancer Research Group. MDA-MB-231 was grown in complete medium. Cell lines BT549 and MDA-MB-468 were grown in DMEM/F12 (Sigma D6421) supplemented with 10% FBS. The murine B16F1 melanoma cell line was transfected with pVitro 2 chimeric HLA-DR401 or pVitro2 human HLA-DP4 (both under the expression of the constitutive IFNγ promotor) by Scancell Ltd and cultured in complete media plus 300µg/mL Hygromycin B [1, 221]. The B16F1 cell line knocked out for MHC Class II, B16F1 H2Ab1 k/o Cl.A2 was produced by Scancell Ltd and grown in complete media. LCLs were produced from healthy donor CD19+ve PBMCs in house by incubation with B95.8 EBV supernatant and culture in complete media. All cell lines cultured at 37°C/5% CO_2. Cell lines utilized were mycoplasma free and authenticated by STR profiling.

2.2 Antibodies

2.2.1 Cell lines and Tumour staining

2.2.1.1 Flow cytometry experiments

Anti-Citrullinated Vimentin (ECV-1) antibody from Eurogentec (Vim 65-76 KLH rabbit polyclonal, Immunization program GB17002, antigen code Vim65-76 cit KLH rabbit polyclonal-1613489-KLH-MBS) was used in all experiments measuring citrullination. Rabbit IgG monoclonal [EPR25A] (Abcam ab178730) used as isotype control for ECV-1. Anti-Vimentin APC (RnD IC2105A) used in starvation, cell density, murine tumour and Epithelial-to-Mesenchymal (EMT) phenotyping assays. Rabbit mAb Vimentin [EPR3776] Alexa Fluor 568 (Abcam ab202504) used for confocal assays. Donkey F(ab')2 Anti-Rabbit IgG H&L Alexa Fluor 488 preabsorbed (Abcam ab181346) used to detect ECV-1, PAD2, PAD4 and Cytokeratin primary antibodies. F(ab')''-Goat anti-Rabbit IgG PE (ebioscience 12-4739-81) and Donkey Anti-Rabbit IgG H&L Alexa Fluor 647 preadsorbed (Abcam ab150063) also used to detect ECV-1 in some experiments. Anti-Mo/Rat Ki67 clone SolA15 efluor 450 (eBioscience 48-5698-82) used to assess proliferation in cell density experiments. PAD enzymes detected in murine tumour assays with Anti-PAD2 (Abcam ab50257) and Anti-PAD4 (Abcam ab50247) antibodies. Cytokeratin expression was tested in murine tumour assays using Anti-Cytokeratin 8 [EP1628Y] (Abcam ab53280) monoclonal antibody. Immune cells detected in murine tumour assays using Anti-CD45 VioBlue (Miltenyi Biotec 130-102-430). For detection of MHC class II, Anti-HLA DR DP DQ [TM] PE-Vio770 (Miltenyi Biotec 130-104-828) was used. To assess EMT phenotype anti-pan reactive cytokeratin clone C11 Alexa fluor 488 (BioLegend 628608) and anti-ms/hu CD324 e-cadherin clone DECMA-1 Brilliant violet 421 (BioLegend 147319) used.

2.2.1.2 Western Blotting

For detection of citrullinated vimentin, ECV-1 antibody described in section 2.2.1.1 used. LC3 antibodies include Anti-LC3 (D3U4C) XP Rabbit mAb Alexa Fluor 647 (CST 13394) for confocal assays and Anti-LC3 (D3U4C) XP Rabbit mAb (CST 12741S) for western blotting. Class II transactivation (CIITA) detected using mouse Anti-CIITA (Sigma C3367). Secondary antibodies for western blotting techniques include IR Dye 800CW Donkey Anti-Rabbit (Licor 926-32213) and IR Dye 680RD Donkey Anti-Mouse (Licor 926-68072). For detection of YAP and phosphorylated YAP, monoclonal antibodies from Cell Signalling Technologies (CST) used; YAP clone D8H1X (CST 14074) and p-YAP Ser127 clone D9W21 (CST 13008).

2.2.1.3 Confocal

For detection of citrullinated vimentin, ECV-1 antibody described in section 2.2.1.1 used. Donkey F(ab')2 Anti-Rabbit IgG H&L Alexa Fluor 488 preabsorbed (Abcam ab181346) used as secondary antibody for ECV-1. LC3 and YAP antibodies described in section 2.2.1.2 used. Rabbit mAb Vimentin [EPR3776] Alexa Fluor 568 (Abcam ab202504) used for detection of vimentin in confocal assays.

2.2.2 PBMC staining

In cell proliferation assays CD25 depletion from PBMCs was confirmed with anti CD25-PE, clone REA570 (Miltenyi Biotec 130-109-075) and anti-CD4 eFluor 450 clone RPA-T4 (ebiosciences 48-0049-42). Antibodies used to phenotype proliferating populations; CD8 VioGreen, clone REA734 (130-110-684), CD134 PEVio770, clone REA621 (130-109-603), CD45RA VioGreen, clone REA562 (130-108-786), CD197 (CCR7) PE-Vio770, clone REA108 (130-099-166), CD127 APC-Vio770, clone REA614 (130-109-517) all from Miltenyi Biotec and CD4 eF450, clone RPA-T4 (48-

0049-42), IFNγ APCeFluor780, clone 4S.B3 (47-7319-42), Granzyme B PE, clone GB11(12-8899-41) from Thermofisher.

2.2.3 TCR experiments

TCR expression was checked on transduced cells using anti-TCR α/β-PE clone IP26 (eBioscience 12-9986-42) or anti-TCR α/β-APC clone IP26 (Biolegend 306714). To assess expression of specific vβ chains the following antibodies were used; TRBV2 = anti-TCR vβ22-PE clone IMMU 546 (IM2051), TRBV25-1 = anti-TCR vβ11-PE clone C21 (IM2290), TRBV20-1 = anti-TCR vβ2-PE clone MPB2D5 (IM2213), TRBV29-1 = anti-TCR vβ4-PE clone WJF24 (IM3602), and TRBV4-3 = anti-TCR vβ2-PE clone ZOE (IM2287). All from Beckman Coulter. TCRs with fully murinised constant region were checked with mouse TCRβ chain clone H57-597 (Biolegend 109208). Truncated CD34 expression was visualised using CD34 FITC clone QBEND/10 (Abcam ab78165). Rat CD2 expression was checked with anti-rat CD2 clone OX-34 (Biolegend 201305). CD4 FITC clone VIT4 (Miltenyi Biotec 130-113-213) was also used in TCR expression analysis of transduced T cells.

T cell activation was measured in antigen presentation assays using CD3 VioBlue clone REA613 (130-114-519), CD69 APC clone FN50 (130-113-520). CD19 FITC clone REA675 (130-113-645) was used to label LCLs and B cells. All from Miltenyi Biotec. Activation levels of APCs was measured using CD80 APC clone 2D10 (Miltenyi Biotec 130-099-710) and CD86 PE clone IT2.2 (eBioscience 12-0869-41). MHC class II expression was checked using HLA DR VioBlue clone AC122 (Miltenyi Biotec 130-113-968) or anti-HLA DR DP DQ [TM] PE-Vio770 (Miltenyi Biotec 130-104-828). CD40L expression on NIH3T3 cell line was assessed regularly using CD154 PE clone 24-31 (Thermofisher 12-1548-42).

2.2.4 Immunohistochemistry

Tissue microarrays (TMAs) described in section 2.21 were stained as stated in section 2.22. Tissues stained for vimentin clone Vim3B4 (Dako M7020) 1 hour at 1/150 dilution, citrullinated vimentin, ECV-1 (Eurogentec) overnight at 1/100 dilution, PAD2 (Abcam ab16478) 1 hour at 1/150 dilution, PAD4 clone OT14H5 (Abcam ab128086) 45 minutes at 1/1000 dilution, MHC-II with anti- HLA-DP, DQ, DR clone CDR/43 (Dako M0775) 45 minutes at 1/3000 dilution, and Ambra1 (Prestige antibodies HPA038535) overnight at 1/20 dilution.

2.3 Recombinant Proteins

For western blotting controls, vimentin recombinant protein (Vim rp) was purchased from Novus Biologicals and was reconstituted prior to *in vitro* deimination assays in 4mM HCl to give a final concentration of 1mg/mL. Enolase1(alpha) recombinant protein (Eno rp) was purchased from Abcam at 1mg/mL in 10% Glycerol, 20mM Tris HCl, 1mM Magnesium Sulphate, pH 7.5. Cytokeratin 8 was purchased from Abcam and reconstituted in 200µL of sterile water to achieve 100µg/mL. Nucleophosmin (0.02% DTT, 0.32% Tris HCl, 10% Glycerol, 0.88% Sodium chloride), GRP78 BiP (0.02% DTT, 0.32% Tris HCl, 20% Glycerol, 0.88% Sodium chloride) and HSP60 (100% PBS) were all purchased from Abcam in solution. P53 was purchased from RnD Systems in 50 mM HEPES pH 7.5, 450 mM NaCl, 10% Glycerol (v/v), 30 µM $ZnCl_2$ at 0.28mg/ml. Peptidylarginine deiminases (PAD) were purchased from MODIQUEST; PAD2 (MQ16.201-2.5) and PAD4 (MQ16.103-2.5). To induce EMT. TGF-β (Peprotech 100-21-10UG) used.

2.4 Peptides

For mouse immunisation experiments conducted by Pete Symonds and Katherine Cook, mice were dosed with 25µg of each MODI1 peptide with 5µg each of CpG ODN 1826 (Invivogen) and MPLA (Sigma) in a total volume of 100µL PBS. MODI1 peptides include; Vimentin 28-49 tri cit (Vim28cit) cit-SYVTTST-cit-TYSLGSAL-cit-PSTS, Vimentin 415-433cit (Vim415cit) LPNFSSLNL-cit-ETNLDSLPL and Enolase 214-260cit (Eno241cit) VIGMDVAASEFF-cit-SGKYDLD. Shorter length MODI1 peptides; Vimentin 28-42 cit (Vim28citS) cit-SYVTTST-cit-TYSLGS, Vimentin 418-431 cit (Vim418citS) FSSLNL-cit-ETNLDSL and Enolase 241-255 cit (Eno241citS) VIGMDVAASEFF-cit-SG. For immune cell proliferation assays, Vim28Cit, Eno241cit and Vim415cit were reconstituted in DMF(10%)/water(90%) at 1mg/mL. For peptide pulsing in antigen presentation assays MODI1 peptides were reconstituted in 100% PBS at 1mg/mL. Vimentin 116-135 Hcit (Vim116Hcit) NYID-hcit-VRFLEQQN-hcit-ILLAEL used as an irrelevant control where stated. Reconstituted in 100% PBS at 1mg/mL. MAGE A3 peptide aa243-258 KKLLTQHFVQENYLEY, reconstituted in 100% PBS at 1mg/mL and used in antigen presentation assays. All peptides manufactured by Genescript.

2.5 Inhibitors

To block the HIPPO pathway the MST1/2 inhibitor XMU-MP-1 (Sigma SML2233) was used at indicated concentrations. To block TGF-β signalling the TGF-β R1 kinase inhibitor VI SB431542 (Sigma 616464) was used at indicated concentrations.

2.6 Stress induction

To induce stress conditions, target tumour cells were plated at $2x10^6$ cells/well and rested overnight before incubating in RPMI medium without FBS (serum starvation),

Krebs-Ringer Bicarbonate Buffer (Sigma, K4002) solution (amino acid starvation), 50ng/mL (100U/mL) recombinant mouse IFNγ (Thermofisher, PMC4031), 20pg/mL IL-1β (Peprotech 211-11B) for 16hrs or 150nM Thapsigargin (Sigma SML1845) for up to 3hrs at 37°C. For cell density assays, B16F1 cells were plated at 0.5, 1, 2, 3 and $5x10^5$ cells/well and incubated for 24hrs before replenishing media with RPMI + 10% FBS (untreated conditions) or Krebs-Ringer Bicarbonate Buffer (Sigma, K4002) solution (amino acid starvation). Cells were treated overnight prior to staining for citrullinated vimentin, Ki67, annexin V or lysing for LC3 western blots. To check apoptosis levels, after staining for cell surface citrullinated vimentin, cells were resuspended in 50µL annexin V binding buffer (10mM HEPES, 140mM NaCl, 2.5mM CaCl2 pH 7.4) and 2.5µl of Annexin V Alexa fluor 350 (Thermofisher A23202) for 30 minutes at 4°C before diluting with 150µL annexin V binding buffer and running on flow cytometer

2.7 MHC class II expression in tumour cell lines

To test the upregulation of MHC class II on TNBC and Ovarian cell lines, cells were plated at $2x10^6$ cells/well and rested overnight before incubating in corresponding media supplemented with recombinant human IFNγ (Thermofisher, PHC4031). Used at indicated concentrations up to 1000U/mL. Cells cultured for 16 hours before harvesting for flow cytometry staining.

2.8 Flow Cytometry

For intracellular staining, cells were fixed and permeabilised using the eBioscience Fixation and Permeabilization buffer set (88-8824-00) as per manufacturer's instructions. Cells were then stained with primary antibodies for 1 hour at 4°C followed by secondary antibodies for 30 minutes at 4°C. For cell surface staining, cells were

incubated with primary and secondary antibodies as described above without fixation and permeabilization. All samples stored in Fixation buffer (eBioscience) until acquisition on MACS Quant 10 flow cytometer (Miltenyi). Data analysed using MACs Quantify software version 2.13.1. All samples were excluded for dead cells and doublets. Isotype controls or unstained samples were used as negatives to apply gates.

2.9 *In vitro* Deimination (Citrullination)

To citrullinated proteins *in vitro*, recombinant proteins were diluted in a deimination buffer consisting of 0.1M Tris HCl pH 7.5 (Fisher, BP1756), 0.1M DTT (Sigma, 43816) and 50mM EDTA (Invitrogen, 15575-038). Samples were incubated with PAD enzymes for 2 hours at 37°C before storing at -80°C overnight or until use.

2.10 Western Blotting

Cell lysates were prepared in RIPA buffer (Merck Millipore 20-188) containing protease inhibitor cocktail (Roche 05892791001) and benzonase (Merck Millipore 70664). Proteins were reduced by addition of sample reducing agent (Invitrogen B0009) and heated to 100°C for 8 minutes before separation in 4-12% Bolt Bis-Tris Gels (Invitrogen NW04125BOX) followed by transfer onto PVDF membranes. The membrane was blocked with 5% BSA before probing with primary antibodies overnight at 4°C. Eurogentec anti-citrullinated vimentin (ECV-1) was used at 0.5µg/ml. In some conditions ECV-1 was blocked prior to western blotting detection (done by Mohammed Gijon), with the antigen peptide (immunogen Vim65-76cit) or depletion peptide (wildtype Vim65-76) at 5:1 peptide to antibody ratio for 4hrs at room temperature whilst rolling. LC3 antibody diluted 1:1000, CIITA antibody diluted 1:1000, YAP antibody diluted 1:1000 and p-YAP dilution 1:1000. Proteins were visualised using fluorescent secondary antibodies against mouse (β-actin) or rabbit

(target protein) and the Licor detection system. Quantification was performed using Image Studio Software and the intensity of respective bands was normalized against the β-actin loading controls. For detection of citrullinated residues in protein samples, the Anti-Citrulline (Modified) Detection Kit (Merck Millipore 17-347B) was used according to manufacturer's protocol. Briefly, proteins were separated in Bis-Tris gels and transferred on to PDVF membranes as described above, before incubating overnight at 37°C in acid solution.

2.11 Microarray

Microarray sets with the identifier numbers 001731_03 and 001731_04 from PEPperCHIP® coated with Poly(ethylene glycol)-based graft copolymer, thickness of 13.5 nm with three amino acid linkers (ß-alanine, aspartic acid, ß-alanine), and contains 337 cyclic citrullinated peptides from the Immune Epitope Database (including the corresponding arginine variants). This included 579 different 10 aa - 17 aa peptides printed in duplicate (1,158 peptide spots each array copy) including citrullinated (Z) Vimentin 65-76: SSAVZLZSSVPG and control SSAVRLRSSVPG peptides (corresponding to ECV-1). HA tags (YPYDVPDYAG, 22 spots), Polio tags (KEVPALTAVETGAT, 20 spots) and c-Myc tags (EQKLISEEDL, 20 spots) were used as control peptides. Peptide cyclization was done via N- to C-terminal thioether formation.

Manufacturer's protocol was followed. Briefly, the peptide microarray was incubated for 15 minutes in standard buffer (PBS, 0.05% Tween20, pH 7.4) before blocking for 30 minutes with standard buffer + 1% BSA and then incubating with secondary antibody IRDye® 800CW Goat anti-Rabbit IgG (H + L) (Licor 926-32213) at 1:5000 in staining buffer (PBS, 0.05% Tween20, 10% blocking buffer) for 45 minutes at room temperature in the dark to ascertain background signal to be excluded from analysis.

Array chip was submerged into dipping buffer twice and air dried before scanning using the Licor SA scanner. Images were exported as 16-bit grayscale (TIFF) file. After pre-staining with secondary antibody, the incubation tray was re-assembled and equilibrated in staining buffer for 15 minutes before incubating with ECV-1 antibody at 1:1000 in staining buffer overnight at 2 to 8 °C. The following day, the microarray was washed in standard buffer 3 times for 1 minute each and secondary antibody added at 1:5000 for 45 minutes at room temperature in the dark. The microarray was washed 3 times for 1 minute in standard buffer before submersion in dipping buffer and scanning as previously described. After staining with primary antibody, the incubation tray was re-assembled and stained with the anti-HA control antibody (PEPperCHIP®) at 1:2000 diluted in staining buffer for 45 minutes as described above. Note all incubations were done at room temperature on an orbital shaker at 140rpm. Data analysed by Mohammed Gijon (Scancell Ltd) using PepSlide® Analyzer. Medians calculated for duplicate peptide samples and corrected for background. Any samples with a standard deviation >40% were not considered true signal.

2.12 Confocal Microscopy

B16F1 cells were plated complete media on 0.22μm glass coverslips in 6-well plates and rested overnight to adhere. The following morning (or after treatment) cells were fixed in 1% Paraformaldehyde (PFA) for 20 min at room temperature. PFA was gently washed away with PBS twice. Cells permeabilised in 0.1% Triton-X100 for 5 minutes at room temperature and then washed with PBS twice before blocking in 1%BSA/PBS for 20 minutes at room temperature. Primary antibodies were diluted in DAPI solution (Thermofisher) and 100μL dropped on to coverslip to form meniscus. Final concentration of DAPI was used at 2μg/mL and incubated overnight at 4°C in the dark. Slides were washed in PBS three times before secondary antibody incubation

for 30 minutes at 4°C in the dark. For ECV-1 stained samples, ECV-1 was incubated alone followed by addition of the secondary antibody and thorough washing before dual staining with LC3 due to species reactivity of the antibodies. To mount slides, cells were washed in PBS twice, one drop of Fluorsave Reagent (Calbiochem 345789) placed on slide and coverslip placed on top using tweezers. Edges were sealed and slides stored at 4°C until imaging with Nikon Ti-E/A1 inverted confocal microscope and images were captured using NIS-Elements Advanced Research software. Images were taken at 60X magnification and saved as TIFF files.

2.13 Murine Melanoma Tumours

2.13.1 Staining

Tumours were excised from female HHDII/DP4 mice challenged with 1-4x10^5 B16F1 HHDII inducible DP4 between 15-60 days post tumour implant. Where indicated, mice were immunised on either day 15 or day 21 post tumour implant with 25µg of each MODI 1 peptide; Vimentin28-49cit, Vimentin 415-433cit and Enolase241-260cit, plus 5µg CpG and 5µg MPLA. Briefly, tumours were disaggregated with scissors and tweezers in complete medium followed by washing and a live cell count, before incubating with antibodies for flow cytometry staining as described in section 2.2.1 and 2.8.

2.13.2 Preparation of Murine Tumour Lysates and Mass Spectrometry

Tumours excised from female HHDII/DP4 mice challenged with 1-4x10^5 B16F1 HHDII inducible DP4 and stored at -80°C until lysis preparation. For lysis, tumours were dipped into liquid nitrogen for ~5 seconds and then powdered using a pre-chillied (-80°C) Biopulveriser. Powdered tumour was reconstituted in lysis buffer (4M Gua*HCL, 100mM TEAB pH 8.5) and sonicated for 10 seconds 4 times. Cell free

supernatants were sent to Proteome Sciences for liquid chromatography tandem mass spectrometry analysis of citrullinated peptide levels. Samples processed using TMTcalibrator™ strategy and all analysis of peptide quantities done by Proteome Sciences.

2.14 Epithelial-to-Mesenchymal Transition (EMT) experiments

To identify the EMT phenotype of the B16F1 cell line, cells were plated at low, medium and high densities (0.5, 2 and $5x10^5$ cells/well respectively) and cultured at 37°C/5% CO_2 for up to 72 hours. Cells were then harvested for staining for vimentin, cytokeratin and e-cadherin expression as described in section 2.8 with antibodies described in section 2.2.1. To induce EMT, recombinant TGF-β added at stated concentrations for up to 72 hours prior to harvesting for phenotype staining. To block EMT, TGF-β inhibitor described in section 2.5 incubated with cells for 48 hours prior to staining.

2.15 Isolation of Peripheral Blood Mononuclear Cells (PBMCs) and Cell Proliferation Assays

PBMCs were isolated by standard methods (SOP 30) from healthy individuals. Proliferation assays for selection of TCRs performed by Ian Daniels (Scancell Ltd). Briefly, 50mls of peripheral blood was taken into blood collection tubes containing Lithium Heparin as an anticoagulant (102 IU, BD vacutainer, 367885). Whole blood was diluted 1:1 with room temperature complete media; RPMI supplemented with 20mM HEPES (Sigma H0887), 2mM L-glutamine (Sigma G7513), and Pen/Strep (Sigma P433, final concentration: 0.1mg/ml streptomycin and 100 units/ml penicillin). Diluted blood was layered over room temperature Histopaque 1077 (Sigma 10771) and centrifuged for density gradient separation of components. The diluted plasma (top layer) was retained whist the PBMC band was carefully removed and the cells

washed twice in room temperature PBS (Sigma D8537). Cells were counted and accessed for viability with trypan blue.

CD25-ve cells were “negatively” selected using CD25 labelled microbeads (Miltenyi Biotec, 130-092-983) on an LS column (Miltenyi Biotech, 130-042-401) according to the manufacturer’s instructions. CD25 depletion was performed as rapidly as possible with all reagents maintained at 4°C. Cells resuspended in sterile filtered MACS buffer (PBS supplemented with 1% FBS and 2mM EDTA) for depletion process. The total number of viable cells available after CD25 depletion determined.

CD25 depleted PBMCs were immediately washed in CFSE loading buffer (PBS supplemented with 5% FBS) and re-suspended in loading buffer to a final concentration of $1x10^7$cells/mL in 3mL of loading buffer. Cells were transferred to a clean 50mL tube. The tube was carefully angled to >45° and pre-prepared CFSE “master mix” (5mM CFSE in DMSO diluted to 50µM in warm PBS) was added to the un-wetted side of the tube at 110µL per 1ml of cells (final [CFSE] 5µM). The tube was capped tightly and inverted to mix the CFSE and cells rapidly. Cells were left in the dark at room temperature for 5 minutes to permit dye loading. Unincorporated dye was removed by washing twice, once in a 10%v/v excess of CFSE loading buffer and again in completed media supplemented with 10%v/v autologous serum. Washed PBMCs were resuspended at a concentration of $2\text{-}3x10^6$/mL in complete media supplemented with 10% autologous plasma. Loaded cells were protected from light at all times. Peptides were added to 1ml of complete media supplemented with 10% autologous serum to give final concentrations of 10µg/mL of citrullinated peptide (or vehicle). 1mL of PBMCs were added to each well of 24 well plates to give a final concentration of $1x10^6$ PBMCs/mL. After gentle mixing plates were incubated at 37ºC in 5% CO_2 for 10 days before phenotyping proliferating populations with antibodies described in section 2.2.2.

2.16 RNA Sequencing Analysis

CD4+ve populations were sorted into non-proliferating and proliferating populations using the MoFlow cell sorter (Beckman Coulter) by Ian Daniels (Scancell), and sent to iRepertoire Ltd for next generation sequencing of T cell receptor (TCR) expressions. Samples subjected to amplicon-rescued multiplex (ARM) PCR technology. Data was analysed by Rachael Metheringham (Scancell Ltd) for identification of TCR sequences. Bulk sequencing data analysed using iRweb online software (iRepertoire) to determine the frequency of TCR alpha and beta chains. Single cell sequencing dad analysed using iPair Software (iRepertoire) to determine pairing of TCR alpha and beta chains in a sample.

2.17 Lentivirus Construct Design

Lentiviral transfer plasmid encoding MAGE A3 TCR was purchased from Creative Biolabs. The TCR nucleotide sequence is under control of the mammalian Eukaryotic promotor EF1 alpha, followed by the alpha variable region (TRAV), alpha constant region (TRAC), a P2A cleavage site, the beta variable region (TRBV), beta constant region (TRBC), a T2A cleavage site and a puromycin resistance gene (Figure 2.1).

Figure 2.1

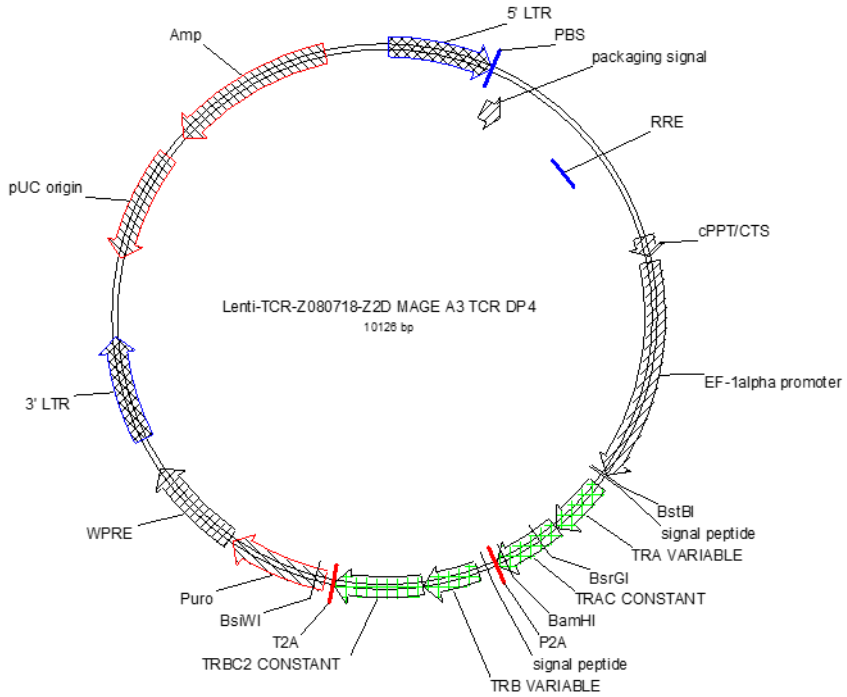


Figure 2.1 Structure of MAGE A3 TCR containing lentiviral plasmid.

In house cloning performed by Rachael Metheringham (Scancell Ltd) to replace MAGE A3 TCR gene with desired TCR sequences. This was done for 1st, 2nd and 3rd generation constructs. The 4th generation constructs were design by Rachael Metheringham (Scancell Ltd) and produced by Genewiz.

2.18 Lentivirus Production

The HEK293T cell line was used as a packaging cell line.

2.18.1 Original method

Cells were seeded at $1.45x10^7$ cells in 1X T175 flask and adhered overnight at 37°C in 5% CO_2. On Day 0, cells were 80% confluent before transfecting with total 60µg DNA at 3:1:1:1 ratios; 30µg Lentiviral plasmid (produced in house) and 10µg of the

three helper plasmids (LentiArt™ Virus packaging kit, 3rd generation) using Lipofectamine 3000 (Invitrogen) in packaging media (OPTI-MEM + 5% FBS + 1mM Sodium Pyruvate). Plasmids and Lipofectamine reagents were pre-incubated for 10 minutes to form complexes before added to cells. Cells were cultured for 6 hours at 37°C in 5% CO_2 and supernatants replenished with fresh packaging media. Supernatants were collected after 48 hours and fresh packaging media applied. Supernatants were collected again at 72 hours. When collected, cell debris was removed by centrifugation. Viral supernatants were stored at 4°C for up to 72 hours before concentrating with Lenti-X concentrator (Takara) according to manufactures protocol. Viral supernatants were resuspended in 1-2mL T cell medium (described in section 2.19) and p24 capsid protein amount measured using Lenti-X GoStix Plus and Lenti-X GoStix Application (Takara) according to manufactures protocol.

2.18.2 Adapted method

Cells were seeded and adhered overnight at 37°C in 5% CO_2. On Day 0 cells were 50% confluent before transfecting with a total of 30µg DNA at 3:1:1:1; 15µg Lentiviral plasmid (produced in house) and 5µg of the three helper plasmids (LentiArt™ Virus packaging kit, 3rd generation) using Turbofect (Thermofisher). Cells were cultured for 48 hours before supernatants were collected and cell debris were removed by centrifugation. Virus particles were concentrated by centrifugation at 10000g for 16 hours at 4°C. Viral pellets were resuspended in 5mL T cell medium (described in section 2.19) and stored at -80°C until use in transductions.

2.19 Lentiviral Transduction

Jurkat transductions: Jurkat 76 cells were resuspended at $1x10^5$ cells/mL. Polybrene was added to 1mL of cells at 8µg/mL. Lentivirus particles were added at multiplicity of infection (MOI) of 10. Cells were centrifuged at 800g for 45 minutes at 32°C to

enhance contact between cells and viral particles. Supernatant was discarded and cells cultured at $1x10^5$ cells/mL at 37ºC/5% CO_2. After 2 days in culture, cells were washed and resuspended in media supplemented with 0.25µg/mL Puromycin. Antibiotics were removed from culture media when cells were used in antigen presentation assays.

Peripheral Blood Mononuclear Cell (PBMC) transductions: PBMCs were isolated from 50-100ml of healthy donor blood on Day -1 using methods described in section 2.15. CD14+ve cells were removed using CD14 microbeads (Miltenyi Biotec 130-050-201) and LS columns (Miltenyi Biotec 130-042-401) according to manufacturer's protocol. Peripheral blood lymphocytes (PBLs) were cultured in T cell medium; RPMI supplemented with 10% autologous plasma, 1% L-Glutamine (Sigma G7513) and 2% HEPES (Sigma H0887). Cells were also cultured with 100U/mL IL-2 (Peprotech 200-02) and CD3/CD28 Dynabeads (Gibco 11131D) added to cells at 75µl per $1x10^6$ cells (equivalent of 3 beads per cell) in 1mL media in 24 well plate, at 37ºC/5% CO_2. On Day 0, lentivirus particles were added to cells at MOI 10 (or as specified) if produced using original transfection method or 1mL of virus produced from adapted method followed by incubation at 37ºC/5% CO_2. Without disturbing cells 1mL of supernatant was removed from wells and fresh T cell media plus 50U/mL IL-2 replenished on Days 3, 5 and 7. Additionally on Day 5, CD3/CD28 dynabeads were removed using a Dynamagnet. TCR expression was checked on Day 7 using antibodies described in section 2.2.3 and method in 2.8. Cells were used in antigen presentation assays on Day 11. Dr Ruhul Choudhury (Scancell Ltd) aided in the T cell transductions of Eno241cit and Vim415cit lentiviral constructs.

2.20 Generation of Monocyte Derived Dendritic Cells

PBMCs were isolated from 50-100mL healthy donor bloods as described in section 2.13. CD14+ve cells were positively selected using CD14 microbeads (Miltenyi Biotec 130-050-201) and LS columns (Miltenyi Biotec 130-042-401) according to manufacturer's protocol. CD14+ve cells were resuspended at $0.5x10^6$ cells/mL in DC medium; RPMI supplemented with 10% autologous plasma, 1% L-Glutamine (Sigma G7513) and 2% HEPES (Sigma H0887), 1000U/mL GM-CSF (Peprotech 300-03) and 400U/mL IL-4 (Immunotools 11340047). Cells were incubated at 37°C/5% CO_2. On Day 3/4 of culture, cells were fed with 50% of total media volume without removing any supernatant. Monocyte derived dendritic cells (DCs) were used for antigen presentation assays on Day 5/6.

2.21 B cell activation and expansion

NIH3T3 CD40L clone 18.2 (referred to as NIH3T3) was used as feeder cell line to activate B cells. Briefly, NIH3T3 cells resuspended at $0.5x10^6$ cells/mL in antibiotic free media, at 2mL per well in a 6 well plate. Mitomycin C (Sigma M4287) was added at final concentration of 10µg/mL for 1 hour at 37°C/5% CO_2. Supernatant was removed and cells washed 6 times with PBS (Sigma D8537) before resuspending at $0.1x10^6$ cells/mL in antibiotic free media, at 2mL per in a 6 well plate followed by incubation at 37°C/5% CO_2 overnight before adding B cells.

PBMCs were isolated from 50-100mL healthy donor bloods as described in section 2.13. CD19+ve cells were positively selected using CD19 microbeads (Miltenyi Biotec 130-050-301) and LS columns and LS columns (Miltenyi Biotec 130-042-401) according to manufacturer's protocol. Cells resuspended at $1.25x10^5$ cells/mL in B cell medium; IMDM supplemented with 10% heat inactivated human AB serum (Sigma H5667), % L-Glutamine (Sigma G7513) and 1% HEPES (Sigma H0887),

5µg/mL Insulin (Thermofisher 12585-014), 50µg/ml Transferrin (Sigma 16052202001), 100U/mL IL-4 (Immunotools 1134048), 50ng/mL IL-2 (Peprotech 200-02), 10ng/mL IL-21 (Peprotech 200-21) and 10ng/mL BAFF (Peprotech 310-13). A total of 4mL of cells were plated on top of Mitomycin C treated NIH3T3 CD40L clone 18.2 in a 6 well plate. B cells cultured with treated NIH3T3 CD40L cells were checked regularly for blasting and expansion by assessing expression of activation markers described in section 2.2.3. B cell medium was renewed and cells split into new wells every 3-4 days at density of $1x10^6$ cells/well. After 14 days of culture cells were frozen for storage in liquid nitrogen.

2.22 Antigen Presentation Assay

2.22.1 CD69 marker expression

Dendritic cells, LCLs, B cells and B16F1 cells were plated at $5x10^4$ cells/100µL in Jurkat 76/T cell medium in U-bottom 96 well plate (conditions plated in triplicate). Cells were rested for 30 minutes before adding 10µg/mL of desired peptides and incubating for a further 2 hours at 37ºC/5% CO_2. Jurkat 76/T cells were plated on top at $5x10^4$ cells/mL and incubated overnight at 37ºC/5% CO_2. The following morning, 100µL of supernatant was collected for ELISA analysis and stored at -20°C until use. Cells from triplicate wells were combined and stained for cell surface expression of CD3, CD4, CD19, CD69 and TCR. For dendritic cells used as APCs, after the addition of peptides and prior to incubated with Jurkats/T cells, DCs were matured with 20µg/mL Poly I:C (Invitrogen tlrl-pic) for 24 hours at 37ºC/5% CO_2.

2.22.2 IFNγ secretion

Prior to assay set up, PVDF ELISpot plates (Millipore MSIPS4610) were coated with capture antibody 1-D1K from IFNγ ELISpot kit (Mabtech 3420-2A) and incubated at

4°C for minimum of 24 hours. Plates were washed 4 times with PBS (Sigma D8537) and blocked in 200µL T cell medium for 1 hour at room temperature. Activated B cells were harvest from culture wells and plated at $2.5x10^4$ cells per well. Peptides were added to a final concentration of 10µg/mL. PHA (Sigma L8754) was added at final concentration of 10µg/mL for positive control. T cells were added to wells at $2.5x10^4$ cells/100µL to have an Effector to Target ratio of 1:1. Plates were incubated overnight at 37°C/5% CO_2 before ELISpot development. Dr Ruhul Choudhury (Scancell Ltd) aided in experiments testing the Eno241cit and Vim415cit TCRs.

2.23 ELISpot

Antibody coating and blocking of ELISpot plates and culture was set up as described in section 2.22. For detection, cells were discarded and plates washed twice (total 8 washes) with automated plated washer using 300µL PBS + 0.05% Tween 20. Anti-human IFNγ Biotinylated detection antibody (mAb 7-B6-1, 1mg/mL) was diluted 1 in 1000 and 50µl added per well. Plates were incubated for 2 hours at room temperature. Plates were washed twice as done previously and Streptavidin Alkaline Phosphatase diluted 1 in 1000 was added at 50µL per well. Plates were incubated for a further 1 hour at room temperature. Plates were washed twice as done previously followed by one wash manually in 200µL PBS. For detection, substrate solution was prepared as follows; for 3 plates 14.4ml water + 600µl development buffer + 150µl Reagent A + 150µl Reagent B (Bio-Rad 170-6432) and 50µl added per well. Plates were developed in dark for ~5 mins. To stop the reaction, the development solution was discarded into the sink and plates were washed thoroughly with tap water. The plastic underdrain from the plates was also removed and rinsed with tap water. Plates were dried overnight at room temperature and wrapped in tissue (to protect from light) until analysed on C.T.L ELISpot analyser.

2.24 ELISA

Maxisorp Nunc-Immuno plate (Thermofisher 439454) coated with 2µg/mL IL-2 capture antibody (MABTECH MT2A91/2C95) overnight at 4°C. The following morning plates were washed twice with 200µL PBS and blocked with 200µL 0.1% BSA in PBS + 0.05% Tween 20, for 1 hour at room temperature. Antigen presentation assay supernatants were diluted 1:1 and 1:2 before adding 100µL to the plate and incubating for 2 hours at room temperature. Cytokine was detected using 0.25µg/mL monoclonal detection antibody (MABTECH MT8G10) followed by Streptavidin HRPO (Life technologies SA1007) according to the manufacturer's instructions. The assay was developed with TMB substrate (BioRad BUF062C) and reaction stopped with 2N H_2SO_4 before absorbance was measured at 450nm. The concentration of cytokine in samples was calculated from human IL-2 standard curve.

2.25 Tissue

All tissue microarrays except ovarian, lung and breast were purchased from AMS Bio.

2.25.1 Head and Neck

The HN802b microarray consists of multiple head and neck tumours alongside some normal tissues, containing 61 cases squamous cell carcinoma, 7 adenoid cystic carcinoma, 1 each of adenocarcinoma and mucoepidermoid carcinoma, plus 10 normal tissues, a single core represents each case. This array was used for staining of Vimentin, Enolase, Citrullinated vimentin, PAD2, PAD4 and MHC-II.

Ambra1 staining was carried out on HN802c, the new version of the array replacing HN802b. This is also a multiple head and neck tumour with normal tissue microarray, containing 61 cases squamous cell carcinoma, 7 adenoid cystic carcinoma, 1 each

of adenocarcinoma and mucoepidermoid carcinoma, 4 larynx tissue, 3 tongue tissue, 1 each of salivary gland tissue, submandibular gland tissue and sublingual gland tissue with a single core per case.

2.25.2 Sarcoma

SO809a, Sarcoma tissue array of soft tissue (adipose, fibrous tissue, smooth muscle and skeletal muscle), including tumour modes and metastasis staging (TNM), clinical stage and pathology grade, 80 cases/80 cores, replaced by SO809b. This contained 20 cases of liposarcoma, 20 fibrosarcoma, 20 leiomyosarcoma, plus 20 rhabdomyosarcoma with a single core per case. This array was used for staining of Vimentin, Enolase, Citrullinated vimentin, PAD2, PAD4 and Ambra1.

The new version of the array, SO809b replacing SO809 was used for staining of MHC-II. Soft tissue sarcoma as control, including TNM, clinical stage and pathology grade, 80 cases/80 cores, containing 20 cases of liposarcoma, 20 fibrosarcoma, 20 leiomyosarcoma, plus 20 rhabdomyosarcoma with a single core per case.

2.25.3 Osteosarcoma

OS804b, Osteosarcoma tissue microarray, containing 40 cases of osteosarcoma with duplicate cores per case, including TNM and clinical stage. This was replaced by OS804c. OS804c is an Osteosarcoma tissue microarray, containing 40 cases of osteosarcoma with duplicate cores per case, including TNM and clinical stage. Also replaced by OS804d. OS804d is an Osteosarcoma tissue microarray, containing 40 cases of osteosarcoma with duplicate cores per case, including TNM and clinical stage. Also replacing OS804c. Vimentin and citrullinated vimentin staining was carried out on OS804b. PAD2, PAD4 and P62 carried out on OS804b. MHC-II staining carried out on OS804c and Ambra1 on OS804d.

2.25.4 Renal

The BC07014a microarray consists of multiple kidney tumours, and a few normal tissues, containing 63 cases of kidney clear cell carcinoma, 6 invasive urothelial carcinomas, plus 3 adjacent normal kidney tissue with single core per case. This array was used for staining for all the markers.

2.25.5 Ovarian

A total of 360 patients were entered into this study and consisted of patients undergoing a laparotomy for primary ovarian cancer between 1984 and 1997 was conducted with approval from the Derby Royal Hospital Ethics Committee and the Nottingham Research Ethics Committee (0205/495). Information on cancer size, stage, presence or absence of residual disease after surgery, histological type and grade, age at diagnosis, and type of adjuvant treatment was collected for all patients.

2.25.6 Lung

The study cohort was comprised of 220 patients subjected to therapeutic resection of histologically identified primary NSCLC (non-small cell lung carcinoma) between the 1st of January 1996 and 31st of July 2006 at the City Hospital, Nottingham, UK and was conducted under the ethical approval of the Biobank (study number ACP000030). All patients treated in the given time period were included in the study, except in the cases where the biological material was unavailable and from 3 patients who received neo-adjuvant therapy.

2.25.7 Breast

Nottingham breast cancer primary series 1998-2006 consist of data from 264 cases of patients presenting with ER-ve, early-stage, primary operable, invasive breast

cancer at Nottingham City Hospital between 1998 and 2006. This work obtained ethics approval by the North West – Greater Manchester Central Research Ethics Committee under the title; Nottingham Health Science Biobank (NHSB), reference number 15/NW/0685. Patients' clinical history and cancer characteristics including tumour type, histological grade, tumour size, lymph node status and Nottingham Prognostic Index were obtained from the Nottingham Breast Pathology Research group (Professor Emad A. Rakha and Professor Ian O Ellis, University of Nottingham, UoN).

2.26 Immunohistochemistry

Immunohistochemistry (IHC) was performed by Mohammed Gijon (Scancell Ltd) for all markers and tissues except vimentin staining on the breast cancer cohort which was stained and scored by Tarek Abdel-Fatah from UoN/NHS. Protein expression was determined by H scoring of arrays, which was double blind and performed by Mohammed Gijon (Scancell Ltd) and a qualified pathologist. Tissue microarrays (TMAs) stated in section 2.25 were stained using the Novolink™ Polymer Detection System (Leica, RE7150K) following the manufacturers protocol. Briefly, tissue sections were heated to 60°C for 10 minutes and dewaxed in xylene before rehydration (Leica Autostainer XL, Leica Biosystems). Antigen retrieval was performed in Citrate buffer pH 6.0 by heating in microwave for 20 minutes. Endogenous peroxidase activity was neutralised with peroxidase block solution and non-specific binding of primary antibodies was attenuated with protein block solution. Tissues were stained with primary antibodies described in section 2.2.4. and were diluted in Novacastra IHC diluent (Leica RE7133). Marker staining was visualised with Novolink™ DAB Polymer (Leica RE7230-K) and tumours counterstained with haematoxylin.

2.27 Statistical Analysis

Comparative analysis of percentage positive events for starvation, cell density and vimentin vs cytokeratin B16F1 tumour staining was performed by applying two-tailed paired t test. Two-tailed paired t test also used to assess significance for YAP and p-YAP expression, phenotyping of murine melanoma tumours and for all TCR experiments that assess activation levels and TCR expression. Welch's t test was performed for analysis of percentage positive events in murine melanoma tumours. One-way ANOVA linear trend analysis was used to identify significance in cell density experiments and multiple comparisons analysis for YAP and p-YAP expression in inhibitor assays. Unpaired t test was performed to analyse significance in ELISA. GraphPad Prism Software was used for statistical analysis of all experiments except TMA and TCGA data. Survival curves and cross tabulations for breast cohort was performed by two BSc students (University of Nottingham). Chi-square log rank test was used to determine significance of survival in TMA cohorts using SPSS v27 and for TCGA data (calculated on UCSC Xena platform). Pearson's correlation was used for TCGA data significance (calculated on UCSC Xena platform). $P < 0.05$ values were considered statistically significant and error bars shown in figures represent median with range.

3 Stress induced Citrullination

3.1 Introduction and Aims

3.1.1 Vimentin

Vimentin is a type III intermediate filament protein (53kDa) expressed by many cells but found at higher levels in mesenchymal cells. As a major cytoskeletal protein, its main role is to maintain cell stability, polarity and structure but is also involved in adhesion and migration in peripheral blood mononuclear cells (PBMCs), fibroblasts and various cancer cells, aiding interactions of endothelial cells with blood vessels [222-224]. Migration of tumour cells involves a process referred to as Epithelial-to-Mesenchymal (EMT) transition and will be discussed in more detail in section 3.1.2.

Elevated vimentin levels were negatively correlated with patient survival in a range of cancers including myeloid leukaemia, colorectal, gastric, non-small cell lung [225-228]. Although vimentin expression was not associated with overall survival and found in <50% of triple negative breast cancer patients (TNBC), it correlated with proliferation marker Ki67 [229]. As discussed in Chapter 1, citrullinated vimentin can be a target for immune recognition, but is also a target for O-glycosylation and methylation facilitating its role in cell migration [230, 231]. Vimentin methylation was associated with poor prognosis in breast cancer patients [231]. Together, these findings highlight vimentin as an important therapeutic target for cancer immunotherapy.

3.1.2 Epithelial - to - Mesenchymal Transition (EMT)

Epithelial to mesenchymal transition (EMT) is a reversible process where epithelial cells remodel their cytoskeleton and disrupt cell-cell adhesion converting into a more

aggressive, metastatic mesenchymal phenotype [224]. Epithelial cells can be characterised by their expression of cytokeratin, E-cadherin and occludin, whereas mesenchymal cells express higher levels of vimentin, N-cadherin, fibronectin and integrin αvβ6. Genes known to regulate EMT include Snail, Zeb and TWIST, which are used in combination with phenotypic protein expression to determine the EMT status of tumour cells in a range of cancers [232]. Most often cells will display a mixed epithelial/mesenchymal phenotype (partial EMT) which allows them to retain their adhesion and enhance their migration properties, forming clusters of circulating tumour cells (CTCs). These CTCs invade and colonize other organs by re-epithelialization of the cells through mesenchymal-to-epithelial transition (MET), forming secondary tumours [233]. Transforming to an intermediate EMT phenotype is also important in wound healing, where cells along the wound edge undergo partial EMT to extend and migrate whilst maintaining cell-to-cell contact, to close the gap [234]. In addition, lack of cell-to-cell contact results in a more mesenchymal phenotype in the presence of TGF-β. MCF7 (breast cancer) cells have an epithelial phenotype whereas SW480 (colorectal cancer) cells display partial EMT, however TGF-β induced higher vimentin, but not E-Cadherin, levels in both cell lines when at 30% confluency compared to when at 100% confluency [235]. TGF-β mediates EMT through many pathways including Smad, ErK/MAPK and Pi3K/Akt most of which result in downregulation of E-Cadherin and upregulation of N-Cadherin and vimentin contributing to cytoskeletal re-organisation and migration [233]. Targeting this mechanism is of high interest, especially as it is thought to be involved in aiding immune evasion and resistance to immunotherapies. For example, expression of checkpoint ligand PD-L1 was significantly correlated with vimentin expression, and negatively correlated with tumour-infiltrating lymphocytes (TILs) in pancreatic cancer suggesting another method by which mesenchymal cells avoid immune regulation [236].

3.1.3 Aims

Our previous studies have shown that citrullinated vimentin is a good target for cytotoxic CD4 T cells. This implies that vimentin is citrullinated within viable cells and then processed and presented on MHC-II for recognition by CD4 T cells. As citrullination is mediated by PAD enzymes which are only activated by high levels of calcium, it is unclear how and where this can occur. In this chapter we sought to understand the cellular stresses that induced citrullination within viable cells.

3.2 Results

3.2.1 Characterisation of anti-citrullinated vimentin anti-serum

To study the stimulation of citrullination under varying conditions of cellular stress, an antiserum was raised against citrullinated vimentin peptide 65-76 (ECV-1). This sequence is a known B cell epitope in Rheumatoid Arthritis patients [237, 238]. Any antibodies recognising the non-citrullinated arginine containing peptide were removed by affinity purification and then citrullinated specific antibodies were affinity purified against the citrullinated peptide. To determine the specificity of this antiserum, recombinant vimentin protein was citrullinated with both PAD2 and PAD4 enzymes *in vitro* and analysed for ECV-1 binding via western blotting. In some cases, ECV-1 was incubated prior to use with the antigen peptide (immunogen sequence Vim 65-76cit) or depletion peptide (wildtype sequence Vim65-76). There was a strong signal for citrullinated vimentin and a weak detection of vimentin wildtype protein in samples treated with both PAD2 and PAD4 (Figure 3.1). Blocking with the antigen peptide, but not the depletion peptide, resulted in a substantial decrease in signal in both PAD treated samples, indicating ECV-1 has a greater specificity for citrullinated vimentin. In addition, ECV-1 did not show any cross reactivity with several other PAD2 and PAD4 treated proteins (Figure 3.2a). Citrullination of these proteins was confirmed using the anti-modified citrulline detection kit which identifies any citrulline in the sample irrespective of the protein. All proteins were successfully deiminated with either PAD2 or PAD4 except p53 (Figure 3.2b). The intermediate filament proteins, vimentin and cytokeratin showed the strongest citrullination. High molecular weight bands between 70-100kDa represent auto-citrullinated PAD2 as determined using an anti-PAD antibody (Appendix 1). There was no citrulline detected in the untreated recombinant proteins. A strong signal was detected for PAD2 treated recombinant vimentin, and PAD2 and PAD4 treated cytokeratin protein but not nucleophosmin,

GRP78 BiP, HSP60, or (Figure 3.2b). The majority of non-deiminated recombinant protein controls were also negative with the ECV-1 antibody. However, there was a faint detection for wild type vimentin and enolase. The signal in these two lanes was considerably lower than found with citrullinated vimentin. The specificity of ECV-1 for citrullinated vimentin was later confirmed via microarray analysis of binding to over 500 citrullinated and non-citrullinated peptides (Peptide list Appendix 2; Figure 3.3). Data analysed by Mohammed Gijon (Scancell Ltd) using PepSlide® Analyzer. The immunogen peptide Vim65-76cit, showed the strongest binding signal closely followed by 4 vimentin peptides that shared all or part of the immunogen peptide sequence (Figure 3.3b). Weak positive signals were identified for two additional peptides corresponding to Human BiP and Human Fibrinogen alpha chain.

Figure 3.1

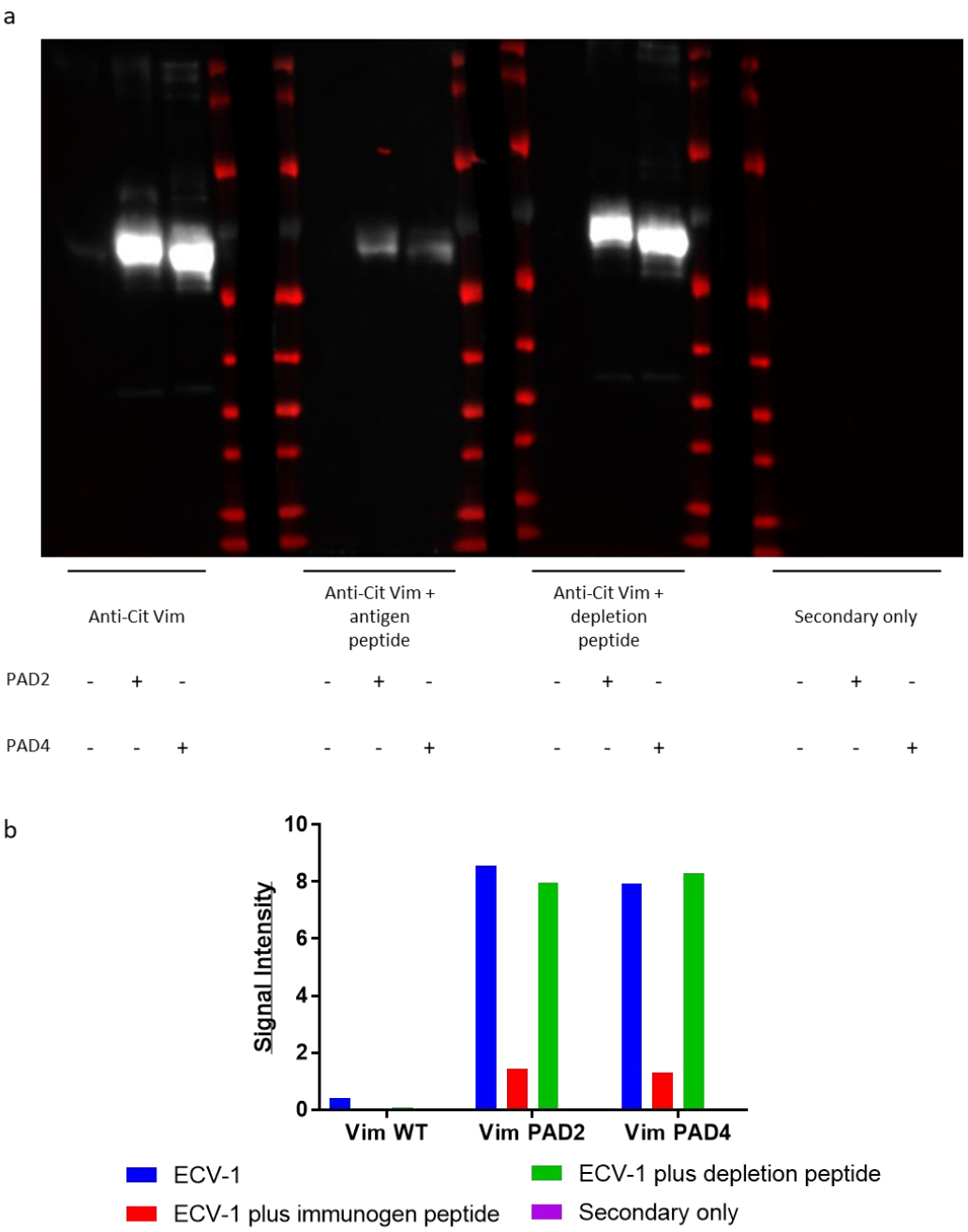


Figure 3.1 Western blot analysis showing binding of ECV-1 to vimentin recombinant protein or vimentin *in vitro* deiminated with PAD2/PAD4, with or without blocking with the antigen peptide (immunogen sequence) or the depletion peptide (wildtype sequence) (a). Quantified vimentin signal (b).

Figure 3.2

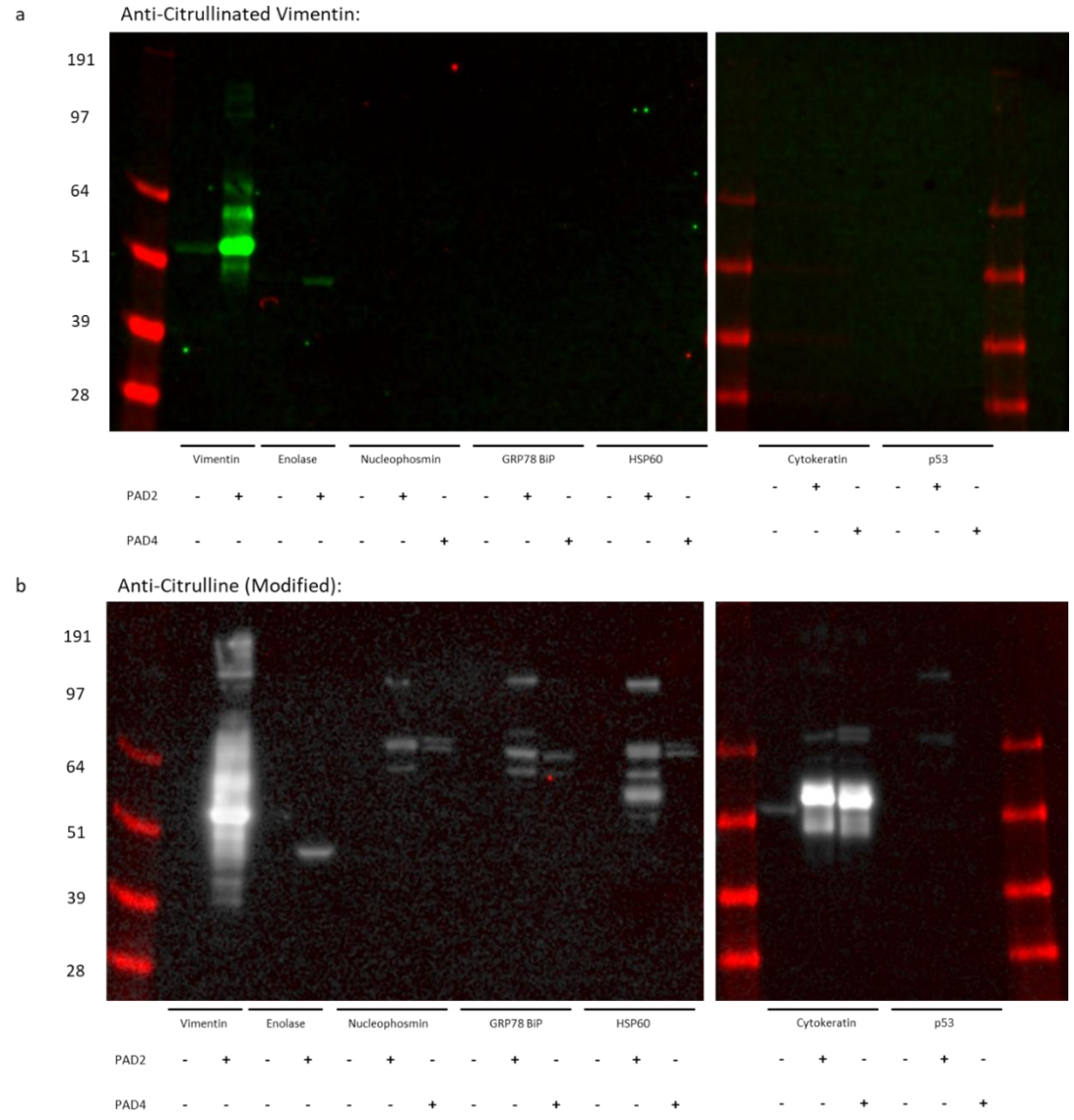
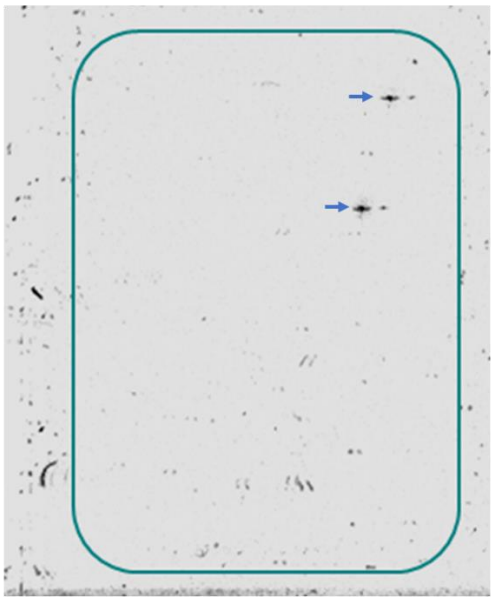


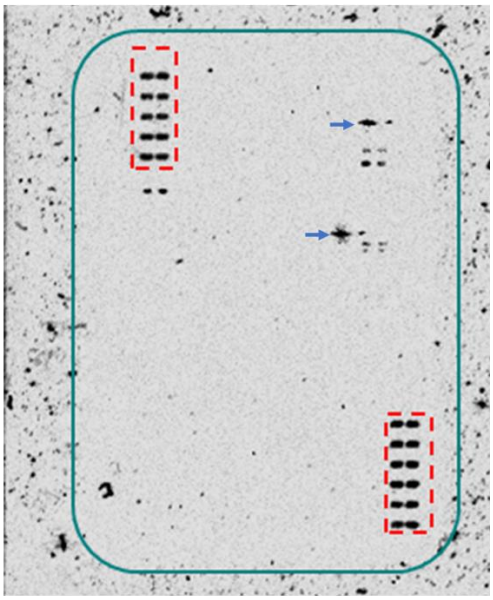
Figure 3.2. Western blot analysis showing the binding of the 0.5µg/ml ECV-1 antibody (a) or total citrullination using the modified citrulline detection kit (b) against recombinant proteins Vimentin, Enolase, Nucleophosmin, GRP78 BiP, HSP60, Cytokeratin and p53 before and after *in vitro* citrullination with PAD2 and PAD4 enzymes.

Figure 3.3

a(i)



a(ii)



b

PEPTIDE SEQUENCE	ANTIGEN	AVERAGE CORRECTED
SSAVZLZSSVPG	Human Vimentin	30.5
GVYATZSSAVZLZSSV	Human Vimentin	14
TZSSAVZLZSSVPGVR	Human Vimentin	8
SAVZLZSSVPGVR	Human Vimentin	6
GVYATZSSAVZLZSSV	Human Vimentin	4
KDVRKDNZAVQKLRREV	Human BIP	2
SZALAZEVDLKDYEDQQ	Human Fibrinogen alpha chain	2

Figure 3.3 Microarray analysis of ECV-1 specificity. Secondary antibody only control (a(i)) showed some non-specific signal (blue arrows) which was excluded from the analysis. Signals outlined with red dashed border correspond to anti-HA control (a(ii)). Binding signal for all positive peptide sequences and the corresponding protein antigen. Amino acid residues highlighted in red are shared with the immunogen peptide for ECV-1; Vim65-76cit (b). Note: Peptide sequence with a standard deviation >40% were excluded from analysis.

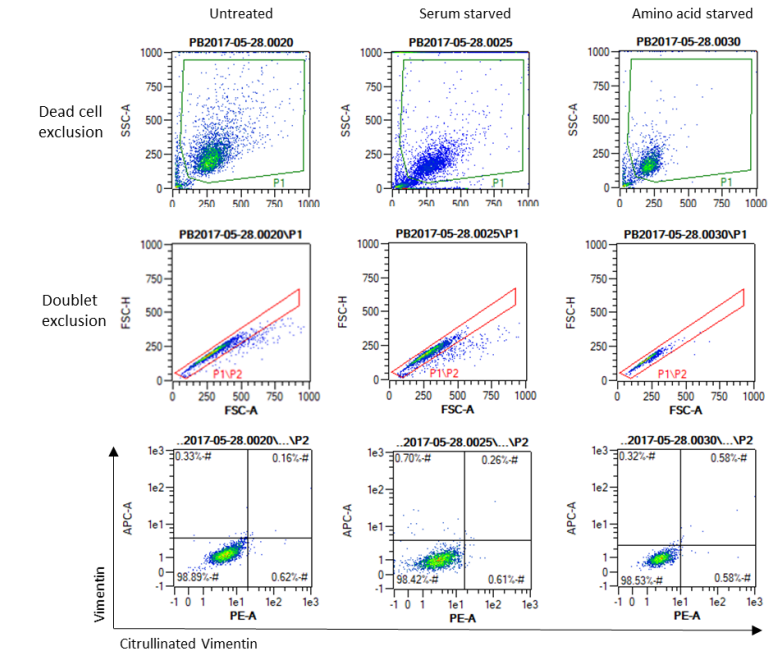
3.2.2 Upregulation of Citrullination by Starvation

As discussed in Chapter 1, nutrient starvation is known to regulate autophagy in cells and CD4 T cell responses to citrullinated peptides were blocked in the presence of an autophagy inhibitor. Due to the low cross-reactivity of ECV-1 with other citrullinated proteins, this antibody was used to detect citrullinated vimentin in other assays. To assess if starvation induced citrullination, B16F1 mouse melanoma cells were subject to overnight incubation with RPMI medium only (serum deficient, SS) or Krebs-Ringer buffer solution (serum and amino acid deficient, AS). Figure 3.4 gives an example of the levels of protein expression and the gating used for flow cytometry analysis of samples stained for vimentin and citrullinated vimentin. All samples were excluded for dead cells and doublets prior to analysis and all gates were applied according to the ECV-1 isotype control (Figure 3.4a). Isotype control samples were stained with rabbit IgG monoclonal and secondary antibody only, no isotype equivalent was used for vimentin. Therefore, vimentin expression was based on an unstained control for the APC channel. Quadrant gating allows the detection of cells in the upper right quadrant as double positive for both vimentin and citrullinated vimentin (stated as double positive citrullinated vimentin from now on). These cells were considered true positives for citrullinated vimentin. Events located in the upper left and lower right quadrants represent vimentin only or ECV-1 positive cells only respectively. The percentage of double positive citrullinated vimentin events were elevated in both AS and SS conditions compared to the untreated control, increasing from 5% to 31% and 23% respectively in the representative data shown (Figure 3.4b). However, expression levels were low suggesting citrullination may not occur within the cytoplasm. There was also a slight increase in ECV-1 single positive events (lower right quadrant) after serum and amino acid starvation compared to untreated controls; increased from 0.2% to 2.6% and 8.7% respectively (Figure 3.4b and c). This may

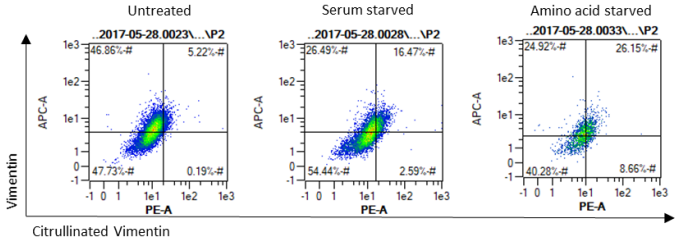
indicate the low levels of cross reactivity of the ECV-1 antibody with other citrullinated proteins.

Figure 3.4

a



b



c

Percentage Positive Events (%)		Untreated	Serum Starvation	Amino acid Starvation
Isotype control	Vimentin only	0.33	0.70	0.32
	Citrullinated vimentin only	0.62	0.61	0.58
	Double positive	0.16	0.26	0.58
Dual stained sample	Vimentin only	46.86	26.49	24.92
	Citrullinated vimentin only	0.19	2.59	8.66
	Double positive	5.22	16.47	26.15

Figure 3.4 Intracellular citrullinated vimentin expression in B16F1 after serum (SS) or serum and amino acid starvation (AS). All gates applied according to the isotype control after dead cell and doublet exclusion (a). Example of a dual stained sample (b) showing the percentage of vimentin (APC) only positive events (upper left quadrant) and double positive citrullinated vimentin (PE) events (upper right quadrant). Percentage positive events of each quadrant shown (c).

Multiple repeats of this experiment were performed and the majority showed an increase in percentage of citrullinated vimentin in B16F1 cells after overnight AS treatment which was statistically significant (P=0.0398 Figure 3.5a). However, no significant increases were observed in median fluorescence intensity (MFI) for these samples (P=0.5223 Figure 3.5b). Although higher percentages of citrullinated vimentin were found with SS treatment this was not significant (P=0.2165 Figure 3.5c). Again, no significant change in MFI was observed with SS (P=0.9003 Figure 3.5d).

Figure 3.5

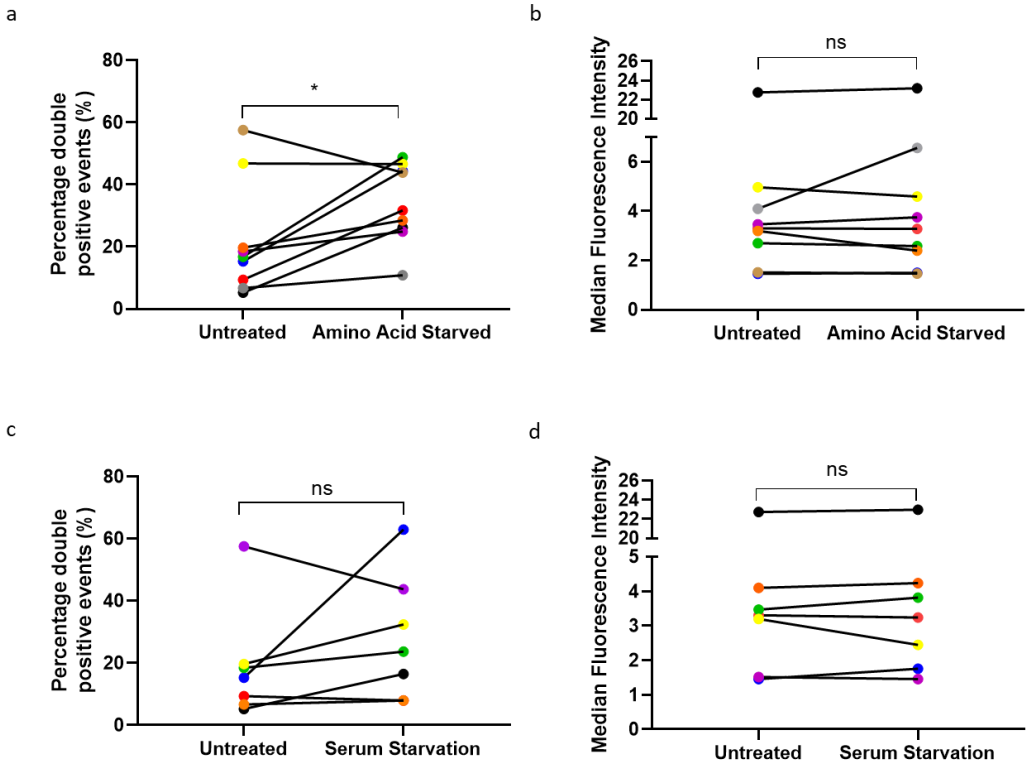
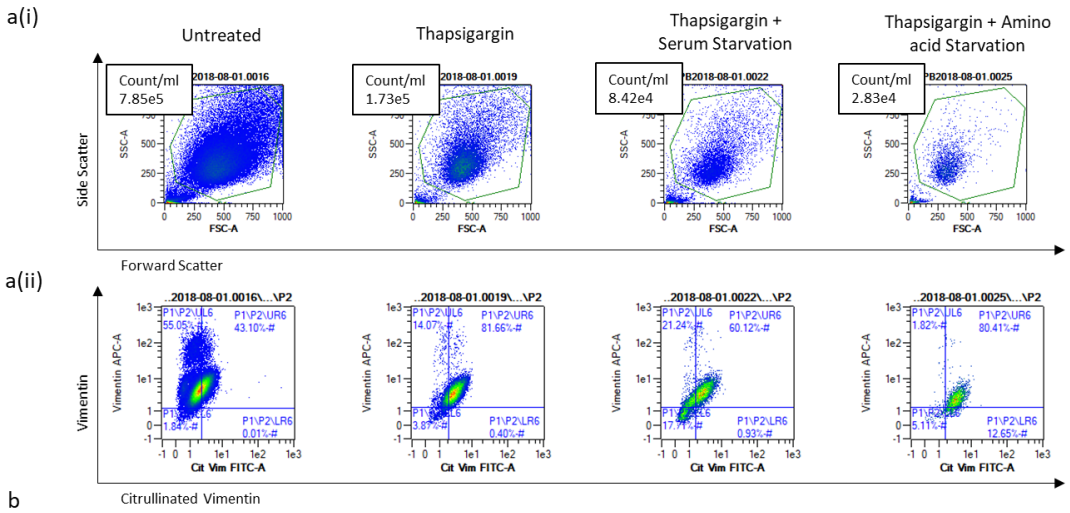


Figure 3.5 B16F1 cells either untreated or treated overnight with amino acid starvation or serum starvation. Collated percentage double positive citrullinated vimentin events (a and c) and median fluorescence intensities (MFI) (b and d) compared between untreated controls and amino acid starved samples (a and b) or serum starved samples (c and d). Data represents at least 7 independent experiments; AS N=9 and SS N=7. Paired t test analysis ns = P ≥ 0.05,* = P < 0.05.

3.2.3 Prolonged Stress results in Cellular Apoptosis

High calcium levels are required for activation of PAD enzymes. The sarco/endoplasmic reticulum Ca2+-ATPase inhibitor Thapsigargin (TG) has been shown to increase intracellular calcium levels and induce accumulation of autophagosomes [239, 240], so it was utilised to observed increases in citrullinated vimentin levels. It was hypothesised that dual stimulation with TG and nutrient starvation would further induce expression of citrullinated vimentin. B16F1 cells were incubated with 150nM TG for 3 hours prior to overnight incubation in either complete media (untreated) or RPMI only (serum starvation) or Krebs-Ringer buffer solution (amino acid starvation). TG concentration based on a preliminary titration experiment (data not shown) and what is described in literature [240]. Cells were harvested and stained for vimentin and citrullinated vimentin using ECV-1. Untreated cultures were 43% positive for citrullinated vimentin and were greatly increased (80%) with TG incubation (Figure 3.6a(ii)). Interestingly, dual stimulation with serum starvation resulted in less citrullinated vimentin (60%) than TG alone and amino acid starvation did not further elevate levels. This experiment was only performed once due to toxicity observed.

Figure 3.6



b

Percentage Positive Events (%)	Untreated	Thapsigargin	Thapsigargin + Serum Starvation	Thapsigargin + Amino acid Starvation
Vimentin only	55.05	14.07	21.24	1.82
Citrullinated vimentin only	0.01	0.40	0.93	12.65
Double positive	43.10	81.66	60.12	80.41

Figure 3.6 Intracellular citrullinated vimentin expression in B16F1 after 3hr Thapsigargin with or without overnight serum/amino acid starvation. Forward scatter vs side scatter and cell count per ml for each sample (a(i)). Quadrant gating (a(ii)) and corresponding percentage positive events (b) shown. N=1.

Due to the high increase in intracellular citrullinated vimentin levels, and reduction in cell number indicating toxicity (Figure 3.6a(i)), with TG and amino acid starvation treatment, cultures were assessed for apoptosis as it is a known trigger of citrullination in non-viable cells. Roughly, 10% of cells were positive for annexin V with TG treatment alone compared to 6% in untreated conditions. Therefore, the elevated intracellular citrullinated vimentin levels (Figure 3.6a) with TG treatment were not just due to apoptosis. However, amino acid starvation alone elevated annexin V expression to 39% compared to untreated conditions. This was further enhanced by the combination of TG and AS up to 49% (Figure 3.7a) suggesting increased citrullinated vimentin levels could be due to starvation induced apoptosis resulting in membrane disruption rather than upregulated autophagy in viable cells. Combination

TG and AS treatment slightly increases apoptosis compared to AS alone as it is an additional stress factor but is not the main cause of toxicity. To support this, the percentage of cell surface citrullinated vimentin and annexin V double positive events increased from 3% in untreated samples to 5%, 11% and 12% with TG, AS and combined TG + AS treatment (Figure 3.7a). Reducing the dose of TG resulted in slightly less toxicity but there was no difference in citrullinated vimentin expression compared to untreated controls (data not shown). Reducing the time of exposure of 150nM TG to 1hr only reduced toxicity to levels seen with amino acid starvation only; 49% annexin V expression with 3 hours dual treatment down to 38% with 1 hour dual treatment (Figure 3.7b). Again, increases in double positive cell surface citrullinated vimentin and annexin V events were observed at 1 hour (14%) and 3 hour (12%) timepoints compared to untreated cells (3%) (Figure 3.7b). This data highlights amino acid starvation as the main cause of apoptosis, not TG treatment.

Figure 3.7

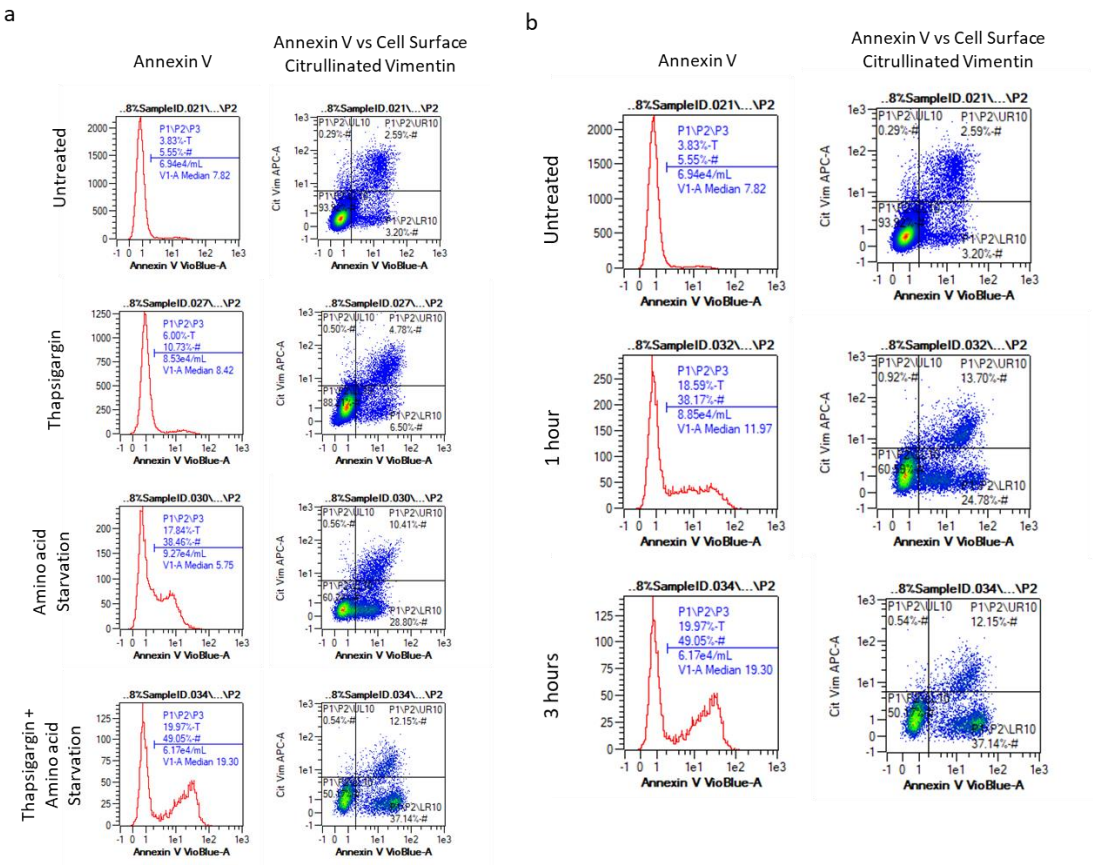


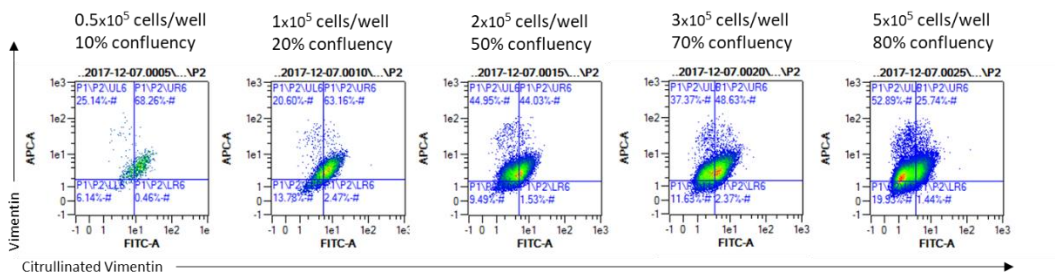
Figure 3.7 Cell surface staining of Annexin V and citrullinated vimentin in B16F1 after treatment with 150nM Thapsigargin and amino acid starvation. Cells were either untreated, amino acid starved overnight, treated with Thapsigargin or a combination of Thapsigargin and amino acid starvation applied. Thapsigargin added for final 3 hours of incubation before staining. N=1 (a). Cells were either untreated or treated with a combination of overnight amino acid starvation and Thapsigargin for 1 or 3 hours. N=1 (b).

3.2.4 Increased Citrullination, Autophagy and Proliferation in Low Density Cells

To assess whether cell-to-cell contact was important for citrullination in viable cells, B16F1 cells were plated at various densities; 0.5, 1, 2, 3 or $5x10^5$ cells/well. Cells were cultured overnight under normal growth conditions before staining for intracellular vimentin (APC) and citrullinated vimentin (FITC) expression using ECV-1. At time of harvest cultures at 0.5, 1, 2, 3 or $5x10^5$ cells/well had reached 10%, 20%, 50%, 70% and 90% confluency respectively, when visualised by brightfield microscopy (Figure 3.8e). All cell densities were >70% positive for vimentin with a slight decrease with increasing densities (Figure 3.8). An increase in citrullinated vimentin expression was observed with decreasing cell density with percentage positive events increasing from 27% at $5x10^5$ cells/well to 68% at $0.5x10^5$ cells/well (Figure 3.8a and b). Cell density experiments were repeated 3 times and the increase in double positive citrullinated vimentin events with decreasing cell density was statistically significant (Figure 3.8c $P \leq 0.0001$). From a total of 11 experiments, the percentage of double positive citrullinated vimentin was significantly greater in low density ($0.5x10^5$ cells/well) conditions compared to high density ($5x10^5$ cells/well) (Figure 3.8d $P \leq 0.0001$), suggesting that cell contact or arrest of cell growth inhibits citrullination.

Figure 3.8

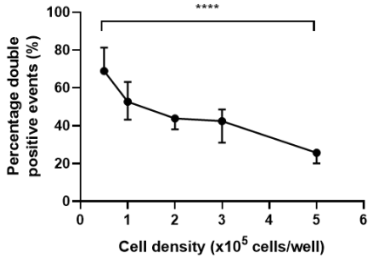
a



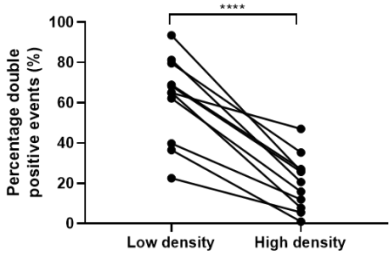
b

Percentage positive events (%)	Cell density (x10^5 cells/well)				
	0.5	1	2	3	5
Vimentin only	25.14	20.60	44.95	37.37	52.89
Citrullinated vimentin only	0.46	2.47	1.53	2.37	1.44
Double positive	68.26	63.16	44.03	48.63	25.74

c



d



e

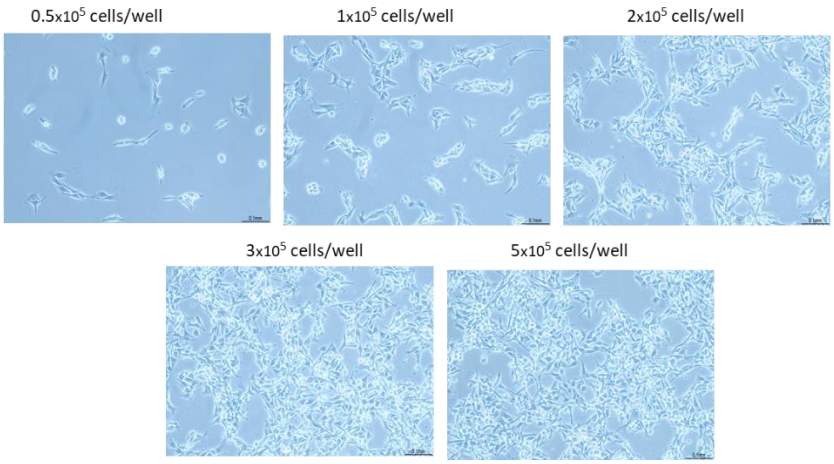


Figure 3.8. Intracellular citrullinated vimentin expression in B16F1 plated at cell densities 0.5, 1, 2, 3 and 5x10^5 cells/well. Quadrant gating (a) with corresponding percentage positive events (b) showing levels of vimentin and citrullinated vimentin. Data representative of 3 experiments. Collated percentages of double positive citrullinated vimentin events at all cell densities (c). Error bars represent median with range N=3. One-way ANOVA linear trend analysis **** = P ≤ 0.0001. Collated double positive citrullinated vimentin events in low (0.5x10^5 cells/well) vs high (5x10^5 cells/well) cell density cultures. N=11. Paired t test analysis **** = P ≤ 0.0001 (d). Images of each cell density (10X magnification) (e).

High levels of calcium can occur in viable cells within double membrane organelles. This can occur within the nuclei and citrullination is a common post-translational modification controlling transcription. Ireland et al (2011) have also shown that citrullination can occur in B cells and that this is elevated if the BCR is activated [204]. Our hypothesis was that this could be the mechanism of citrullination within cancer cells. To determine if there is an association between cell density and autophagy, the microtubule-associated protein light chain 3 (LC3) was used to detect levels of autophagy in B16F1. LC3-I (cytoplasmic) and LC3-II (phagosome associated) can be distinguished in western blotting techniques by two distinct bands at 14kDa and 16kDa, respectively. Low cell density samples 1 and 2 showed weak signals for both LC3-I and LC3-II (Figure 3.9b). Normalisation against β-actin shows the level of LC3-I increased as density increased to density 3 and then remained constant at high density from 3 to 6. In contrast, LC3-II normalised against β-actin, showed that the signal decreased with increasing cell density 3 to cell density 6 (Figure 3.9c). This suggests a decrease in autophagy with increasing density. Expression of citrullinated vimentin protein within these lysates was assessed in parallel, however no signal was detected in the cell density lysates despite a strong band with the positive control, *in vitro* deiminated vimentin (Figure 3.9a). This is consistent with the low expression of citrullinated vimentin as measured by indirect immunofluorescence. Also if vimentin is citrullinated prior to degradation, or citrullinated and degraded within autophagosomes this would make it difficult to detect as a whole protein.

Figure 3.9

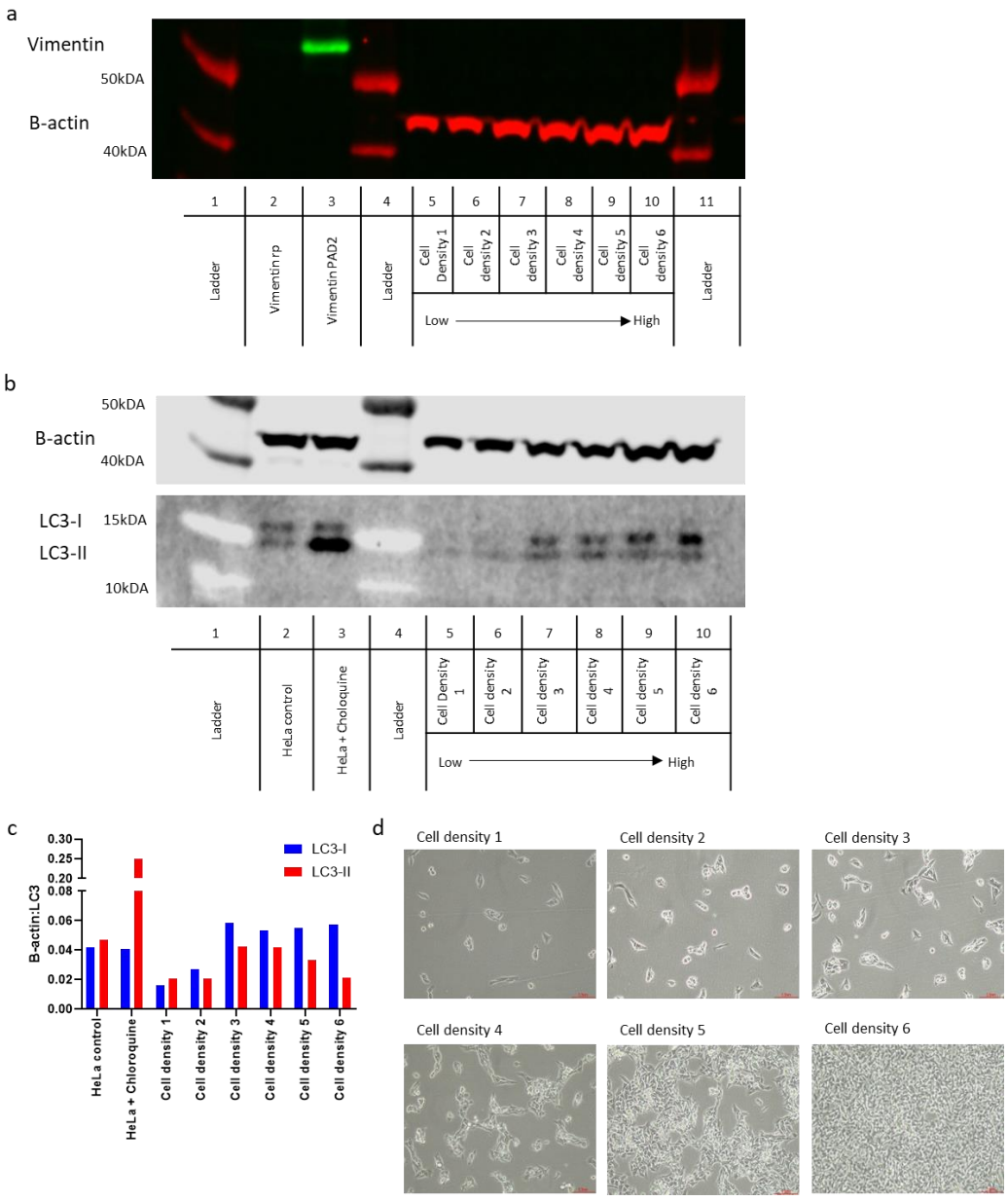


Figure 3.9 B16F1 cultured at various cell densities were tested for citrullinated vimentin (a) and LC3 (b) expression. ECV-1 used at 0.5µg/mL and LC3 antibody used at 1:100 according to manufactures instructions. 0.5µg of Vimentin recombinant protein and PAD2 invitro deiminated vimentin used as negative and positive control for citrullinated vimentin blot. HeLa control and HeLa + Chloroquine (CST #11972) used as negative and positive controls respectively for LC3 blot. Cell density 1 corresponds to the lowest density plating ($0.54x10^5$ cells/T25), doubling in cell number to cell density 6 ($21.60x10^5$ cells/T25). LC3 signal was normalised against β-actin loading controls (c). Bright-field images taken of each cell density (d). N=1.

Confocal analysis of LC3 staining in low and high cell density conditions supported these findings. More LC3 puncta, corresponding to LC3-II bound phagosomes, were observed in low density conditions compared to high density conditions (Figure 3.10a). Initial staining with ECV-1 showed a similar punctate staining pattern (Figure 3.10b), suggesting that vimentin was citrullinated and degraded within autophagosomes. However, not all repeated experiments showed clear punctate staining, suggesting not all variables were being controlled. B16F1 at low and high density were dual stained for LC3 and ECV-1 to assess whether they co-localise. Stronger, dispersed cytoplasmic staining for both LC3 and ECV-1 were observed with some areas with rounded punctate staining, highlighted by white arrows (Figure 3.11a). The staining intensity for both LC3 and ECV-1 was greater in low density cultures compared to high density cultures despite the reduced size of puncta (Figure 3.11a). However no co-localisation of LC3 and citrullinated vimentin was seen (Figure 3.11b), perhaps reflecting that the antiserum did not recognise the degraded citrullinated vimentin

Figure 3.10

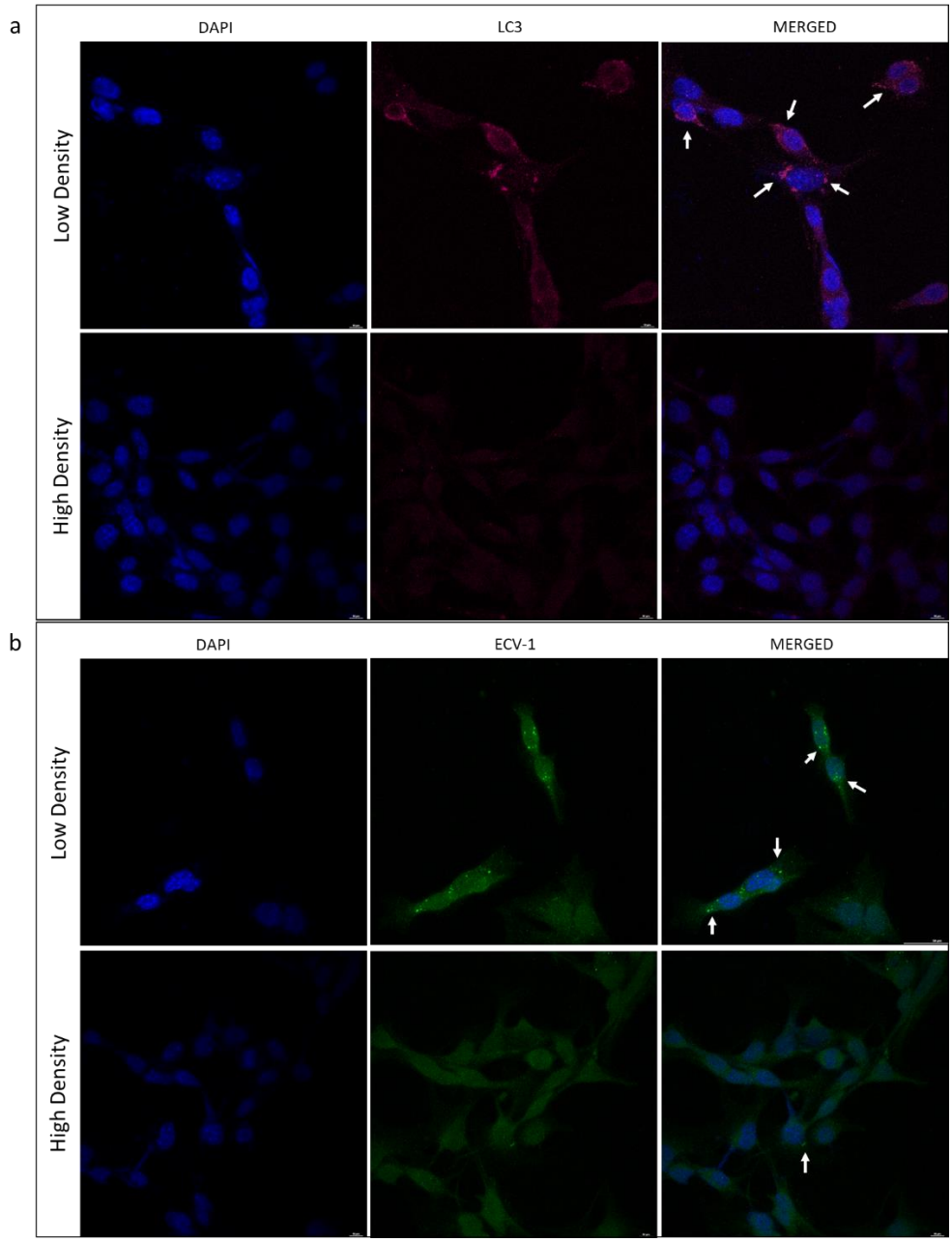


Figure 3.10 Confocal microscopy images (60X lens) of low, $0.5x10^5$ cells/well and high, $5x10^5$ cells/well density plated cells single stained for either LC3 at 1:50 dilution (a) or ECV-1 at 1:500 dilution (b). Maximum intensity profiles combining all Z stacks shown. White arrows indicate areas of LC3 puncta corresponding to LC3-II associated phagosomes or positive citrullinated vimentin staining. Nuclei stained with DAPI. N=1.

Figure 3.11

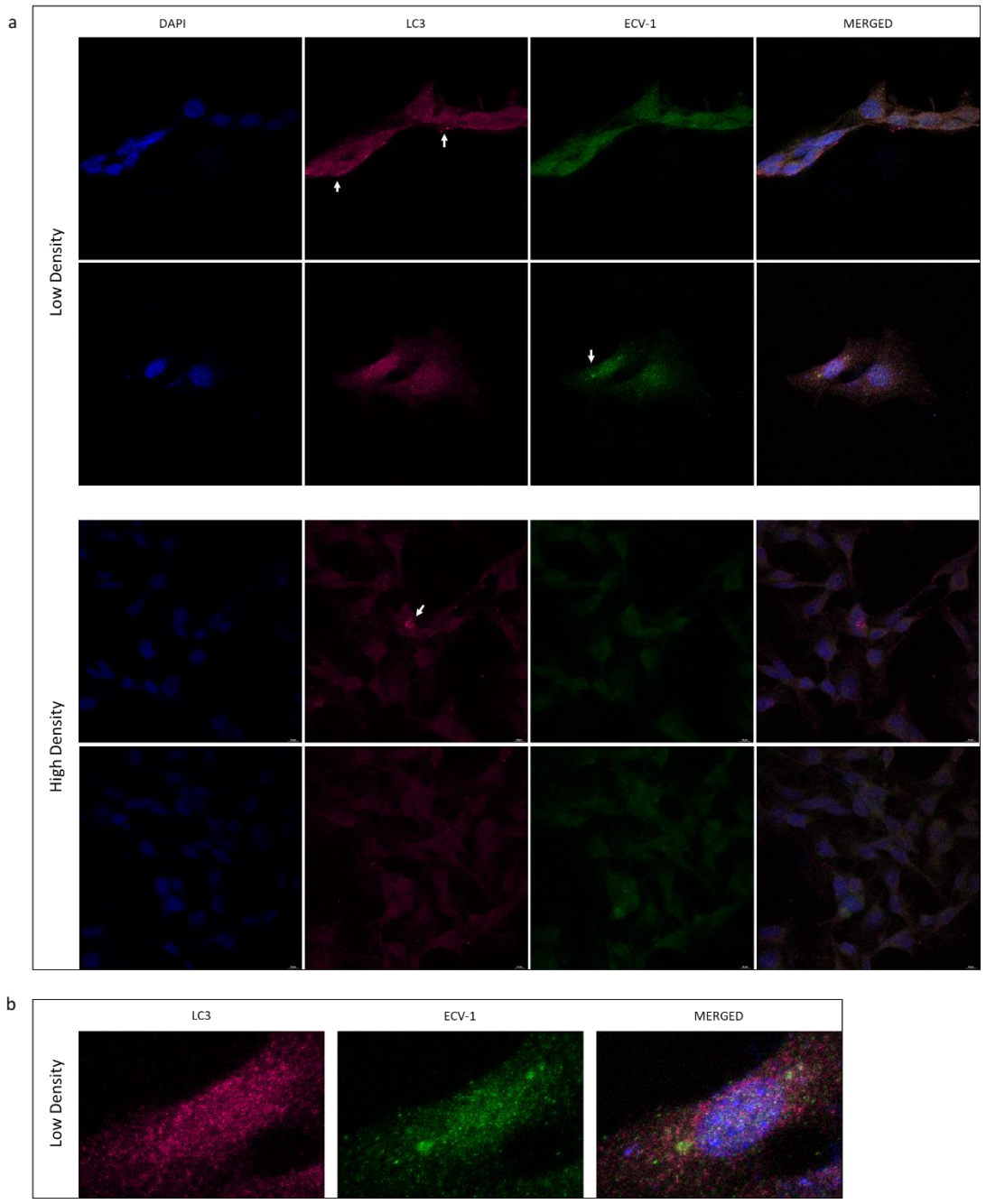


Figure 3.11 Confocal microscopy images (60X lens) of low, $0.5x10^5$ cells/well and high, $5x10^5$ cells/well density plated cells dual stained for LC3 at 1:50 dilution and ECV-1 at 1:500 dilution. Maximum intensity profiles combining all Z stacks shown. White arrows indicate areas of LC3 puncta corresponding to LC3-II associated phagosomes or positive citrullinated vimentin staining (a). More detailed view of one cell at low density (b). Nuclei stained with DAPI. N=1.

To determine true autophagy staining and to increase the potential of visualising co-localisation of LC3 and ECV-1, the lysosomal acidification inhibitor Chloroquine (CQ) was used to block degradation and allow accumulation of phagosomes in cell density experiments. Prior to confocal analysis, B16F1 cells were treated with CQ for 0, 1, 4 and 20 hours at 37°C and lysates prepared for western blotting. After 20 hours CQ treatment, the low density plated cells were rounded and unhealthy with many non-adherent cells (Figure 3.12c). Normalised LC3-II signal was greater at low density compared to high density in all CQ treatment conditions. In addition, the level of LC3-II increased in low density samples with longer CQ treatment time. Taken together, the data indicates that cells plated at low density underwent more autophagy compared to cells plated at high density and this effect can be observed to a greater extent with the use of CQ (Figure 3.12a and b).

Figure 3.12

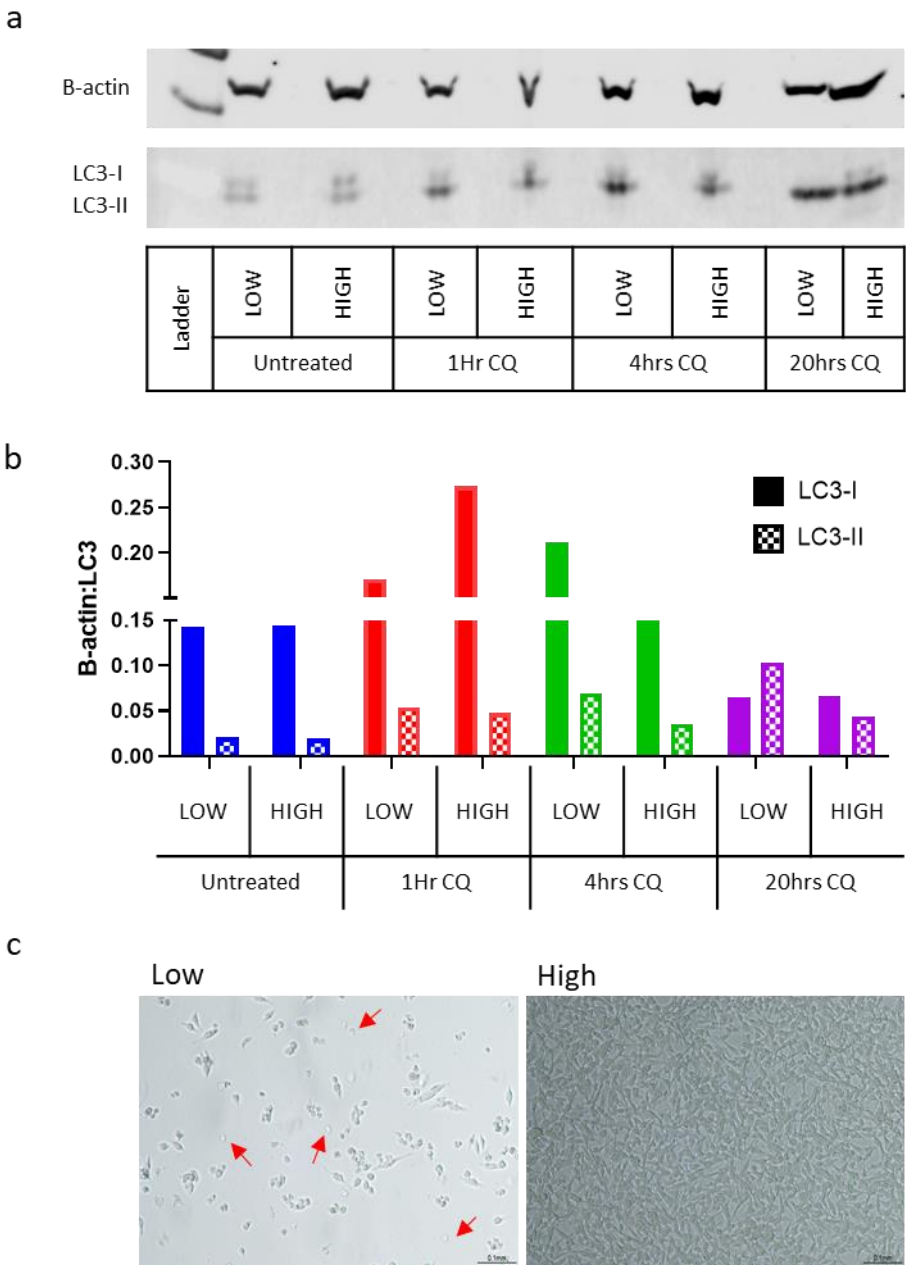
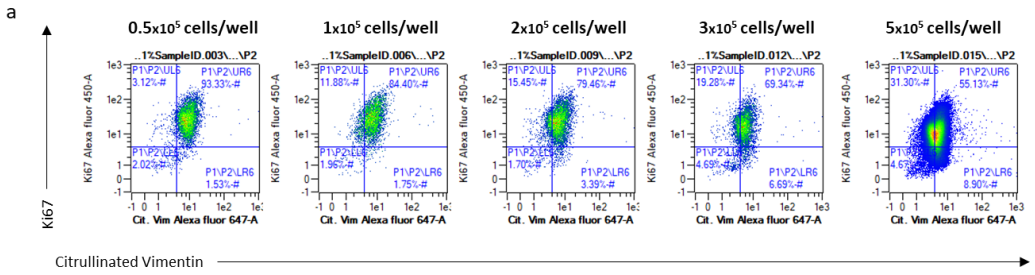


Figure 3.12 B16F1 cultured at low ($0.5x10^5$ cells/well) and high ($5x10^5$ cells/well) densities were tested for LC3 expression after 50μM Chloroquine (CQ) treatment for 0, 1, 4 or 20 hours. Antibody used at 1:1000 according to manufactures instructions (a). LC3 signal was normalised against β-actin loading controls (b). Brightfield images (10X) for low and high density cultures after 20 hours CQ treatment. Non-adherent cells highlighted by red arrow (c). N=1.

It was hypothesised that actively growing cells may have a requirement for high energy levels which were inducing autophagy and stress induced citrullination. To investigated this, B16F1 cells were plated at densities 0.5, 1, 2, 3 or $5x10^5$ cells/well and stained for nuclear expression of proliferation marker Ki67 in combination with citrullinated vimentin. More than 85% of cells were positive for Ki67, of which 55% of cells were also positive for citrullinated vimentin (Figure 3.13a and b). A decrease in Ki67 and citrullinated vimentin double positive events as well as Ki67 median fluorescence intensity, was observed with increasing cell density, indicating that there is a correlation between proliferation and citrullination. These experiments were conducted three times, and both were statistically significant, P=0.0024 and P=0.0006, respectively (Figure 3.13c and d).

Cells plated at various densities were also grown in serum and amino acid starvation (AS) media to test whether nutrient deprivation can further induce citrullinated vimentin expression in these cultures. Quadrant gating analysis shows an increase in double positive citrullinated vimentin events (upper right quadrants) with decreasing cell density in both untreated and AS conditions (Figure 3.14a-c). However, these percentages were consistently lower in AS cultures compared to untreated controls (Figure 3.14d) therefore the addition of nutrient deprivation did not have an additive effect on citrullinated vimentin expression. Ki67 levels were also assessed; all densities in both untreated and AS conditions were greater than 85% positive for Ki67, however, as seen previously, Ki67 MFI decreased with increasing densities (Figure 3.14e). Interestingly, the MFI of AS cell densities was consistently lower than untreated conditions suggesting AS inhibited cell proliferation and therefore resulted in less citrullinated vimentin expression (Figure 3.14f). This experiment was performed once and must be repeated to confirm the effect of AS on Ki67 expression.

Figure 3.13



b

Percentage positive events (%)	Cell density (x10⁵ cells/well)				
	0.5	1	2	3	5
Ki67 only	3.12	11.88	15.45	19.28	31.30
Citrullinated vimentin only	1.53	1.75	3.39	6.69	8.90
Double positive	93.33	84.40	79.46	69.34	55.13

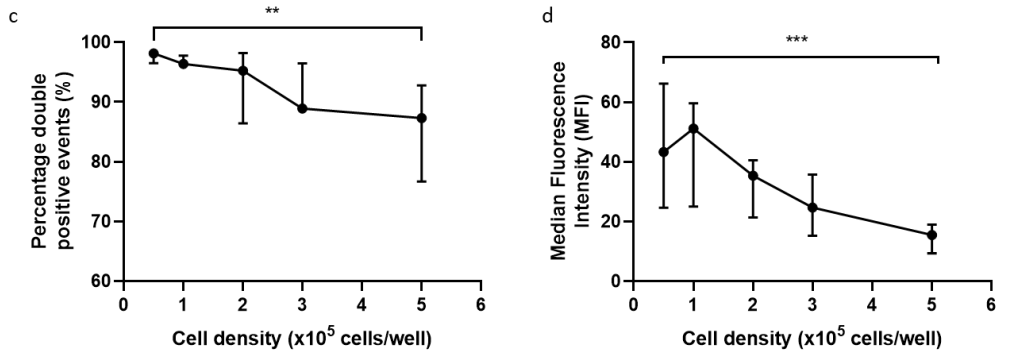
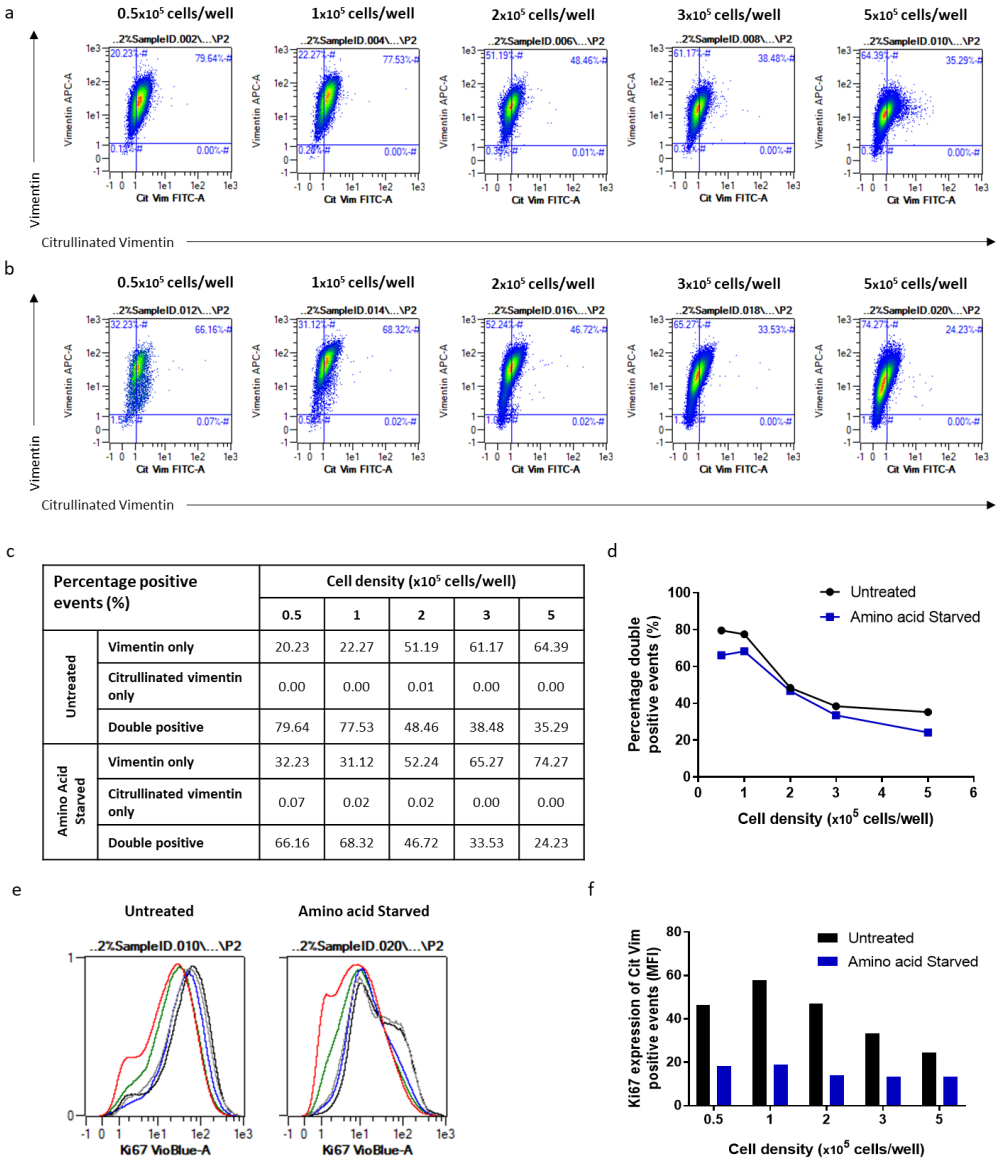


Figure 3.13 Intracellular Ki67 and citrullinated vimentin expression in B16F1 plated at cell densities 0.5, 1, 2, 3 and $5x10^5$ cells/well. Quadrant gating showing cells double positive for Ki67 and citrullinated vimentin (a). Percentage positive events of each quadrant; Ki67 only (upper left), Citrullinated vimentin only (lower right) and double positive (upper right). Data representative of 3 experiments (b). Collated data for percentage Ki67 and citrullinated vimentin double positive events (c) Collated median fluorescence intensities for Ki67 staining (d). Error bars represent median with range N=3. One-way ANOVA linear trend analysis ** = P <0.01, *** = P<0.001.

Figure 3.14



Percentage positive events (%)		Cell density (x10⁵ cells/well)				
		0.5	1	2	3	5
Untreated	Vimentin only	20.23	22.27	51.19	61.17	64.39
	Citrullinated vimentin only	0.00	0.00	0.01	0.00	0.00
	Double positive	79.64	77.53	48.46	38.48	35.29
Amino Acid Starved	Vimentin only	32.23	31.12	52.24	65.27	74.27
	Citrullinated vimentin only	0.07	0.02	0.02	0.00	0.00
	Double positive	66.16	68.32	46.72	33.53	24.23

Figure 3.14. Intracellular citrullinated vimentin, vimentin and Ki67 expression in B16F1 plated at cell densities 0.5, 1, 2, 3 and 5x10^5 cells/well cultured in complete media (untreated) or Krebs-Ringer Buffer solution (serum and amino acid depleted media; stated as amino acid starved). Quadrant gating of untreated (a) and amino acid starved (b) conditions, showing cells double positive for vimentin and citrullinated vimentin. Percentage positive events of each quadrant; Vimentin only (upper left), Citrullinated vimentin only (lower right) and double positive citrullinated vimentin (upper right) (c). Percentage of double positive citrullinated vimentin events at each density (d). Data representative of 2 experiments N=2. Ki67 expression of untreated and amino acid starved conditions. Histogram overlay line colours represent the following densities; Grey = 0.5x10^5, Black = 1x10^5, Blue = 2x10^5, Green = 3x10^5

and Red = 5_{x10^5} cells/well (e). Ki67 Median fluorescence intensities (MFI) of citrullinated vimentin positive events in untreated and amino acid starved conditions(f). N=1.

3.2.5 Involvement of the HIPPO pathway in citrullinated protein expression

There are many signalling pathways implicated in cellular stress and survival. One heavily studied pathway involved in regulating proliferation and apoptosis is the HIPPO pathway, whose two major downstream effectors YAP and TAZ are commonly used to determine the signalling activity in cells [241, 242]. This pathway is switched on during cell-to-cell contact and YAP/TAZ is phosphorylated blocking its translocation to the nucleus and therefore inhibiting transcription of genes promoting proliferation. When cell-to-cell contact is absent, the pathway is switched off, allowing YAP/TAZ to translocate to the nucleus and bind to a family of transcription factors known as TEAD, triggering proliferative genes [241, 242]. Pavel et al (2018) showed that autophagy could be inhibited when the HIPPO pathway was switched on [243]. The relationship between the HIPPO signalling pathway and citrullination was investigated in B16F1 cultures grown at low and high density. Confocal staining of YAP in these density cultures found co-localisation of YAP (Alexa fluor 488 – green) with the Nucleus (DAPI – blue) in low density conditions suggesting the HIPPO pathway was active in these conditions (Figure 3.15). At high density, YAP staining was more cytoplasmic with some cells showing a distinct absence of signal in the nucleus (Figure 3.15). Protein expression of YAP and phospho-YAP (p-YAP) were also examined in low and high density B16F1 cultures by western blotting. Bands at 65kDa observed for both YAP and p-YAP (Figure 3.15a). The signal intensities of YAP and p-YAP were normalised against β-actin in 4-5 experiments. There was no significant difference in either YAP or p-YAP protein in both low and high densities, YAP P=0.4947 and p-YAP P=0.8030 (Figure 3.16b).

Figure 3.15

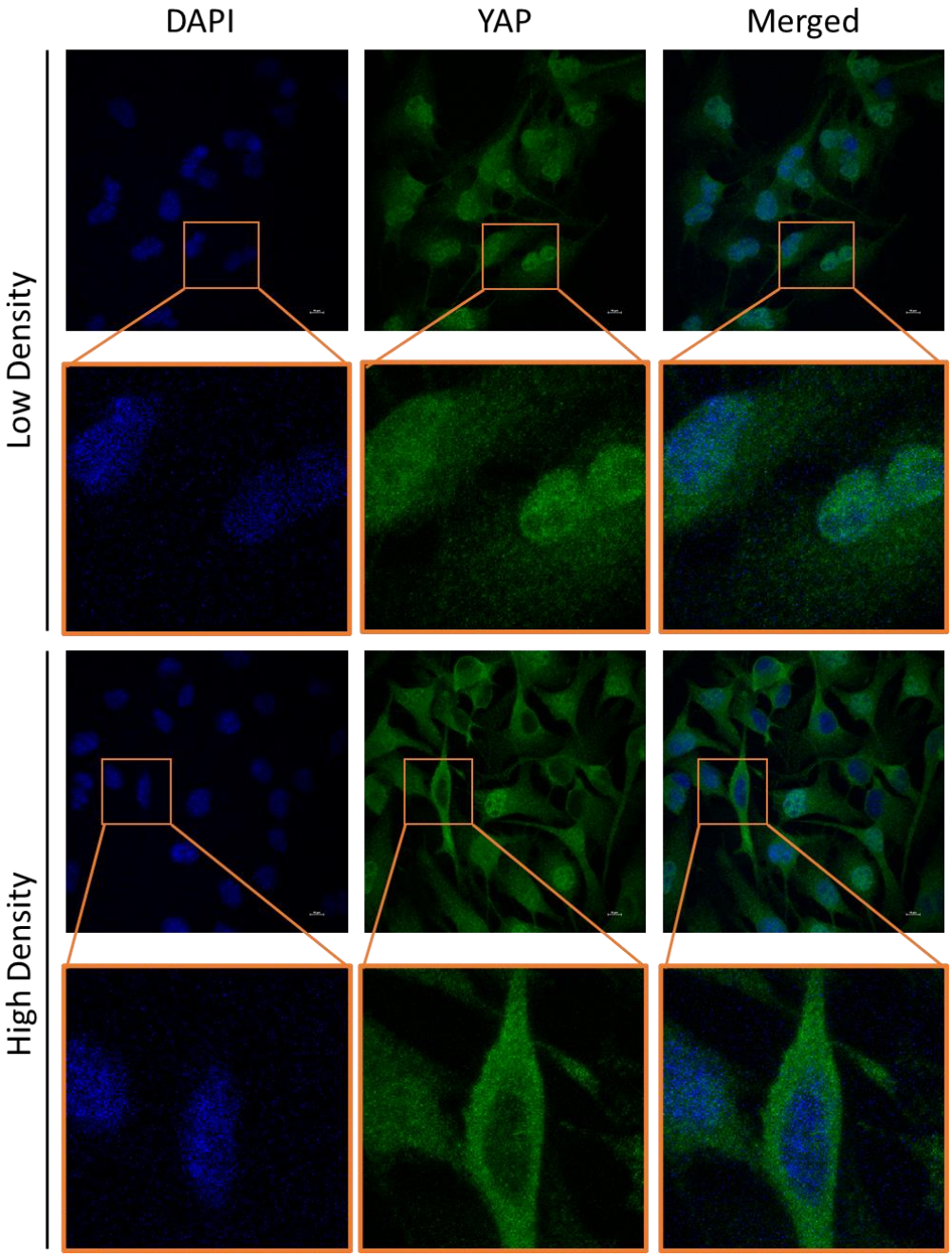


Figure 3.15. Confocal microscopy images (60X lens) of low, $0.5x10^5$ cells/well and high, $5x10^5$ cells/well density plated cells dual stained for YAP at 1:100 dilution. Maximum intensity profiles combining all Z stacks shown. Nuclei stained with DAPI. N=1.

Figure 3.16

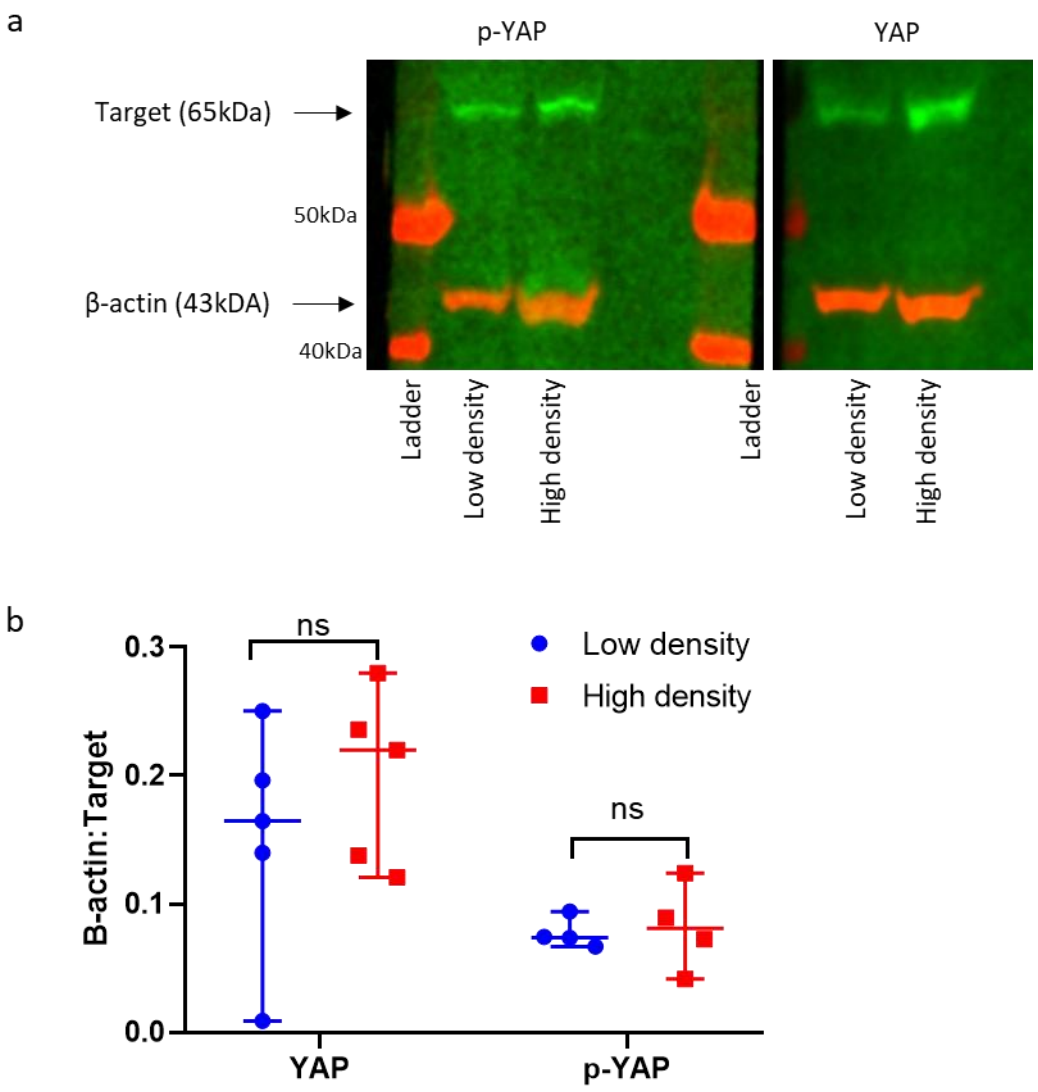


Figure 3.16. B16F1 cells plated at low and high density overnight before lysis to measure protein expression of YAP and p-YAP via western blotting (a). Experiments collated and target proteins normalised against β-actin expression. Paired t test analysis, ns = P≥0.05, N>4 (b). All error bars show median with range.

To block HIPPO signalling and switch the pathway off, the inhibitor XMU-MP-1 was utilised. This is a reversible ATP-competitive inhibitor of upstream kinase MST1 and MST2, which blocks its phosphorylation and subsequently the phosphorylation of downstream molecules such as YAP/TAZ, allowing the active form to translocate to the nucleus and bind to TEAD [244, 245]. B16F1 cells grown at low and high density overnight were treated with XMU-MP-1 at 0, 1, 3 and 10μM. Both YAP and p-YAP signals were faint in cells harvested after 15 minutes of XMU-MP-1 exposure with slightly stronger band detection in high density cultures, with increasing concentrations showing no effect in both densities (Figure 3.17a). High density plated cells treated with 0, 3 and 10μM XMU-MP-1 for 6 hours showed no significant difference between concentrations for YAP expression (P=0.8289 and P=0.3006 for 3μM and 10μM compared to untreated) and p-YAP expression (P=0.1785 and P=0.3104 for 3μM and 10μM compared to untreated) (Figure 3.17b). Although higher levels of LC3-II were seen at low density compared to high density, expression levels were not altered with 6 hours XMU-MP-1 treatment (Figure 3.17c(i)). Normalisation against β-actin showed similar low levels of LC3-II with 3μM XMU-MP-1 which was slightly elevated with 10μM XMU-MP-1, however the median expression was still less than the untreated control (Figure 3.17c(ii)).

Figure 3.17

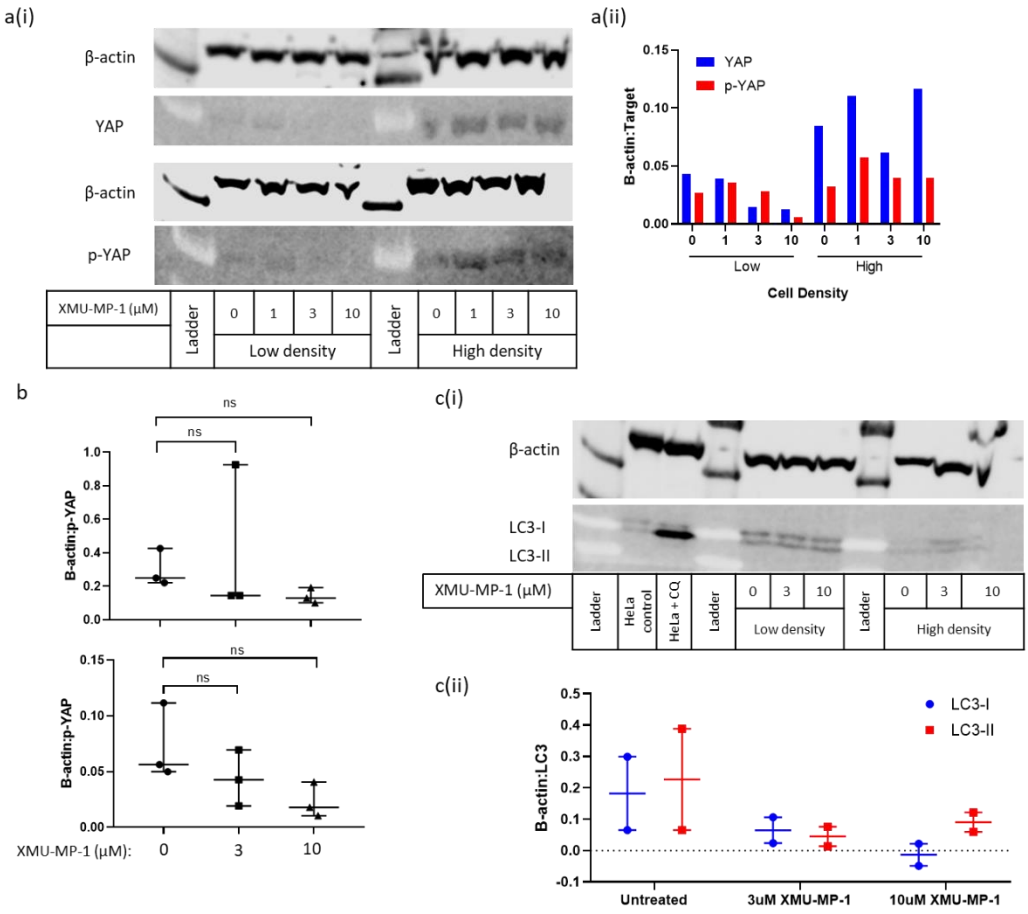


Figure 3.17. Expression of YAP and phospho-YAP in low and high density plated B16F1 treated with MST-1/2 inhibitor, XMU-MP-1, for 15mins at 0, 1 3 and 10μM. N=1 (a(i) and (ii)). Expression of YAP and p-YAP in high density plated B16F1 incubated with XMP-MP-1 at 0, 3 and 10μM for 6 hours. N=3 One-way ANOVA multiple comparisons analysis, ns = P≥0.05 (b). LC3 expression of low and high density (c(i)) and only high density (c(ii)) plated B16F1 treated with 0, 3 and 10μM XMU-MP-1 for 6 hours. N≤2 (c(i)). Target proteins normalised against β-actin.

High density plated cells (cultured and adhered overnight) were also treated with 0, 3 and 10µM XMU-MP-1 for 1, 3, 6 and 24 hours prior to western blotting analysis of YAP and p-YAP and staining for citrullinated vimentin with ECV-1. YAP expression levels remained constant in untreated conditions over the 24 hour time course but there was an increase in p-YAP at 24 hours (Figure 3.18d). There was also a slight increase in both YAP and p-YAP with 3µM but not 10µM XMU-MP-1 after 1 hour of treatment. This was reduced at 3 and 6 hours for both YAP and p-YAP (Figure 3.18d). After 24 hours of incubation, p-YAP levels were slightly elevated with 3µM XMU-MP-1 treatment in comparison to levels seen at 3 and 6 hours however this was still lower than untreated conditions (Figure 3.18d(ii)). Citrullinated vimentin expression ranged from 40-80% in all treatment conditions with 6 hours XMU-MP-1 incubation and did not show any difference with concentration (Figure 3.18a). After 24 hours, citrullinated vimentin expression was depleted to 20% in untreated cells. Cells treated with XMU-MP-1 remained constant at ~60% citrullinated vimentin expression for both doses compared to at 6 hours but much greater than untreated conditions; ~60% for both 3µM and 10µM (Figure 3.18b). Some toxicity was observed in cultures treated with 10µM but not 3µM XMU-MP-1 for 24 hours as shown by the diminished number of events in flow cytometry scatter plots (Figure 3.18c). Apoptosis levels using annexin V staining should be tested in these conditions for confirmation of toxicity. This data suggests culturing high density cells for prolonged time periods can induce p-YAP in B16F1 cells and levels can be reduced by inhibiting MST-1/2. Citrullinated vimentin expression is also reduced in high density cells cultured for extended periods but levels can be increased by blocking the HIPPO pathway. This data is from preliminary experiments and needs to be repeated to confirm the effects of the HIPPO pathway on citrullination in tumour cells.

Figure 3.18

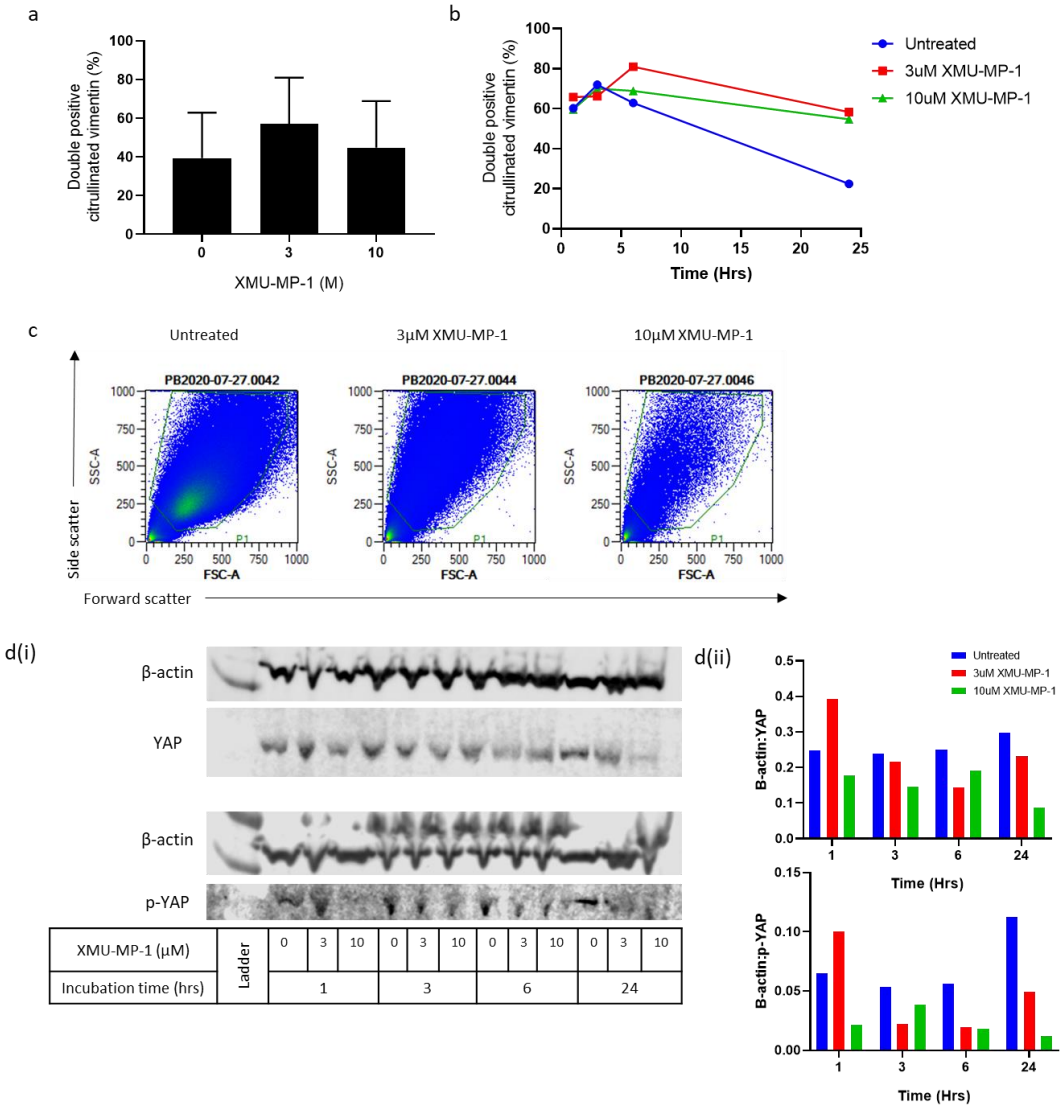


Figure 3.18. Citrullinated vimentin expression in high density plated B16F1 treated with 0, 3 and 10µM XMP-MP-1 for 6 hours. N=2 (a). Expression of citrullinated vimentin by flow cytometry (b) and YAP and phospho-YAP by western blotting (d(i)) in high density plated B16F1 treated with 0, 3 and 10µM XMU-MP-1 for 1, 3, 6 and 24 hours. Target proteins normalised against β-actin. N=1 (d(ii)). Forward scatter vs side scatter dot plots of B16F1 either untreated or treated with 3µM and 10µM XMU-MP-1 for 24 hours (c).

3.2.6 Citrullination in Murine Melanoma Tumours

Immunisation with MODI1 peptides; Vimentin28-49Tri Cit[28,36,45] (Vim28cit), Vimentin415-433Cit[424] (Vim415cit) and Enolase241-260Cit[253] (Eno241cit), has shown potent induction of CD4 T cells which mediate regression of tumours [1, 2, 77, 220]. This response is dependent upon MHC class II expression within the tumours which is required for presentation of these citrullinated peptides [1]. To assess if a difference in citrullinated vimentin could be detected within MODI1 immunised groups, B16F1 tumours were extracted from a total of 30 tumour bearing mice, disaggregated and stained for CD45 (VioBlue) before intracellular staining for Vimentin (APC), Citrullinated Vimentin (FITC), PAD2 (FITC) and PAD4 (FITC). Growth curves show tumour expansion from day 17 onwards in both unimmunised and immunised groups (Figure 3.19). Tumour bearing mice were immunised on either day 15 or day 21 with most tumours showing complete regression. In some cases tumours from immunised mice displayed regression until days 30-40 before re-growth (Figure 3.19). Immunisations and tumour excisions were performed by Peter Symonds and Dr Katherine Cook (Scancell Ltd).

Figure 3.19

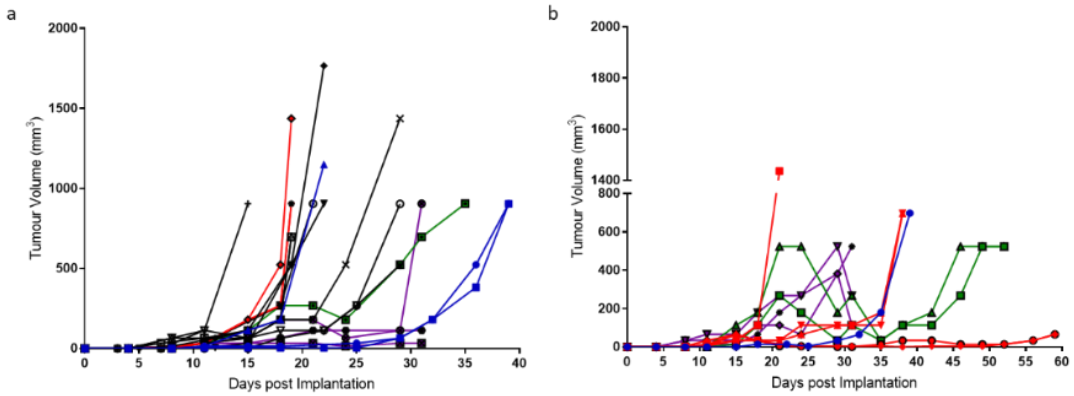


Figure 3.19. Growth curves of unimmunised (a) and MODI1 peptide immunised (b) B16F1 tumours from tumour bearing mice. Unimmunised N=19. Immunised N=11. Coloured lines (Blue, Red, Green and Purple) indicate matched studies.

Example of gating strategy shown in Figure 3.21a. As immune cells also express citrullinated vimentin (Figure 3.21) all CD45 positive cells (and doublets) were excluded prior to analysis of vimentin, citrullinated vimentin, PAD2 and PAD4. Quadrant gating confirmed the presence of cells double positive for citrullinated vimentin. Mice were either unimmunised or immunised with MODI 1 peptides. Immunised tumours were sub-divided into three groups based on their growth status at time of harvest; immunised but non-regressing, immunised and regressed but grew back and immunised and regressed (Figure 3.20b).

Citrullinated vimentin expression was seen in all tumour samples, ranging between 2-34% positive with differential staining in both unimmunised and immunised groups, suggesting many more would need to be analysed to make definite conclusions. There was no significant difference in the percentage of double positive citrullinated vimentin events between unimmunised and immunised tumours, P=0.8656 (Figure 3.20b(i)). The citrullinated vimentin MFI of immunised samples was lower than those of the unimmunised group indicating a reduced expression of citrullinated vimentin per cell, however this was not significant, P=0.0635 (Figure 3.21c).

CD45 was used as a general infiltrating immune cell marker. As immune cells have previously been shown to express citrullinated vimentin (Figure 3.21), samples were eliminated of any CD45 positive events. In the majority of tumours, CD45 expression was low with the highest percentage reaching 25% and with no significant difference between unimmunised and immunised samples, P=0.7670 (Figure 3.20b(ii)).

As PAD enzymes catalyse the citrullination of proteins, expression levels of PAD2 and PAD4 in tumours were also assessed. No distinct population of PAD positive cells were identified, instead cells differentially expressed these enzymes (Figure 3.20a). Both PAD enzymes were found at 5-40% of all tumours with no significant difference between unimmunised and immunised groups, PAD2 P=0.8820 and PAD4 P=0.2200 (Figure 3.20b(iii) and b(iv)).

Figure 3.20

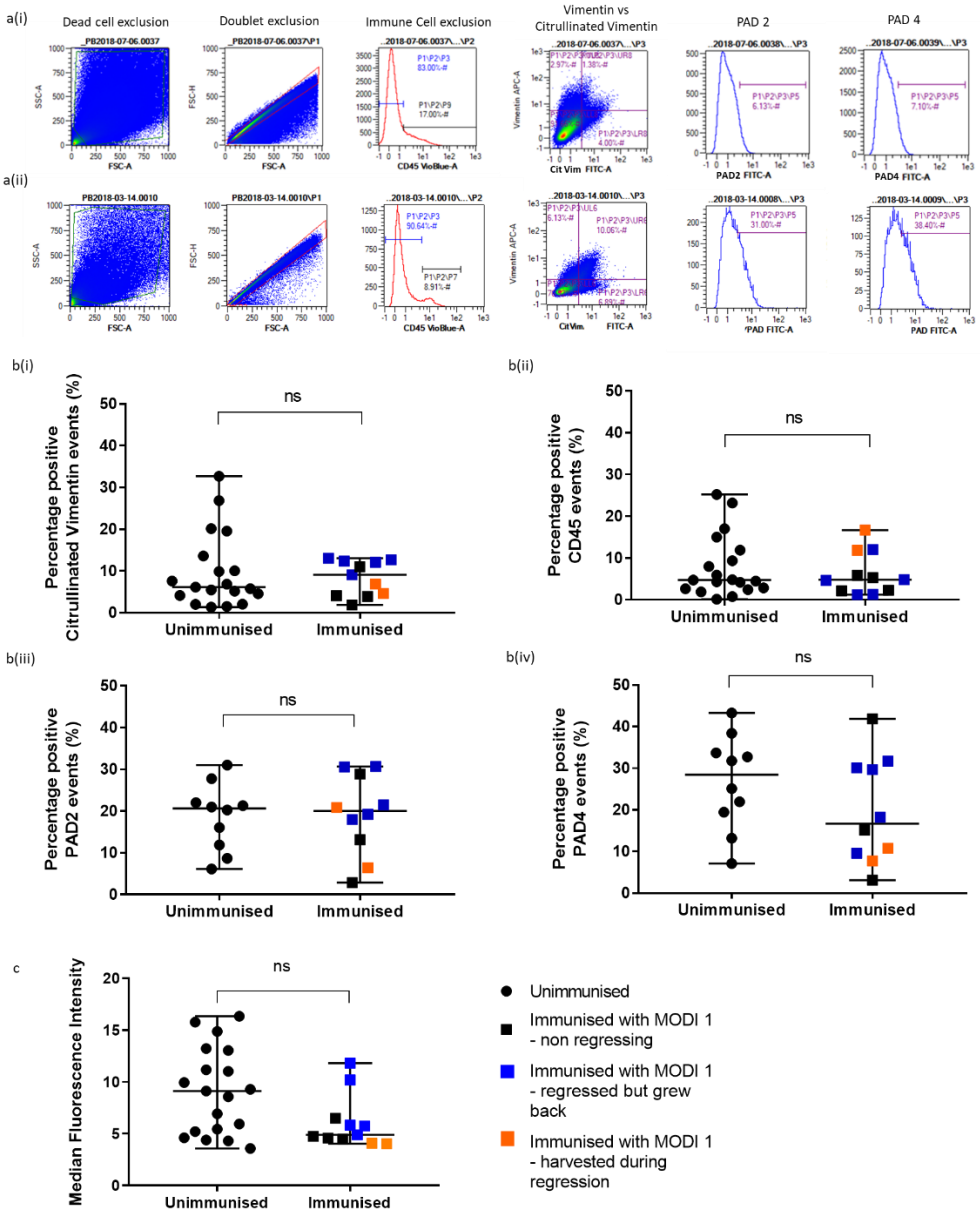


Figure 3.20. Murine melanoma tumours stained for CD45 (VioBlue), Vimentin (APC) and Citrullinated Vimentin (FITC). PAD2, PAD4 and Cytokeratin expressions also checked. Doublets and immune cells (CD45 positive) were excluded prior to vimentin, citrullinated vimentin, PAD2 and PAD4 analysis. Example of low (a(i)) and high (a(ii)) citrullinated vimentin and PAD expressing tumour. Percentage positive events for double positive citrullinated vimentin (i), CD45 (ii), PAD2 (iii) and PAD4 (iv) compared for unimmunised (black circle) and samples immunised with MODI1 peptides (b). Immunised sample divided into 3 groups; non-regressing (black square), regressed but grew back (blue square) and harvested during regression (orange square). Median fluorescence intensity (MFI) of double positive citrullinated vimentin in unimmunised and immunised groups (c). Data shown as median with range. N≥9. Welch's t test analysis for PAD2 and PAD4 staining ns = P > 0.05. Mann-Whitney test for citrullinated vimentin and CD45 staining ns P> 0.05.

Figure 3.21

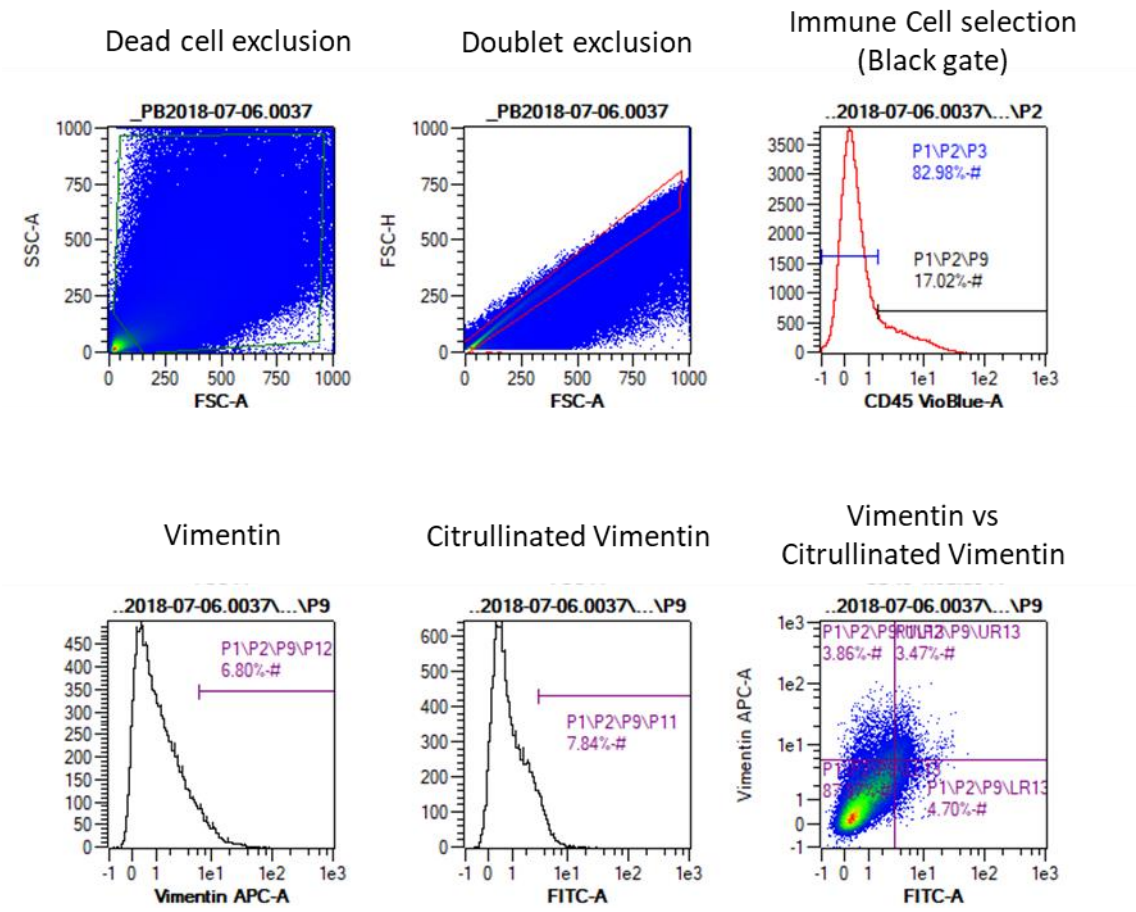


Figure 3.21 Murine melanoma tumours stained for CD45 (VioBlue), Vimentin (APC) and Citrullinated Vimentin (FITC). Doublets were excluded prior to selection of CD45 positive immune cells and subsequent gating for vimentin and citrullinated vimentin.

To confirm the presence of the ECV-1 citrullinated epitope, Vim65-76cit SSAV-Cit-L-Cit-SSVPG, in B16F1 tumours, 5 tumour samples (A1, A2, A4, A7 and A8) from unimmunised tumour bearing mice were pulverised and prepared as cell-free lysates and sent to Proteome Sciences for analysis of citrullinated peptide sequences via mass spectrometry. Tumours excised from mice by Peter Symonds (Scancell Ltd). Abundance of peptide sequences containing any part of the ECV-1 epitope are shown in Table 3.1 with amino acids corresponding to the immunogen peptide highlighted in green. No peptides containing the full immunogen peptide were found in any of the tumours but a total of 18 peptides containing partial sequences were identified. Of these, only one sequence was citrullinated (termed deiminated in table) and contained the immunogen peptide amino acids 65-71 plus an additional citrullinated residue at position 64, SSSPGGAYVT-cit-SSAV-cit-L-cit. The abundance of this sequence was greatest in tumours A7 and A8, 0.164 and 0.157 (3s.f) respectively, compared to tumours A1 0.0844 (3s.f), A2 -0.688 (3s.f) and A4 -0.541 (3s.f). The remaining 17 sequences identified were either not deiminated, SSAVRLR, or contained parts of the immunogen peptide without an arginine. The latter was found for 12 out of 17 un-deiminated sequences (Table 3.1). The abundance of un-deiminated arginine containing sequences were greater in most tumours. For example the direct wildtype equivalent for the citrullinated sequence found, SSPGGAYVTRSSAVRLR, was more abundant in tumours A1 0.195 (3s.f), A4 0.291 (3s.f), A7 0.289 (3s.f). This suggests that Vim65-76 is not preferentially citrullinated in B16F1 tumours and may explain the low levels of citrullinated vimentin staining with ECV-1.

Table 3.1

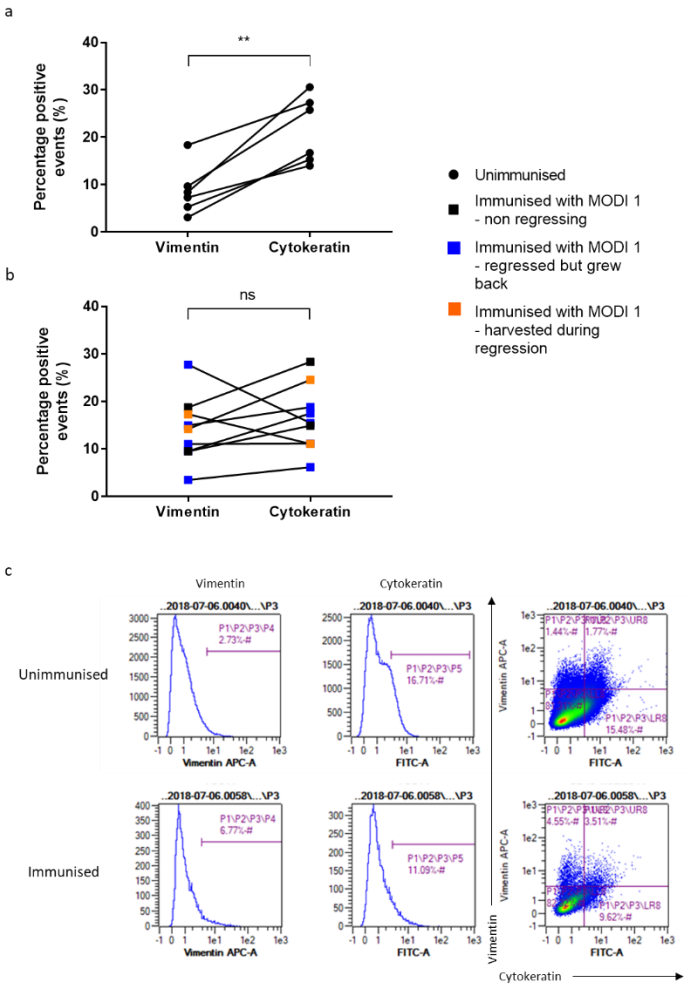
Sequence	Modification	Abundance				
		A1	A2	A4	A7	A8
SSSPGGAYVT-cit-SSAV-cit-L-cit	N-Term(TMT6plex); R11(Deamidated); R16(Deamidated); R18(Deamidated)	0.08435	-0.688240311	-0.54063	0.164183	0.157416
SSSPGGAYVTRSSAVR	N-Term(TMT6plex)	0.322089	-0.393643888	0.122427	0.122309	0.087138
SSVPGVRLLQDSVDF	N-Term(TMT6plex)	0.444606	0.099288443	0.061833	0.732237	0.422833
SVPGVRLLQDSVD	N-Term(TMT6plex)	0.07668	-0.60682061	0.235061	0.508425	0.434796
SSPGGAYVTRSSAVRLR	N-Term(TMT6plex)	0.194834		0.290558	0.288696	-0.01003
SSPGGAYVTRSSAVR	N-Term(TMT6plex)		0.38350888	0.043504	-0.0369	0.19552
SSPGGAYVTRSSA	N-Term(TMT6plex)	0.385093		-0.65696	-0.49932	1.007113
SSSPGGAYVTRSSAVRLR	N-Term(TMT6plex)		-0.312278472	-0.16852	0.457216	-0.38771
SSSPGGAYVTRSSAVRL	N-Term(TMT6plex)		-0.289348795	0.462598	0.966708	0.446757
SSSPGGAYVTRSSA	N-Term(TMT6plex)	1.098484		0.573708	-0.22264	0.54029
SSVPGVRLLQDSVDFSLAD	N-Term(TMT6plex)	0.37313	0.14987132	0.454907	-1.60705	
SSVPGVRLLQDSVDFSLA	N-Term(TMT6plex)		-0.261513913	-0.22433	0.682972	-0.18301
SSVPGVRLLQDSVDFS	N-Term(TMT6plex)	-0.06217		0.160187	0.398208	0.341366
SSVPGVRLLQDSVD	N-Term(TMT6plex)	-0.13412	0.010934666	-0.00417		-0.15013
SSVPGVRLLQ	N-Term(TMT6plex)		0.365152904	-0.57923	-0.0412	0.258214
SSVPGVRLL	N-Term(TMT6plex)		0.377900996	-0.57089	0.060098	0.296907
SSVPGVRL	N-Term(TMT6plex)	0.611585	0.132152421		0.650775	0.15134
YSSSPGGAYVTRSSA	N-Term(TMT6plex)		-0.241203635	0.114436	-0.35433	0.464237

Table 3.1 Abundance of peptide sequences identified by mass spectrometry in B16F1 tumours (A1, A2, A4, A7 and A8) from unimmunised tumour bearing mice which include the epitope for anti-citrullinated vimentin antibody ECV-1; SSAV-cit-L-cit-SSVPG or its non-deiminated equivalent. Matched amino acids highlighted in green. TMTcalibrator™ strategy by Proteome Sciences.

3.2.7 Involvement of EMT in citrullinated protein expression

Epithelial-to-mesenchymal transition (EMT) is involved in the progression and metastasis of many tumours and there is some evidence that lack of cell-to-cell contact can induce this aggressive phenotype [224, 235]. As B16F1 is a mouse melanoma cell line that can potentially undergo an EMT-like process. One of the characteristics of this process includes the change in the cells main cytoskeletal filament protein from cytokeratin, normally associated with a less invasive/aggressive state, to vimentin, a more metastatic state. Tumours from unimmunised tumour bearing mice were compared for their vimentin and cytokeratin expression. Interestingly, the proportion of cells expressing greater levels cytokeratin compared to vimentin was significantly higher ($P=0.0025$) in all unimmunised tumours, showing the B16F1 tumours mostly consisted of cells with an epithelial phenotype (Figure 3.22a). This was not found in immunised samples ($P=0.3960$), suggesting immunisation caused phenotypic changes in the tumour cells (Figure 3.22b). However, a small percentage of cells in the unimmunised tumour were also co-expressed vimentin and cytokeratin showing partial EMT (Figure 3.22c and d). In addition, some immunised tumours displayed greater vimentin expression compared to cytokeratin (Figure 3.22b) showing a pronounce switch to a mesenchymal/invasive phenotype.

Figure 3.22



d

Percentage positive events (%)		
Unimmunised	Vimentin only	1.44
	Cytokeratin only	15.48
	Double positive	1.77
Immunised	Vimentin only	4.55
	Cytokeratin only	9.62
	Double positive	3.51

Figure 3.22. Vimentin vs Cytokeratin expression in B16F1 tumours from unimmunised (a) and MODI1 peptide immunised (b) tumour bearing mice. Unimmunised N=6. Immunised N=6. Paired t test analysis ** = P ≤0.01. ns = P>0.05. Example of histogram and quadrant gating for vimentin and cytokeratin in unimmunised and immunised tumours (c) showing percentage positive events for each quadrant (d). Upper left = Vimentin only. Lower right = Cytokeratin only. Upper right = Double positive for Vimentin and Cytokeratin. Data representative of 6 unimmunised and 6 immunised tumours.

Researchers analysing 43 ovarian cell lines were able to determine the EMT phenotype of each cell line depending just on the expression of vimentin, cytokeratin and e-cadherin [246]. Firstly, cells positive or negative for e-cadherin were labelled as epithelial or mesenchymal respectively. If the e-cadherin positive cells were positive for cytokeratin but negative for vimentin they were considered as Epithelial. But if they were positive for both vimentin and cytokeratin they were thought to show an Intermediate Epithelial phenotype. On the other side of the spectrum, if e-cadherin negative cells were positive for both vimentin and cytokeratin they were classified as Intermediate Mesenchymal. Finally on the furthest end, Mesenchymal cells were only positive for vimentin [246]. This spectrum was used to assess the EMT phenotype of B16F1 before investigating the relationship between EMT and citrullination. As cell density has shown to effect citrullination levels, the EMT phenotype was first checked within these cultures. B16F1 was plated at low ($0.5x10^5$cells/well), medium ($2x10^5$cells/well) or high density ($5x10^5$cells/well) in 6 well plates for 24 and 48 hours before staining for vimentin, cytokeratin and e-cadherin. All three markers were expressed at high levels (>80%) in all densities at 24 hours however there was a slight increase in cytokeratin and e-cadherin levels from 85% at low density to 95% at medium and high densities (Figure 3.23a). Vimentin expression remained constant at >95% throughout all densities at both 24 and 48 hour timepoints. However, cytokeratin and e-cadherin levels were reduced at 48 hours; from 85% to 80% in low density cultures, and from 95% to 60-80% in medium and high density cultures. Cytokeratin levels fluctuated but in general were lower in medium and high density cultures at 48 hours compared to at 24 hours. Increasing density reduced the expression of e-cadherin from 80-60% at 48 hours but this density dependent effect was not observed at 24 hours (Figure 3.23a). B16F1 cells cultured at medium density for up to 72 hours showed cytokeratin expression was further reduced to ~70% however vimentin expression remained constant (Figure 3.23b).

Figure 3.23

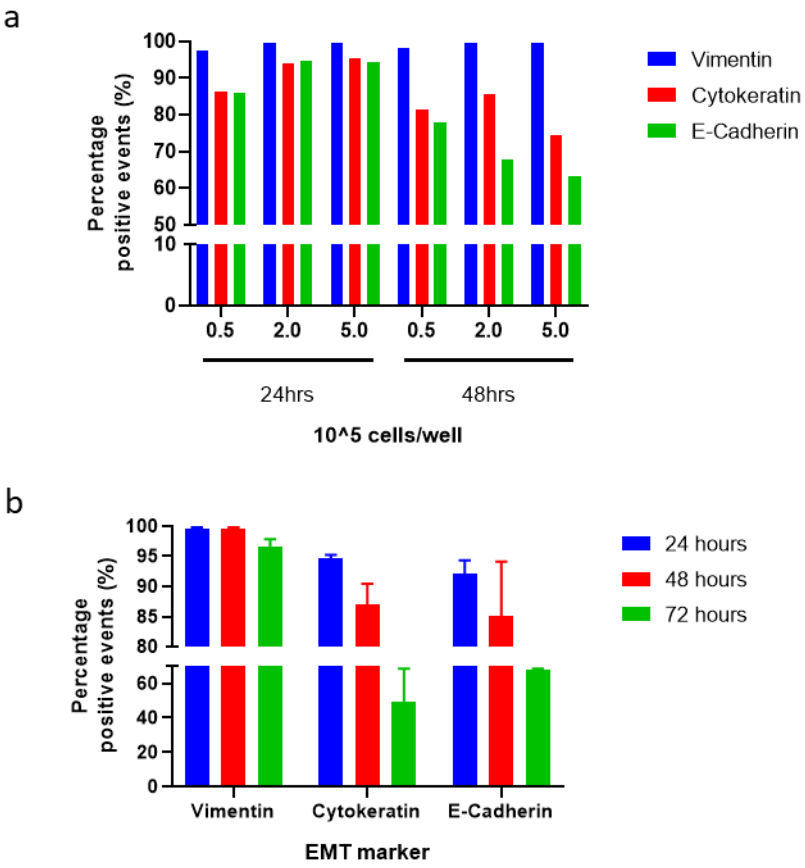


Figure 3.23. Expression of EMT markers Vimentin, Cytokeratin and E-cadherin in B16F1 cell line plated at increasing densities for 24 and 48 hours (a) and only at 2_{x10^5} cells/well for 24-72 hours (b). N≥2.

Studies have shown TGFβ can induce EMT *in vitro* [235], and so was used to induce EMT in B16F1 and check its effect on citrullinated vimentin expression. TGFβ was incubated with medium density plated B16F1 at 0, 1 5 and 20ng/ml for 24, 48 and 72 hours before staining for vimentin, cytokeratin and e-cadherin. Although a decrease in cytokeratin and e-cadherin expression was found at 48 and 72 hours, there was no change in EMT marker expression at any TGFβ dose for any timepoint (Figure 3.24a). Higher doses of TGFβ were tested ranging from 0-500ng/ml and expression of EMT markers plus citrullinated vimentin using ECV-1 were assessed after 48 hours exposure. Cells were almost 100% positive for vimentin, approximately 80% and 40% positive for e-cadherin and cytokeratin respectively. However, there was no change in EMT marker or citrullinated vimentin expression with increasing TGFβ concentration; citrullinated vimentin ranged between 40-60% (Figure 3.24b(i)).

It was hypothesised that B16F1 secrete and regulate TGFβ and so the effect of external TGFβ would be masked. Therefore, the same cell conditions were incubated with the TGFβ Type 1 Receptor (R1) Kinase inhibitor SB431542 at 0, 1, 3, 10 and 30μM for 48 hours to block EMT, inducing the opposing mechanism Mesenchymal-to-Epithelial (MET) transition, and to test its effect on citrullinated vimentin expression. The percentage of citrullinated vimentin positive events fluctuated between 50-80% however there was no correlation with TGFβ inhibitor dose. Untreated conditions showed ~100%, 80% and 45% expression of vimentin, e-cadherin and cytokeratin respectively. TGFβ inhibitor titration did not affect vimentin and cytokeratin levels however an increase in e-cadherin expression from 80% at 3μM to 100% at 10μM and 30μM was observed (Figure 3.24b(ii)). This experiment was performed once and needs to be repeat to confirm the effects of inhibiting TGFβ.

Figure 3.24

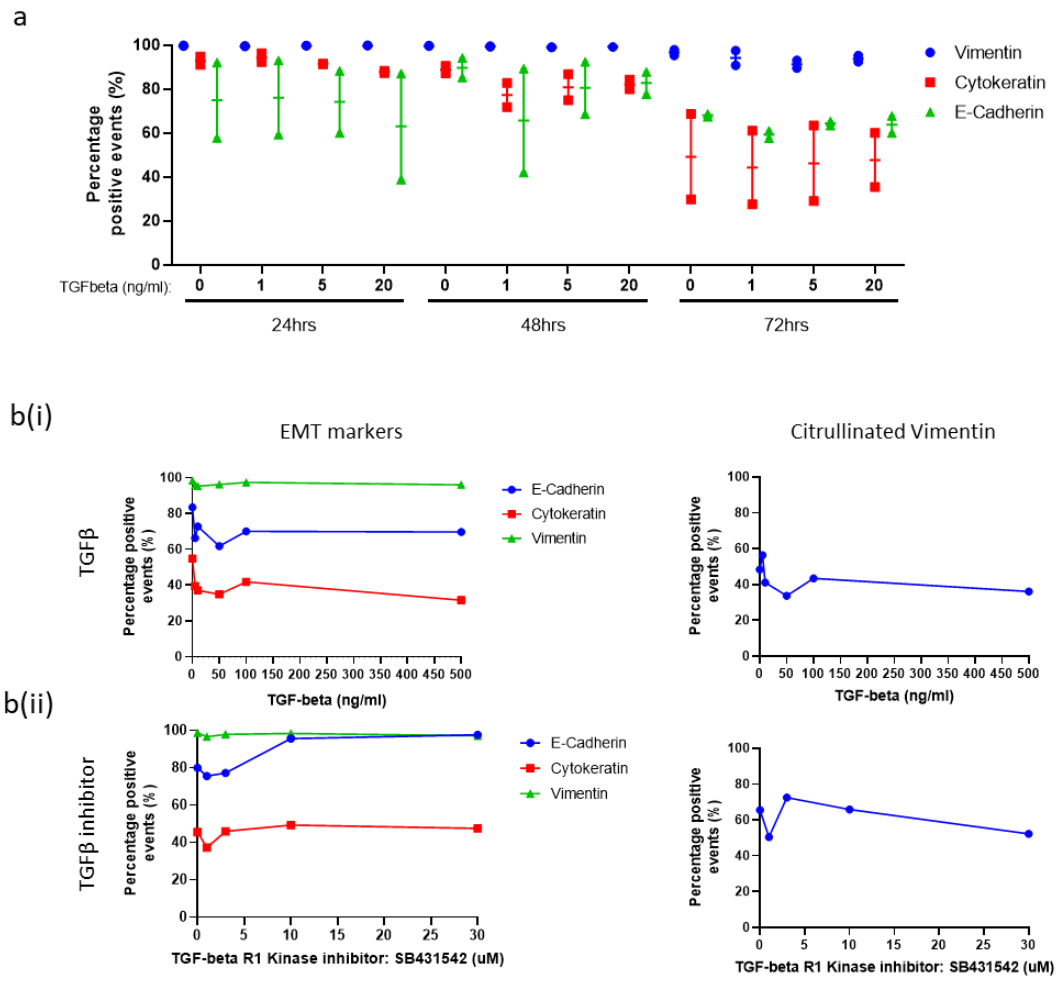


Figure 3.24. Induction of EMT with TGFβ treatment. B16F1 cells either untreated or treated with 1, 5 or 20 ng/ml TGFβ for 24, 48 and 72 hours before staining for EMT markers vimentin, cytokeratin and e-cadherin. N=2 (a). EMT marker and citrullinated vimentin expression of B16F1 cells treated with 5-500ng/ml TGFβ (b(i)) or 1-30μM TGF-β kinase inhibitor SB431542 (b(ii)) for 48 hours. N=1.

3.2.8 Citrullination and Autophagy in human cancers

A panel of human cancer tissue microarrays (TMAs) including head and neck, sarcoma, osteosarcoma, renal, ovarian, lung and breast (ER negative) were stained for citrullinated vimentin expression using ECV-1, and other citrullination markers such as PAD2 and PAD4, and autophagy marker such as Ambra1. TMAs were also stained for vimentin to compare levels of citrullination on this protein in human tumours. H scoring was used to evaluate expression as negative (0), low (1-100), medium (101-200) or high (201-300). TMA staining and scoring was performed by Mohammed Gijon (Scancell Ltd). The percentage of positive cases were calculated from the number of TMAs scored as low, medium or high within an array data set. Examples of staining intensities for citrullinated vimentin in ovarian cancer shown in Figure 3.25b and for remaining markers in ovarian cancer in the Appendix 3. The total number of cases in each cancer array ranged from 67-321 (Table 3.2, 3.3, 3.4, 3.5 and 3.6). All cancers were greater than 50% positive for citrullinated vimentin except for Renal cancer which only showed 35.8% of positive cases. For some cancers expression was very high; sarcoma 80%, osteosarcoma 86%, breast 94%, lung 97% and ovarian 97%. Head and neck cancer was moderately positive displaying 58% of citrullinated vimentin positive cases (Table 3.2).

The distribution of citrullinated vimentin expression varied between the different cancers. Cases with high expression (>200) were only seen in sarcoma, ovarian and breast cancers. The median citrullinated vimentin expression ranged between 50-100 for most cancers except head and neck and renal which had medians of 20 and 0 respectively (Figure 3.25a). Therefore, citrullinated vimentin expression was low (or negative for renal) for the majority of cases within these cancers. Ovarian, breast, lung, osteosarcoma and sarcoma cancers with the highest percentage of positive cases displayed mostly low (55-80%) to moderate (20-40%) citrullinated vimentin

expression with only <10% of ovarian, breast and sarcoma cases with high expression (Figure 3.26a). Head and neck and renal cancers were mostly negative (~40% and 60% respectively) with some low (~30%) and moderate (~20% and 5% respectively) expression (Figure 3.26a). Citrullinated vimentin staining was cytoplasmic in all cancers with some nuclear staining observed; nuclear localisation seen in strongly stained example (Figure 3.25b).

Figure 3.25

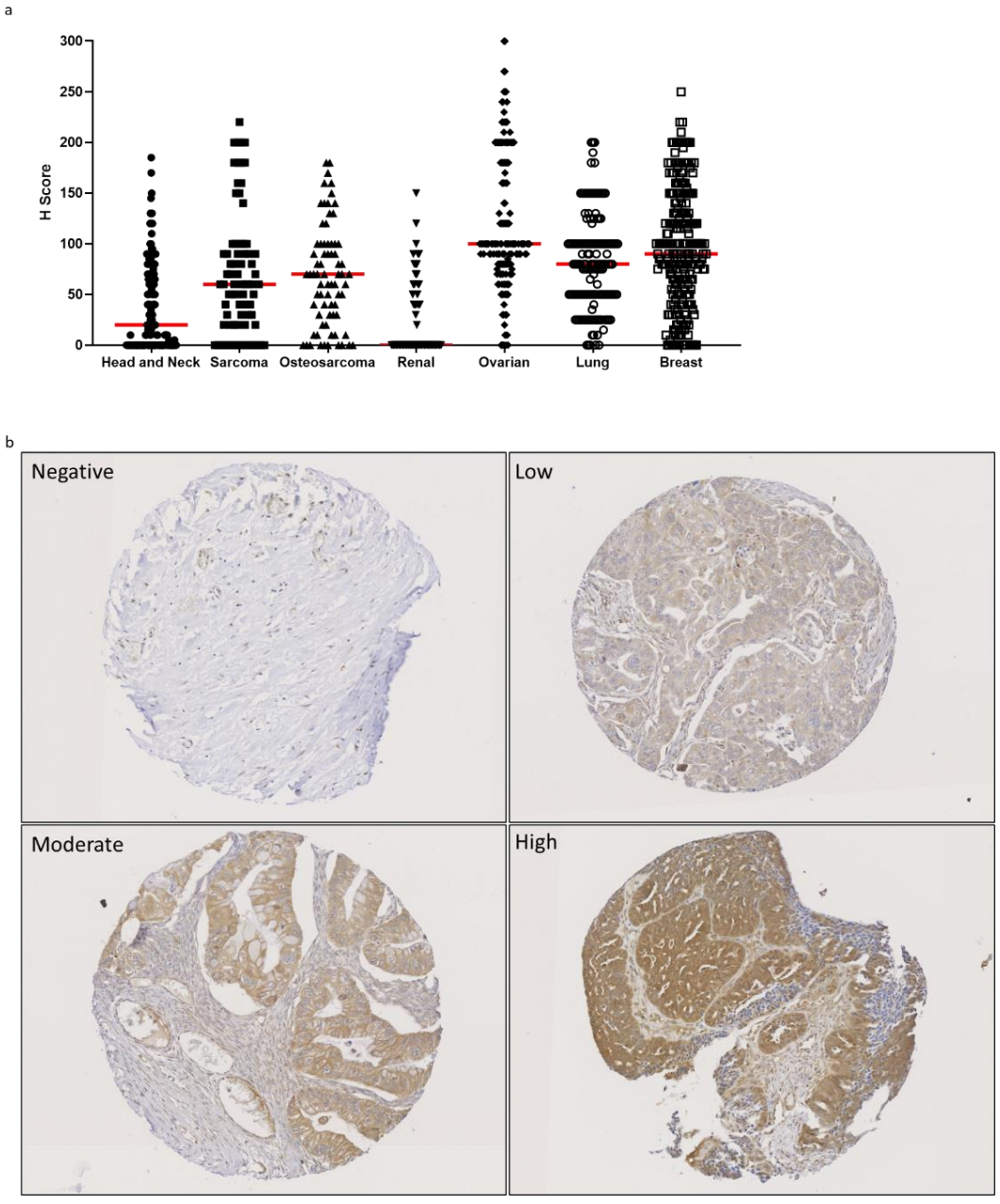


Figure 3.25. Distribution of H score values for Citrullinated Vimentin in head and neck, sarcoma, osteosarcoma, renal, ovarian, lung and breast (ER negative) cancers (a). Red bar represents the median. Citrullinated vimentin staining intensities showing examples of negative, low, moderate and high expression in ovarian TMA (b).

Table 3.2

Cancer Type	Positives	
	Cases	Percentage
Head and Neck	70/121	57.9
Sarcoma	60/75	80.0
Osteosarcoma	63/73	86.3
Renal	24/67	35.8
Ovarian	155/160	96.9
Lung	149/154	96.8
Breast Erneg	244/260	93.8

Table 3.2 Percentage of citrullinated vimentin positive cases in a range of cancers based on H score percentages. TMAs scored as low, moderate or high considered as 'positive'.

In contrast, vimentin expression was mostly negative in breast and lung cancers, only showing 15% and 40% of positive cases, despite the high levels of citrullinated vimentin. Renal cancer was also mostly negative for vimentin (~75%) however this correlated with citrullinated vimentin levels (Figure 3.26a and Table 3.3). Alternatively, sarcoma and osteosarcoma were almost 95% positive for vimentin and up to 60% of these cases displayed high expression. Approximately 65-67% of head and neck and ovarian cancers were vimentin positive, with mostly low and less moderate and high expression (Figure 3.26a and Table 3.3).

PAD enzymes are essential for citrullination of proteins and the different types vary slightly in function and location. The two mainly studied enzymes PAD2 and PAD4 were assessed in the panel of human TMAs depending on their cellular location;

cytoplasmic PAD2 and nuclear PAD4. All cancers were greater than 49% positive for cytoplasmic PAD2 displaying mostly low (40-60%) to moderate (10-40%) and some high (2-10%) (Figure 3.26c and Table 3.4). In contrast, nuclear PAD4 was found at >94% in all cancers assessed with the majority of cases expressing high levels (70-95%) of the enzyme (Figure 3.26d and Table 3.5).

Lastly, expression of the autophagy regulator Ambra1 was measured. This protein was found in >50% of cases in all cancers with breast, lung and ovarian cancers 97-98% positive (Table 3.6). Of the positive cases, expression levels were similar throughout the groups with greater low (40-60%) expression and less moderate (10-30%) to high (2-15%) expression. No cases with high Ambra1 expression were seen in head and neck cancers (Figure 3.26e).

Table 3.3

Cancer Type	Positives	
	Cases	Percentage
Head and Neck	80/122	65.6
Sarcoma	72/76	94.7
Osteosarcoma	69/73	94.5
Renal	16/67	23.9
Ovarian	127/205	66.8
Lung	34/226	15.0
Breast Erneg	112/283	39.6

Table 3.3 Percentage of vimentin positive cases in a range of cancers based on H score percentages. TMAs scored as low, moderate or high considered as 'positive'.

Table 3.4

Cancer Type	Positives	
	Cases	Percentage
Head and Neck	112/122	91.8
Sarcoma	39/80	48.8
Osteosarcoma	72/78	92.3
Renal	47/67	70.1
Ovarian	212/222	95.5
Lung	133/201	66.2
Breast Erneg	175/321	60.7

Table 3.4 Percentage of cytoplasmic PAD2 positive cases in a range of cancers based on H score percentages. TMAs scored as low, moderate or high considered as 'positive'.

Table 3.5

Cancer Type	Positives	
	Cases	Percentage
Head and Neck	121/122	99.2
Sarcoma	78/80	97.5
Osteosarcoma	78/78	100.0
Renal	63/67	94.0
Ovarian	260/260	100.0
Lung	211/216	97.7
Breast Erneg	313/313	100.0

Table 3.5 Percentage of nuclear PAD4 positive cases in a range of cancers based on H score percentages. TMAs scored as low, moderate or high considered as 'positive'.

Table 3.6

Cancer Type	Positives	
	Cases	Percentage
Head and Neck	79/118	66.9
Sarcoma	43/79	54.4
Osteosarcoma	61/80	76.3
Renal	53/67	79.1
Ovarian	254/259	98.1
Lung	97/100	97.0
Breast Erneg	282/291	96.9

Table 3.6 Percentage of Ambra positive cases in a range of cancers based on H score percentages. TMAs scored as low, moderate or high considered as 'positive'.

Figure 3.26

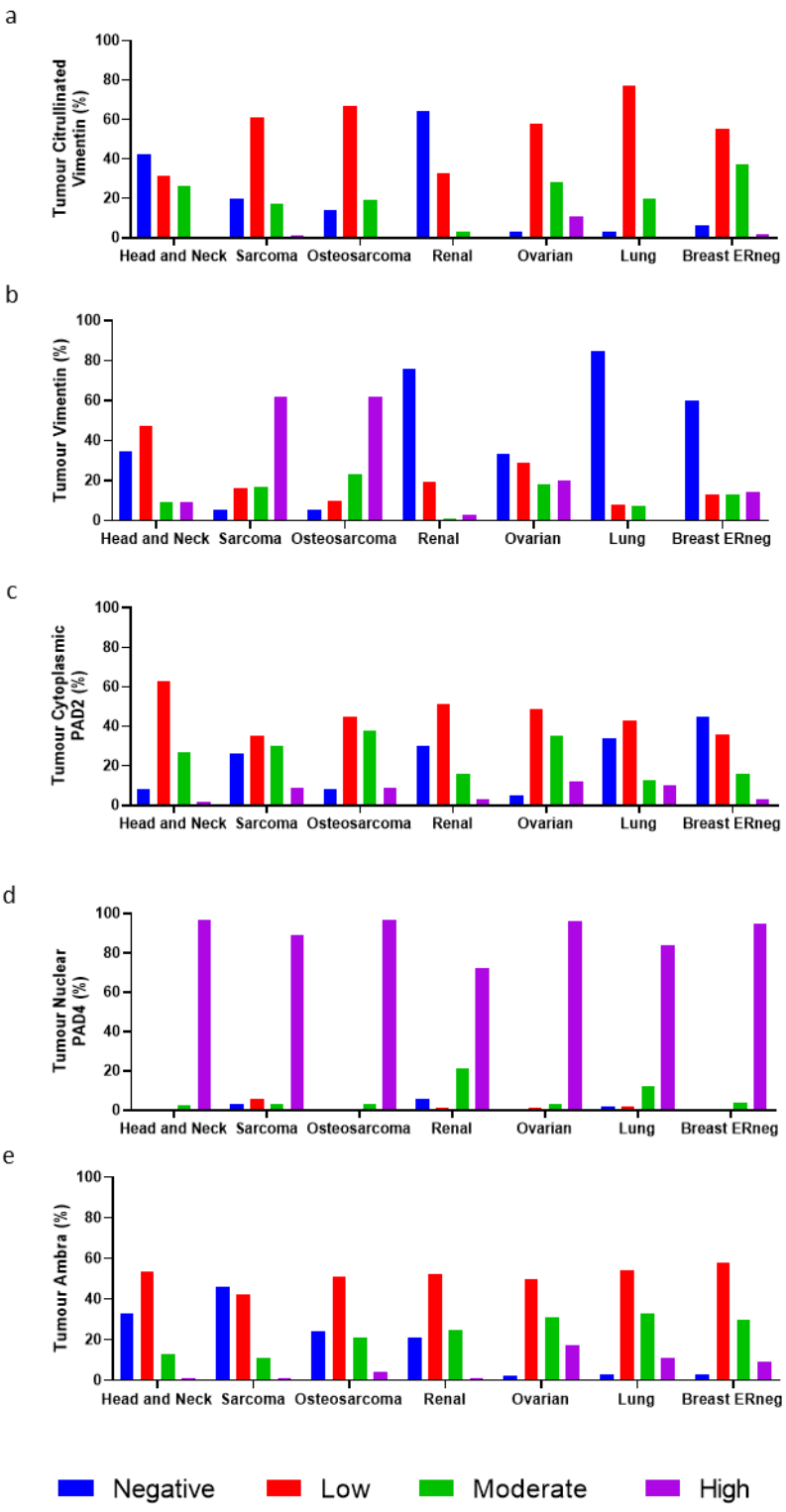

a
Tumour Citrullinated Vimentin (%)
b
Tumour Vimentin (%)
c
Tumour Cytoplasmic PAD2 (%)
d
Tumour Nuclear PAD4 (%)
e
Tumour Ambra (%)
0
20
40
60
80
100
Head and Neck
Sarcoma
Osteosarcoma
Renal
Ovarian
Lung
Breast ERneg
Negative
Low
Moderate
High

Figure 3.26. Protein expression of citrullinated vimentin (a), vimentin (b), cytoplasmic PAD2 (c), nuclear PAD4 (d) and Ambra (e) in a panel of human cancers; Head and Neck, Sarcoma, Osteosarcoma, Renal, Ovarian, Lung, ER negative Breast.

Clinical data was available for ovarian, lung and breast TMA cohorts so expression of citrullinated vimentin, PAD2 and Ambra1 (latter two not done for breast cancer) were assessed as prognostic factors. Low citrullinated vimentin expression correlated with better survival in ovarian and breast cancers however this was not significant, P=0.164 and P=0.393 respectively (Figure 3.27a and c). Alternatively, high expression of citrullinated vimentin in lung cancer resulted in significantly greater survival than cases with low expression, P=0.016 (Figure 3.27b). PAD2 expression in these cancers also varied. Negative cases displayed significantly better survival for up to 19 years in ovarian cancer (P=0.020) but PAD2 positive expression correlated with higher survival rates over 16 years in lung cancer (Figure 3.28a and c), however the latter was not significant (Figure 3.28c). Expression levels of citrullinated vimentin and PAD2 in relation to survival were similar in these cancers; low/negative expression of both markers correlated with greater survival probability in ovarian cancer, whereas survival was higher in lung cancer patients with high/positive expression.

There was no significant difference in survival between Ambra1 positive and negative individuals with ovarian cancer (P=0.662), however those with Ambra1 outlived those in the negative group (Figure 3.29b). The prognostic effect of Ambra1 was more pronounced in the lung cohort. Positive expression was significantly correlated with better survival, P=0.009 (Figure 3.28d).

Figure 3.27

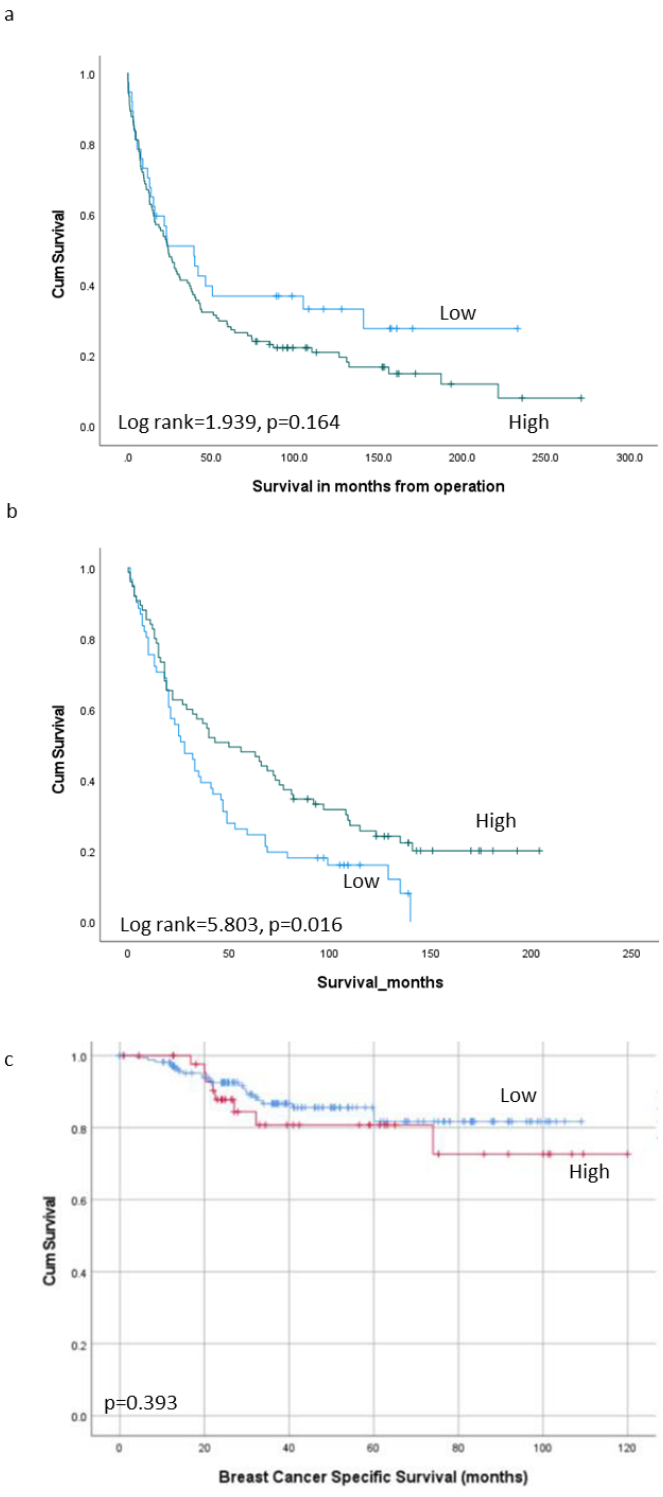


Figure 3.27. Kaplan-meier survival curves for ovarian (a), lung (b) and breast (c) cancer data sets based on citrullinated vimentin expression. Chi-square log rank test significance P≤0.05.

Figure 3.28

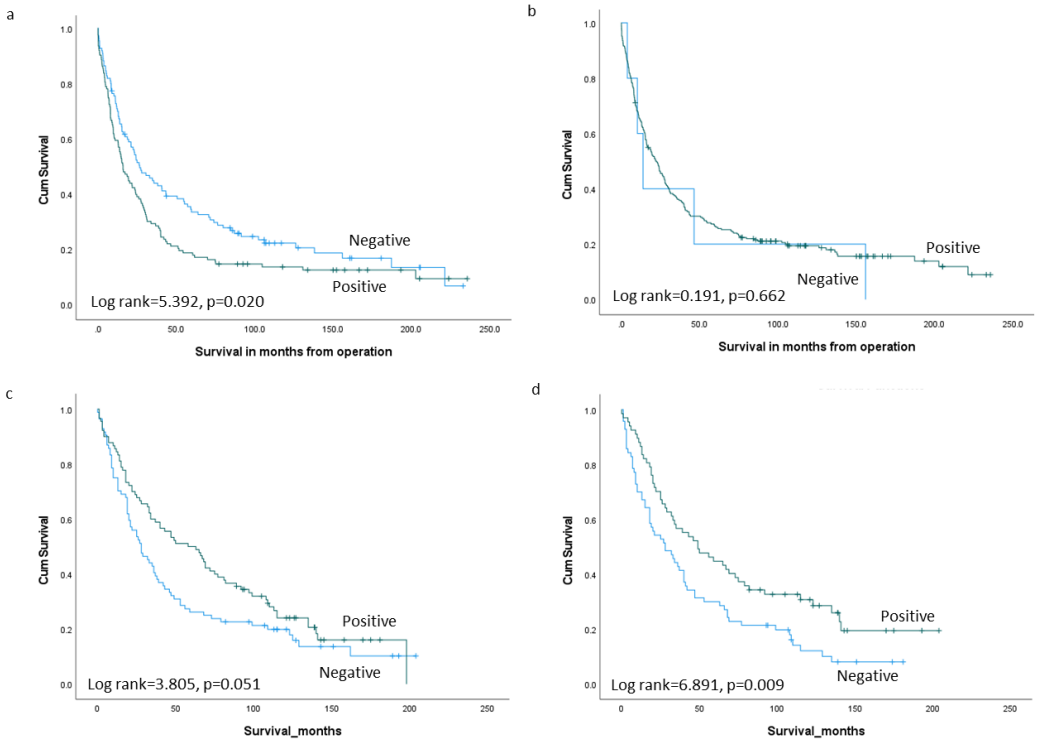


Figure 3.28. Kaplan meier survival curves for ovarian (a and b) and lung (c and d) cancer data sets based on PAD2 (a and c) and Ambra1 (b and d) expression. Chi-square log rank test significance P≤0.05.

Although, citrullinated vimentin expression did not correlate with survival in ovarian cancer, expression of this modified protein did positively correlate with Ambra1. A larger proportion of cases expressing Ambra1 also had significantly greater citrullinated vimentin expression; 14.5% and 85.5% of citrullinated vimentin high cases were found in Ambra1 low and high groups respectively, P=0.017 (Table 3.7). Elevated percentages of high citrullinated vimentin expressing cases were also found in both negative and positive groups for vimentin and PAD2 but this was not significant, P=0.054 and P=0.388 respectively (Table 3.7).

Similarly ranged percentages, between 43-57%, were seen with Ambra1 vs citrullinated vimentin in Lung cancer indicating no correlation (Table 3.8). However, greater levels of high citrullinated vimentin expressing cases were observed in vimentin and PAD positive (72-75%) compared to negative (36-50%) groups. This difference was only significant for PAD2 and not vimentin correlations, P<0.001 and P=0.088 respectively (Table 3.8).

In the breast cancer cohort, citrullinated vimentin expression was significantly correlated with PAD2 and Ambra1 expression with a greater percentage in high groups (32% and 49% respectively) compared to low groups (~17% for both markers), P=0.013 and P<0.001 respectively (Table 3.9).

Table 3.7

Marker	Group	Ovarian		
		Citrullinated Vimentin		Significance
		Low	High	Chi-Square p-value
Vimentin	Negative	33.3%	66.7%	0.054
	Positive	17.6%	82.4%	
PAD2	Negative	25.9%	74.1%	0.388
	Positive	19.4%	80.6%	
Ambra1	Low	31.8%	68.2%	0.017
	High	14.5%	85.5%	

Table 3.7 Percentage of Vimentin, PAD2 and Ambra1 negative and positive cases in Ovarian cancer patients with low or high expression of Citrullinated vimentin. Chi-squared log rank test significance. P≤0.05.

Table 3.8

Marker	Group	Lung		
		Citrullinated Vimentin		Significance
		Low	High	Chi-Square p-value
Vimentin	Negative	50.8%	49.2%	0.088
	Positive	25.0%	75.0%	
PAD2	Negative	63.8%	36.2%	<0.001
	Positive	28.0%	72.0%	
Ambra1	Negative	50.7%	49.3%	0.405
	Positive	43.7%	56.3%	

Table 3.8 Percentage of Vimentin, PAD2 and Ambra1 negative and positive cases in Lung cancer patients with low or high expression of Citrullinated vimentin. Chi-squared log rank test significance. P≤0.05.

Table 3.9

Marker	Group	Breast		
		Citrullinated Vimentin		Significance
		Low	High	Chi-Square p-value
Vimentin	Low	80.5%	19.5%	0.463
	High	73.9%	26.1%	
PAD2	Low	82.9%	17.1%	0.013
	High	67.7%	32.3%	
Ambra1	Low	83.2%	16.8%	<0.001
	High	51.4%	48.6%	

Table 3.9 Percentage of Vimentin, PAD2 and Ambra1 negative and positive cases in Breast cancer patients with low or high expression of Citrullinated vimentin. Chi-squared log rank test significance. P≤0.05.

3.2.9 Results summary

In summary, although nutrient starvation did induce citrullination this was mostly in apoptotic dying cells, and cell density was shown to be a stronger trigger with up to 70% of low density plated cells expressing citrullinated vimentin. Expression was mostly cytoplasmic with some cases showing punctate staining, increased phagosome associated LC3-II and increased proliferation in low density compared to high density cultures. This suggests actively growing cells undergo more autophagy and have greater potential to express citrullinated epitopes. Confocal analysis showed the presence of active YAP/TAZ in low density cells, a major downstream effector of the HIPPO pathway involved in regulation of proliferative and survival genes. Inhibition of upstream phospho-protein MST1/2 using XMU-MP-1, prevents phosphorylation of YAP/TAZ allowing it's active form to translocate to the nucleus. B16F1 cells cultured for 24hrs showed reduced citrullinated vimentin expression compared to the untreated control but XMU-MP-1 treatment reduced this effect and produced citrullinated vimentin levels comparable to untreated conditions at this time point. This suggests the HIPPO pathway may play a role in citrullination however more work is required to confirm its involvement. B16F1 tumours implanted in HHDII/DP4 mice showed no difference in percentage of citrullinated vimentin or PAD enzyme expression after immunisation with citrullinated peptides, however the citrullinated vimentin levels per cell (MFIs) were significantly reduced in immunised tumours. Citrullinated vimentin was also expressed in human cancers head and neck (58%), sarcoma (80%), osteosarcoma (86%), renal (36%), ovarian (97%), lung (62%) and ER negative breast (90%). High expression significantly correlated with survival in lung ($P=0.016$) but not ovarian ($P=0.164$) or breast ($P=0.393$) cancers. Additionally, citrullinated vimentin positively correlated with PAD2 and Ambra1 in these cancers.

3.3 Discussion

Research into the links between citrullination and cancer progression is fairly new despite the abundant evidence of PAD enzyme expression and involvement in many cancers [181, 247, 248]. Previously, we have shown potent anti-tumour responses to citrullinated peptides in a B16F1 mouse model, to be mediated by CD4 T cells. These peptides were presented by an autophagy dependent MHC class II pathway and responses were inhibited in the absence of PAD inhibitors [1, 2]. Although autophagy is an ongoing mechanism carried out by all cells, it can be upregulated in response to cellular stress. For these reasons, it was hypothesised that the post-translational modification, citrullination can be induced by stress. In this chapter, we have used the polyclonal antibody ECV-1 to determine citrullinated vimentin expression in B16F1, and surprisingly the biggest trigger for citrullination was growing cells at low density without contact inhibition, which was correlated with increased proliferation and high levels of autophagy. Pavel et al (2018) also reported involvement of the HIPPO pathway, switched off by lack of cell-to-cell contact, was associated with cell survival [243]. The two main transcriptional activators downstream of this pathway are the yes-associated protein (YAP) and its co-activator with a PDZ-binding domain (TAZ). When this pathway is activated by cell-to-cell contact, a series of serine/threonine kinases are phosphorylated. Briefly, MST1/2 are activated and phosphorylate LATS1/2 which in turn phosphorylates YAP/TAZ. This inhibits YAP/TAZ from translocating to the nucleus and binding to a family of transcription factors TEAD that regulate cell proliferation genes [241, 249]. In addition, nutrient deprivation has been found to protect against apoptosis through YAP dependent autophagy in the epithelial breast cancer cell line MCF7 [250]. However, high confluency resulted in YAP inactivation, reduced autophagy and proliferation, promoting apoptosis when exposed to stress factors such as hypoxia and glucose starvation [243]. This

coordinates with our findings where confocal analysis of YAP co-localisation with the nucleus at low density but was mostly cytoplasmic at high density.

Western blotting analysis of YAP and p-YAP protein expressed was inconclusive, with no distinct changes in expression in low or high density cultures. To test the involvement of the HIPPO pathway on autophagy and citrullinated vimentin expression, cells were treated with the MST1/2 inhibitor, XMU-MP-1. This was hypothesised to elevate un-phosphorylated YAP levels in high density cultures but no changes were observed. There was also no effect on LC3-II expression after XMU-MP-1 treatment. Two additional molecules can act to inhibit YAP-TEAD interactions; VGLL4 blocks YAP binding to TEAD in the nucleus and 14-3-3ζ/σ binds to phosphorylated YAP and sequesters it in the cytoplasm [242, 251-253]. These interactions can occur independent of MST1/2 activity and could explain the lack of changes in YAP/p-YAP observed. Although autophagy and YAP expression levels were not affected by MST1/2 inhibition, citrullination vimentin levels were greater in XMU-MP-1 treated B16F1 compared to untreated cells in culture for 24 hours. However, expression was not elevated compared to XMU-MP-1 treated samples at earlier time points suggesting blocking the HIPPO pathway prevented the decrease in citrullination rather than induced citrullination. The citrullinated vimentin depletion in untreated cultures was likely due to increased growth and therefore more contact inhibition, switching on the HIPPO pathway to limit cell proliferation. Our data on the correlation of citrullination and this signalling pathway are inconclusive and require further work and it is possible this pathway is not involved in citrullination. But research has shown the HIPPO pathway plays an important role in cancer progression. For example, the reduced cell proliferation and colony formation in breast cancer models, and ablated tumour growth plus increased cell death in oesophageal adenocarcinoma when YAP is knocked down or inhibited [252, 254]. High expression of VGLL4 and low YAP correlated with increased survival, reduced

tumour size and less lymph node metastasis in breast, colorectal and gastric cancer patients [252, 255, 256]. Therefore, active YAP expression is desirable for tumour growth.

Cells grown at low density also expressed greater amounts of the proliferation marker Ki67 which is routinely used as a cellular proliferative marker for prostate and breast tumours due to its presence in the active cell cycle phases G1, S, G2 and mitosis, and absence in G0 resting cells [257]. In addition, autophagy has been showed to be cell cycle dependent with the greatest levels of LC3-II accumulation in the G1 and S phases [258]. B16F1 cells were found to have elevated levels of both Ki67 and LC3-II at low density compared to high density suggesting these actively growing cells require more energy which is obtained through autophagy. Literature has also shown citrullinated protein expression is linked to increased proliferation in tumours. Immunohistochemical (IHC) analysis of prostate tumours showed elevated PAD2 which correlated with higher citrullinated protein expression and Ki67 levels, compared to healthy tissues [247]. The high levels of cellular proliferation marker Ki67 in prostate tumours and larger LNCaP tumours in male Balb/c athymic nude mice after overexpression of PADI2 [247], indicate PAD2 dependent citrullination promotes proliferation in tumour cells. Together, this suggests high levels of citrullination occur in actively growing tumour cells. IHC staining of B16F1 tumours from tumour bearing mice for nuclear Ki67 (active), ECV-1 and LC3 must be performed to confirm increased citrullinated vimentin expression correlates with higher levels of autophagy and proliferation.

Pavel et al (2018) also saw reduced LC3-II associated autophagy at high density which correlated with apoptosis induction in MCF10A, a non-cancerous cell line [243]. Hypoxia and starvation treatment of these cells at low density, but not high density, increased apoptosis. Western blot analysis showed increased LC3-II in low density

compared to high density cultures in B16F1, and clear vesicle staining of both ECV-1 and LC3 in single stained confocal images was observed. PAD expression and activity within autophagosomes have previously been reported in Rheumatoid Arthritis patient synoviocytes and B cells [204, 259]. Therefore, it is hypothesised that citrullinated vimentin would co-localise with LC3. Chloroquine treatment allowed better visualisation of LC3-II expression via western blotting, so could be used to better identify localisation of citrullinated vimentin within autophagosome, however this is yet to be confirmed. As single stained confocal images also showed cytoplasmic citrullinated vimentin expression, it is still unclear whether citrullination occurs within autophagosomes and whether proteins are modified prior to protein degradation or post-degradation within these or other double membrane vesicles. Traditionally, extracellular proteins processed via the endosomal/lysosomal pathway are presented via MHC class II but we know cytoplasmic proteins can also be presented through autophagy [260]. Autophagosomes then fuse with MHC class II containing compartments (MIICs) forming multi-vesicular bodies (MVBs) which expresses LC3-II [207]. To avoid apoptosis from high calcium levels, viable cells must undergo citrullination within these vesicles. Therefore, the presence of cytoplasmic citrullinated vimentin in confocal experiments could suggest the cells were unhealthy. Confocal experiments should be repeated for cell density dependent citrullinated vimentin expression to confirm signal seen in single stained images. In addition, annexin V expression or an intracellular apoptosis marker should be checked in cell density experiments to exclude early apoptosis as a reason for the cytoplasmic citrullination observed.

Interestingly, significant differences were only found after serum and amino acid (AS) and not serum (SS) starvation alone despite increases in percentage positives. It is possible that AS causes higher levels of autophagy than SS and therefore a greater amount of cargo is made available for citrullination. Further evidence to support this

theory is the activation of the general amino acid control (GAAC) pathway to enhance amino acid uptake in parallel to deactivation of mTOR (inhibitor of the autophagy) under serum and glutamine starvation. The addition of glutamine starvation resulted in the upregulation of amino acid transporters and only transient autophagy as seen by the decrease in LC3-II puncta after 12 hours, however serum plus amino acid starvation resulted in prolonged autophagy [261]. In addition, serum starvation alone did not effectively reactivate mTOR suggesting glutamine deprivation is required for increasing amino acid intake, reducing the need for autophagy. To simulate serum starvation in these experiments, glutamine supplemented RPMI was used. Therefore, this condition would allow reactivation of mTOR by the time of harvest (16 hours), blocking autophagy and reducing the level of phagosomal cargo for citrullination. To confirm higher levels of autophagy are induced by AS than SS, expression of mTOR and LC3-II should be assessed in both conditions.

An alternative explanation for the higher levels of citrullination in AS conditions could be due to autophagy induced cell death as indicated by Annexin V staining. During apoptosis the cell membrane will flip exposing phosphatidylserine (PS), a membrane phospholipid normally located on the cytoplasmic side. Annexin V will bind to cell surface PS highlighting unhealthy, apoptotic cells [262]. Cell death poses a major caveat in experiments when inducing autophagy *in vitro*, especially in the context of citrullination. Membrane flipping as indicated by annexin V staining, will allow an influx of calcium that could induce PAD activation increasing the chances of citrullination. AS treatment elevated apoptosis compared to untreated controls. When B16F1 cells were incubated with the sarco/endoplasmic reticulum Ca2+-ATPase inhibitor Thapsigargin (TG) alone, intracellular citrullinated vimentin expression doubled with limited toxicity compared to untreated controls suggesting upregulation in viable cells due to elevated levels of TG-dependent free calcium ions in the cytoplasm. However, the combination of AS and TG further increased apoptosis compared to AS alone.

This suggests AS induced high levels of cellular stress, pushing the cells from autophagy into apoptosis and TG further contributed to this effect. Autophagy was induced in almost 100% of glioma cells when nutrient starved for 1 day but this also induced apoptosis in 15% of cells and prolonged nutrient starvation further elevated cell death [263]. To confirm this, an intracellular apoptosis marker such as Caspase 3/7 should be stained alongside citrullinated vimentin to exclude apoptotic cells from the analysis. All data depended on specificity of EVC-1 antibody used to assess citrullination of vimentin.

Indeed, some cross-reactivity was found with the ECV-1 antibody in flow cytometry assays. In addition, a higher percentage of citrullinated vimentin positive cases were also seen in ovarian, lung and breast cancers compared to vimentin staining suggesting binding of ECV-1 to other proteins. However, cross-reactivity of this antibody was very low and in general ECV-1 only exhibited strong binding to citrullinated vimentin from microarray analysis. Cross-reactivity of anti-citrullinated protein antibodies (ACPA) in Rheumatoid Arthritis (RA) has been extensively reported. For example, an anti-citrullinated MBP antibody was able to detect citrullinated fibrinogen via western blotting, and an anti-citrullinated pro-filaggrin antibody cross reacted with a number of citrullinated Epstein-Barr virus (EBV) peptides from EBNA-1 [264, 265]. In addition, citrullinated antibodies have shown cross reactivity to multiple post-translational modifications including citrullination, homocitrullination and acetyllysine.[266]. The data from these experiments show much stronger recognition of citrullinated vimentin peptide sequences compared to the PAD2 *in vitro* deiminated Enolase, human BIP and human fibrinogen peptides detected. There were no similarities in amino acid residues between citrullinated vimentin and BIP/fibrinogen sequences however the small overlap in recognition may be due to the structural confirmation of the epitopes. A study by Ge et al (2019), analysed the structure of citrullinated peptides in antibody binding grooves. They

found interactions with 3 hydrogen bonds deep within the groove were essential for recognition of the citrulline residue in the side chain, which biased against positively charged arginine residues. However, hydrogen bonds between main chain residues and antibody complementary determining regions (CDRs) also contributed to the cross-reactivity between peptides [267].

Immunisation with MODI1 citrullinated peptides; Vim28cit, Vim415cit and Eno241cit, have shown great anti-tumour responses, increased survival and regression of tumours in B16F1 tumour bearing mice [1]. Even when mice with larger bulky tumours were immunised, most tumours showed complete regressed, but in some cases tumours were found to regress and grow back. When these tumours were analysed for expression of citrullinated vimentin they did not show any difference in percentage of citrullinated vimentin or PAD2/4 positive cells compared to unimmunised controls. However, the citrullinated vimentin MFI was significantly lower in progressing immunised tumours, suggesting although the number of cells expressing citrullinated vimentin was not affected, the level of citrullination per cell was lower in the immunised tumours. Antibody ECV-1 utilised throughout this work has been useful to detect upregulation of citrullinated vimentin in tumour cell lines in response to stress. Interestingly, mass spectrometry showed that the epitope that this antibody binds, Vim65-76cit, is not preferentially expressed in B16F1 tumours. This could explain the low levels of staining observed in B16F1 tumours, when compared to the cell line. It would be of interest to repeat the mass spectrometry on the cell line to see if Vim65-76 is more widely expressed. It is also of interest that Vim65-76cit is a commonly citrullinated epitope associated with stimulating antibody responses in RA in response to extracellular citrullination of vimentin [237]. There are many other non-tumour cells such as immune cells, fibroblasts and endothelial cells in the tumour microenvironment that interfere with the flow cytometric analysis of tumour cells. Although immune cells were excluded from the analysis using CD45 gating, a tumour

isolation cell kit should be used for a cleaner preparation and removal of non-tumour cells. CD45 staining did not show any difference in the percentage of immune cells between groups however this does not conclude a lack of immune response. Elevated IFNγ and IL-17 was released from splenocytes of immunised tumour bearing mice compared to unimmunised tumour bearing mice, showing subcutaneous immunisations resulted not only in local inflammation (as seen by tumour regression) but also a circulating immune repertoire to citrullinated epitopes [1]. Therefore, even though the total immune cell count was not changed, there may be a difference in the phenotype of tumour infiltrating immune cells. This can be assessed using a range of antigen presenting cell or T cell markers in B16F1 tumour flow cytometry assays.

Interestingly, unimmunised tumours displayed a partial EMT phenotype with the majority in an epithelial (cytokeratin expressing) state and a smaller percentage also in a mesenchymal (expressing vimentin) state. Immunisation caused phenotypical changes in the tumours as seen by the varied expressions of vimentin and cytokeratin, with no relation to tumour regression status. However, some immunised tumours showed a majority shift to a mesenchymal phenotype suggesting the aggressive, metastatic adaptation of the tumour in response to immunisation. Inflammation is known to induce tumour progression through the release of certain cytokines such as IL-6, TNF-α, IL-10 and TGF-β promoting angiogenesis and EMT [268]. It is possible that the vaccine induced inflammation resulted in EMT and that the increased vimentin expression presented more targets for citrullination, resulting in the great survival rates, of up to 100%, observed with MODI1 peptides compared to unimmunised controls [1, 2, 77].

Partial EMT was also observed in B16F1 culture *in vitro*, displaying high levels of vimentin, cytokeratin and E-cadherin. Expression of these markers was not affected by density at 24 hours but there was a slight decrease in e-cadherin expression with

increasing density at 48 hours. In addition, there was a reduction in epithelial markers cytokeratin and E-cadherin was found in prolonged culture up to 72 hours at medium density. Vimentin levels remained constant with ~100% of cells expressing this mesenchymal marker. As discussed earlier, cultures incubated for long periods would consist of densely packed cells with no contact inhibition. YAP expression induced the expression of mesenchymal phenotype related transcription factors and cytoskeletal proteins Snail, fibronectin, vimentin and n-cadherin and reduced epithelial markers occludin and e-cadherin in lung tumour and MCF10A (non-malignant breast epithelial) cells, correlating with increased metastasis and migration [269, 270]. This indicates a regulatory role of TEAD controlled genes in the induction of EMT and could explain the reduced cytokeratin and e-cadherin expression seen in long B16F1 cultures. However, these experiments were preliminary and must be repeated. Protein and gene expressions of mesenchymal markers would be useful to confirm the induction of EMT in these cultures.

Co-culture with immune cells or pre-incubation with inflammatory cytokines can induce EMT *in vitro* which resulted in reduced T cell viability and an increase in regulatory T cells [271]. The most influential cytokine for EMT induction is TGF-β, which mediates this conversion through Smad, ErK/MAPK and Pi3K/Akt pathways [233]. TGF-β treatment did not induce phenotypical changes in B16F1 however incubation with a TGF-β inhibitor increased expression of epithelial marker E-cadherin. Many tumour cells secrete TGF-β as a method of evading T cell cytotoxicity [272, 273], so it is possible that B16F1 also releases this cytokine. Experiments need to be repeated and cell culture supernatants need to be checked for TGF-β levels.

Citrullinated vimentin was also expressed in human cancers head and neck (58%), sarcoma (80%), osteosarcoma (86%), renal (36%), ovarian (97%), lung (62%) and ER negative breast (90%). The expression levels varied between cancers with the

majority displaying low to moderate expression, and only sarcoma, ovarian and breast cancer displaying cases of high expression. Due to the difficulty in producing and isolating a citrullinated protein specific antibody, to date no studies have reported expression levels of citrullinated vimentin in human cancer tissues via immunohistochemistry. Citrullination in cancer is measured by anti-citrulline antibodies, PAD expression or analysis of tumour cell lines [182, 247, 274]. Citrullinated vimentin expression was mostly cytoplasmic with some nuclear staining. This correlates with findings from Baka et al (2011) who showed cytoplasmic citrullination in lung adenocarcinoma TMAs [274]. High expression significantly correlated with survival in lung (P=0.016) but not ovarian (P=0.164) or breast (P=0.393) cancers. Lung cancer patients also showed better survival with PAD2 and autophagy marker Ambra1 expression and there was a positive correlation between citrullinated vimentin expression with both markers. It is known that smoking is a causative factor for lung cancer with links to RA, and that PAD enzyme levels are higher in smokers [274, 275]. Increased T cell responses to citrullinated vimentin peptides 60-75cit and 415-433cit have also been reported in cigarette smoke mouse models compared to a non-smokers group. In this environment, IFNγ levels were reduced and IL-10 secretion increased, promoting suppression of T cells [275]. It is possible that the high levels of citrullination in lung cancer provide neoepitopes for the immune system to recognise and counterattack growing tumour cells.

Interestingly, the reverse was seen in ovarian and breast TMA cohorts, where low expression of citrullinated vimentin correlated with increased survival rates. Better patient survival was also seen in ovarian cancer patients with no PAD2 expression and there was no correlation with Ambra1 expression. However, there was a positive correlation between citrullinated vimentin and PAD2 and Ambra1 expression in both ovarian and breast cancers. High citrullination in these cancers may promote metastasis, decreasing chances of survival. Research has shown PAD inhibition

reduced proliferation, migration and invasion of triple negative breast cancer (TNBC) and regulated cytoskeletal proteins inducing mesenchymal to epithelial transition (MET) in mammary ductal carcinoma cells [181, 276]. Although 40% of cases were negative for PAD2 in the breast cancer TMA cohort, both ovarian and breast cancers displayed some cases with moderate to high expression. In addition, PAD4 was involved in citrullination of the extracellular matrix (ECM) in metastatic colorectal cancer, modifying fibrillin-1, emilin-1 and collagens in metastatic tumours compared to adjacent normal liver tissues. Citrullination of collagen in the ECM was shown to be important for adhesion suggesting metastatic tumour cells use this mechanism to establish a new base [248]. PAD4 levels in all cancer TMAs stained were high for nuclear expression. The lung TMA cohort also expressed mostly low to moderate citrullinated vimentin expression with no high expressing cases. Ovarian and breast cancers showed more cases with moderate and high citrullinated vimentin expression. Tumour associated inflammatory cells usually provide a good prognosis for the cancer, as seen by increased survival rates with tumour associated neutrophils (TANs) and tumour-infiltrating lymphocytes (TILs) [277-279]. However as mentioned earlier, inflammation can also promote tumour progression. High percentages of tumour-associate macrophages (TAMs) were associated with reduced disease free survival and overall survival in colorectal cancer [277]. This is normally the case with chronic inflammation where TAMs produce angiogenic factors and release cytokines such as TNF-α and IL-6 which promote tumour survival through NF-κB/JNK and JAK/STAT pathways respectively, regulating tumour suppressor genes. Both cytokines have also shown to induce cancer stem cell development [280]. We know citrullinated epitopes can be recognised by T cells and induce the release of inflammatory mediators [1, 2, 77, 220]. High levels of citrullinated vimentin expression witnessed in some ovarian and breast cancers may have promoted chronic inflammation and therefore resulted in reduced survival. This could indicate a delicate balance in citrullination levels for patient prognosis where low levels of citrullinated

vimentin can sufficiently prime an immune response without promoting excessive tumour proliferation and metastasis through chronic inflammation.

To conclude, low cell density plated cells were the best produces of citrullinated vimentin, the most proliferative and with the highest levels of autophagy. Although nutrient deprivation significantly induced citrullinated vimentin expression, the treated cells also showed high levels of apoptosis which could have produced false positives in these assays. Apoptosis could be the leading cause of cytoplasmic citrullination due to a high influx of calcium. As previous research has shown citrullinated epitopes are presented through autophagy via MHC class II, we know these target cells are viable. Citrullinated vimentin expression was seen in a range of human cancers highlighting this as a broad target antigen.

4 The importance of MHC class II expression in tumours

4.1 Introduction

4.1.1 MHC regulation by CIITA

As discussed in Chapter 1, processed peptides can be presented on the surface of cells via the Major Histocompatibility Complex (MHC). Two classes exist; MHC class I which presents peptides to CD8 T cells and MHC class II which presents to CD4 T cells. There are many molecules involved in the MHC class II presentation pathway such as invariant chain or CD74 (Ii), and MHC-associate molecules DM (HLA-DM) and DO (HLA-DO) [18]. Gene expression of all MHC class II alleles, HLA- DR, - DP, -DQ and the associated molecules HLA-DM, -DO, are under the control of the Class II Transactivator (CIITA) [281, 282]. This transcriptional activator is also known to regulate MHC class I expression and many non-MHC related genes [281, 283]. CIITA is thought to modulate MHC class II expression through the upstream MHC class II specific regulatory module SXY which consists of four sequence boxes; S, X, X2 and Y. The latter three bind to regulatory factors RFX, CREB and NFY respectively (Figure 4.1) [282].

Activation and expression of CIITA is also regulated at the transcription level. Four distinct promotors known as pI, pII, pIII and pIV have been identified (Figure 4.1) [284]. The function of pII is still unknown but advancements have been made in understanding pI, pII and pIV mechanisms. Each of these promotors generate three different isoforms of CIITA that vary at their 5' ends [282]. CIITA pI is responsible for constitutive MHC class II expression in conventional dendritic cells (DCs) and macrophages, whereas pIII controls expression in B cells, T cells and plasmacytoid

DCs [285]. The pIV is the main isoform expressed after IFN-γ treatment controlling the induction of MHC class II in non-professional antigen presenting cells [284]. However, there is some evidence of pIV activation by IFNγ in B cells [286]. Upstream of pIV is a GAS element, E box and interferon response element (IRE) that requires binding of STAT1, USF-1 and IRF-1 respectively to activate the promotor [287]. IFNγ regulates the expression of STAT1 and IRF-1, and coordination between STAT1 and the other transcription factors are required for successful CIITA induction via pIV [285, 287-290]. Induction and recruitment of these transcription factors can be inhibited by statins, therefore modulating CIITA induced MHC class II expression [291].

Figure 4.1

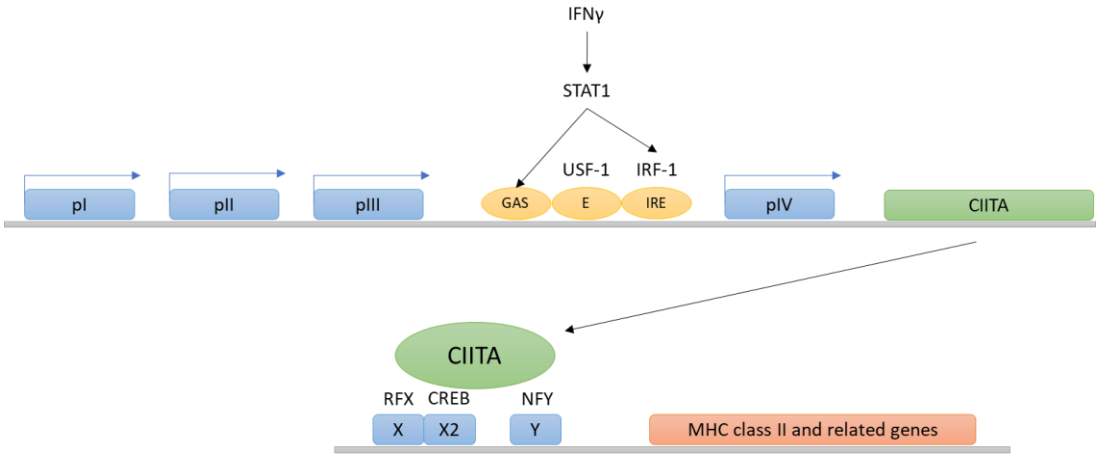


Figure 4.1 Activation of CIITA via four different promoters; pI, pII, pIII and pIV. The latter is IFNγ inducible and requires binding on STAT1, USF-1 and IRF-1 to upstream GAS element, E box and interferon responsive element (IRE) for activation. CIITA exhibits its effects through the SXY regulatory module that binds transcription factors RFX, CREB and NFY and induces expression of MHC class II related genes.

4.1.2 Aims

Citrullinated peptides are presented by MHC class II inducing a CD4 response. In this chapter we investigated the expression of MHC class II in human cancers. We also assessed the upregulation of MHC class II in ovarian and breast cancer cell lines after IFNγ treatment and the involvement of CIITA in this response.

4.2 Results

4.2.1 MHC class II expression in human cancer cell lines

MHC class II (MHC-II) has been thought to be restricted to only antigen presenting cells (APCs) but literature describes many non-APCs with the ability to upregulate MHC-II expression in response to inflammatory cytokines such as Interferon gamma (IFNγ). The levels of MHC-II were assessed in a panel of Triple Negative Breast cancer (TNBC) and ovarian cancer cell lines after overnight incubation with various concentrations of IFNγ. On average, between 5-45% of untreated tumour cells were positive for MHC-II varying between cells lines tested within a cancer type. Overnight incubation with 1000U/mL IFNγ significantly induced MHC-II in 3/4 ovarian cancer cell lines and 2/4 TNBC cell lines ($P=\leq 0.01$ and $P=\leq 0.001$ respectively) (Figure 4.2a).

Titration experiments with IFNγ show the highest level of MHC-II expression was reached with 100U/mL IFNγ for MDA-MB-231 (75%), MDA-MB-468 (15%), OVCAR 8 (37%), SKOV3 (45%), OVCAR3 (50%), OAW42 (80%) after overnight incubation, with no further increases in percentage with increasing IFNγ concentration (Figure 4.2b(i) and (ii)). There was a smaller increase in median fluorescence intensity (MFI) readings for these cell lines with increases only found for MDA-MB-231 and OAW42 (Figure 4.2b(iii)) and b(iv)). This suggests IFNγ exposure converts an MHC-II negative cell to a positive cell rather than increasing the number of MHC-II molecules on the cell surface. Repeated experiments with 1000U/mL IFNγ showed lower MHC-II expression in untreated OAW42 (10-20%) with no elevation after treatment (Figure 4.2a). Only two of the cell lines tested, BT549 and DU4475 displayed no changes in percentage of MFI or MHC-II positive cells at any IFNγ concentration, however expression in DU4475 was constant at 45%-50% (Figure 4.2b(i) and b(iii)).

Figure 4.2

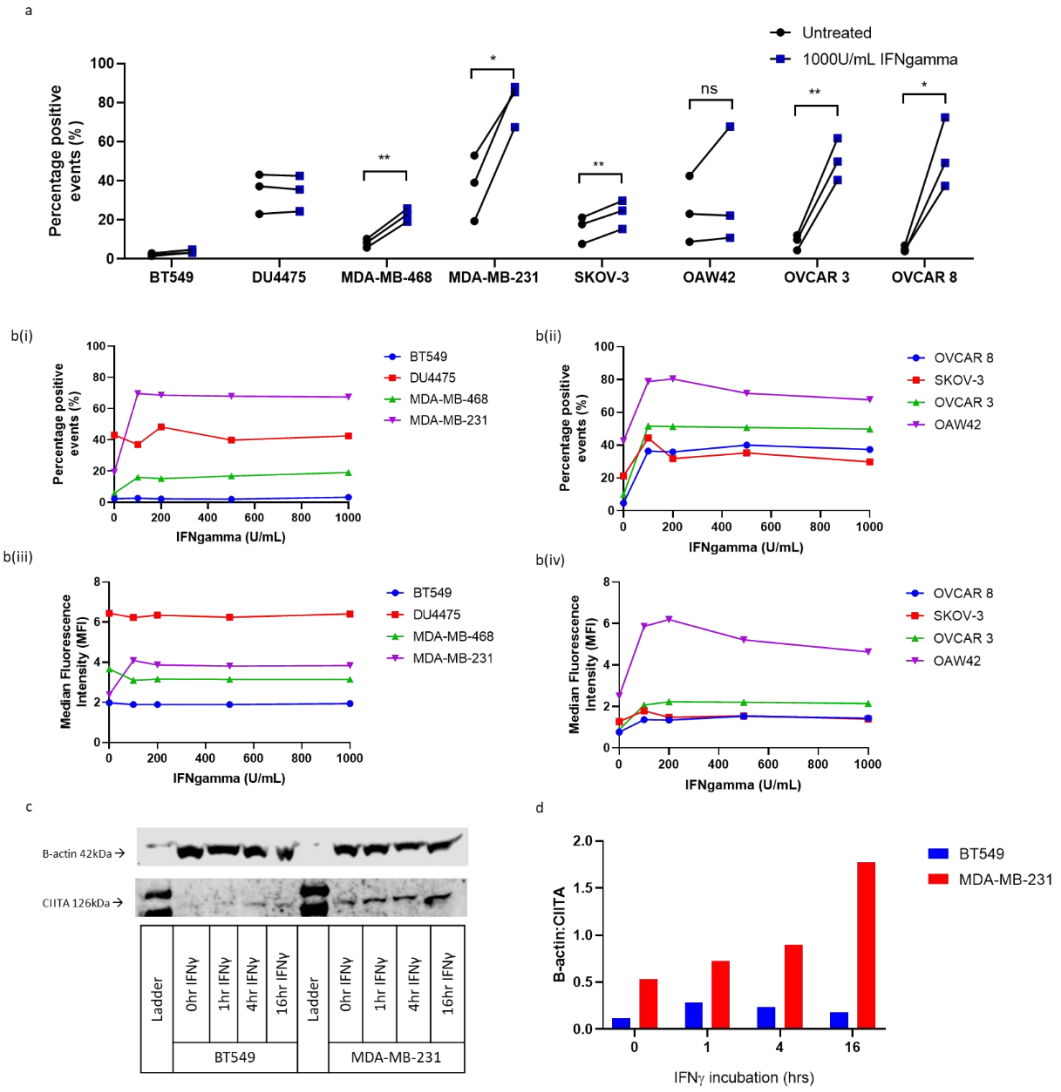


Figure 4.2 Induction of MHC class II expression in human Triple Negative Breast cancer (TNBC) BT459, DU4475, MDA-MB-468 and MDA-MB-231 and Ovarian cancer cell lines OVCAR 8, SKOV-3, OVCAR 3 and OAW42 with overnight titration of Interferon Gamma (IFNγ), N=3. Paired t test significance ns = P≥0.05, * = P≤0.01, ** = P=≤0.001 (a). Percentage and median fluorescence intensities (MFI) of MHC class II positive events in TNBC (b(i) and (iii)) and Ovarian cancer (b(ii) and (iv)) cell lines treated with or without IFNγ for 16 hours, N=1. CIITA protein expression in BT549 and MDA-MB-231 cell lines after treatment with IFNγ for 0, 1, 4 and 16 hours (c). CIITA signal normalised against B-actin (d). N=1.

The expression of MHC-II is tightly regulated by the CIITA and tumour cells expressing this activator can effectively prime CD4 T cells [292]. However not all tumour cells produce CIITA protein despite its detection at a transcriptional level, resulting in a loss of MHC-II expression [293]. BT549 (class II negative) and MDA-MB-231 (IFNγ inducible class II) were tested for CIITA protein expression after incubation with 1000U/ml IFNγ after 0, 1, 4 or 16 hours. As predicted, BT549 was negative for CIITA in untreated conditions and failed to upregulate CIITA even after overnight incubation with IFNγ. In contrast, MDA-MB-231 showed low levels of CIITA protein expression in untreated conditions which was further induced with increasing IFNγ incubation times (Figure 4.2c and d). Taken together, the results indicate that the lack of MHC-II expression in BT549 was probably due to absence of IFNγ-dependent CIITA. However, this data was preliminary and needs to be repeated, including the other TNBC and ovarian cancer cell lines tested via flow cytometry.

4.2.2 Gene expression of CIITA, IRF-1 and HLA-DPA1 in human cancers

To further investigate the importance of CIITA expression, the Cancer Genome Atlas (TCGA) was used to assess RNA levels of CIITA, HLA class II histocompatibility antigen DP alpha 1 chain (HLA-DPA1) and DP beta chain 1 (HLA-DPB1) which encode the alpha and beta chain of the DP allele respectively, and Interferon Regulatory Factor (IRF-1) which regulates the transcription of IFNγ and IFNγ related genes in various cancers.

A high probability of survival over a 5-year period (1825 days) was found in melanoma, head and neck, lung, breast, ovarian and sarcoma cancers, when CIITA expression was greater than the median (Figure 4.3a-f and Table 4.1). However, CIITA expression was only significantly correlated with survival in melanoma and head and neck cancers (P=1.89e-5 and P=0.03632 respectively) (Figure 4.3a and b). Somatic mutations including deletion, missense and silenced were assessed for their correlation with survival in the cancer panel. The frequency of a mutation in the CIITA gene was low in many cancers with <10 cases in ovarian, pancreatic, breast, renal (papillary and clear cell) and sarcoma despite the large total number of cases analysed (Table 4.1). However, in some cancers there was a higher occurrence of mutations e.g 12, 24 and 28 cases in head and neck, lung and colorectal cancer respectively. The greatest number of mutations was seen in melanoma (48 out of 451 total cases) and this was significantly correlated with 5-year survival (P=0.0228) (Figure 4.3g). A similar trend was also seen for breast cancer however the number of cases with mutations was much smaller (only 8 out of 790) and this was not significant (P=0.4391) (Figure 4.3j). Kaplan-Meier curves highlight better survival probability in head and neck, lung, ovarian and sarcoma in cases without a mutation in the CIITA gene but this was not significantly greater than those with a mutation (Figure 4.3h, i, k and l).

Figure 4.3

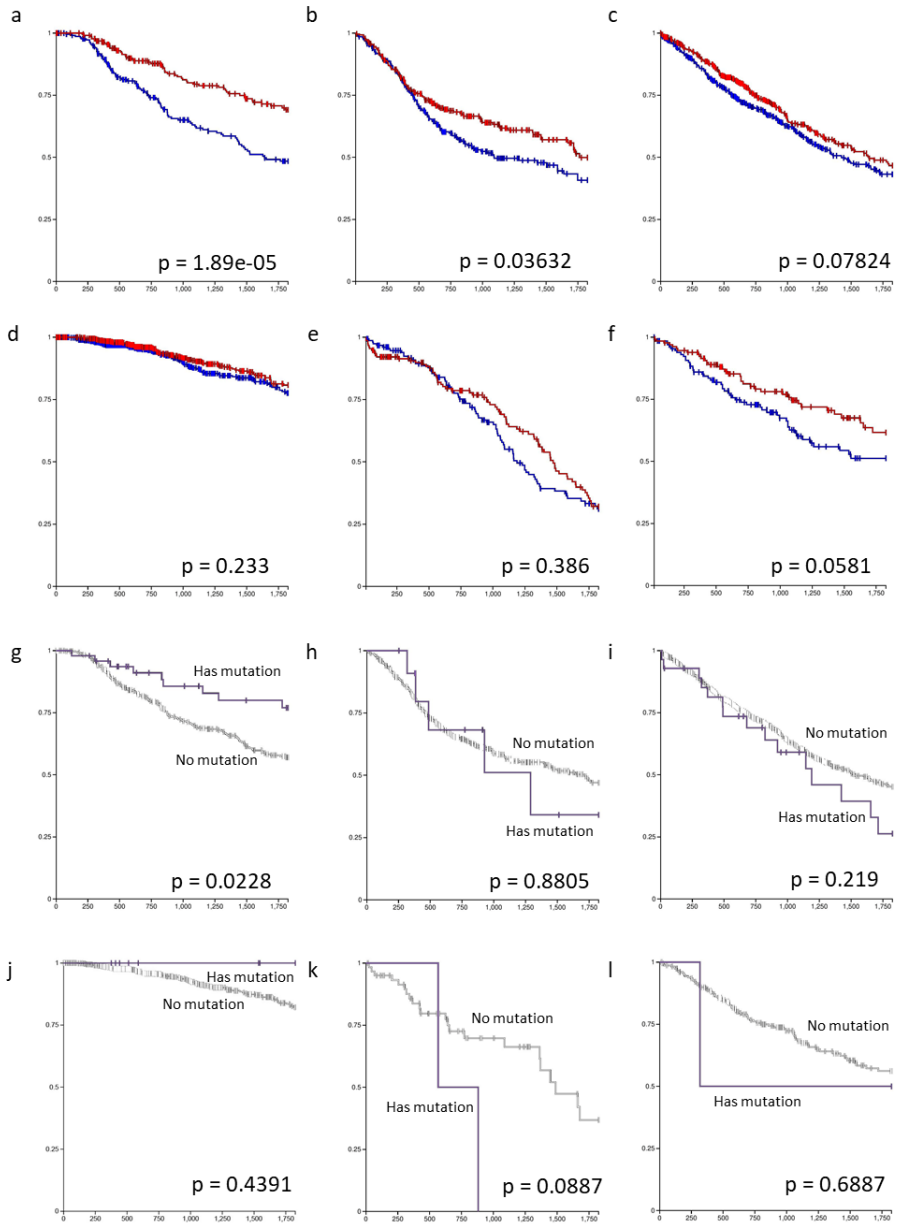


Figure 4.3 Kaplan-Meier curves showing the 5 year survival probability correlated with CIITA expression (a-f) and with or without somatic mutations (g-l) for cancer types melanoma (a and g), head and neck (b and h), lung (c and i), breast (d and j), ovarian (e and k) and sarcoma (f and l). Median used to divide samples into two groups for CIITA expression; blue line < median, red line > median. Medians and sample numbers shown in Table 4.2. TCGA database analysed using UCSC Xena. Chi-squared log rank test significance P≤0.05.

Table 4.1

Cancer type	Overall Survival		Median	Number of Samples		Survival cutoff (Days)	Significance of mutation relating to survival (p-Value)	White-No mutation	Purple-Has mutation
	Significance	p-Value		Group A (Blue) < median	Group B (Red) >median				
Melanoma	Yes	1.89E-05	8.016	229	229	1825	0.0228	403	48
Head and Neck	Yes	0.03632	7.939	283	282	1825	0.8805	495	12
Lung	No	0.07824	8.752	556	506	1825	0.219	950	28
Ovarian	No	0.386	9.292	154	153	1825	0.0887	61	2
Pancreatic	No	0.8372	8.905	92	91	1825	0.8942	175	2
Breast	No	0.233	7.858	609	605	1825	0.4391	782	8
Renal (kidney papillary cell)	No	0.2301	7.818	162	160	1825	0.00000193	278	2
Renal (kidney clear cell)	No	0.8557	8.561	303	303	1825	0.3143	364	4
Sarcoma	No	0.0581	7.551	133	135	1825	0.6887	234	2
Colorectal	No	0.3194	7.173	214	216	1825	0.06212	353	24

Table 4.1 Expression of CIITA in various cancers based on TCGA database analysed using UCSC Xena. Chi-squared log rank test significance P≤0.05.

As there are three classical MHC-II genes in humans that code for HLA-DP, -DQ and -DR, and many different alleles exist within each haplotype, it is difficult to correlate MHC-II gene expression with survival. As, the MHC-II DP molecule is less polymorphic and has been shown to present citrullinated peptides [77], MHC-II expression in the TCGA databases were investigated by analysis of HLA-DPA1 and beta 1 chain (HLA-DPB1). These genes encode for the alpha and beta chain of the DP molecule which forms a dimer to complete the MHC class II allele. The majority of cancers analysed showed greater survival probability with HLA-DPA1 and HLA-DPB1 expression, including breast, head and neck, lung, melanoma, ovarian, renal and sarcoma (Appendix 4). However, this was only significant for three cancers; HLA-DPA1 expression was significantly correlated with survival in melanoma (P=9.386e-5), head and neck (P=0.03058) and sarcoma (P=0.02667) (Table 4.2a and Figure 4.4a-c). All three of these cancers also showed better survival with greater CIITA expression (Figure 4.3a, b and f). Significant association between HLA-DPB1 and survival was observed in melanoma (P=2.224e-5) and renal papillary cell (P=5.727e-3) (Table 4.2b and Figure 4.4d and e). There was not much difference in survival between colorectal cancer patients with high vs low HLA-DPA1 and HLA-DPB1 but

slightly improved prognosis was found in HLA low groups by 5 years (Appendix 4). A clear difference in survival was observed in pancreatic cancer, where survival was reduced in patients with HLA-DPA1 and HLA-DPB1 expression after 2 years (Appendix 4).

Table 4.2

a

Cancer type	Overall Survival		Median	Number of Samples		Survival cutoff (Days)
	Significance	p-Value		Group A (Blue) < median	Group B (Red) >median	
Melanoma	Yes	9.386E-05	12.24	230	228	1825
Head and Neck	Yes	0.03058	11.63	283	282	1825
Lung	No	0.07622	12.86	556	506	1825
Ovarian	No	0.3473	12.52	154	153	1825
Pancreatic	No	0.9244	12.55	92	91	1825
Breast	No	0.3335	12.26	606	608	1825
Renal (kidney papillary cell)	No	0.2299	12.15	162	160	1825
Renal (kidney clear cell)	No	0.5259	13.54	302	304	1825
Sarcoma	Yes	0.02667	12.01	133	132	1825
Colorectal	No	0.8667	11.07	214	216	1825

b

Cancer type	Overall Survival		Median	Number of Samples		Survival cutoff (Days)
	Significance	p-Value		Group A (Blue) < median	Group B (Red) >median	
Melanoma	Yes	2.224E-05	11.7	231	227	1825
Head and Neck	No	0.1037	11.21	283	282	1825
Lung	No	0.12	12.27	557	505	1825
Ovarian	No	0.1573	11.36	153	154	1825
Pancreatic	No	0.4016	12.28	91	92	1825
Breast	No	0.07531	11.54	605	609	1825
Renal (kidney papillary cell)	Yes	5.727E-03	11.65	162	160	1825
Renal (kidney clear cell)	No	0.6656	12.79	302	304	1825
Sarcoma	No	0.1668	11.6	132	133	1825
Colorectal	No	0.603	10.42	213	217	1825

Table 4.2 Expression of HLA-DPA1 (a) and HLA-DPB1 (b) in various cancers based on TCGA database analysed using UCSC Xena. Chi-squared log rank test significance. P≤0.05.

Figure 4.4

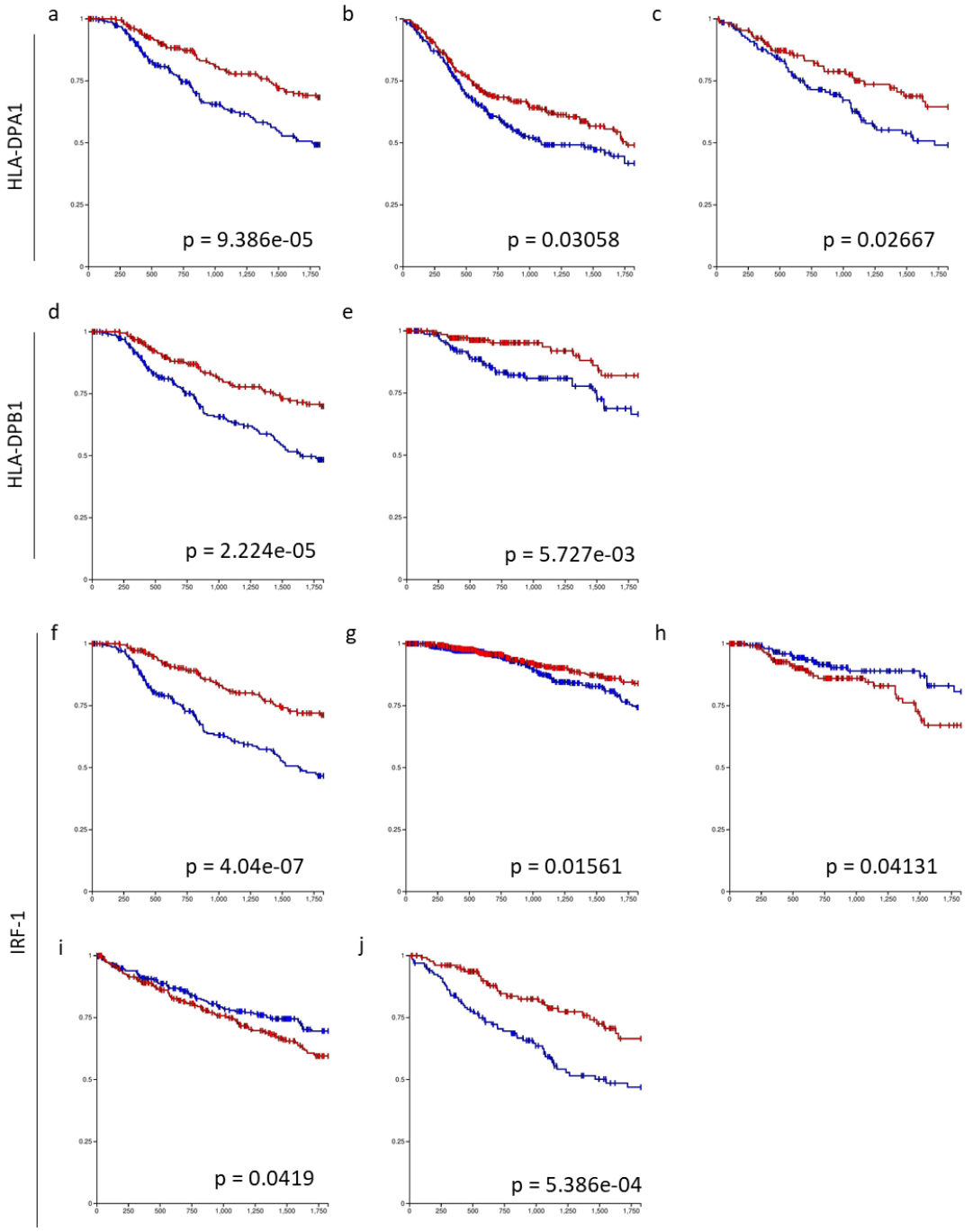


Figure 4.4 Kaplan-Meier curves showing the 5-year survival probability correlated with HLA-DPA1 expression for cancer types melanoma (a), head and neck (b) and sarcoma (c), with HLA-DPB1 for melanoma (d) and renal papillary cell (e), and with IRF-1 expression for cancer types melanoma (f), breast (g), renal- papillary cell (h), renal- clear cell (i) and sarcoma (j). Median used to divide samples into two groups for CIITA expression; blue line < median, red line > median. Medians and sample

numbers shown in Tables 4.3 and 4.4. TCGA database analysed using UCSC Xena. Chi-squared log rank test significance P≤0.05.

As previously discussed, CIITA expression can be upregulated by IFNγ. This is partly regulated by the interaction of IRF-1 to its binding site along promotor IV (pIV) of the CIITA gene [284]. Therefore, it was hypothesised that IRF-1 levels in tumours would positively correlate with CIITA and a higher probability of patients whose tumours express these markers having better survival. Kaplan-Meier curves show expression of IRF-1 was positively correlated with survival of patients in 3 (melanoma, head and neck and sarcoma) out of 10 cancers studied (Table 4.3 and Figure 4.4f, g and j). The opposite was observed in renal cancers, both papillary cell and clear cell carcinomas, where higher expression of IRF-1 significantly resulted in a poorer survival of cancer patients (P=0.04131 and P=0.0419 respectively) (Figures 4.4h and i). IRF-1 expression was not significantly correlated with survival in patients with head and neck, lung, ovarian, pancreatic or colorectal cancer (Table 4.3). As expected, strong positive correlations were found between CIITA and IRF-1 expression in almost all cancers with Pearson correlation coefficients ranging from 0.5-0.85 except for pancreatic cancer which displayed moderate correlation between these two factors (P=0.4512) (Table 4.4). Again, the best results were seen in melanoma, showing the strongest correlation between IRF-1 and CIITA (Pearson rho = 0.8582) (Figure 4.5).

Table 4.3

Cancer type	Overall Survival		Median	Number of Samples		Survival cutoff (Days)
	Significance	p-Value		Group A (Blue) < median	Group B (Red) >median	
Melanoma	Yes	4.04E-07	9.96	228	230	1825
Head and Neck	No	0.05771	10.85	283	282	1825
Lung	No	0.7143	10.58	553	509	1825
Ovarian	No	0.2493	10.72	154	153	1825
Pancreatic	No	0.1468	10.44	92	91	1825
Breast	Yes	0.01561	10.02	608	606	1825
Renal (kidney papillary cell)	Yes	0.04131	9.332	162	160	1825
Renal (kidney clear cell)	Yes	0.0419	10.48	303	303	1825
Sarcoma	Yes	5.386E-04	9.913	133	132	1825
Colorectal	No	0.9	10.79	215	215	1825

Table 4.3 Expression of IRF-1 in various cancers based on TCGA database analysed using UCSC Xena. Chi-squared log rank test significance. P≤0.05.

Table 4.4

Cancer type	IRF1 vs CIITA correlation	
	Pearson's rho	p-Value
Melanoma	0.8582	1.083e-138
Head and Neck	0.7573	2.136e-106
Lung	0.6172	1.826e-119
Ovarian	0.7083	3.752e-48
Pancreatic	0.4512	1.469e-10
Breast	0.7281	1.314e-201
Renal (kidney papillary cell)	0.5079	1.409e-22
Renal (kidney clear cell)	0.6622	1.082e-77
Sarcoma	0.6769	3.177e-37
Colorectal	0.7378	1.075e-75

Table 4.4 Correlation between CIITA and IRF-1 RNA expression in various cancers. Analysis of TCGA dataset using UCSC Xena. Pearson's rho significance = P≤0.05

Figure 4.5

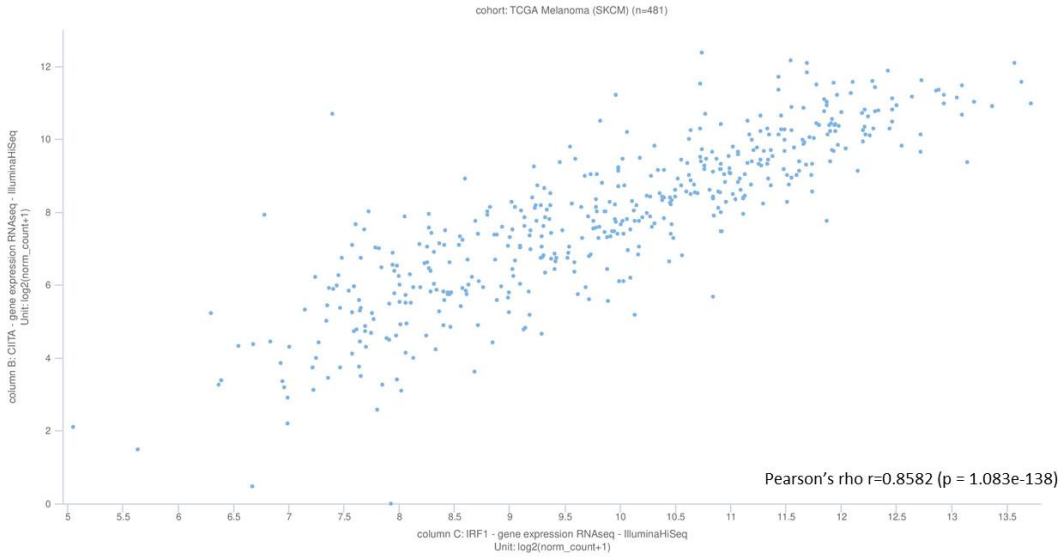


Figure 4.5 Correlation analysis between CIITA and IRF-1 RNA expression in melanoma from TCGA database. UCSC Xena used for analysis. N=481 and 634 respectively.

4.2.3 MHC class II protein expression in human cancers

As gene expression of CIITA was seen in a wide range of tumours it was important to determine if MHC-II protein expression was also observed. A pan class II monoclonal antibody that recognises all HLA- DR, DP and DQ proteins was used to stain a panel of human cancer tissue microarrays (TMAs) including head and neck, sarcoma, osteosarcoma, renal, ovarian, lung and breast (ER negative). H scoring was used to evaluate expression as negative (0), low (1-100), medium (101-200) or high (201-300). TMA staining and scoring performed by Mohammed Gijon (Scancell Ltd). The percentage of MHC-II positive cases were calculated from the number of TMAs scored as low, medium or high within an array data set. MHC-II staining intensity shown in Figure 4.6c with examples of negative, low, moderate and high staining cases for ovarian, lung and breast cancers. Expression was found in both the cytoplasm and membrane of tumour cells.

The total number of cases in each cancer array ranged from 67-276 and approximately 26-55% of cases from all cancers where positive for MHC-II (Table 4.5a). The lowest percentage of MHC-II positive cases was found in ovarian, lung and breast TMAs at 31%, 26.9% and 27.2% respectively. More than 40% of sarcoma and renal cancers were positive whilst head and neck and osteosarcoma TMAs had the highest percentage of MHC-II positive cases at > 50% (Table 4.5). The mean MHC-II H scores were similar in all cancers tested, at approximately 25-30, however strong positive scores from 100-300 were also observed (Figure 4.6b). Despite the greater percentage of positive cases in head and neck and osteosarcoma cancers, the majority of these were classified with low MHC class II expression, 49% and 48% respectively, with 10% of cases expressing moderate levels (Figure 4.6a). Renal and sarcoma cancers also showed mainly low expression (~40%) with 5-10% moderate expression, but the later also had a few cases (<2%), that depicted high levels of

MHC-II. Interestingly, cancers with the greatest percentage of cases expressing high MHC-II were ovarian, lung and breast, which were also found to have the lowest percentage of total positive cases (Figure 4.6 and Table 4.5). These results show that MHC-II is expressed by a wide range of human tumours. This may be further enhanced by cancer vaccines which stimulate IFNγ release at the tumour site .

Table 4.5

Cancer Type	Positives	
	Cases	Percentage
Head and Neck	59/107	55.1
Sarcoma	35/80	43.8
Osteosarcoma	42/79	53.2
Renal	32/67	47.8
Ovarian	54/174	31.0
Lung	53/197	26.9
Breast Erneg	75/276	27.2

Table 4.5 Percentage of MHC class II positive cases in a range of cancers based on H score percentages. TMAs scored as low, medium or high considered as 'positive'.

Figure 4.6

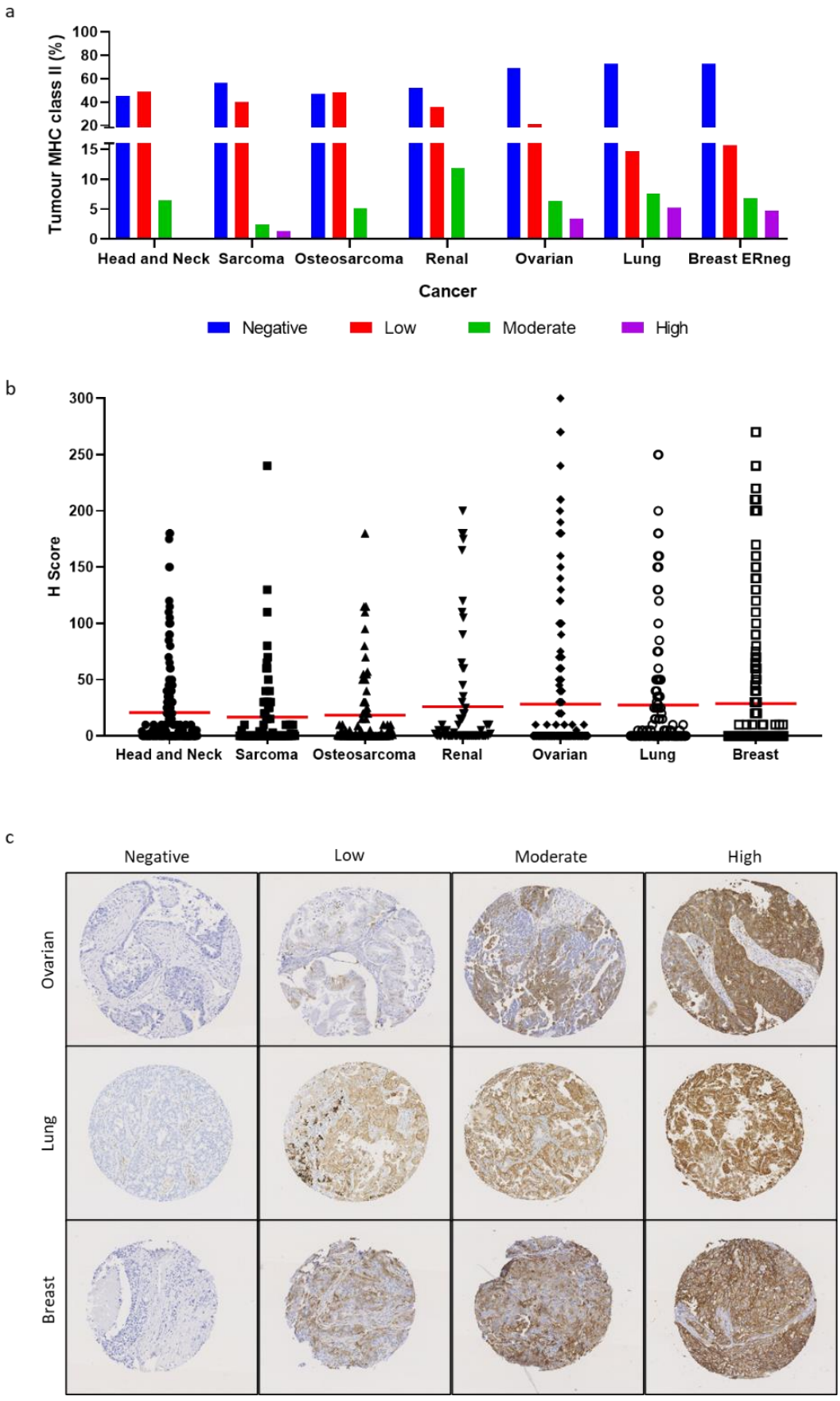

a
Tumour MHC class II (%)
100
80
60
40
20
15
10
5
0
Head and Neck
Sarcoma
Osteosarcoma
Renal
Ovarian
Lung
Breast ERneg
Cancer
Negative
Low
Moderate
High
b
H Score
300
250
200
150
100
50
0
Head and Neck
Sarcoma
Osteosarcoma
Renal
Ovarian
Lung
Breast
c
Negative
Low
Moderate
High
Ovarian
Lung
Breast

Figure 4.6 H score analysis of MHC class II divided into negative, low, moderate and high expression in a range of cancer TMAs (a). Individual cases plotted for each cancer with red bar representing the median value (b), Examples of MHC class II staining showing negative, low, moderate and high intensity in ovarian, lung and breast (ER negative) cancers. Cytoplasmic and membrane staining in tumour cells (c).

Clinical data was available for ovarian and lung TMA data cohorts; Kaplan-Meier curves were produced to determine the survival probability of patients with or without MHC-II expression. It was hypothesised that the presence of MHC-II increases the chance of survival in cancer patients. This was true for the breast cancer cohort which showed patients positive for MHC-II had a significantly better overall survival compared to those without expression (P=0.004) (Figure 4.7c(i)). MHC-II expression was also positively correlated with disease free interval survival and lower occurrence of distant metastasis (Figure 4.7c(i) and (ii)). However, expression was not significantly correlated with overall survival in ovarian or lung cancers when divided into negative and positive populations (P=0.883 and P =0.343 respectively) (Figure 4.7a and b(i)). However, lung cancer patients with positive expression showed improved survival probability in the first 12 years (Figure 4.7a). There was no difference in patient survival between MHC-II positive and negative cases in ovarian cancer throughout the 20-year data collection period (Figure 4.7b(i)). When dividing the ovarian cancer MHC-II expression data into negative, weak and strong populations, there was a significant difference in survival between the 3 groups (P=0.035) (Figure 4.8a). Survival was significantly reduced in ovarian patients with strong compared to weak MHC-II expression, but not those with negative expression as shown by post-hoc analysis (P=0.008 and P=0.332 respectively) (Figure 4.8b). Weak MHC-II expression initially correlated with better survival compared to no expression, but rates dropped to lower levels after the initial 19-year period and this was not significant (P=0.194) (Figure 4.8b). This suggests that low levels of MHC-II expression were better than no expression but high levels correlated with a poor

prognosis in ovarian cancer. These results suggest that up regulation of MHC-II may initially allow immune recognition and a good prognosis but chronic or high expression may drive to a non-productive tumour promoting immune response. Therefore, moderate MHC-II expressing or negative tumours may show a better response to a cancer vaccine than high expressing tumours.

Data has previously been reported to support evidence of the IFNγ receptor as a prognostic marker in ovarian cancers [294]. Positive expression of IRF-1 and IFNγ receptor was significantly correlated with increased survival (P=0.036 and P=0.016 respectively) (Figure 4.7b(ii) and b(iii)).

Figure 4.7

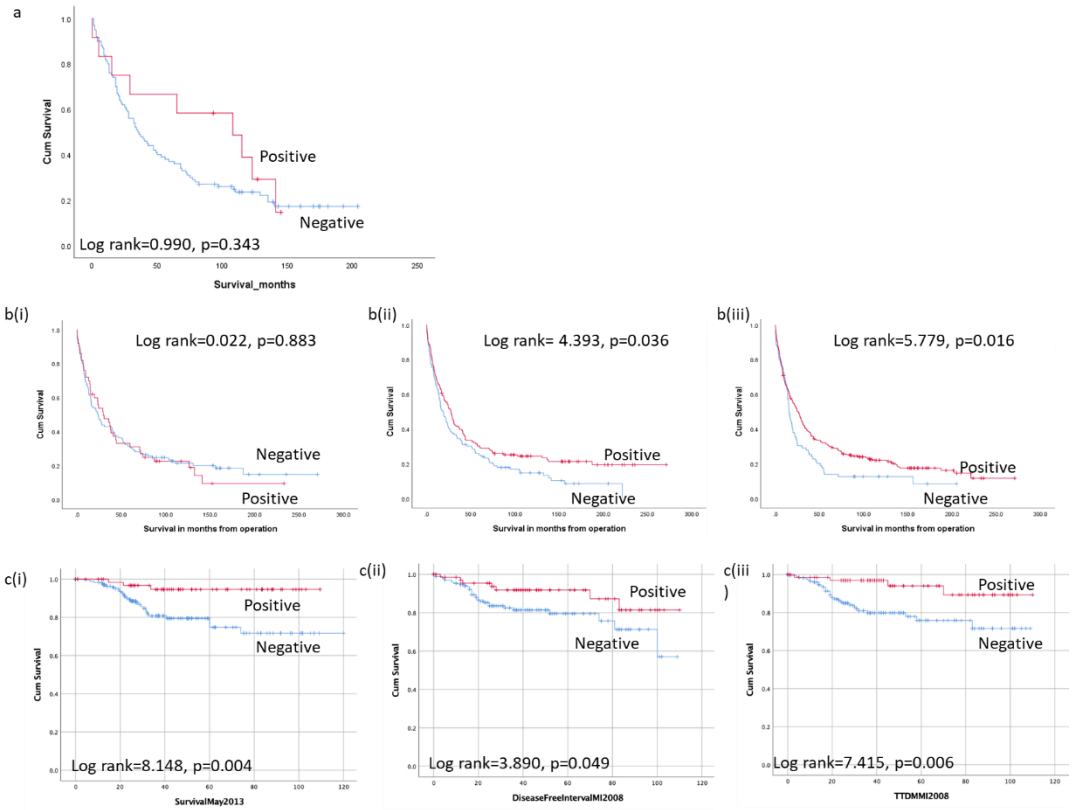
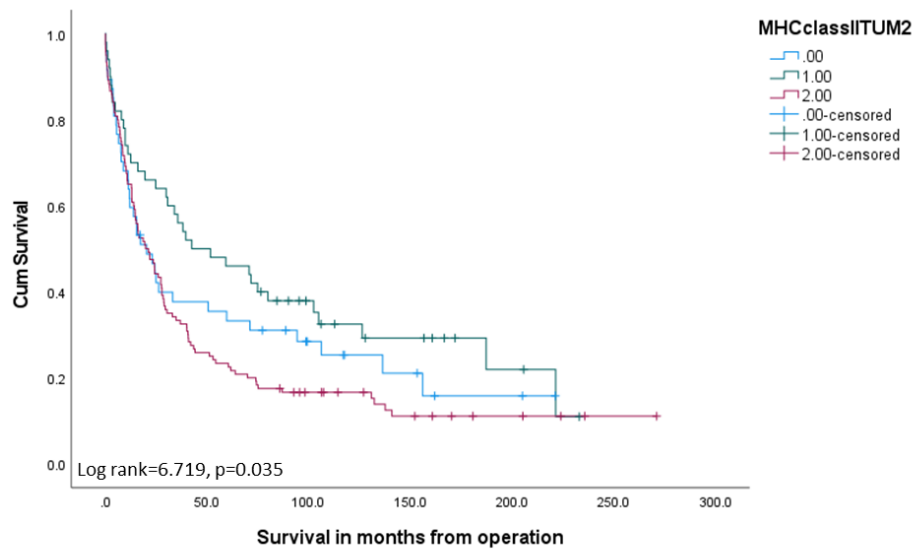


Figure 4.7 Kaplan-Meier survival curves for lung (a) and ovarian (b(i)) and breast (c(i)) cancer data sets based on MHC class II expression, N=197, 175 and 234 respectively. Correlation of IRF-1 (b(ii) and IFNγ receptor (b(iii)) expression with survival in ovarian cancer, N=279 and 350 respectively. Correlation of MHC class II expression and disease-free interval survival (c(ii)) and time to distant metastasis (c(iii)) in Breast cancer, N=245 for both Kaplan-meier graphs. Chi-square log rank test significance P≤0.05.

Figure 4.8

a



b

Pairwise Comparisons

		.00		1.00		2.00	
	MHCclassIITUM2	Chi-Square	Sig.	Chi-Square	Sig.	Chi-Square	Sig.
Log Rank (Mantel-Cox)	.00			1.684	.194	.941	.332
	1.00	1.684	.194			7.002	.008
	2.00	.941	.332	7.002	.008		

Figure 4.8 Kaplan-Meier survival curve for ovarian data set in three groups (negative 0, weak 1 and strong 2) (a) with multiple comparisons shown in table below (b). Chi-square log rank test significance P≤0.05.

4.2.4 MHC class II correlations with citrullination and autophagy markers

The Ovarian cancer cohort was analysed for correlations between MHC-II expression and other citrullination and autophagy markers. Increasing MHC-II expression was significantly correlated with high citrullinated vimentin (P<0.001), PAD2 (P<0.001), autophagy related marker Ambra1 (P=0.016) and IFNγ receptor (P=0.003) (Table 4.6 and Figure 4.9a, c, d and e). Citrullinated vimentin low and PAD2, Ambra1 and IFNγ receptor negative patients displayed equally low levels of each MHC-II expression group. However, high/positive expression of these markers showed positive correlations with MHC-II; percentages increased from 9.1%, 6.7%, 18.7% and 18% in negative groups to 66.7%, 73%, 57.1% and 56.6% in patients expressing strong MHC-II for citrullinated vimentin high, PAD2, Ambra1 and IRF-1 positive populations respectively (Table 4.6 and Figure 4.9a, c, d and e). Interestingly, all Ambra1 negative patients were also 100% negative for MHC class II expression (Table 4.6). Correlations between MHC-II and markers vimentin and IRF-1 were not found to be significant (P=0.242 and P=0.697 respectively), strong MHC-II expression was elevated in both vimentin and IRF-1 negative and positive populations (Table 4.6 and Figure 4.9b and f). The percentages of strong MHC-II expression were similar in negative and positive vimentin (49.1% vs 59.4%) and IRF-1 (60% vs 54.2%) groups. These results are consistent with but do not prove the hypothesis that high levels of PAD2 and autophagy result in citrullinated vimentin which can be expressed on MHC-II for recognition by cytotoxic CD4 T cells.

Table 4.6

Marker	Group	MHC class II			Significance
		Negative	Weak	Strong	Chi-Square
Citrullinated Vimentin	Low (Q1)	38.7%	32.3%	29.0%	<0.001
	High (Q2, Q3, Q4)	9.1%	24.2%	66.7%	
Vimentin	Negative	24.5%	26.4%	49.1%	0.242
	Positive	14.2%	26.4%	59.4%	
PAD2	Negative	30.7%	33.3%	36.0%	<0.001
	Positive	6.7%	20.2%	73.0%	
Ambra	Negative	100.0%	0.0%	0.0%	0.016
	Positive	18.7%	24.2%	57.1%	
IFNγ receptor	Negative	41.9%	6.5%	51.6%	0.003
	Positive	18.0%	25.4%	56.6%	
IRF-1	Negative	18.8%	21.2%	60.0%	0.697
	Positive	22.5%	23.3%	54.2%	

Table 4.6 Percentage of citrullinated vimentin, vimentin, PAD2, Ambra, IFNγ receptor, IRF-1 negative and positive cases in MHC class II negative, weak or strong Ovarian cancer patients. Chi-squared log rank test significance. P≤0.05.

Figure 4.9

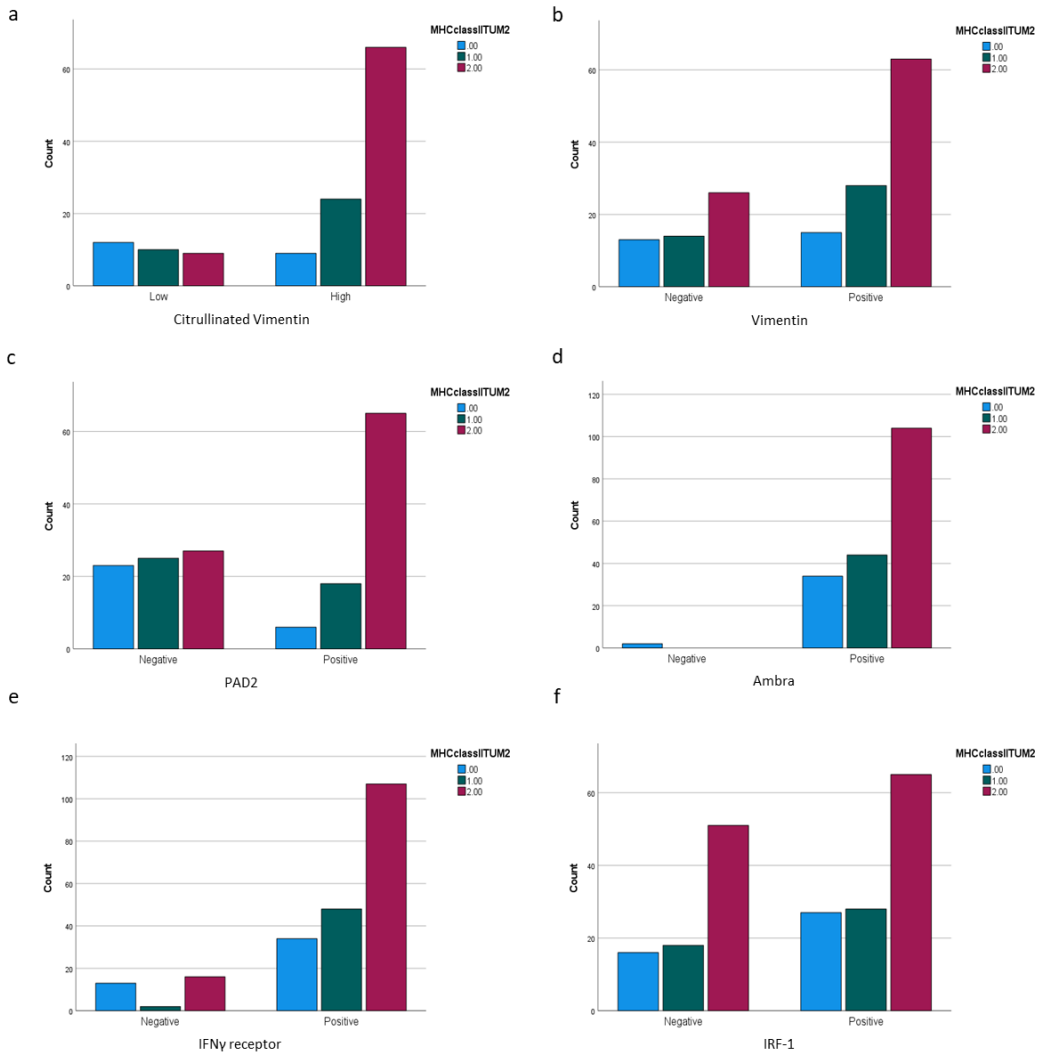


Figure 4.9 Distribution of cases either low or high for citrullinated vimentin (a) and negative or positive for vimentin (b), PAD2 (c), Ambra1 (d), IFNγ receptor (e), and IRF-1 (f) compared to MHC class II in Ovarian cancer patients. Expression levels of MHC class II divided into 3 groups; negative (blue 0), weak (green 1) and strong (purple 2).

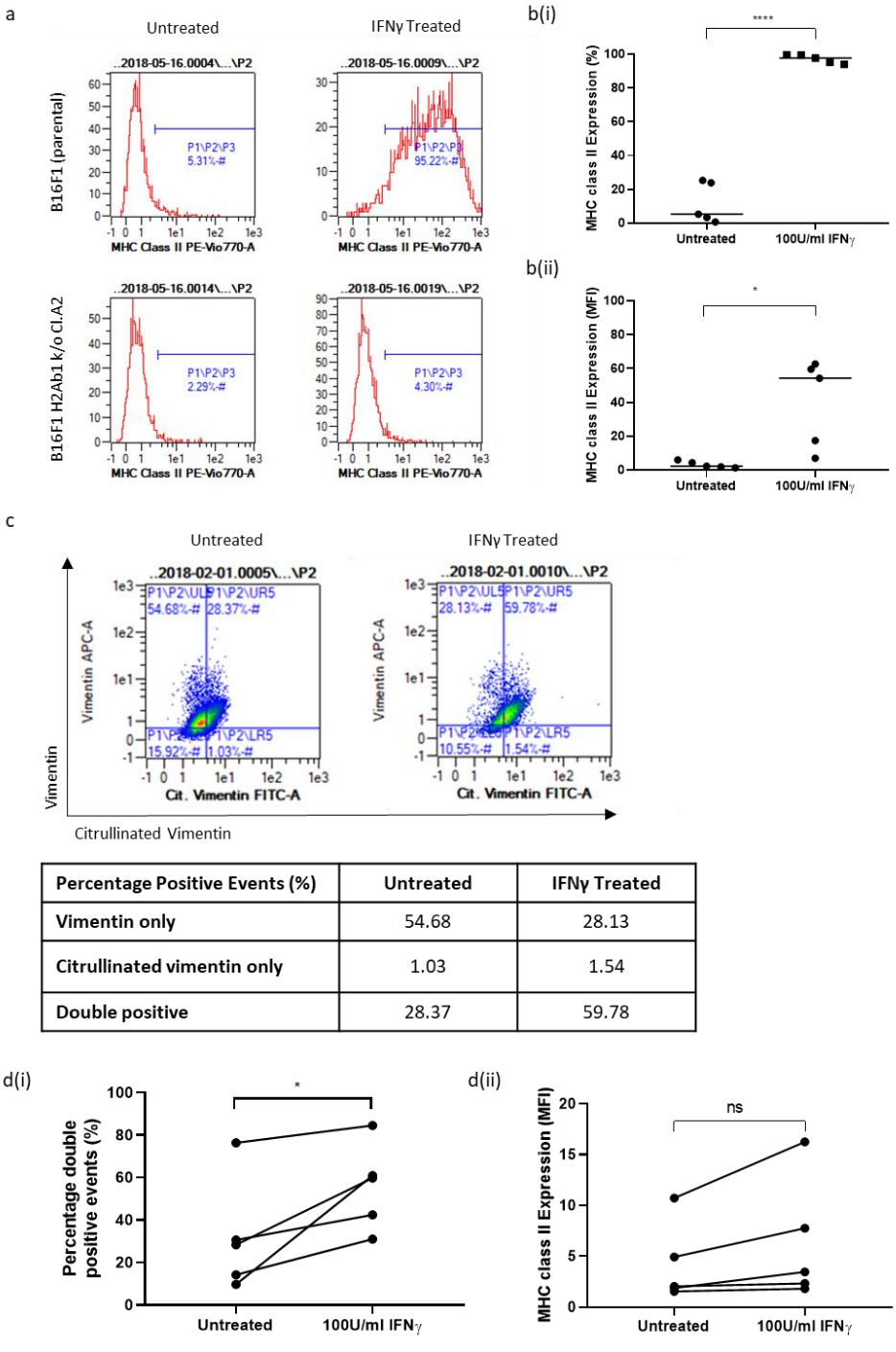
4.2.5 IFNγ upregulates MHC class II and citrullination in B16F1 cell line

The citrullinated vimentin peptide vaccine stimulated potent anti-tumour responses in the murine B16 melanoma model. To understand the expression of MHC-II in these murine models, the induction of MHC-II by IFNγ in the murine melanoma cell line B16F1 was tested. Upregulation of MHC-II expression was observed in B16F1 parental cells after incubation with mouse IFNγ recombinant protein at 100U/mL, and detected with an anti-mouse MHC-II (I-A/I-E) antibody. Percentage of MHC-II positive events increased from 5.31% to 95.22% in B16F1 parental cells, but not the MHC-II knockout line B16F1 H2Ab1 k/o Cl.A2; 2.29% to 4.32% (Figure 4.10a). Data from 5 individual experiments assessing MHC-II induction by 100U/mL IFNγ in B16F1 parental cells was collated. There was a significant increase in the percentage and median fluorescence intensities (MFI) of MHC-II positive cells in all experiments ($P<0.0001$ and MFI $P=0.0367$) (Figure 4.10b).

As IFNγ is one of the inflammatory cytokines released by APCs in the tumour microenvironment, it could also be a possible factor for inducing cellular stress. To test this, the expression of citrullinated vimentin was checked in IFNγ treated and untreated conditions. As before B16F1 cells were plated at $2x10^5$ cells/well in a 6-well plate and incubated with 100U/mL IFNγ overnight before intracellular staining using an antibody that detects citrullinated vimentin (ECV-1). Untreated cells expressed moderate levels of double positive citrullinated vimentin (28%) which was elevated after overnight IFNγ treatment to 51% (Figure 4.10c). Quadrant gating showed that the majority of untreated cells were vimentin positive but citrullinated vimentin negative (Figure 4.10c upper left quadrant). However, a significant rightward shift in the population was observed after exposure to IFNγ resulting in more double positive citrullinated vimentin events (Figure 4.10c upper right quadrant). This experiment was repeated 5 times and increases in the percentage but not MFI of MHC class II positive

cells after treatment with 100U/mL IFNγ was found to be statistically significant (P=0.0388 and P=0.0998) (Figure 4.10d). This result shows that IFNγ can upregulate both citrullination and MHC-II expression and explains the good recognition by CD4 T cells.

Figure 4.10



Percentage Positive Events (%)	Untreated	IFNγ Treated
Vimentin only	54.68	28.13
Citrullinated vimentin only	1.03	1.54
Double positive	28.37	59.78

Figure 4.10 IFNγ upregulation of MHC class II expression in B16F1 parental cells and B16F1 cells knocked out for MHC class II, B16F1 H2Ab1 k/o Cl.A2 (a). Percentage positive events (b(i)) and median fluorescence intensities (MFI) (b(ii)) of MHC class II in B16F1 parental cells with or without 100U/mL IFNγ treatment, N=5. Paired T test analysis * = P<0.05, **** = P<0.0001. Quadrant gating with corresponding percentage positive events (c) showing levels of vimentin and citrullinated vimentin in B16F1 with or without 100U/mL IFNγ treatment. Collated percentages of citrullinated vimentin double positive events (d(i)) and MFI (d(ii)), N=5. Paired t test analysis ns = P≥0.05, * = P<0.05.

4.2.6 Results summary

In a panel of Triple negative breast cancer (TNBC) and ovarian cancer cell lines, 4/8 lines expressed MHC-II. This was enhanced in 3/4 ovarian and 2/4 TNBC cell lines following exposure to IFNγ. Up regulation of MHC-II by IFNγ is dependent on activation of the CIITA which is controlled by the pIV promoter. This was confirmed by showing upregulation of CIITA after IFNγ incubation in MDA-MB-231 (MHC class II positive) but not BT549 (MHC class II negative). In addition, a strong correlation between IRF-1 and CIITA mRNA expression was found in 10 cancers analysed from the TCGA database. Interestingly, CIITA mRNA expression alone correlated with good prognosis in melanoma (P=1.89e-5), head and neck cancer (P=0.03632), lung (P=0.07824) and ovarian cancers (P=0.0581). Melanoma cancer patients also had significantly improved survival with HLA-DPA1 (P=9.386e-5), HLA-DPB1 (P=2.224e-5) and IRF-1 (4.04e-7) mRNA expression. IFNγ also increased citrullinated vimentin expression in the murine melanoma cell line B16F1. Measuring MHC-II protein expression in human tumours showed 55% of head and neck cancers, 53% of osteosarcomas, 48% of renal cancers, 44% of sarcomas, 31% of ovarian and 27% of breast and lung cancers were positive. Positive expression was associated with survival in breast (P=0.004) but not with lung (P=0.343) and ovarian (P=0.883) cancers. However, dividing ovarian cancer patients into MHC-II expression into negative, low and high groups resulted in significantly better survival (P=0.008) for

the MHC-II low compared to the MHC-II high expressing group. In addition, MHC class II positively correlated with citrullinated vimentin ($P<0.001$), PAD2 ($P<0.001$), IFNγ receptor ($P=0.003$) and autophagy marker Ambra1 ($P=0.016$). In breast cancer patients, MHC class II expression was correlated with increased survival ($P=0.004$), disease free interval survival ($P=0.049$) and less distant tumour metastasis ($P=0.006$). Taken together this data shows MHC class II is present in human tumour cells at low levels but can be further induced by inflammatory cytokine IFNγ that is dependent on CIITA expression.

4.3 Discussion

The main focus of anti-tumour activity has been focused on CD8 T cells due to the constitutive MHC class I and lack of MHC class II (MHC-II) expression on tumour cells. However, in this chapter we have shown MHC-II is expressed at low to moderate levels on tumour cells and can be further induced by IFNγ. Traditionally, CD4 T cells have been considered as only helper cells to promote and support CD8 T cell effector functions. Especially as CD8 memory responses are deficient when CD4 T cells are removed [295-297]. More recent research has shown CD4 T cells can express a cytotoxic phenotype when activated by peptide-MHC-II [1, 77], and this is due to the termination of transcription factor thPOK controlling the expression of CD8 T cell lineage genes [78]. When activated, CD4 T cells are able to upregulate similar cytotoxic functions such as perforin and granzyme B release, directly killing tumour cells expressing peptide-MHC-II, independently of CD8 T cells [80-83]. In addition, neo-epitopes from random mutations in tumour are pre-dominantly recognised by MHC-II compared to MHC-I, producing a strong CD4 response. RNA vaccinations including these neo-epitopes in B16F1 mouse models showed 60% survival which was reduced to 20% in the presence of an anti-CD4 blocking antibody [298]. Furthermore, a clinical trial involving immunisation with personalised peptide vaccines based on the mutated neoantigens sequenced from the patient tumour, showed the majority of *ex vivo* IFNγ responses were CD4 mediated rather than CD8 [299]. This highlights the importance of MHC-II expression in tumours and their ability to present neo-epitopes and stimulate a robust, cytotoxic CD4 T cell response.

A strong correlation exists between MHC-II expression and infiltrating CD4 and CD8 T cells with reduced metastasis in Triple Negative Breast Cancer (TNBC) tumours. In contrast, the lack of MHC class II expression correlated with reduced infiltrating lymphocytes and increased tumour cell metastasis [300-303]. Antigen presenting

cells constitutively express MHC-II whereas expression in most other cells including tumours can be induced by IFNγ. Measuring MHC-II protein expression in human tumours showed 55% of head and neck cancers, 53% of osteosarcomas, 48% of renal cancers, 44% of sarcomas, 31% of ovarian and 27% of breast and lung cancers were positive. These cancers displayed mostly low to moderate expression of MHC class II, with high expression cases only seen in sarcoma, ovarian, lung and breast. This correlates with MHC class II expression recorded in TNBC where the majority of patients (479) were negative for MHC-II, and only 86 patients expressed low and 116 patients expressed high levels of MHC-II [304]. In a panel of TNBC and ovarian cancer cell lines, 4/8 lines showed moderate expression of MHC-II. This was enhanced in 3/4 ovarian and 2/4 TNBC cell lines following exposure to IFNγ. Together, this indicates MHC-II is present in human tumour cells at low levels and can be further elevated by inflammatory cytokine IFNγ.

Three MHC class II gene groups exist in humans; HLA-DP, -DQ and -DR. Expression of genes that code for the alpha and beta chain of MHC-II haplotype HLA-DP (HLA-DPA1 and HLA-DPB1 respectively) were found to correlate with survival in most cancers. However, survival was only significantly associated with HLA-DPA1 expression in melanoma, head and neck and sarcoma, and with HLA-DPB1 expression in melanoma and renal papillary cell carcinoma. In contrast, high expression of these MHC-II genes correlated with reduced survival in pancreatic cancer patients and this difference was observed after 2 years. As discussed in chapter 3, inflammation can be tumour suppressive but chronic inflammation can also promote tumour progression. A leukocyte count greater than $10x10^9$ cells/L correlated with a higher hazard ratio in pancreatic cancer [305]. Furthermore, long term survivors (>6 years) had more CD8 T cells and less CD4 T cells in tumours compared to short term survivors (<1 year) [306]. This cancer type also has a low tumour mutational burden (TMB) and the occurrence of neoantigens is fairly low with high neoantigen

expression associated with >70% survival rates [134, 306]. Low levels of neoantigens and high MHC-II expression could have contributed to chronic inflammation with reduced tumour specific cytotoxic effects, resulting in the poor prognosis of MHC-II high patients in our pancreatic cancer cohort.

As survival probabilities were divided based on low and high expression of these MHC-II genes, it is possible that some patients expressed greater levels of HLA-DR or HLA-DQ rather than HLA-DP which may have a more significant impact on prognosis. It is interesting that the presence of each chain can contribute individually to a patient's outcome despite pairing of both chains required to form a stable MHC molecule and present peptide. In addition, survival rates between subtypes of renal cancer differed suggesting varying degrees of dependency on MHC-II expression based on the tumour site. In general, the survival probabilities of each chain were similar in each cancer type (survival curves in Appendix 4). As HLA-DP is less polymorphic than HLA-DR, a few alleles appear with higher occurrence in the population e.g DPA1*0103/DPB1*0401 (DP401) [307]. HLA-DP molecules are known to form stable dimers in the absence of invariant chain (Ii) and HLA-DM, only requiring peptide [308]. More recently, the polymorphic HLA-DP alleles were subdivided into two groups based on their amino acid residue at position 84. Those that held aspartic acid such as HLA-DP1, -DP5 and -DP8, associate with Ii and CLIP. Alternatively, alleles with a glycine at position 84 such as DP2 and DP4, do not associate with Ii through CLIP but can via non-CLIP interactions [309]. This suggests that DP2 and DP4 (and others in the second group) bind endogenous peptide more efficiently as they do not need to associate with Ii and CLIP. These endogenous peptides are a source of unique tumour associated antigens (TAAs) that can be recognised by CD4 T cells explaining the greater survival probabilities seen in majority of cancers.

The expression of all class II associated HLA-molecules including HLA-DM and DO are regulated by CIITA which is under the control of four distinct CIITA promotors. CIITA promotor IV is best known for its role in IFNγ-mediated MHC-II expression as discussed in section 4.1 [284, 286]. It was hypothesised that CIITA regulated MHC-II expression in TNBC and ovarian tumour cell lines and this was confirmed by showing upregulation of CIITA after IFNγ incubation in MDA-MB-231 (MHC class II positive) but not BT549 (MHC class II negative). Experiments performed by Van der Stoep and colleagues showed that the lack of CIITA induction in various tumour cell lines was due to the methylation of CIITA promotor IV [310]. Tumours can also fail to respond to IFNγ by different molecular mechanisms and one of which is the downregulation of the IFNγ receptor. This has been shown in breast cancer tissues by the lack of either IFNGR1 or IFNGR2 (the two subunits that form the IFNγ receptor). STAT1 activation was ablated in the absence of IFNGR1 [311, 312]. In these cells, CIITA induction and therefore MHC class II expression would be inhibited. Another reason tumours do not respond to IFNγ is due to defects in downstream signalling involving the Janus kinases JAK1 and JAK2, and signal transducer and transcriptional activator STAT1, referred to as the JAK-STAT. These molecules have been greatly studied in a range of cancers for their contribution to tumour progression and metastasis. Genetic mutations causing loss of function were found to occur in both JAK1 and JAK2 in melanoma and non-small lung cancer but to a greater extent in JAK2. In addition, JAK2 deficient cell lines were non-responsive to IFNγ treatment and showed inhibition of STAT1 [313, 314]. Again, this would reduce CIITA activation, ablating MHC class II expression. By these methods, tumours are able to avoid immune recognition.

The strong correlation between CIITA and IRF-1 from TCGA database cancer panel further highlights the importance of IFNγ induction of CIITA. Many links between IFNγ and CIITA expression in cancer have been reported in literature. Incubation with IFNγ for up to 48 hours induced phosphorylated STAT1, CIITA, and HLA-DR, -DP, -DQ in

melanoma and glioblastoma cell lines [315, 316]. In addition, pIV was detected in 82% of glioma tissue samples [316]. The lack of CIITA pIV reduced expression of CIITA and MHC class II in metastatic breast cancer cell line MDA-MB-435 [301]. Analysis of the TCGA database showed CIITA mRNA expression correlated with good prognosis in melanoma (P=1.89e-5), head and neck (P=0.03632), lung (P=0.07824) and ovarian cancer (P=0.0581). These cancers, especially melanoma, are considered immunogenic due to their high TMB expression of TAAs; MAGE, NY-ESO1, MELOE-1, and p53 [134, 317-319]. The increased survival of cancer patients expressing high CIITA could be due to the stimulation of T cell responses against these TAAs. Mutations in CIITA also significantly correlated with increased survival in melanoma patients suggesting an upregulation of CIITA and therefore MHC-II. A mutation can either upregulate or down-regulate expression of the gene and is a more common characteristic of the cancer if it allows the tumour to escape immunosurveillance. Lung cancers also have high TMB due to related carcinogenic factors such as smoking. However, CIITA mutations in this cohort were not correlated with survival. A more detailed analysis of the mutation and its effect on CIITA expression is required to establish whether they contribute to a better prognosis. Melanoma cancer patients (from TCGA) also displayed significantly better survival with IRF-1 (4.04e-07) mRNA expression. Treatment with DNA methyltransferase inhibitors have been shown to enhance CIITA and MHC-II expression in the murine ovarian cancer cell line ID8 and this was correlated with a reduction in tumour size [320]. Taken together, the data suggests upregulation of CIITA by tumour cells is advantageous for patients resulting in immune related tumour regression.

In breast cancer patients, MHC-II expression was significantly correlated with survival (P=0.004), disease free interval survival (P=0.049) and less distant tumour metastasis (P=0.006). A similar prognosis was observed in lung cancer patients, with greater survival in the MHC-II group compared to negative, however this was not

significant. Survival is most like due to MHC-II presentation of TAAs which are recognised by CD4 T cells, initiating a pro-inflammatory response. Work conducted by Park et al (2017) support this theory; both low and high expression of MHC-II in TNBC correlated with increase tumour-infiltrating lymphocytes compared to the MHC-II negative group, and both CD4 and CD8 T cell numbers were further elevated in the high compared to low expressing group [304]. Although there was no association with disease-free survival in the total patient population, MHC-II was significantly correlated with disease-free survival in patients with lymph node metastasis [304], suggesting immune recognition was vital to avoid a severe prognosis with metastatic tumours. In ovarian cancer, IRF-1 and IFNγ but not MHC class II expression, associated with patient survival. However, MHC-II expression was positively correlated with IFNγ. This cytokine pathway is downregulated in many tumours to avoid immune regulation and promote tumour survival and progression. More mutations were found in the IFNγ pathway in melanoma patients that did not respond to immunotherapy compared to those that did respond and these mutations were associated with reduced survival [321]. Recently, non-small cell lung cancer (NSCLC) cells were found to restrict IFNγ induced MHC class II expression via MEK/ERK signalling pathways [322]. In lung cancer, the outcome was dependent on IFNγ dose; low levels correlated with reduced patient survival and increased Epithelial to Mesenchymal (EMT) markers, adhesion and stem-cell like molecules, whereas high levels resulted in increased tumour cell apoptosis [323]. Apoptosis induction as well as increased TAA presentation through MHC-II expression may have contributed to the increased IFNγ and IRF-1 associated survival levels witnessed.

MHC-II expression was also positively correlated with expression of autophagy marker Ambra1 in ovarian cancer. This protein binds to Beclin-1 inducing autophagosome formation [324]. As with most other autophagy related proteins, Ambra1 is regulated by the autophagy inhibitor mTOR, which blocks its activity [325].

The MHC-II presentation pathway overlaps with the autophagy pathway with the formation of multivesicular bodies (MVB) [207], so a correlated increase in both was expected. In addition, 100% of Ambra1 negative cases were also negative for MHC-II indicating a strong connection between autophagy and MHC-II expression.

Interestingly, MHC-II expression also positively correlated with citrullinated vimentin expression. In addition to previous findings showing autophagy dependent recognition of citrullinated epitopes by CD4 cells [1], this suggests presentation of this TAA via autophagy and MHC-II in ovarian cancer. In these experiments, increased IFNγ production was observed in responding CD4 T cells [1, 77, 220]. IFNγ is known to be secreted from a multitude of immune cells including macrophages, dendritic cells and B cells but more predominantly by natural killer (NK) cells, Th1 effector T cells and cytotoxic T cells [326-329], which can contribute to MHC-II induction in cancer. For example, adoptive transfer of TRP-1 CD4 specific T cells increased MHC-II expression in tumour cells in mouse models and tumour regression was reduced in the presence of a IFNγ neutralising antibody [125].

We have highlighted another role for IFNγ in tumour cells; the augmentation of citrullination. Citrullinated vimentin levels were increased in the B16F1 cell line following overnight exposure to IFNγ. This suggests that this inflammatory cytokine promotes a state of cellular stress resulting in citrullination. Cytokines can induce endoplasmic reticulum (ER) stress in cells. A combination of IFNγ and TNF-α or IL-1β treatment increased ER stress related proteins ATF4, BiP/GRP78 and Chop in mesenchymal stem/stromal and pluripotent stem cells [330, 331]. This feedback mechanism of IFNγ induced citrullinated vimentin provides a very promising effect of utilising citrullinated epitopes as TAAs for immunotherapy. Immunisation with citrullinated peptides stimulated epitope specific IFNγ responses [1, 77, 220], therefore activated T cells releasing this cytokine can further elevate expression of

citrullinated proteins in neighbouring tumour cells, increasing the efficacy of this vaccine.

To conclude, MHC-II is expressed in human cancers at low levels, however expression can be elevated by IFNγ induced CIITA activation through promoter IV. CIITA correlates with survival in a range of cancers highlighting the importance of this transactivator for MHC-II expression in tumours. The good prognosis of CIITA and MHC-II positive cancers is due the activation of T cell responses, allowing immune control over the growth and metastasis of tumours. In addition, IFNγ induction of both MHC-II and citrullination provides a secondary mechanism by which activated citrullinated protein specific T cells can recognise and eliminate tumour cells.

5 Identification of citrullinated protein specific T cell receptors

5.1 Introduction and Aims

5.1.1 T cell receptor repertoires; Public and Private T cell receptors

T cell receptor (TCR) repertoires to various infectious and autoimmunity diseases have been greatly studied by researchers. These works have identified a range of public TCRs that are shared between different individuals and are often clonally dominant; found at a higher copy number within the TCR repertoire. In contrast, private TCRs are unique to the individual but are more prevalent. Over the past two decades, scientists have aimed to understand the structural and genetic factors that influence the responding T cell repertoire to a particular antigen, in the hope to utilise this phenomenon for therapeutical benefits. One highly recognised mechanism that shapes public TCRs known as ‘convergent recombination’ involves the production of the same nucleotide sequence from the convergence of multiple recombination events that then converge to encode for the same amino acid sequence.

At the first stage, a shared TCR sequence is more likely to have been spliced from germline D regions in multiple ways due to the homology between the 3’ end of the V region and 5’ end of the D region but still resulting in the same nucleotide sequence. Fewer splicing options of the D region would be available for private TCR [42]. This has also been seen in TCR repertoire responses to HIV and CMV [332, 333] and when observing repertoires in grafted human thymus in mouse models [334]. The latter study also identified shorter CDR3 lengths due to fewer nucleotide additions in shared TCRs. The ability for amino acids to be coded by various nucleotide sequences forms the second stage of this mechanism, a more likely occurrence in

shared TCRs [335]. During the final stage of convergent recombination, the many amino-acid sequences will conform to a certain amino-acid motif contributing to the TCRs biological function [42, 336]. High throughput TCR sequencing of CD8 T cells specific to the CMV epitope (NEGVKAAW) termed NW8, found conserved amino acid motifs in both TCRα and TCRβ chains which were encoded by multiple V genes and identified in public TCRs. In contrast, no conserved amino acid motifs were observed in private TCRs [332].

Further work in this field highlighted an additional phenomenon that contributes to public TCR occurrence known as recombinational bias. In this scenario, responding TCR repertoires display a skewed usage of V, D and J gene segments where recombination of these segments are not random. The usage frequencies differed between each V-J combination but showed similar expression patterns from 3 individual mice [337] and in mice with grafted human thymus, approximately 25% and 100% of shared CDR3β chains from different thymi contained the same V and J genes respectively [334].

Research into cancer related shared TCR repertoires has also been of high interest. In HLA-A2 positive breast cancer patients, 18 public TCRs were identified from both the tumour infiltrating lymphocyte (TIL) and peripheral blood lymphocyte (PBL) populations. Only 4 of these TCRs were found in HLA-A2 healthy individuals [338]. There was a higher number of unique TCRβ sequences in tumour tissue compared to PBL in 5 pancreatic cancer patients [339]. Both suggest expansion of these shared TCRs were in response to tumour. In lung adenocarcinoma patients, CD4 TILs carried more diverse TCR repertoires than CD8 TILs and great clonality of CD8 TILs, not CD4 TILs, was associated with patient relapse [340]. CD4 T regulatory (Treg) cells were clonally expanded in bladder cancer patient TILs however cytotoxic CD4 effector memory and effector T cells were also identified. In *ex vivo* experiments cytotoxic

activity of CD4 TILs was inhibited by the presence of Tregs [82]. In these examples, CD4 T cells could promote survival however recovery was dependent on repertoire and phenotype diversity. V gene usage was varied in rheumatoid arthritis patients based on the CD4 T cell subset analysed, however compared to healthy controls TRBV3-1 usage was notable elevated and TRBJ2-7 was decreased in naïve, effector memory and TH17. Additionally, higher diversity in Treg and lower diversity of TH17 and effector memory cell repertoires were found in RA patients compared to healthy controls, and the presence of shared TCR clonotypes of the effector memory and TH17 subsets were correlated with increased disease activity [341]. These findings suggest that although public TCRs are preferentially expanded in response to tumour antigen, private TCRs and a more diverse CD4 repertoire are essential in fighting both cancer and autoimmune disease.

5.1.2 Aims

The hypothesis is that T cells responses to stress induced post-translational modifications (siPTMs) show clonal restriction and citrullinated protein specific TCRs can be identified and isolated.

5.2 Results

5.2.1 Expression of MODI1 peptides in B16F1 tumours

We have previously shown that immunisation with MODI1 citrullinated peptides Vim28-49cit[28,36,45], Vim415-433cit[424] and Eno241-260cit[253] are presented on HLA-DR4 or DP4 in tumour cells and stimulate strong CD4 mediated anti-tumour responses [1, 2]. To confirm the presence of these citrullinated epitopes in B16F1 tumours, 5 tumour samples (A1, A2, A4, A7 and A8) from unimmunised B16F1 tumour bearing mice were pulverised and prepared as cell-free lysates and sent to Proteome Sciences for analysis of citrullinated peptide sequences via mass spectrometry. Tumours were excised by Peter Symonds (Scancell Ltd). All MODI1 peptide epitopes were found to be citrullinated (stated as deiminated in data tables) in the tumours. The abundance of each MODI1 peptide and their wildtype equivalent were assessed in each tumour sample with a higher value signifying a greater amount, and the estimated concentration across all samples given in pmol/mg (Table 5.1). The shorter length peptide Vimentin28-42cit[28,36] (Vim28citS) containing two citrullinated residues was also searched. In addition, two versions of Eno241cit and Eno241wt were found, the second containing an oxidation of Methionine at position 4. A greater abundance and estimated concentration was observed for all citrullinated peptides compared to its wildtype form; 0.704pmol/mg Eno241cit vs 0.058pmol/mg Eno241wt, 1.704pmol/mg Vim415cit vs 1.649pmol/mg Vim415wt, and 0.856pmol/mg Vim28cit vs 0.020pmol/mg Vim28wt. Out of all wildtype peptides searched, only Vim415wt showed expression however abundance was slightly lower than its citrullinated equivalent. Interestingly, a higher concentration was estimated for Vim28citS, 1.886pmol/mg, compared to the full length Vim28cit peptide suggesting preferential cleavage of this sequence within tumour cells (Table 5.1).

Table 5.1

Peptide	Sequence	Modifications	Abundance					pmol/mg
			A1	A2	A4	A7	A8	
Vim28-49wt	RSYVTTSTRTYSLGSALRPSTS	N-Term(TMT6plex)	-0.74	-0.92	-0.83	-1.40	-0.63	0.020
Vim28-49Cit	cit-SYVTTST-cit-TYSLGSAL-cit-PSTS	N-Term(TMT6plex); R1(Deimidated); R9(Deimidated); R18(Deimidated)	-0.08	1.01	0.36	0.10	0.97	0.856
Vim28-42Cit	cit-SYVTTST-cit-TYSLGS	N-Term(TMT6plex); R1(Deimidated); R9(Deimidated)	0.02	-0.74	-0.49	-0.32	-0.27	1.886
Vim415wt	LPTFSSLNLRETNLESLPL	N-Term(TMT6plex)	-1.67	-1.51	-1.82	-1.20	-1.34	1.649
Vim415-433Cit	LPTFSSLNL-cit-ETNLESLPL	N-Term(TMT6plex); R10(Deimidated)	-0.59	-0.32	-0.29	-0.19	0.04	1.704
Eno241-260wt	VIGMDVAASEFYRSGKYDLD	N-Term(TMT6plex); K16(TMT6plex)	-3.09	-2.74	-3.07	-3.06	-2.46	0.058
Eno241-260wt	VIGMDVAASEFYRSGKYDLD	N-Term(TMT6plex); M4(Oxidation); K16(TMT6plex)	-2.45	-2.55	-2.66	-2.44	-1.91	
Eno241-260Cit	VIGMDVAASEFY-cit-SGKYDLD	N-Term(TMT6plex); R13(Deimidated); K16(TMT6plex)	-0.66	-0.54	-0.86	-0.51	-0.31	0.704
Eno241-260Cit	VIGMDVAASEFY-cit-SGKYDLD	N-Term(TMT6plex); M4(Oxidation); R13(Deimidated); K16(TMT6plex)	-1.94	-1.88	-1.89	-1.85	-1.61	

Table 5.1 Abundance of MODI1 peptides Vim28-49cit, Vim415-433cit and Eno241-260cit and their equivalent wildtype (wt) forms in B16F1 tumours from unimmunised tumour bearing mice, as detected by mass spectrometry. Relative abundance of sequences from each tumour sample, A1, A2, A4, A7 and A8 and their corresponding estimated concentration in pmol/mg. TMTcalibrator™ strategy by Proteome Sciences. N=5.

In addition to searching specifically for MODI1 peptide sequences, a full list of all citrullinated vimentin and enolase peptides was generated and their abundance in each tumour was collated (Table 5.2). A total of 40 vimentin and 12 enolase citrullinated peptides were identified. Peptides containing amino acids corresponding to Vim28cit, Vim415cit, Eno241cit and the immunogen peptide used to raise the anti-citrullinated vimentin antisera termed ECV-1 are highlighted in Red, Blue, Purple and Green, respectively. Almost half (19/40) of the total citrullinated vimentin sequences corresponded to the Vim28cit peptide, and just under a third of sequences (13/40) corresponded to Vim415cit, showing selective citrullination of these epitopes. The only other citrullinated sequence to appear frequently at various lengths was LIKTVET-cit-DGQVINETSQHHDDLE, resembling vimentin amino acids 443-466. Of the citrullinated enolase peptides analysed, two thirds (8/12) matched Eno241cit. Two additional sequences, found at different lengths or with alternative citrullinated residues, were identified; Enolase33-63 AAVPSGASTGIYEALEL-cit-DNDKT-cit-

FMGKGVS and Enolase308-342 TASAGIQVVGDDLTVTNPK-cit-IAKAASEKSCNCLLL.

Table 5.2

Protein	Sequence	Modification	Abundance				
			A1	A2	A4	A7	A8
Vimentin	NL-cit-ETNLESLPLVDTHSKRTL	N-Term(TMT6plex); R3(Deimidated); K18(TMT6plex)	0.428968	-0.34112	0.338993	0.2209	0.518329
	cit-SYVTTSTRTYSL	N-Term(TMT6plex); R1(Deimidated)	0.324936	-0.03572	0.024163	0.183907	0.13236
	cit-SYVTTSTRT	N-Term(TMT6plex); R1(Deimidated)	0.472054	-0.59289	-0.07776	-0.08623	-0.48485
	SSSPGGAYVT-cit-SSAV-cit-L-cit	N-Term(TMT6plex); R11(Deimidated); R16(Deimidated); R18(Deimidated)	0.08435	-0.68824	-0.54063	0.164183	0.157416
	ST-cit-TYSLGSAL-cit-PSTS	N-Term(TMT6plex); R3(Deimidated); R12(Deimidated)	-1.09757	-0.08193	-0.56213	0.190826	0.407221
	SYVTTST-cit-TYSLGS	N-Term(TMT6plex); R8(Deimidated)	0.39149	-0.0435	0.056524	0.236218	0.080716
	T-cit-TYSLGSAL-cit-PSTS	N-Term(TMT6plex); R2(Deimidated); R11(Deimidated)	0.13943	-0.26432	0.347748	0.363259	0.481051
	TYSLGSAL-cit-PSTS	N-Term(TMT6plex); R9(Deimidated)	0.150931	0.055	0.211275	0.596018	-0.29485
	VTTST-cit-TYSLGSAL-cit-PSTS	N-Term(TMT6plex); R6(Deimidated); R15(Deimidated)	0.151492	0.400457	-0.24603	0.03327	0.160199
	IKTVET-cit-DGQVINETSQHHDDLE	N-Term(TMT6plex); K2(TMT6plex); R7(Deimidated)	0.26989		-0.05244	0.213226	0.021786
	IKTVET-cit-DGQVINETSQ	N-Term(TMT6plex); K2(TMT6plex); R7(Deimidated)	0.07688	-0.17554		0.189104	0.37514
	KTVET-cit-DGQVINETSQHHDDLE	N-Term(TMT6plex); K1(TMT6plex); R6(Deimidated)		-0.69132	0.15501	0.220248	-0.32663
	KTVET-cit-DGQVINETSQHHDD	N-Term(TMT6plex); K1(TMT6plex); R6(Deimidated)	0.585791	-0.38899	-0.43714		0.37555
	KTVET-cit-DGQVINETSQ	N-Term(TMT6plex); K1(TMT6plex); R6(Deimidated)		-0.23327	0.267653	0.165713	0.313986
	LIKTVET-cit-DGQVINETSQHHDDLE	N-Term(TMT6plex); K3(TMT6plex); R8(Deimidated)	0.470477		0.062254	-0.02177	0.268222
	LPTFSSLNL-cit-ETNLESLPL	N-Term(TMT6plex); R10(Deimidated)	0.230335		0.162192	0.271725	-0.17346
	LPTFSSLNL-cit-ETNL	N-Term(TMT6plex); R10(Deimidated)	0.016178		0.154198	0.081303	-0.14935
	NL-cit-ETNLESLPLVDTHSKRTLLIK	N-Term(TMT6plex); R3(Deimidated); K18(TMT6plex); K24(TMT6plex)	-0.23478	0.106823	0.045813		0.359752
	NL-cit-ETNLESLPLVDTHSKRTLL	N-Term(TMT6plex); R3(Deimidated); K18(TMT6plex)	0.240006	-0.23262		0.380492	0.150758
	NL-cit-ETNLESLPLVDTHSKRT	N-Term(TMT6plex); R3(Deimidated); K18(TMT6plex)	0.986191	-0.16199	0.347468		0.735833
	NL-cit-ETNLESLPLVDTHSKR	N-Term(TMT6plex); R3(Deimidated); K18(TMT6plex)	1.373402	-0.02391		-0.13115	0.751872
	NL-cit-ETNLESLPLVDTHS	N-Term(TMT6plex); R3(Deimidated)	0.785468	-0.36611	0.328113		0.476312
	NL-cit-ETNLESLPLVDTH	N-Term(TMT6plex); R3(Deimidated)		-0.47117	0.325039	0.140603	0.512526
	NL-cit-ETNLESLPLVDT	N-Term(TMT6plex); R3(Deimidated)	0.259476	-0.06612	0.431682		0.288696
	NL-cit-ETNLESLPLVD	N-Term(TMT6plex); R3(Deimidated)		0.038251	0.311944	-0.03816	0.466581
	cit-SYVTTST-cit-TYSLGSAL-cit-PST	N-Term(TMT6plex); R1(Deimidated); R9(Deimidated); R18(Deimidated)		0.306813	0.029177	-0.22336	-0.21319
	cit-SYVTTST-cit-TYSLGSA	N-Term(TMT6plex); R1(Deimidated); R9(Deimidated)	-0.29455		0.213235	-0.11518	-0.44203
	cit-SYVTTST-cit-TYSL	N-Term(TMT6plex); R1(Deimidated); R9(Deimidated)		0.894108	0.13997	-0.78455	0.15358
	cit-SYVTTST-cit-TY	N-Term(TMT6plex); R1(Deimidated); R9(Deimidated)	0.190413	-0.01045	0.294118		0.150489
	SYVTTST-cit-TYSLGSAL-cit-PSTS	N-Term(TMT6plex); R8(Deimidated); R17(Deimidated)	-0.05183	0.035331	-0.03249		-0.05217
	TTST-cit-TYSLGSAL-cit-PSTS	N-Term(TMT6plex); R5(Deimidated); R14(Deimidated)	0.241749	-0.29951		0.088906	-0.1288
	VET-cit-DGQVINETSQHHDDLE	N-Term(TMT6plex); R4(Deimidated)	0.636468	-0.13517		0.834674	0.263789
	NL-cit-ETNLESLPLVDTHSK	N-Term(TMT6plex); R3(Deimidated); K18(TMT6plex)		-0.19616		-0.02725	0.592126
	cit-SYVTTST-cit-TYSLGSAL-cit-PSTS	N-Term(TMT6plex); R1(Deimidated); R9(Deimidated); R18(Deimidated)	0.094476			0.05324	-0.08481
	cit-SYVTTST-cit-TYSLGS	N-Term(TMT6plex); R1(Deimidated); R9(Deimidated)	0.256446		0.138452		-0.22353
	cit-SYVTTST-cit-TYSLG	N-Term(TMT6plex); R1(Deimidated); R9(Deimidated)	0.015967		-0.16629		-0.02066
	cit-SYVTTSTRTYS	N-Term(TMT6plex); R1(Deimidated)		-0.08319	0.324867		0.099685
	cit-TYSLGSAL-cit-PSTS	N-Term(TMT6plex); R1(Deimidated); R10(Deimidated)	0.418486	-0.24723			0.022429
	YVTTST-cit-TYSLGSAL-cit-PSTS	N-Term(TMT6plex); R7(Deimidated); R16(Deimidated)	-0.16998	0.01835			0.23003
	TFSSLNL-cit-ETNLESLPL	N-Term(TMT6plex); R8(Deimidated)		0.20429		-0.20356	
Enolase	VIGMDVAASEFY-cit	N-Term(TMT6plex); M4(Oxidation); R13(Deimidated)	-0.29005	0.093165	0.18822	-0.16394	-0.03933
	AAVPSGASTGIYEALELRDNDKT-cit-FMGKGVS	N-Term(TMT6plex); K22(TMT6plex); R24(Deimidated); K28(TMT6plex)	0.245698	0.439423	0.223463	0.111716	0.17027
	AAVPSGASTGIYEALEL-cit-DNDKTRFMGKGVS	N-Term(TMT6plex); R18(Deimidated); K22(TMT6plex); K28(TMT6plex)	0.245698	0.439423	0.223463	0.111716	0.17027
	MDVAASEFY-cit-SGKYDLD	N-Term(TMT6plex); M1(Oxidation); R10(Deimidated); K13(TMT6plex)	0.300504	-0.21199	0.106615	-0.01269	0.464024
	ASAGIQVVGDDLTVTNPK-cit-IAKAASEKSCNCLLL	N-Term(TMT6plex); K18(TMT6plex); R19(Deimidated); K22(TMT6plex); K27(TMT6plex); C29(Carbamidomethyl); C31(Carbamidomethyl)	-0.12438	0.290798	-0.08899		0.251617
	IGMDVAASEFY-cit-SGKYDLD	N-Term(TMT6plex); M3(Oxidation); R12(Deimidated); K15(TMT6plex)	-0.07839	0.027015		0.199778	0.170742
	IGMDVAASEFY-cit-SGKYDLD	N-Term(TMT6plex); R12(Deimidated); K15(TMT6plex)	0.031893	-0.13262		-0.29324	-0.30317
	TASAGIQVVGDDLTVTNPK-cit-IAKAASEKSCNCLLL	N-Term(TMT6plex); K19(TMT6plex); R20(Deimidated); K23(TMT6plex); K28(TMT6plex); C30(Carbamidomethyl); C32(Carbamidomethyl)	-0.3077	-0.00097	0.019465		0.16162
	VIGMDVAASEFY-cit-SGKYDLD	N-Term(TMT6plex); R13(Deimidated); K16(TMT6plex)	0.017263	0.016689	0.111706		-0.09615
	VIGMDVAASEFY-cit-SGKYD	N-Term(TMT6plex); M4(Oxidation); R13(Deimidated); K16(TMT6plex)	0.22333		0.62365	-0.56058	0.008836
	VIGMDVAASEFY-cit-SGKYDLD	N-Term(TMT6plex); M4(Oxidation); R13(Deimidated); K16(TMT6plex)	0.001243		0.181218		-0.16395
	VIGMDVAASEFY-cit-SGKYDL	N-Term(TMT6plex); M4(Oxidation); R13(Deimidated); K16(TMT6plex)	-0.1383			0.080624	0.105686

Table 5.2 Abundance of deiminated Vimentin and Alpha-Enolase peptide sequences identified by mass spectrometry in B16F1 tumours from tumour bearing mice; A1, A2, A4, A7 and A8. Sequences containing amino acids that correspond to those found in MODI1 peptides Vim28-49cit, Vim415-433cit and Eno241-260cit are highlighted in Red, Blue and Purple respectively. Sequences corresponding to anti-citrullinated vimentin epitope ECV-1 highlighted in green. TMTcalibrator™ strategy by Proteome Sciences. N=5.

5.2.2 MODI1-specific CD4 T cell repertoire in healthy individuals

To determine whether healthy individuals have T cell repertoires that can recognise and respond to citrullinated peptides, PBMCs were isolated from 5 individuals, depleted of CD25 positive (regulatory T) cells. Representative plot from one donor showing percentage of CD25+ve cells before and after depletion (Figure 5.1a). Cells were then labelled with CFSE (for tracking proliferation) prior to incubation with or without citrullinated peptides for 10 days. Samples were taken from the cultures at Day 10 to assess and phenotype the proliferating T cells. Dead cells and doublets were excluded from the analysis prior to gating on CD4 or CD8 positive cells (Figure 5.1b). The T cell subsets were then gated for CFSE expression according to vehicle (DMSO) only negative controls (Figure 5.1c); low CFSE intensity corresponds to proliferating cells. PBMCs from healthy donors BD41 and BD11 processed by Ian Daniels (Scancell Ltd). Variations in healthy donor responses to citrullinated peptides Vim28cit, Eno241cit and Vim415cit were observed, as seen by a range of increased percentages in low CFSE populations compared to vehicle control, with a greater number of proliferating CD4 T cells compared to CD8 T cells (Figure 5.1d). There was a significant difference between proliferating CD4 T cells in Vim28cit cultures ($P=0.0303$) but not Eno241cit ($P=0.0636$) or Vim415cit ($P=0.2532$). This data suggests that responses to citrullinated peptides are CD4 mediated but not all donors respond to every epitope.

Figure 5.1

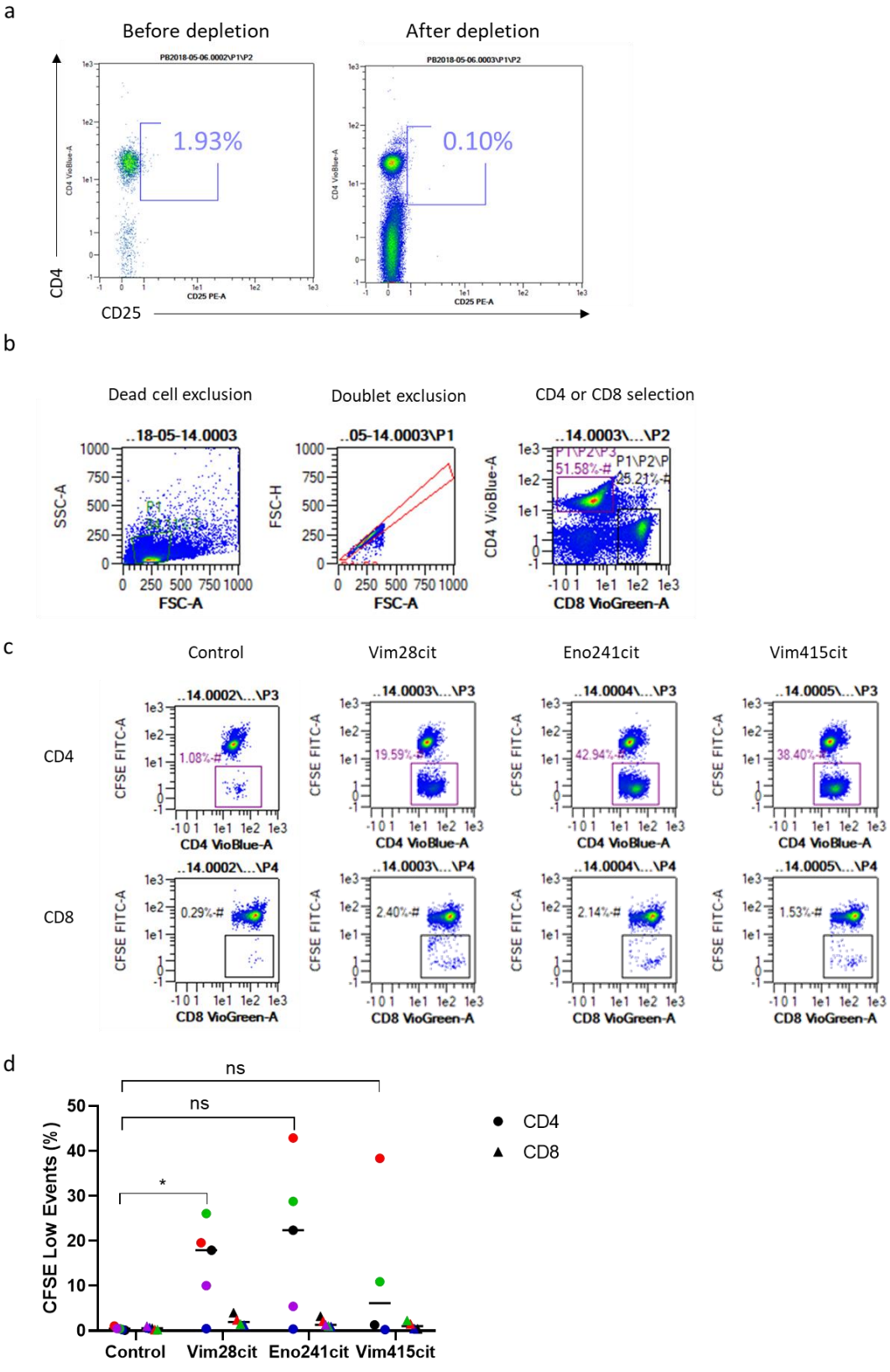

a
Before depletion
After depletion
1.93%
0.10%
CD4
CD25
b
Dead cell exclusion
Doublet exclusion
CD4 or CD8 selection
SSC-A
FSC-A
FSC-H
CD4 VioBlue-A
CD8 VioGreen-A
c
Control
Vim28cit
Eno241cit
Vim415cit
CD4
CD8
CFSE FITC-A
1.08%
19.59%
42.94%
38.40%
0.29%
2.40%
2.14%
1.53%
d
ns
*
CFSE Low Events (%)
CD4
CD8
Control
Vim28cit
Eno241cit
Vim415cit

Figure 5.1 PBMCs isolated from 5 healthy donors and labelled with CFSE (FITC) prior to incubation with citrullinated peptides for 10 days. Example of CD25 depletion of PBMCs; plots show percentage of CD25+ve cells before and after depletion in 1 donor prior to CFSE labelling (a) Dead cells and doublets excluded from analysis prior to selection of CD4 or CD8 positive populations (b). Example of gating to identify proliferating (CFSE low) CD4 and CD8 T cells incubated with citrullinated peptides (c). Collated CD4 and CD8 proliferation data from 5 healthy donors (d). Vehicle only (DMSO) used as negative control to gate for CFSE low populations. Coloured circles represent matched donors; black circle = BD14, blue circle = BD25, red circle = BD38, green circle = BD11 and purple circle = BD41. Paired t test significance, ns = $p \geq 0.05$, * = $p < 0.05$, N=5.

After identifying CD4 responses to citrullinated peptides, the activation and functionality of the proliferating population was assessed. Activation of the proliferated CD4 T cell population was determined by staining for CD134 (OX40, tumour necrosis factor receptor expressed by activated T cells), and functionality was assessed by staining for IFNγ (inflammatory cytokine secreted by activated T cells) and Granzyme B (serine protease secreted by cytotoxic T cells). The expression of these activation factors varied between the responding donors; proliferated after culture with Vim28cit for 10 days (Figure 5.2a). BD14 and BD11 showed the greatest percentage of CD134, IFNγ and Granzyme B in CFSE low populations when cultured with Vim28cit suggesting the proliferated cells were activated cytotoxic CD4 T cells (Figure 5.2a). However, no positive marker expression was seen in BD25, and BD38 only showed elevated expression of activation marker CD134 in the low CFSE population under these conditions (Figure 5.2a). Overall, the levels of activation markers varied between donors and only 2/4 showed increased expression in response to citrullinated peptides (Figure 5.2b).

Figure 5.2

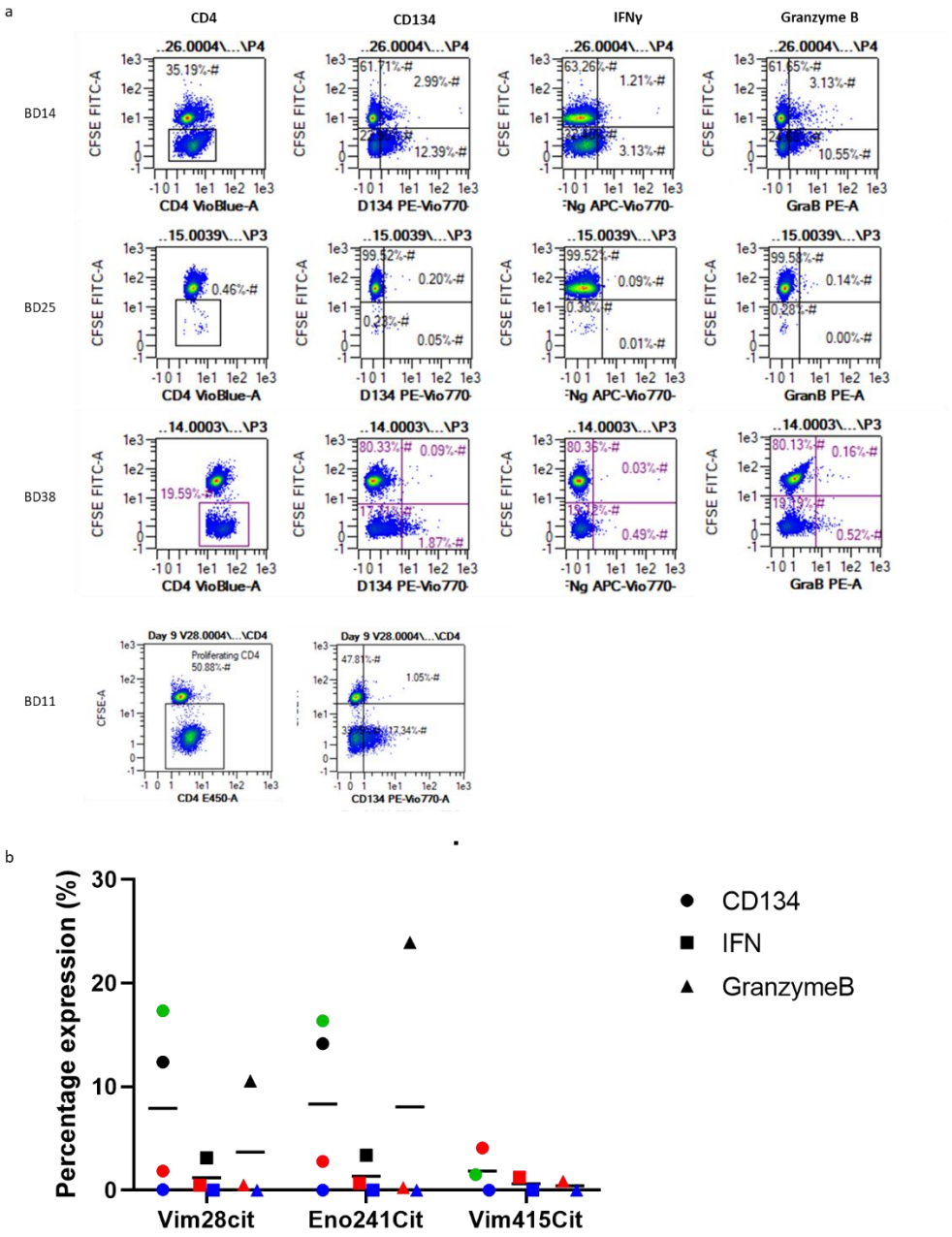
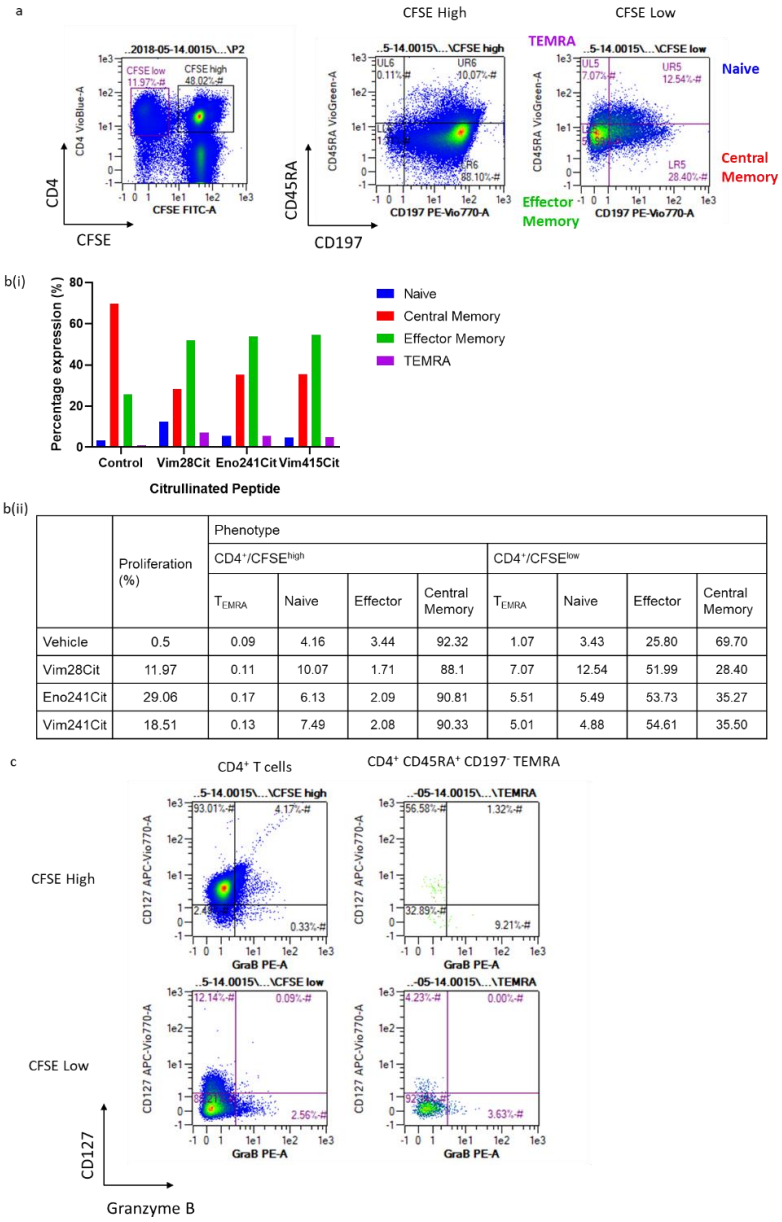


Figure 5.2 CD4 proliferation populations stained for activation markers CD134, IFNγ and granzyme B. Example of gating strategy of PBMCs from 3 healthy donors incubated with Vim28cit for 10 days (9 days for BD11) (a) and collated data from all citrullinated peptide conditions shown (b). Colours represent matched donors; black = BD14, blue = BD25, red = BD38, green = BD11. Vim415cit only tested for BD25 and BD38. Only CD134 levels measured in BD11 cultures. N≤4.

Further phenotyping was performed on healthy donor BD38 to determine the distribution of Naïve (upper right quadrant), Central Memory (lower right quadrant), Effector Memory (lower left quadrant) and CD45RA+ve Effector Memory, TEMRA (upper left quadrant) (Figure 5.3a). The CD4 positive population was gated for low or high CFSE signal before gating against CD45RA and chemokine receptor CCR7 (CD197) as described by Tian et al (2017) [79]. Cultures incubated with vehicle only had a high percentage of central memory (92.32%) T cells with only 4.16% naïve and 3.44% effector memory in the CFSE high population. Of the proliferating cells, 25% were found to be effector memory, 69% were central memory and only 3.43% and 1% were naïve and TEMRA, respectively (Figure 5.3b(ii)). Incubation with citrullinated peptides doubled the percentage of effector memory cells in the CFSE low population compared to the vehicle control, resulting in a reduction of central memory cells (Figure 5.3b). The percentage of TEMRA cells increased to 5%, 5.5% and 7% in the proliferating CFSE low cultures incubated with Vim415cit, Eno241cit and Vim28cit, respectively (Figure 5.3b(ii)). This shift in phenotype was not observed in the CFSE high populations and TEMRA percentages remained below 1% in both the vehicle only control and citrullinated peptide cultures (Figure 5.3b(ii)). Activated and terminally differentiated T cells can be identified by a reduction in the expression of the IL-7 receptor (CD127) [342]. Proliferating cultures incubated with Vim28cit showed a decrease in IL-7 receptor (CD127) expression and increase in Granzyme B compared to the CFSE high population of the same culture. Gating on TEMRA positive cells in these cultures prior to gating on CD127 and Granzyme B found that TEMRA also have a reduced percentage of CD127 but with a relatively low expression of Granzyme B (Figure 5.3c). This data suggests that healthy individuals have a CD4 T cell repertoire that is able to recognise and respond to citrullinated peptides, promoting the expansion of T cells with a cytotoxic effector memory phenotype.

Figure 5.3



	Proliferation (%)	Phenotype							
		$CD4^+/CFSE^{high}$				$CD4^+/CFSE^{low}$			
		T_{EMRA}	Naive	Effector	Central Memory	T_{EMRA}	Naive	Effector	Central Memory
Vehicle	0.5	0.09	4.16	3.44	92.32	1.07	3.43	25.80	69.70
Vim28Cit	11.97	0.11	10.07	1.71	88.1	7.07	12.54	51.99	28.40
Eno241Cit	29.06	0.17	6.13	2.09	90.81	5.51	5.49	53.73	35.27
Vim241Cit	18.51	0.13	7.49	2.08	90.33	5.01	4.88	54.61	35.50

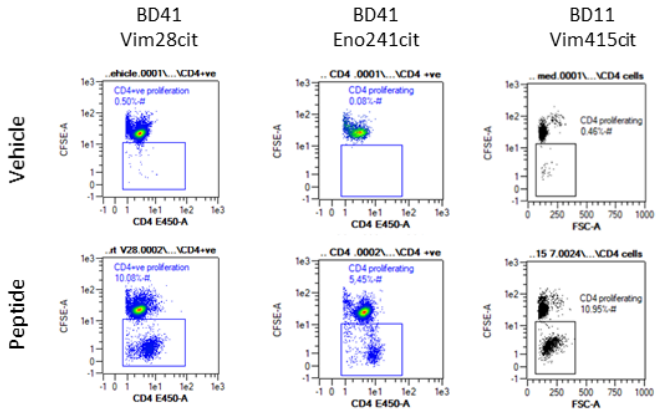
Figure 5.3 Partial phenotyping of CD4 T cells cultured with or without citrullinated peptides for 10 days. Vehicle only (DMSO) used as negative control. CD4 positive cells gated according to low or high CFSE expression prior to CD45RA vs CCR7 (CD197). Quadrants divided as follows: TEMRA = Upper left, Naïve = Upper right, Effector memory = Lower left, Central memory = Lower right (a). Expression of T cell phenotypes in proliferating (CFSE low) populations (b(i)) and percentages of detailed (b(ii)). CD4 population and TEMRA cells from Vim28cit highlighted also gated for CD127 vs Granzyme B (c). N=1.

5.2.3 Identification of MODI1 T cell receptors

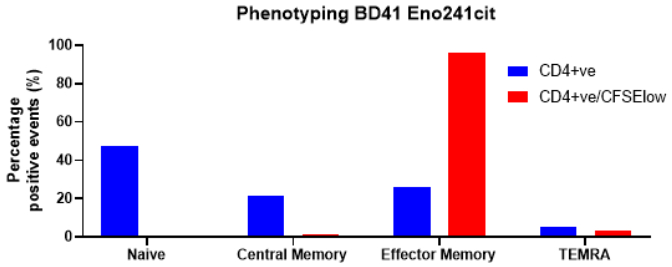
PBMCs from healthy donors BD41 and BD11 were cultured with citrullinated peptides for 10 days before assessing levels of proliferation using CFSE staining by Ian Daniels (Scancell Ltd). Non-proliferating and proliferating CD4+ve populations from BD41 Vim28cit and Eno241cit and BD11 Vim415cit cultures were purified via cell sorting and sent to iRepertoire for TCR repertoire sequencing using next generation sequencing. The total number of cells from each population is shown in Figure 5.4d. Fewer cells were isolated from the proliferating population (CFSE low) compared to proliferating (CFSE high) populations. This correlates with the percentage of proliferating cells identified via flow cytometry, which ranged from 5-11% of the CD4+ve population (Figure 5.4a). Further phenotyping was performed on BD41 Eno241cit and BD11 Vim415cit cultures as shown in Figure 5.3 and described in section 5.3.2. As seen with previous donors, the proliferating populations expressed a stronger effector memory phenotype with a slight increase in the highly cytotoxic TEMRA population compared to the total CD4s (Figure 5.4b and c).

Figure 5.4

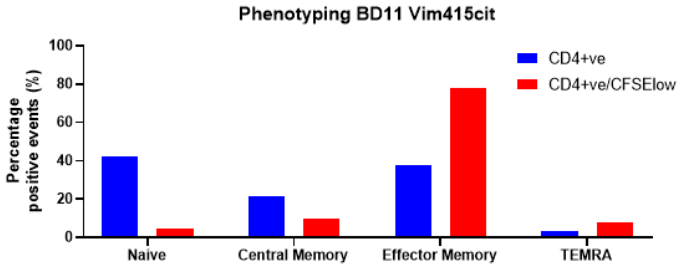
a



b



c



d

	Number of cells/vial for RNA sequencing		
	BD41 Vim28cit	BD41 Eno241cit	BD11 Vim415cit
CFSEhigh	230000	155000	150000
CFSElow	23000	14000	23000

Figure 5.4 PBMCs from 2 healthy donors (BD41 and BD11) were isolated and cultured with citrullinated peptides Vim28cit, Eno241cit and Vim415cit for 10 days before sorting proliferating and non-proliferating populations for RNA sequencing. Proliferating CD4+ve cells identified as $CFSE^{low}$ populations (a). Phenotyping of BD41 Eno241cit (b) and BD11 Vim415cit (c) identified percentage of CD4+ve and $CD4+/CFSE^{low}$ cells within Naïve, Central Memory, Effector Memory and TEMRA populations. Number of cells sorted and sent to IRepertoire for TCR RNA sequencing (d). N=1.

Bulk TCR repertoire sequencing was initially performed by iRepertoire on the non-proliferating and proliferating CD4+ve populations (with part of the sample put aside for downstream single cell sequencing), to identify the frequency of different alpha and beta chain CDR3 sequences in each culture. CFSE high populations for both TRAV (alpha chain) and TRBV (beta chain) showed a very diverse repertoire of sequences, at low frequencies as seen by the number and small size of each spot. In contrast, CFSE low populations were oligoclonal suggesting expansion of a selection of T cells with certain TCRs (Figure 5.5). This was observed in all citrullinated peptide cultures. The top ten most frequent CDR3 sequences for Vim28cit (Table 5.4), Eno241cit (Table 5.5) and Vim415cit (Table 5.6) are shown for both CFSE high and low populations. Of the ten top sequences in the Vim28cit TRAV chain CFSE low population, 9 were not seen in the most abundant sequences in the CFSE high population. One sequence, AVSDEGAQKLV, was observed in both populations but was 67 times more abundant in the CFSE low population (Table 5.4b). For Vim28cit beta sequences, two CDR3 peptides, SVWTSVQETQY and SARFRKNEKTQY, were found in both CFSE low and high population. But again SVWTSVQETQY was 70 times and SARFRKNEKTQY was 50 times more abundant in CFSE low populations (Table 5.4b). The highest frequency sequence seen in the Eno241cit TRAV chain CFSE low population, ATRTGANNLF, and TRBV chain CFSE low population, ASSDGGVDTEAF, were also the most abundant, and second most abundant, in the CFSE high population respectively. CDR3 sequence ATRTGANNLF was 44 times and ASSDGGVDTEAF was 103 times more abundant in the proliferation population (Table 5.5b). The remaining 9 sequences of each chain group were unique to the proliferating population (Table 5.5). No matching sequences were observed between the CFSE high and low TRAV chain populations in Vim415cit cultures but one sequence, SVRKSGDTQY, was found in both low and high beta populations (Table 5.6a). This was 8 times more abundant in the proliferating population (Table 5.6b).

For all of these shared sequences, abundance was greater in the CFSE low populations compared to CFSE high indicating expansion of these T cell clones.

Figure 5.5

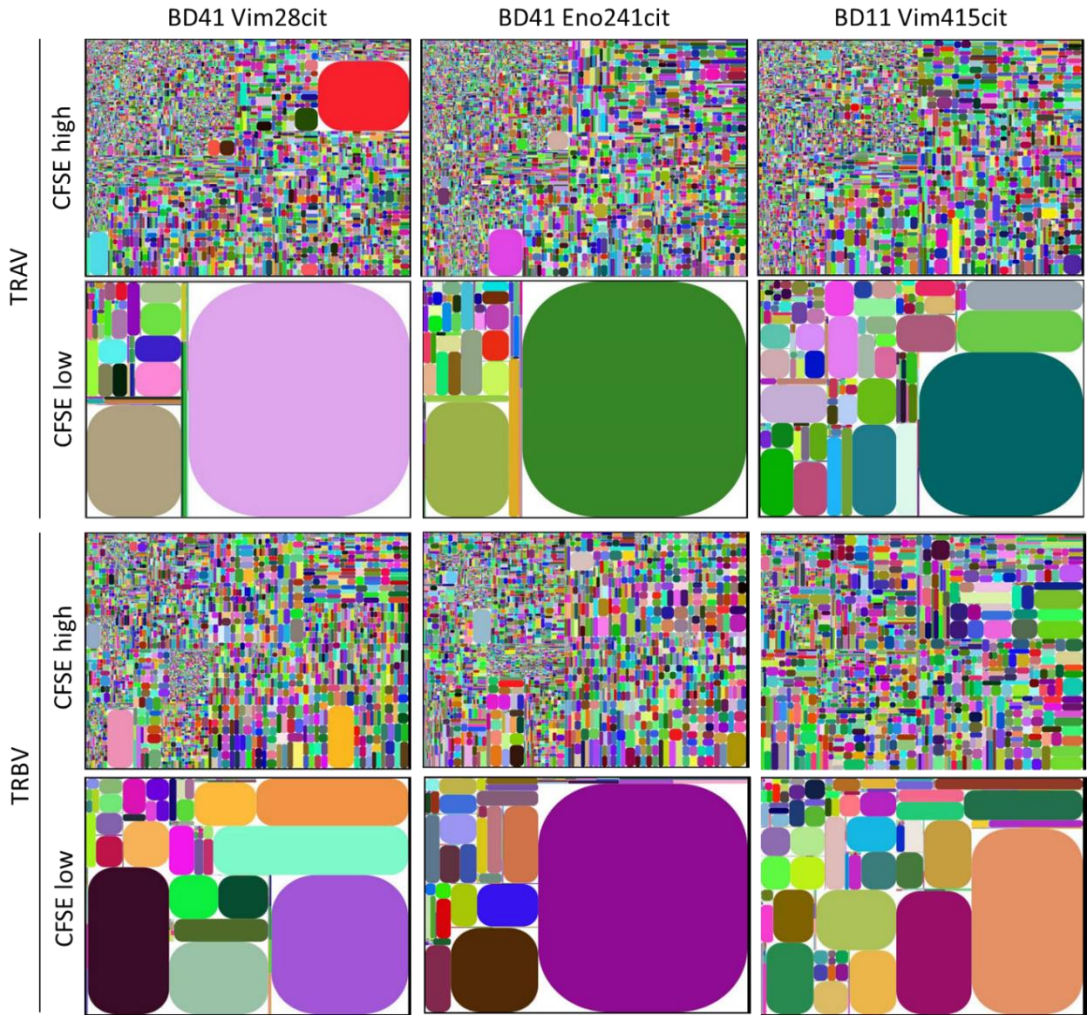


Figure 5.5 Tree maps displaying the diversity of TCR sequences identified in CFSE high and CFSE low populations of CD4 T cells from BD41 PBMCs cultured with Vim28cit and Eno241cit, and BD11 PBMCs cultured with Vim415cit. Each spot represents a unique V-J-CDR3 sequence and the size of each spot denotes the relative frequency. N=1.

Table 5.4

a

ALPHA Vim28cit CFSE high				ALPHA Vim28cit CFSE low			
CDR3 (peptide)	**V domain**	**J domain**	**Copy**	**CDR3 (peptide)**	**V domain**	**J domain**	**Copy**
ATRTGANNLF	hTRAV17	HTRAJ36	58062	AMREVGDYKLS	hTRAV14/DV4	hTRAJ20	442899
AVKDPGNQFY	hTRAV12-2	hTRAJ49	7684	AVSGPGGAQKLV	hTRAV8-6	hTRAJ54	254680
AYRSTNTGNQFY	hTRAV38-2/DV8	hTRAJ49	3926	AVSDEGAQKLV	hTRAV8-6	hTRAJ54	100579
AMREVGDYKLS	hTRAV14/DV4	hTRAJ20	2782	AVVASGTYKYI	hTRAV22	hTRAJ40	45064
AYNNDYKLS	hTRAV38-2/DV8	hTRAJ20	2263	ILRVSFGNEKLT	hTRAV26-2	hTRAJ48	22623
ASASSNFGNEKLT	hTRAV8-6	hTRAJ48	2142	AVRDRRGYQKVT	hTRAV1-1	hTRAJ13	20960
ALDRAGTALI	hTRAV6	hTRAJ15	1648	AVSGYGGSQGNLI	hTRAV8-6	hTRAJ42	18340
ALRNEKLT	hTRAV16	hTRAJ48	1601	AVSEGYGGATNKLI	hTRAV8-6	hTRAJ32	15438
AVSDEGAQKLV	hTRAV8-6	hTRAJ54	1512	AAPDLNFGNEKLT	hTRAV20	hTRAJ48	14892
ALKTRAGADGLT	hTRAV38-2/DV8	hTRAJ45	1420	AVAQLGAAGNKLT	hTRAV8-3	hTRAJ17	13296
BETA Vim28cit CFSE high				**BETA Vim28cit CFSE low**			
CDR3 (peptide)	**V domain**	**J domain**	**Copy**	**CDR3 (peptide)**	**V domain**	**J domain**	**Copy**
ASSDGGVDTEAF	hTRBV25-1	hTRBJ1-1	10921	SVWTSVQETQY	hTRBV29-1	hTRBJ2-5	525848
SVPGGSTDTQY	hTRBV9-1	hTRBJ2-3	7766	SHRDNTDQY	hTRBV29-1	hTRBJ2-3	145439
SVWTSVQETQY	hTRBV29-1	hTRBJ2-5	7475	SVEDQEGTDTQY	hTRBV29-1	hTRBJ2-3	120024
ASSREDRSNYGYT	hTRBV4-1	hTRBJ1-2	4367	SARFRKNEKETQY	hTRBV29-1	hTRBJ2-5	82146
SVQLTGYYGYT	hTRBV29-1	hTRBJ1-2	2363	AISEDQGNEQF	hTRBV10-3	hTRBJ2-1	39534
SVKVRTQY	hTRBV29-1	hTRBJ2-5	2219	ASSYPPRPPNEQF	hTRBV6-5	hTRBJ2-1	27186
SARFRKNEKETQY	hTRBV29-1	hTRBJ2-5	1666	ASSPGGSGRGTGELF	hTRBV5-4	hTRBJ2-1	14834
SVLTALAEAYEQY	hTRBV29-1	hTRBJ-7	1606	ASRELGLLQPQH	hTRBV19	hTRBJ1-5	14581
AWSRQTGGRRGYT	hTRBV30	hTRBJ1-2	1533	ASSRPRDSYNEQF	hTRBV6-6	hTRBJ2-1	8370
SVVLPGANTEAF	hTRBV29-1	hTRBJ1-1	1334	SARQANMGLRNNEQF	hTRBV20-1	hTRBJ2-1	5583

b

Chain	**CDR3 (peptide)**	**Copy number**		**Ratio**
		CFSE high	**CFSE low**	
ALPHA	AVSDEGAQKLV	1512	100579	1:67
BETA	SVWTSVQETQY	7475	525848	1:70
BETA	SARFRKNEKETQY	1666	82146	1:50

Table 5.4 Top 10 most frequent CDR3 peptide sequences identified for both alpha and beta chains in BD41 Vim28cit CFSE high and CFSE low cultures. Rows highlighted in blue show sequences present in the top 10 of both CFSE high and CFSE low populations (a). Ratios of shared sequences in CFSE high and low cultures (b). N=1.

Table 5.5

a

ALPHA Eno241cit CFSE high				ALPHA Eno241cit CFSE low			
CDR3 (peptide)	**V domain**	**J domain**	**Copy**	**CDR3 (peptide)**	**V domain**	**J domain**	**Copy**
ATRTGANNLF	hTRAV17	hTRAJ36	12210	ATRTGANNLF	hTRAV17	hTRAJ36	539750
AVKDPGNQFY	hTRAV12-2	hTRAJ49	2938	ILRTENEKLT	hTRAV26-2	hTRAJ48	98053
AVSEPYNQGGKLI	hTRAV8-6	hTRAJ23	1496	ATDAGTDKLI	hTRAV17	hTRAV34	16566
ALSSSNTGKLI	hTRAV19	hTRAJ37	1489	AFMRGGGADGLT	hTRAV38-1	hTRAJ4	13839
ALDTGRRALT	hTRAV6	hTRAJ5	1263	ALSGGSNYKLT	hTRAV38-2/DV8	hTRAJ53	9227
ALPGYSSASKII	hTRAV6	hTRAJ3	1249	AYRSVYGGATNKLI	hTRAV38-2/DV8	hTRAJ32	8362
ASASSNFGNEKLT	hTRAV8-6	hTRAJ48	978	AVTQPGRDDKII	hTRAV8-4	hTRAJ30	5962
VVSDHGRGSTLGRLY	hTRAV8-2	hTRAJ18	961	AYGKLT	hTRAV13-3	hTRAJ52	5855
AYRGMEYGNKLV	hTRAV38-2/DV8	hTRAJ47	857	ALGYTGGFKTI	hTRAV6	hTRAJ9	5765
IVGYSTLT	hTRAV26-1	hTRAJ11	815	ILNEWSGSEKLV	hTRAV26-2	hTRAJ57	5748
BETA Eno241cit CFSE high				**BETA Eno241cit CFSE low**			
CDR3 (peptide)	**V domain**	**J domain**	**Copy**	**CDR3 (peptide)**	**V domain**	**J domain**	**Copy**
SVLTALAEAYEQY	hTRBV29-1	hTRBJ2-7	4754	ASSDGGVDTEAF	hTRBV25-1	hTRBJ1-1	478247
ASSDGGVDTEAF	hTRBV25-1	hTRBJ1-1	4655	SVPGGSTDTQY	hTRBV29-1	hTRBJ2-3	73481
AVEPAGQVNIQY	hTRBV29-1	hTRB2-4	3214	SPDAGTSGAPPHLVFSYNEQF	hTRBV20-1	hTRBK2-1	26810
AWSRGIMDEQF	hTRBV30	hTRBJ2-1	2256	SVEKGWNEQF	hTRBV29-1	hTRBJ2-1	25990
SVVLPGANTEAF	hTRBV29-1	hTRABJ1-1	2111	ASSYRVSRYT	hTRBV28	hTRBJ1-2	16939
AWSVGWLAGEKTEAF	hTRBV30	hTRBJ1-1	1709	SVGVAGITYEQY	hTRBV29-1	hTRBJ2-5	11184
SVSSSGANVLT	hTRBV29-1	hTRBJ2-6	1562	ASSDGQKYQETQY	hTRBV6-6	hTRBJ2-5	10890
SVTGTGGLNQPQH	hTRBV29-1	hTRBJ1-5	1452	ASSQDQGTPYEQY	hTRBV4-3	hTRBJ2-7	9963
SVVSGANVLT	hTRBV29-1	hTRBJ2-6	1396	ASSRAESTDTQY	hTRBV19	hTRBJ2-2	9526
AWSPFRGGSEKLF	hTRBV30	hTRBJ1-4	1390	ASSRLPTHSSYNEQF	hTRBV3-1	hTRBJ2-1	9291

b

Chain	**CDR3 (peptide)**	**Copy number**		**Ratio**
		CFSE high	**CFSE low**	
ALPHA	ATRTGANNLF	12210	539750	1:44
BETA	ASSDGGVDTEAF	4655	478247	1:103

Table 5.5 Top 10 most frequent CDR3 peptide sequences identified for both alpha and beta chains in BD41 Eno241cit CFSE high and CFSE low cultures. Rows highlighted in blue show sequences present in the top 10 of both CFSE high and CFSE low populations (a). Ratios of shared sequences in CFSE high and low cultures (b). N=1.

Table 5.6

a

ALPHA Vim415cit CFSE high				ALPHA Vim415cit CFSE low			
CDR3 (peptide)	**V domain**	**J domain**	**Copy**	**CDR3 (peptide)**	**V domain**	**J domain**	**Copy**
AVTLNSGNTPLV	hTRAV8-6	hTRAJ29	2516	IVRGASGTQGAQKLV	hTRAV26-1	hTRAJ54	170373
IVRSGGTSYGKLT	hTRAV26-1	hTRAJ52	2228	ILRDVGNQGGKLI	hTRAV26-2	hTRAJ23	33328
AVSSGGYQKVT	hTRAV8-6	hTRAJ13	1397	ALLSLLAGGTSYGKLT	hTRAV9-2	hTRAJ52	22039
IVRGTHGGANSKLT	hTRAV26-1	hTRAJ56	1309	ILRALNEKLT	hTRAV26-2	hTRAJ48	22039
AVSDVRTGRRALT	hTRAV8-6	hTRAJ5	1262	ALSGGSNYKLT	hTRAV16	hTRAJ53	15975
ALGRGDYKLS	hTRAV6	hTRAJ20	1113	AMSGGADGLT	hTRAV12-3	hTRAJ45	14003
AVAPGYNFNKFY	hTRAV22	hTRAJ21	1061	ILRGFILSGAGSYQLT	hTRAV26-2	hTRAJ28	13877
IVRAKNYGGSQGNLI	hTRAV26-1	hTRAJ42	981	IVAAYKLS	hTRAV26-1	hTRAJ20	12075
VVRGGGGNKLT	hTRAV10	hTRAJ10	923	ALLNQAGTALI	hTRAV20	hTRAJ15	11663
AVILNTGRRALT	hTRAV8-6	hTRAJ5	885	VVRIMDTGRRALT	hTRAV12-1	hTRAJ5	11521
BETA Vim415cit CFSE high				**BETA Vim415cit CFSE low**			
CDR3 (peptide)	**V domain**	**J domain**	**Copy**	**CDR3 (peptide)**	**V domain**	**J domain**	**Copy**
AVGLLVGVADTQY	hTRBV30	hTRBJ2-3	8632	ASSLTDTQY	hTRBV6-6	hTRBJ2-3	210421
AWITGGTEAF	hTRBV30	hTRBJ1-1	7456	SVEAPEEETQY	hTRBV29-1	hTRBJ2-5	94738
AWTGSNWAYEQY	hTRBV30	hTRBJ2-7	5199	ASSQPAIKRWEQF	hTRBV4-1	hTRBJ2-1	49598
AWSDSEQF	hTRBV30	hTRBJ2-1	4809	ASSRGTDGTNEQY	hTRBV5-1	hTRBJ2-7	36204
AWSQRRGLGTEAF	hTRBV30	hTRBJ1-1	4707	ASQEAGAFYNSPLH	hTRBV19	hTRBJ1-6	34665
AWSRDRGRTEAF	hTRBV30	hTRBJ1-1	4661	SVRKSGDTQY	hTRBV29-1	hTRBJ2-3	33107
SVRWADTQY	hTRBV29-1	hTRBJ2-3	4084	ASSLMSGTSYDQY	hTRBV7-3	hTRBJ2-3	30199
ASRGQDFTDTQY	hTRBV6-1	hTRBJ2-3	3758	ASSWNTEAF	hTRBV2	hTRBJ1-1	21847
AWTENYGYT	hTRBV30	hTRBJ-2	3453	ASRRTGGQGNEKLF	hTRBV11-2	hTRBJ1-4	17910
AWSVPGGAQDTQY	hTRBV30	hTRBJ2-3	3416	ASSWWTGQETQY	hTRBV5-1	hTRBJ2-5	16463

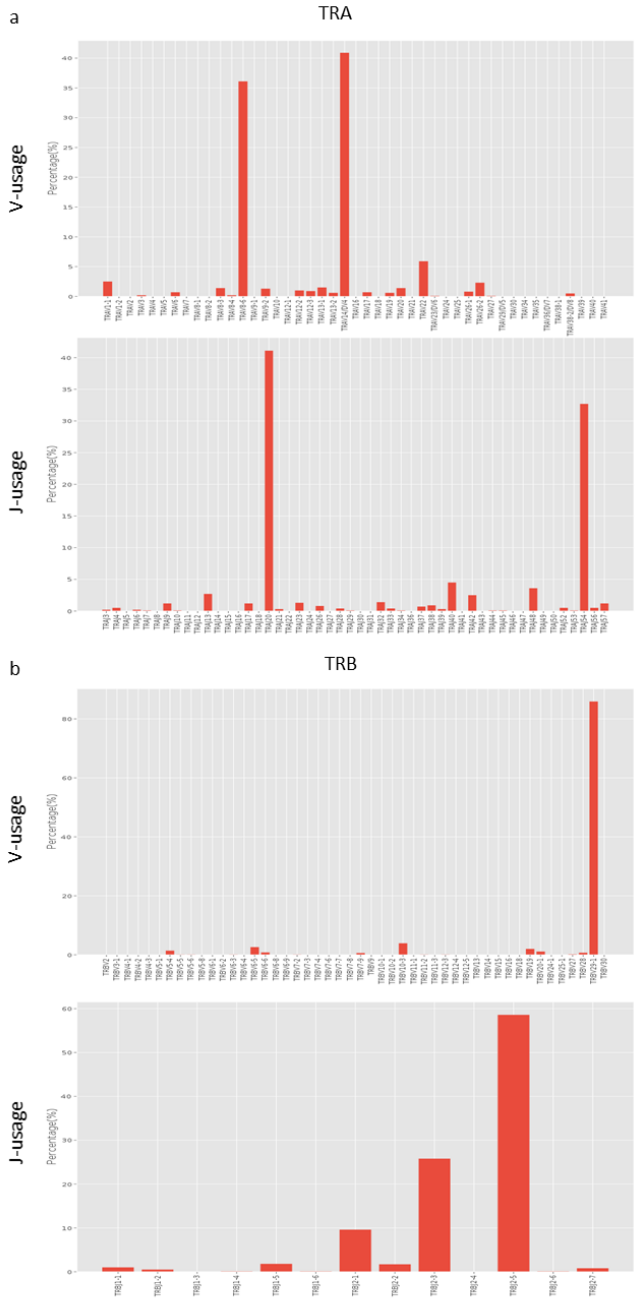
b

Chain	**CDR3 (peptide)**	**Copy number**		**Ratio**
		CFSE high	**CFSE low**	
BETA	SVRWADTQY	4084	33107	1:8

Table 5.6 Top 10 most frequent CDR3 peptide sequences identified for both alpha and beta chains in BD41 Vim415cit CFSE high and CFSE low cultures. Rows highlighted in blue show sequences present in the top 10 of both CFSE high and CFSE low populations (a). Ratios of shared sequences in CFSE high and low cultures (b). N=1.

Further analysis of bulk sequencing data determined the most prevalent V- and J-segments in alpha and beta chains of proliferating Vim28cit (Figure 5.6), Eno241cit (Figure 5.7) and Vim415cit (Figure 5.8) cultures. Although many V- and J- segments were found in each proliferating culture, higher percentages of up to 2 dominant V-, J- segments were identified. Percentages of these dominant V- and J- segments ranged between 13-85% of the total population. The TRBV29-1 gene was dominant with percentage usage of 85%, 15% and 19% in Vim28cit, Eno241cit and Vim415cit cultures respectively (Figure 5.6, 5.7 and 5.8). For the alpha chain, TRAV26-2 was also shared between all three peptides but was only identified as dominant in Eno241cit and Vim415cit cultures. Analysis of J-usage found TRAJ54 and TRBJ2-3 were both dominant in Vim28cit and Vim415cit cultures (Figures 5.6 and 5.8) with no shared dominant segments with Eno241cit (Figure 5.7).

Figure 5.6

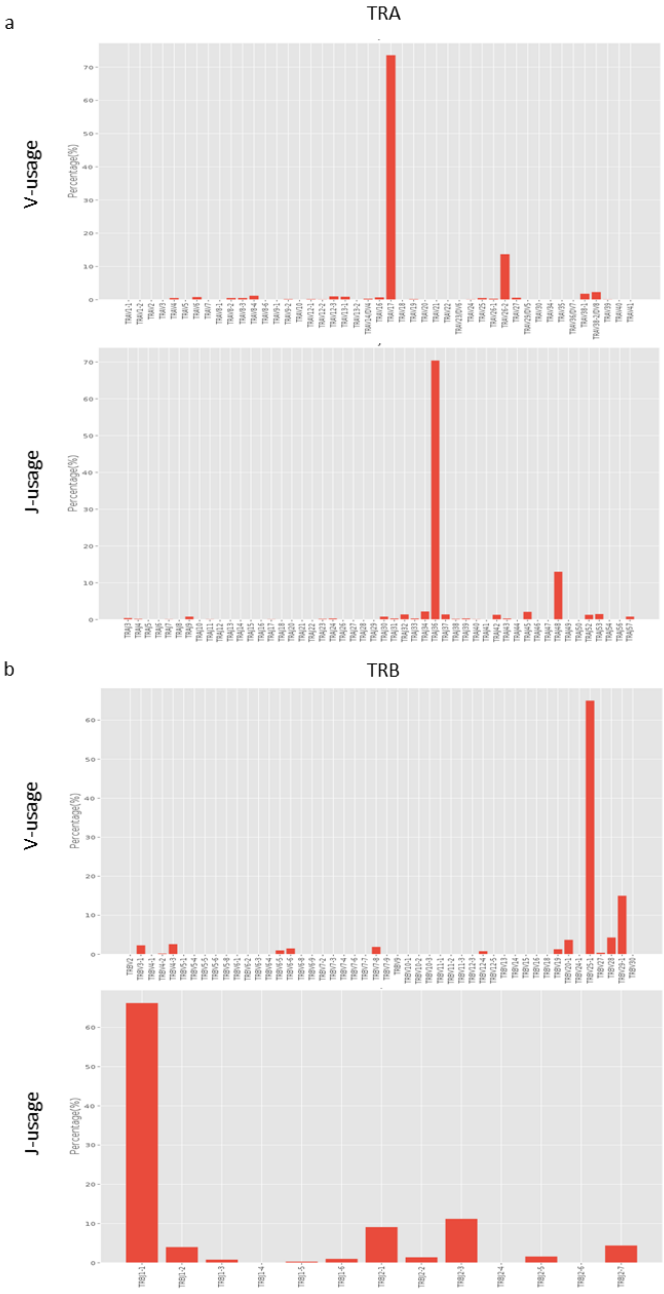


c

TRA				TRB			
V-usage		J-Usage		V-usage		J-usage	
TRAV14/DV4	41%	TRAJ20	41%	TRBV29-1	85%	TRBJ2-5	59%
TRAV8-6	36%	TRAJ54	33%	-		TRBJ2-3	25%

Figure 5.6 V- and J- usage in alpha (a) and beta (b) chains of BD41 Vim28cit proliferating (CFSE low) cultures. Highest frequency V and J domains listed for alpha (TRA) and beta (TRB) chains (c). N=1.

Figure 5.7

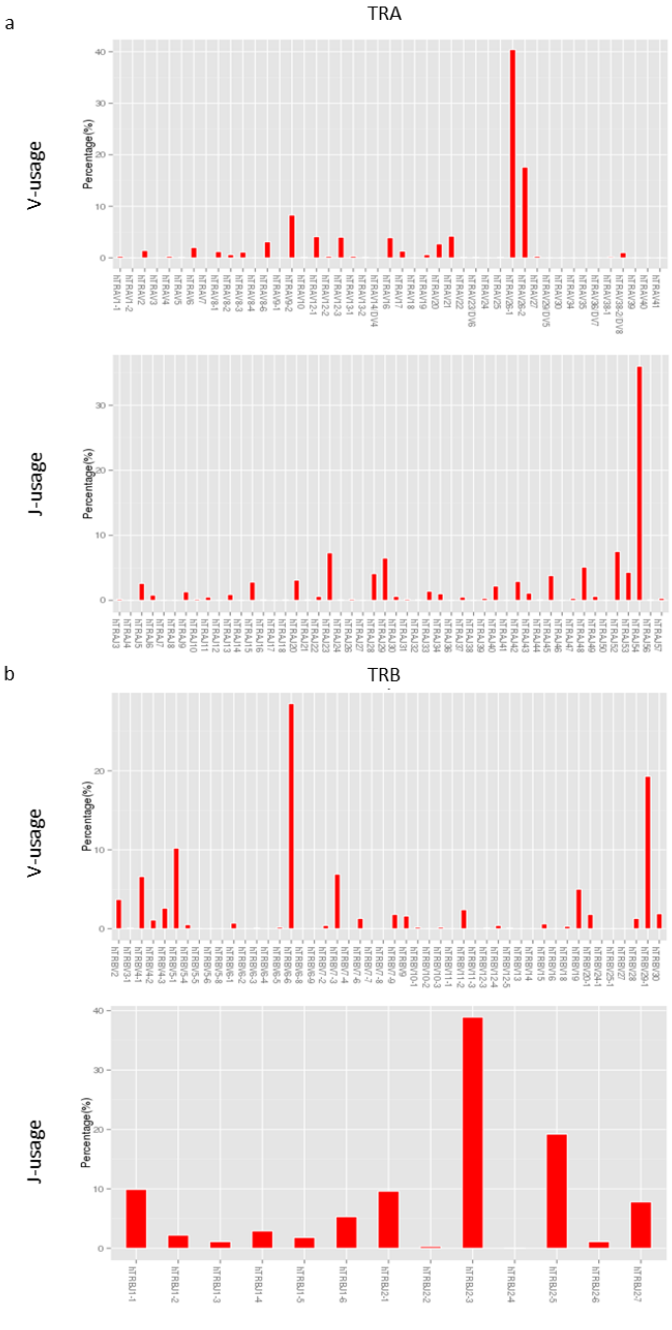


c

TRA				TRB			
V-usage		J-Usage		V-usage		J-usage	
TRAV17	72%	TRAJ36	70%	TRBV25-1	64%	TRBJ1-1	65%
TRAV26-2	13%	TRAJ48	30%	TRBV29-1	15%	-	

Figure 5.7 V- and J- usage in alpha (a) and beta (b) chains of BD41 Eno241cit proliferating (CFSE low) cultures. Highest frequency V and J domains listed for alpha (TRA) and beta (TRB) chains (c). N=1.

Figure 5.8



c

TRA				TRB			
V-usage		J-Usage		V-usage		J-usage	
TRAV26-1	40%	TRAJ54	36%	TRBV6-6	28%	TRBJ2-3	39%
TRAV26-2	18%	-		TRBV29-1	19%	TRBJ2-5	19%

Figure 5.8 V- and J- usage in alpha (a) and beta (b) chains of BD11 Vim415cit proliferating (CFSE low) cultures. Highest frequency V and J domains listed for alpha (TRA) and beta (TRB) chains (c). N=1.

After determining the clonality of proliferating populations, single cell sequencing was performed and iPair software was used to determine the frequency of specific alpha and beta chain pairing. Data analysis was performed by Rachael Metheringham (Scancell Ltd). Potential TCRs were listed and numbered according to occurrence frequency; the number of wells with matched alpha and beta chains (Table 5.7). Bulk sequencing was performed on remaining cells that were not used for single cell sequencing. This allowed ranking of chains found in single cell sequencing according to their frequency in the bulk sample and was termed 'Bulk Rank'. Each alpha and beta chain identified was also compared to sequences detected in equivalent non-proliferating populations and labelled as 'Shared' if found in both populations or 'Unique' if only observed in proliferating populations. In Vim28cit cultures, 14/52 wells had identical CDR3 peptides highlighting this TCR as a likely candidate (Table 5.7a). Both alpha and beta chains were registered as shared as they were found in bulk CFSE high and low populations. Read counts for both chains were high (30000-100000) in non-proliferating populations however increased to >4000000 in proliferating populations. Many other sequences were also detected with some wells containing more than two chains, an additional alpha or beta chain with a low read count (highlighted in red). Some of these CDR3 peptides were shared but at lower read counts in non-proliferating populations (<32000) with variable increases in frequency in proliferating populations (400-4000000). Only TCRs 4, 10 and 13 contained both alpha and beta unique chains.

A more clonal response was seen in Eno241cit cultures with the most frequent TCR identified in 61/75 wells and only 3 other potential TCRs (Table 5.7b). Again, CDR3 sequences for the top TCRs were shared in bulk samples with non-proliferating populations found at read counts 205734 and 83304 for alpha and beta chains respectively. Both chains increased in frequency to >6300000 in the proliferating population. TCR 3 also contained shared alpha and beta chains, found at lower

frequencies in CFSE high (read counts 505-24534) which was elevated in CFSE low (read counts 32791-975476) populations. TCR 2 contained a shared alpha chain but unique beta chain and both chains were unique in TCR 4.

The sequences determined from the Vim415cit culture were not as clonal as seen with Vim28cit and Eno241cit, with a total of 8 TCRs detected in only 2-5 wells out of 35 wells analysed (Table 5.7c). In addition, only TCR 3 and TCR 6 contained both shared alpha and beta chains which were seen at lower read counts in non-proliferating populations compared to shared sequences identified in Vim28cit and Eno241cit cultures; read counts between 892-34959. TCRs 1, 2, 5 and 7 contained a shared alpha chain but unique beta chain, and TCRs 4 and 8 contained unique chains only. All TCRs listed were tested for reactivity to the corresponding citrullinated peptide.

Table 5.7

a

TCR	FREQUENCY (28/52 WELLS)	WELLS	CDR1 Peptide	CDR2 Peptide	CDR3 Peptide	V Gene	D Gene	J Gene	C Gene	Read Count	Comparison with bulk data set			
											Bulk Rank	Unique / shared	Normalised read counts	
													CFSE high	CFSE low
1	13/14	A05/A08/A10/B01/B03/B11/C07/D11/E04/F06/F12/H07/H08/H04	SQVTM	ANQGSEA	SVWTSVQETQY	hTRBV29-1	hTRBD2	hTRBJ2-5	hTRBC	2935	1	S	110892	4922545
			TSDQSYG	QGSYDEQN	AMREVGDYKLS	hTRAV14/DV4	*	hTRAJ20	hTRAC	2350	1	S	31227	4016372
2	3	B08/D06/H02	SQVTM	ANQGSEA	SHRDNTDTQY	hTRBV29-1	hTRBD2	hTRBJ2-3	hTRBC	3149	2	S	9865	1361477
			TISGTDY	GLTSN	ILRVSFGNEKLT	hTRAV26-2	*	hTRAJ48	hTRAC	1615	5	S	662	205153
3	2	G07/H03	SQVTM	ANQGSEA	SARFRKNEKETQY	hTRBV29-1	*	hTRBJ2-5	hTRBC	2707	4	S	24715	768981
			NSASDY	IRSNMDK	AEAYSGGYQKVT	hTRAV13-2	*	hTRAJ13	hTRAC	2141	17	S	1178	54854
4	2	D02/E06	SEHKS	YYEKEE	ASSLGSRSGYT	hTRBV5-5	hTRBD2	hTRBJ1-2	hTRBC	791	26	U	N/A	13826
			SSVSVY	YLSGSTLV	AVSGYGGSQGNLI	hTRAV8-6	*	hTRAJ42	hTRAC	6006	7	U	N/A	166313
5	2/3	F05/G05/G02	MNHNY	SVGAGI	ASSRPRDSYNEQF	hTRBV6-6	*	hTRBJ2-1	hTRBC	1369	9	S	712	78352
			TRDTTYY	RNSFDEQN	ALSATYNQGGKLI	hTRAV19	*	hTRAJ23	hTRAC	3303	20	S	617	47182
6	2	A03/A06	SEHNR	FQNEAQ	ASSLFPGTGNTEAF	hTRBV7-9	hTRBD1	hTRBJ1-1	hTRBC	212	32	U	N/A	10681
			DSASNY	IRSNVGE	AAPYSSASKII	hTRAV13-1	*	hTRAJ3	hTRAC	6401	29	S	89	16586
7	1	E01	SQVTM	ANQGSEA	SHRDNTDTQY	hTRBV29-1	hTRBD2	hTRBJ2-3	hTRBC	4399	2	S	9865	1361477
			TSDQSYG	QGSYDEQN	AMREVGDYKLS	hTRAV14/DV4	*	hTRAJ20	hTRAC	851	1	S	31227	4016372
8	1	E02	SEHNR	FQNEAQ	APGGTSGRGEQF	hTRBV7-9	hTRBD2	hTRBJ2-1	hTRBC	625	14	U	N/A	26716
			DRGSQS	IYSNGD	AVNAGNNRKLI	hTRAV12-2	*	hTRAJ38	hTRAC	1829	13	S	2076	90937
9	1/2	C06/B12	DFQATT	SNEGSKA	SALDGQGGLNEQF	hTRBV20-1	hTRBD1	hTRBJ2-1	hTRBC	3091	11	S	637	36761
			DSASNY	IRSNVGE	AASTGGYNKLI	hTRAV13-1	*	hTRAJ4	hTRAC	2512	19	S	303	49486
10	1	C12	SGHDT	YYEEEE	ASSQTGSEAF	hTRBV5-6	hTRBD1	hTRBJ1-1	hTRBC	1313	25	U	N/A	14023
			YGATPY	YFSGDTLV	AVGFSGGYQKVT	hTRAV8-3	*	hTRAJ13	hTRAC	3428	28	U	N/A	18000
11	5	D03/F04/F07/H01/H11	MNHEY	SVGAGI	ASSYPPRPPNEQF	hTRBV6-5	*	hTRBJ2-1	hTRBC	2107	6	S	1335	254492
			ATGYPS	ATKADDK	ALTLNTGGFKTI	hTRAV9-2	*	hTRAJ9	hTRAC	802	11	S	246	120264
12	1	H06	LNHDA	SQIVND	ASSLQTSGGLDEQF	hTRBV19	hTRBD2	hTRBJ2-1	hTRBC	945	16	S	845	22841
			SSVSVY	YLSGSTLV	AVSEGYGGATNKLI	hTRAV8-6	*	hTRAJ32	hTRAC	3803	8	S	617	139997
13	1	E03	MNHEY	SMNVEV	ASRQTGPYGYT	hTRBV27	hTRBD1	hTRBJ1-2	hTRBC	508	24	U	N/A	14397
			YGATPY	YFSGDTLV	AVAQLGAAGNKLT	hTRAV8-3	*	hTRAJ17	hTRAC	4530	10	U	N/A	120573
14	1	D01	LNHDA	SQIVND	ASRELGLLQPQH	hTRBV19	*	hTRBJ1-5	hTRBC	539	8	S	29	477
			SSVSVY	YLSGSTLV	AVSDEGAQKLV	hTRAV8-6	*	hTRAJ54	hTRAC	4559	3	S	16972	912087
15	1	C03	SEHNR	FQNEAQ	ASSRSGWGGELF	hTRBV7-9	hTRBD2	hTRBJ2-2	hTRBC	1455	23	S	311	14519
			SVFSS	VVTGGEV	AGDFGTASKLT	hTRAV27	*	hTRAJ44	hTRAC	3319	39	U	N/A	9775
16	1	B05	MDHEN	SYDVKM	ASTTPWREGEQF	hTRBV28	hTRBD2	hTRBJ2-1	hTRBC	1600	13	S	1097	30835
			DSASNY	IRSNVGE	AAKRRGQNFV	hTRAV13-1	*	hTRAJ26	hTRAC	3345	15	S	1212	80744

b

TCR	FREQUENCY (75 WELLS)	WELLS	CDR1 Peptide	CDR2 Peptide	CDR3 Peptide	V Gene	D Gene	J Gene	C Gene	Read Count	Comparison with bulk data set			
											Bulk Rank	Unique / shared	Normalised read counts	
													CFSE high	CFSE low
1	61	A02/A03/A04/A05/A06/A07/A08/A09/B01/B02/B03/B04/B06/B08/B10/B11/C01/C02/C03/C04/C05/C06/C07/C08/D01/D02/D04/D05/D06/D07/D09/D10/D11/E01/E02/E04/E05/E06/E08/E09/E10/F01/F02/F03/F04/F05/F08/F09/F10/F11/G02/G03/G05/G07/G08/G09/G10/G11/H04/H06	MGHDK	SYGVNS	ASSDGGVDTEAF	hTRBV25-1	hTRBD2	hTRBJ1-1	hTRBC	546	1	S	83304	6348835
			TSINN	IRSNERE	ATRTGANNLF	hTRAV17	*	hTRAJ36	hTRAC	11339	1	S	205734	6935476
2	4	D03/E03/G04/H07	DFQATT	SNEGSKA	SPDAGTSGAPPHLVFSYNEQF	hTRBV20-1	hTRBD2	hTRBJ2-1	hTRBC	57	3	U	N/A	355908
			TISGTDY	GLTSN	ILRTENEKLT	hTRAV26-2	*	hTRAJ48	hTRAC	5822	2	S	3841	1259924
3	2	E12/H05	SQVTM	ANQGSEA	SVPGGSTDTQY	hTRBV29-1	*	hTRBJ2-3	hTRBC	2410	2	S	24534	975476
			NSAFQY	TYSSGN	AMSRGGWGKLQ	hTRAV12-3	*	hTRAJ24	hTRAC	534	16	S	505	32791
4	1	A10	LGHNA	YSLEER	ASSQDLGLAFTEQF	hTRBV4-3	hTRBD2	hTRBJ2-1	hTRBC	192	21	U	N/A	29709
			NSAFQY	TYSSGN	AMSVSGGSQGNLI	hTRAV12-3	*	hTRAJ42	hTRAC	3357	14	U	N/A	46116

c

TCR	FREQUENCY (35 WELLS)	WELLS	CDR1 Peptide	CDR2 Peptide	CDR3 Peptide	V Gene	D Gene	J Gene	C Gene	Read Count	Comparison with bulk data set			
											Bulk Rank	Unique / shared	Normalised read counts	
													CFSE high	CFSE low
1	5	B04/D02/D04/D12/G10	LNHDA	SHIVND	ASQEAGAFYNSPLH	hTRBV19	hTRBD2	hTRBJ1-6	hTRBC	1704	5	U	N/A	448227
			TISGTDY	GLTSN	ILRDVGNQGGKLI	hTRAV26-2	*	hTRAJ23	hTRAC	29379	2	S	1741	692542
2	4	F09/GO7/H05/HO8	MGHRA	YSYEKL	ASSQPAIKRWEQF	hTRBV4-1	*	hTRBJ2-1	hTRBC	1276	3	U	N/A	2586
			TISGNEY	GLKNN	IVRGASGTQGAQKLV	hTRAV26-1	*	hTRAJ54	hTRAC	18994	1	S	16694	350284
3	3	C06/G05/H11	MNHNY	SVGAGI	ASSLTDTQY	hTRBV6-6	*	hTRBJ2-3	hTRBC	11529	1	S	34959	2720797
			ATGYPS	ATKADDK	ALSPASGNTPLV	hTRAV9-2	*	hTRAJ29	hTRAC	10006	12	S	892	149592
4	2	C02/C04	SGHRS	YFSETQ	ASSRGTSGTNEQY	hTRBV5-1	hTRBD2	hTRBJ2-7	hTRBC	3074	4	U	N/A	468126
			ATGYPS	ATKADDK	ALLSLLAGGTSYGKLT	hTRAV9-2	*	hTRAJ52	hTRAC	9615	3	U	N/A	530711
5	2	D08/D11	SGHAT	FQNNGV	ASRRTGGWGNEKLF	hTRBV11-2	hTRBD1	hTRBJ1-4	hTRBC	7740	9	U	N/A	231580
			NSAFQY	TYSSGN	AMSGGGADGLT	hTRAV12-3	*	hTRAJ45	hTRAC	14581	6	S	1996	290976
6	2	A06/B03	SGHTA	FQGTGA	ASSLMSGYSTDTQY	hTRBV7-3	*	hTRBJ2-3	hTRBC	11276	7	S	1085	390480
			DSAIYN	IQSSQRE	AVNSGNTPLV	hTRAV21	*	hTRAJ29	hTRAC	14247	11	S	4778	236825
7	2	D03/F02	SNHLY	FYNNEI	ASHGVAGAGEQF	hTRBV2	hTRBD2	hTRBJ2-1	hTRBC	9698	24	U	N/A	59427
			DSAIYN	IQSSQRE	AVGKGNTPLV	hTRAV21	*	hTRAJ29	hTRAC	7186	23	S	573	77279
8	2	B09/F07	LGHNT	FRNRAP	ASGLTGGSNTGELF	hTRBV12-5	hTRBD2	hTRBJ2-2	hTRBC	365	60	U	N/A	9335
			YGGTVN	YFSGDPLV	AVISVVAGNTPLV	hTRAV8-1	*	hTRAJ29	hTRAC	17301	16	U	N/A	101736

Table 5.7 TCR sequences identified in CFSE low populations from BD41 cultured with Vim28cit (a) and Eno241cit (b) peptides and BD11 cultured with Vim415cit peptide (c) using single cell sequencing and iPair software analysis. Read counts refers to the stitched and filtered reads associated with that particular CDR3 peptide from that well. The bulk rank is the position in which that single cell CDR3 matched with the bulk sample. Sequences were also ranked as unique or shared depending on whether they were also found in the CFSE high population. Read counts given for CDR3 sequence as found in bulk samples. Unique sequences only found in CFSE low bulk population so marked as N/A for CFSE high read count. Wells highlighted in red contained more than one alpha or beta chain and chains with highest read counts taken into consideration. N=1.

5.2.4 TCR transductions of Jurkat 76 cell line

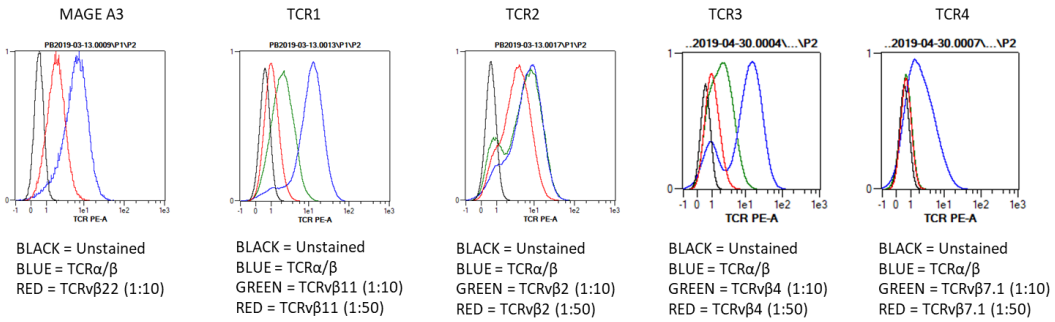
A TCR with known antigen specificity was required for use as a positive control and for optimisations of transfection and transduction protocols. Mouse experiments have shown MODI1 peptides can be presented by HLA-DR4 and HLA-DP4 [2, 221]. Therefore, due to its HLA-DP4 restriction, the TCR specific for MAGE A3$^{243\text{-}258}$ was selected [343, 344].

The Jurkat 76 (J76) cell line is a derivative of the human T cell lymphoma cell line Jurkat E6.1, which is characterised by its lack of TCR alpha and beta chain expression [345]. Therefore it will only express the transduced TCR making it a useful model to check TCR transduction efficiency. This cell line is also negative for cell surface expression of CD3 and CD4/CD8 so upregulation of CD3 should correlate with TCR expression. J76 were transduced using lenti viral particles at a multiplicity of infection (MOI) of 10 for 48 hours prior to puromycin selection. TCR expression was assessed using pan-TCR (anti-TCRα/β) at 1:25 dilution and vβ specific (vβ22/11/2/4/7.1) antibodies at 1:10 and 1:50 dilutions 7 days post transduction (Figure 5.9a). Expression levels with the pan-TCR antibody were greater than 80% and higher than seen with the corresponding vβ specific antibody in all conditions, except for Eno241cit TCR4 which was only ~60% positive with pan-TCR antibody. The signal with vβ specific antibody staining of Eno241cit TCR4 transduced cells was much lower, only showing 2% positive at 1:10 dilution. For MAGE A3 and Eno241cit TCR1-3 transduced J76, there was approximately 20% increase in TCR expression with pan TCRα/β antibody compared to vβ specific antibodies (at 1:10 dilution). Median fluorescence intensity (MFI) values also increased from ~2.5 to 6.68 and 12.21 for MAGE A3 and Eno241cit TCR1 respectively. No difference in MFI was observed for TCR2 but a larger difference was found between vβ specific (2.95) and pan-TCR (13.20) in TCR3 transduced cultures.

To increase and stabilise TCR expression, all transduced lines were enriched using magnetic selection (data not shown) or by cell sorting using pan-TCR antibody (Figure 5.9b). This greatly improved the percentage of TCR positive cells in Eno241cit TCR4 transduced J76 increasing from 35% (MFI 2.36) to 80% (MFI 3.75) post-sorting. The original Eno241cit TCR2 culture displayed reduced TCR expression at the time of sorting, 61% (MFI 3.10), however sorting elevated expression to 96.77% (MFI 8.41). The percentage of TCR expression in MAGE A3 and Eno241cit TCR1 and TCR3 transduced J76 were >91% but still increased to >99% after sorting. Higher MFIs were also observed post-sorting from 7.38, 6.68 and 6.20 to 13.87, 11.69 and 12.98 in MAGE A3, Eno241cit TCR1 and TCR3 cultures respectively. Overall, staining with pan-TCR gave the best signal and TCR expression was improved after sorting.

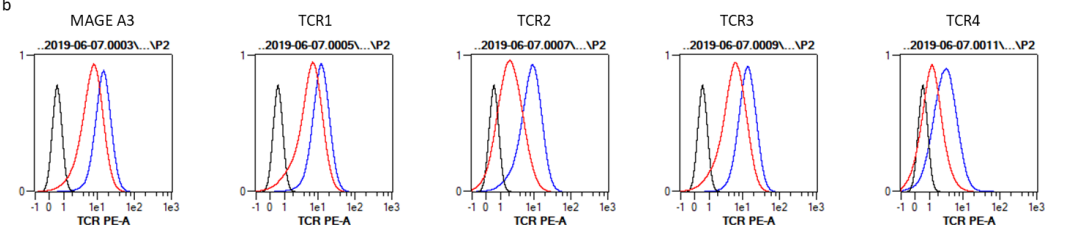
Figure 5.9

a



	MAGE A3		TCR1		TCR2		TCR3		TCR4	
	%	MFI	%	MFI	%	MFI	%	MFI	%	MFI
TCRα/β	94.25	6.68	94.83	12.21	88.50	7.54	82.19	13.20	58.82	3.29
Vβ specific (1:10)	68.72	2.40	71.10	2.75	80.96	7.36	62.39	2.95	2.01	1.67
Vβ specific (1:50)	N/A	N/A	23.63	1.81	82.87	4.32	23.77	1.90	1.52	1.66

b

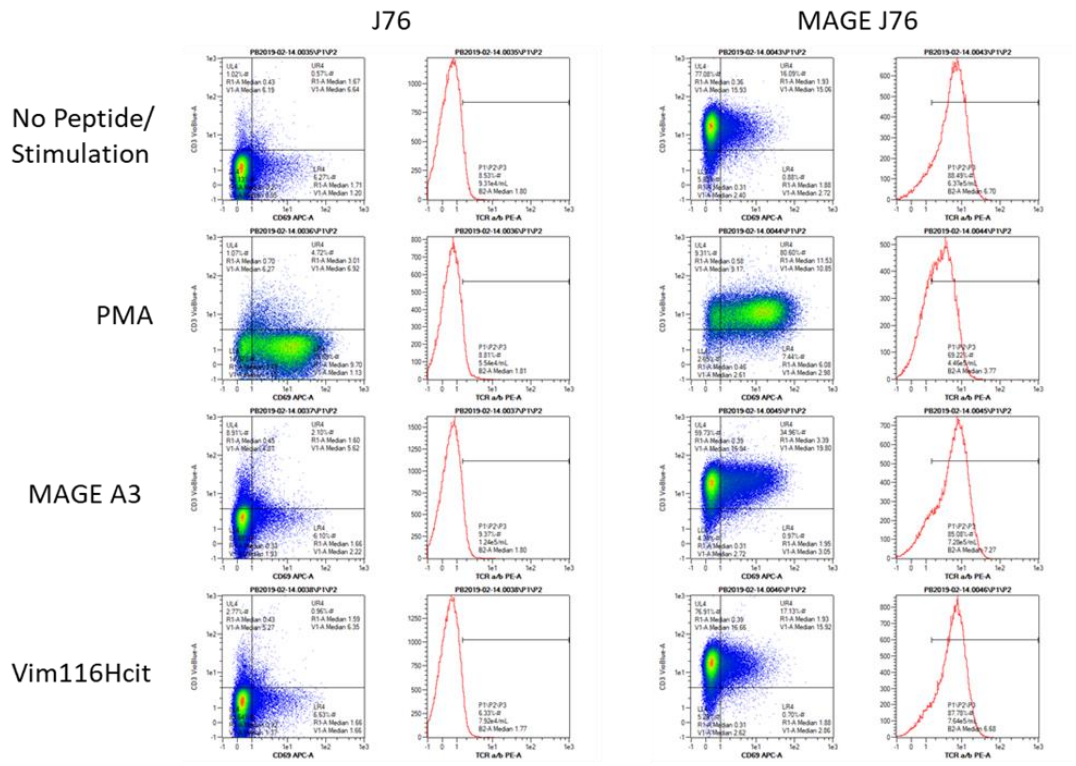


	MAGE A3		TCR1		TCR2		TCR3		TCR4	
	%	MFI	%	MFI	%	MFI	%	MFI	%	MFI
Original	95.59	7.38	91.58	6.68	61.05	3.10	91.62	6.20	35.14	2.36
Sorted	99.77	13.87	99.51	11.69	96.77	8.41	99.72	12.98	79.74	3.75

Figure 5.9 Jurkat 76 cell line transduced with either MAGE A3 TCR, Eno241cit TCR1, Eno241cit TCR2, Eno241cit TCR3, or Eno241cit TCR4 and stained for TCR expression after 7 days of culture using pan-TCR (TCRα/β) at dilution 1:25 or vβ specific antibodies at indicated dilutions. Puromycin (0.25µg/ml) selection was applied at day 2 of culture (a). Cell lines sorted based on pan-TCR (TCRα/β) antibody to increase TCR expression (c). Percentages and median fluorescence intensities (MFI) shown for each culture. N=1.

To assess the functionality and specificity of the MAGE A3 TCR transduced J76, the cells were cocultured in an antigen presentation assay and recognition was checked using the early activation marker CD69 [346]. Monocyte derived Dendritic cells (DCs) were generated from healthy HLA-DP4 positive donor. DCs were pulsed with the MAGE A3 (aa243-258 KKLLTQHFVQENYLEY) or irrelevant peptide Vim116Hcit (aa116-135 NYID-hcit-VRFLEQQN-hcit-ILLAEL) for 1 hour and then matured overnight with 20µg/ml Poly I:C. The following day DCs were cocultured overnight with untransduced (J76) or MAGE A3 TCR transduced J76 (MAGE J76) at a range of effector: target (E:T) ratios; 1:1, 2:1, 5:1, and 10:1. Cells were harvested and checked for CD3 (VioBlue), CD69 (APC) and TCR (PE) expression. CD3 and TCR expression in J76 was low; <5% and <10% respectively, however transduction with MAGE A3 TCR induced both CD3 and TCR expression up to ~90% (Figure 5.10). Cells that co-expressed CD3 and CD69 were considered as activated J76. Phorbol 12-myristate 13-acetate (PMA) was used as a positive control for activation to compare against peptide pulsed conditions. PMA stimulation induced high levels of activation as seen by > 80% CD3/CD69 double positive events in both untransduced and transduced conditions (Figure 5.10). In comparison, MAGE A3 peptide pulsed DCs induced 34% CD3/CD69 expression in MAGE J76 when cultured at 5:1 effector:target (E:T) ratio; lower than seen with PMA stimulation but double the background induced by the irrelevant peptide Vim116Hcit (Figure 5.10). The healthy donor used in this assay has previously shown to proliferate in response to Vim116Hcit (Appendix 5), therefore this peptide should be presented by the donors DCs.

Figure 5.10



Condition	CD3/CD69 double positive cells (%)		TCR expression (%)	
	J76	MAGE J76	J76	MAGE J76
No peptide/stimulation	0.57	16.09	8.53	88.49
PMA	4.72	80.60	8.81	69.22
MAGE A3	2.10	34.96	9.31	85.08
Vim116Hcit	0.96	17.13	6.33	87.78

Figure 5.10 Dendritic cells (DCs) pulsed with MAGE A3 or Vim116Hcit peptides for 1hr, and matured with 20 µg/ml Poly I:C overnight prior to coculture with untransduced and MAGE A3 TCR transduced Jurkat 76 at E:T ratio 5:1. Expression of activation marker CD69 (APC) alongside CD3 (VioBlue) and TCR (PE). CD3/CD69 double positive cells were considered as activated Jurkats. PMA stimulation used as positive control. N=1.

Activation levels were amplified by increasing the number of DCs in coculture. A greater percentage of MAGE J76 cells were activated after peptide pulsing with MAGE A3 peptide when cocultured at 1:1 (70%) or 1:2 (62%) E:T ratios (Figure 5.11a). At all coculture ratios CD3/CD69 double positive expression was higher in MAGE A3 peptide pulsed conditions compared to irrelevant peptide Vim116Hcit pulsed conditions suggesting specific recognition of the MAGE A3 peptide (Figure 5.11a). Supernatants from coculture ratios 1:1 and 2:1 were also tested for IL-2 levels (Figure 5.11b). The dotted line shows the minimum level of detection of the assay. No detectable levels of IL-2 were produced from no peptide/stimulation and control Vim116Hcit peptide pulsed conditions. In contrast, PMA stimulation induced up to 80 pg/ml of IL-2 at coculture ratio 1:1 but only 25 pg/ml at coculture ratio 2:1. For both ratios, approximately 60 pg/ml IL-2 was detected after peptide pulsing with MAGE A3, mirroring the increase in activation of MAGE J76 cells observed via flow cytometry. This increase in IL-2 was significantly greater than the no peptide/stimulation control; P=0.0071 for 1:1 conditions and P=0.046 for 2:1 conditions (Figure 5.11b). The elevated activation levels when cocultured with greater numbers of peptide pulsed APCs further supports MAGE J76 recognition and specificity for MAGE A3 peptide. This data shows that the MAGE A3 TCR restricted by HLA-DP4 can be used as a positive control for screening TCR reactivity to specific peptides in antigen presentation assays.

Figure 5.11

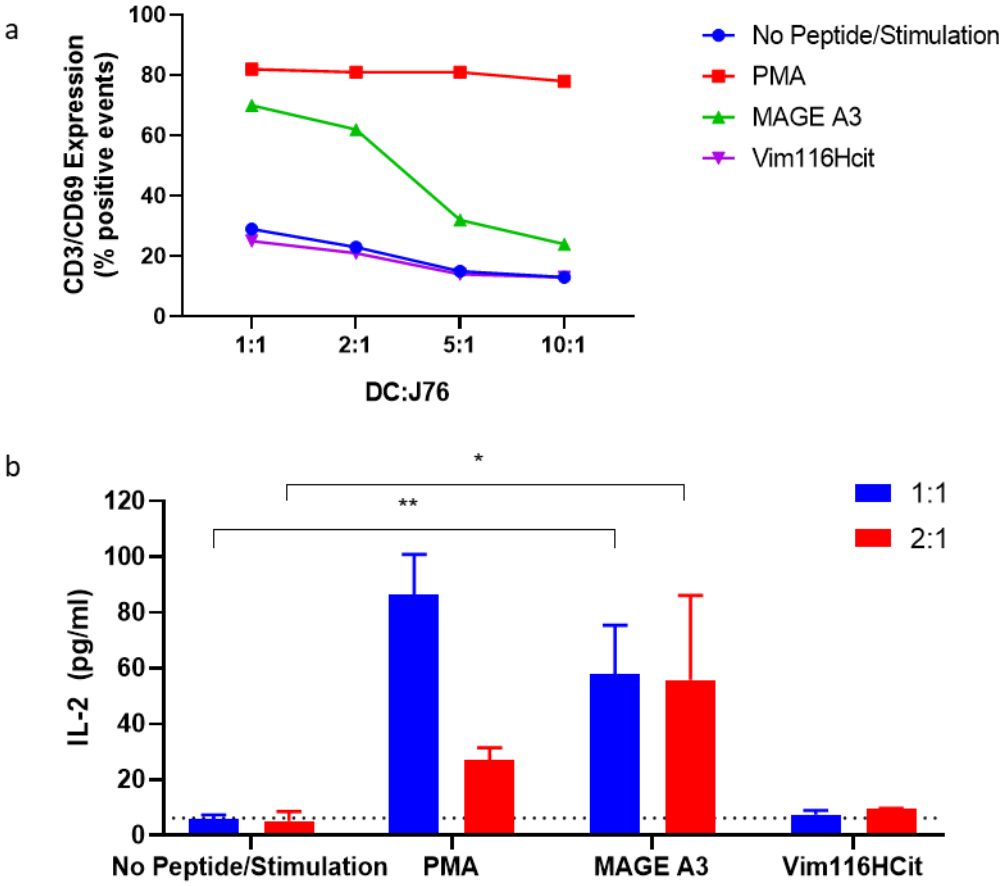


Figure 5.11 Dendritic cells (DCs) pulsed with 10 µg/ml MAGE A3 or Vim116Hcit peptides for 1hr, and matured with 20µg/ml Poly I:C overnight prior to coculture with untransduced and/or MAGE A3 TCR transduced Jurkat 76 (J76). Percentage of CD3/CD69 double positive expression of MAGE A3 TCR transduced J76 cocultured with peptide pulsed DCs at E:T ratios 1:1, 2:1, 5:1 and 10:1 (a). IL-2 secretion of cocultures 1:1 and 2:1 (b). Unpaired t test, * = $p<0.05$, ** = $p<0.01$. Errors bars representative of multiple wells, N=1..

To confirm HLA-DP4 restriction of the MAGE A3 TCR, MAGE A3 peptide was incubated in media alone (No APC control) or with B16F1 cells constitutively expressing HLA-DP4 (B16F1cDP4) or HLA-DR4 (B16F1cDR4) for 2 hours at 37°C before overnight coculture at 2:1 E:T ratio, with MAGE A3 TCR transduced Jurkat 76 (MAGE J76). Cells were harvested and stained for CD3 (Vioblue), CD69 (APC) and TCR (PE) expression (Figure 5.12). Minimal activation was seen in the no APC control and when cocultured with B16F1cDR4 (<15% CD3/CD69 double positives). Total CD69 expression increased when cocultured with peptide pulsed B16F1cDP4 (36%) however CD3 and TCR expression was greatly reduced. This could be due to CD3 recycling after TCR engagement, the control mechanism to avoid hyperstimulation following TCR activation.

Figure 5.12

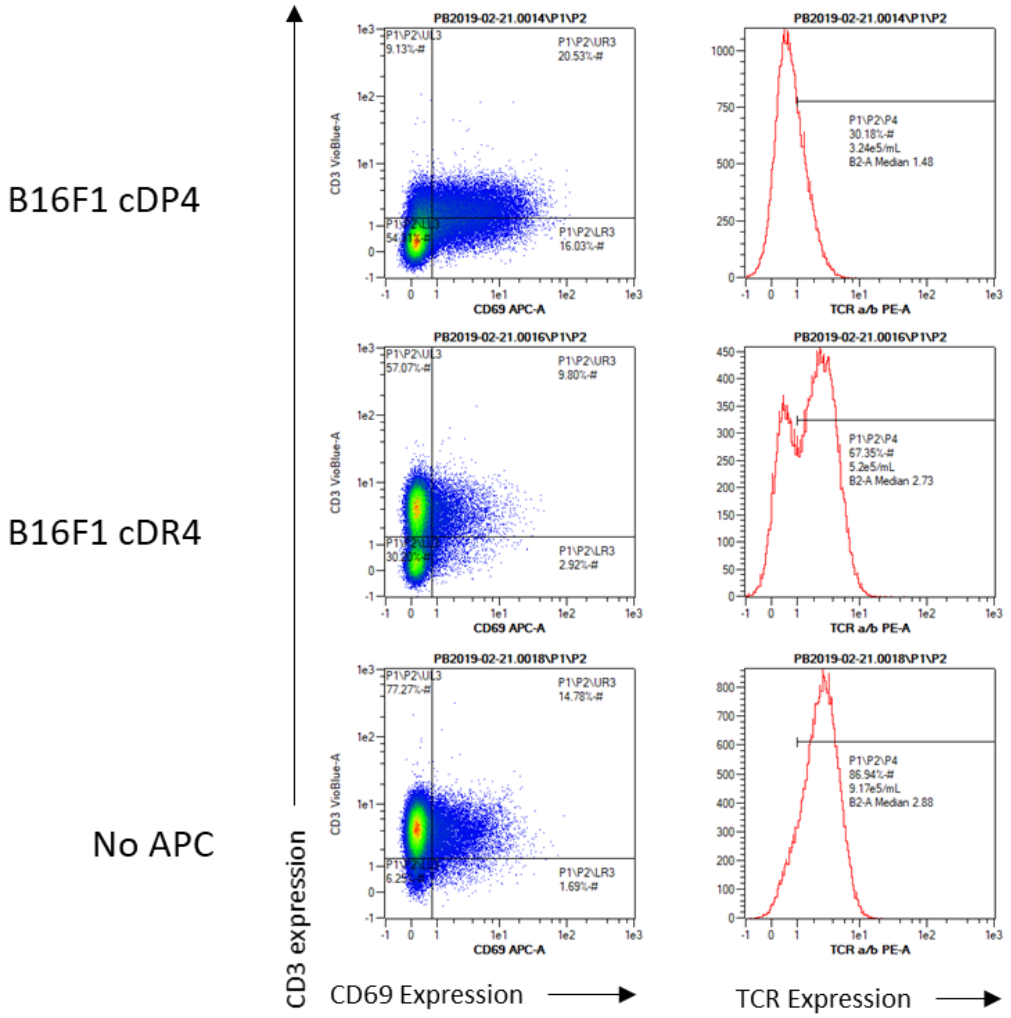


Figure 5.12 B16F1 cDP4 and B16F1 cDR4 pulsed with MAGE A3 peptide for 2 hours at 37°C before overnight coculture with MAGE A3 TCR transduced Jurkat 76 (J76) at E:T ratio 2:1. No APC = media only control. Expression of activation marker CD69 (APC) alongside CD3 (VioBlue) and TCR (PE). CD3/CD69 double positive cells were considered as activated J76. N=1.

5.2.5 Improved T cell transduction efficiencies

Four high frequency TCRs identified from the healthy donor BD41 in response to Eno241cit, were transduced into J76 and tested for TCR recognition. No activation (CD3/CD69 double positive events) above background was seen when Eno241cit TCR1 and Eno241cit TCR2 J76 were cocultured with peptide pulsed BD41 DCs, despite ~30% CD3/CD69 expression with MAGE A3 control (Figure 5.13a). Increased levels of APC activation markers CD80, CD86 and MHC class II (MHC-II) seen in DCs show these have successfully matured overnight (Figure 5.13b). EBV transformed B cells (LCLs) produced from BD41 were used as antigen presenting cells (APCs). Infection with the Epstein Barr Virus to induces continuous proliferation of the B cells. Recognition of citrullinated protein specific TCRs were also tested using peptide pulsed BD41 LCLs at 2:1 E:T ratio. The MAGE A3 TCR J76 positive control exhibited some activation in response to MAGE A3 (18-28%) which was above the background levels induced by irrelevant peptide Eno241cit, however the difference was not significant (Figure 5.13c). Expression of activation markers CD80, CD86 and MHC-II were found in LCLs however they were not as high when compared to DCs (Figure 5.13d).

The lack or lowered expression of costimulatory molecules and impaired signalling in Jurkat cells was thought to have contributed to the low responses found in coculture assays using transduced J76 [345, 347]. As T cells express high levels of costimulatory molecules it was hypothesised that they may give stronger responses in coculture assays.

Figure 5.13

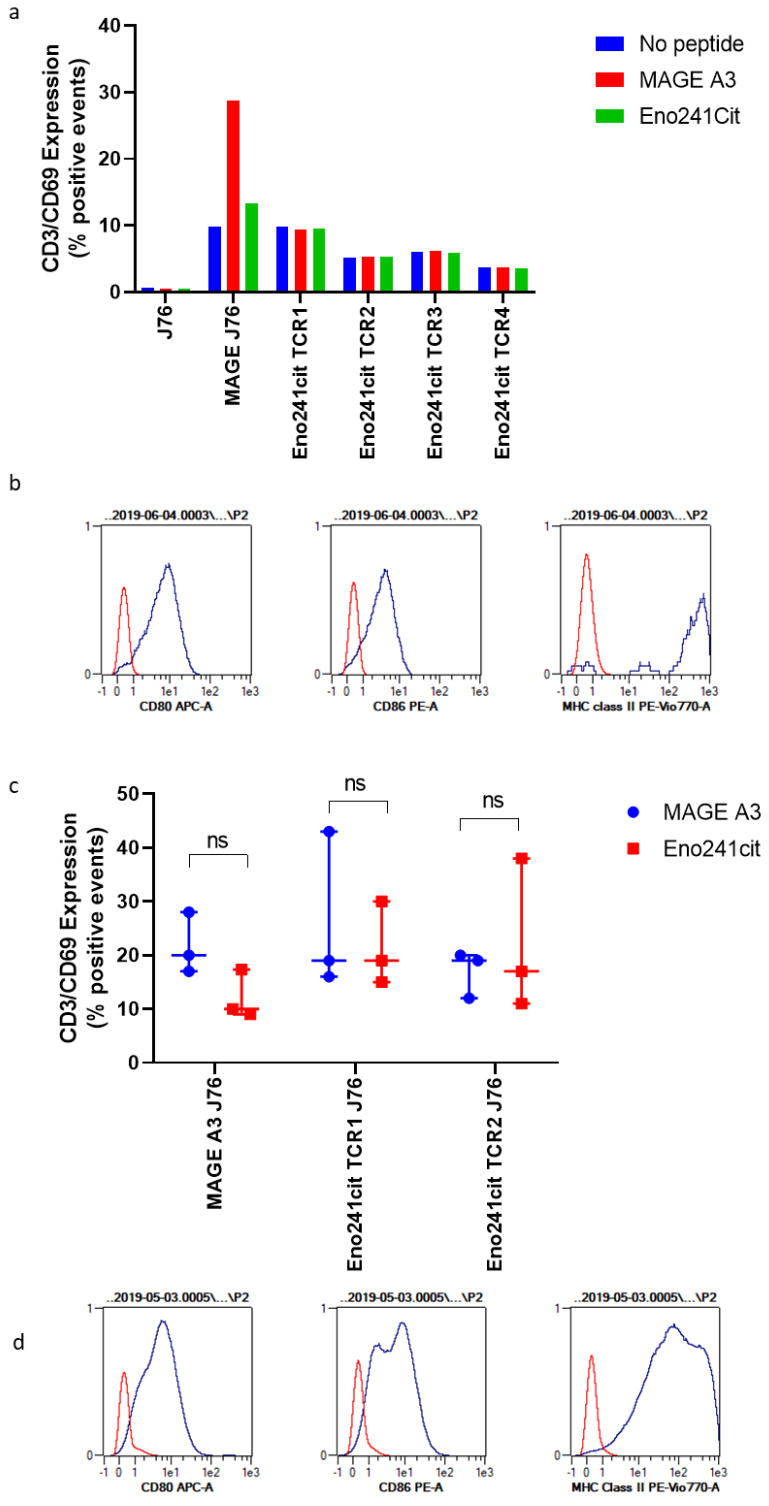


Figure 5.13 Percentage of CD3/CD69 double positive events. DCs peptide pulsed overnight with either MAGE A3 or Eno241cit before coculture with TCR transduced J76 at 2:1 E:T ratio, N=1 (a). BD41 B-LCL peptide pulsed with either MAGE A3 or Eno241cit for 2 hours before coculture with TCR transduced

J76 at 2:1 E:T ratio, N=3. Multiple Paired t test analysis ns = P > 0.05 (c).. Expression of activation markers CD80, CD86 and MHC class II in BD41 dendritic cells (b) and BD41 B-LCLs (d). Red line = unstained. Blue line = stained.

Prior to transductions of T cells, all TCR constructs were in their simplest form and only expressed the desired TCR sequence plus puromycin resistance and were known as 1st generation (Figure 5.14 and Table 5.8). To further improve transduction efficiency, the constructs were modified to enhance TCR expression on the T cell surface. These techniques included murinisation (9 amino acid replacements) of the constant region, inclusion of a cysteine residue in both alpha and beta chains to produce an additional disulphide bridge to prevent mispairing, and codon optimisation for preferential protein expression [348-350]. These modifications form the 2nd generation of constructs. A further optimisation was included to allow better assessment of transduction efficiency. The 3rd generation of constructs included all the 2nd generation modifications but the puromycin selection gene was replaced with selection markers such as rat CD2, truncated CD34 and GFP, or contained a fully murinised constant region. The constructs were then simplified and any markers/resistance genes were removed and replaced with a furin cleavage site (RAKR) and SGSG linker between the alpha and beta chain sequence. These belong to the 4th generation of constructs (Figure 5.14 and Table 5.8). As the MAGE A3 TCR was used for optimisation of all experiments, it was produced in all 4 construct generations. The Eno241cit TCRs were also produced as all 4 generations however only Eno241cit TCR 1 was made in the 2nd and 3rd generation (Rat CD2) versions whilst experiments were optimised. Once transfection and transduction techniques were optimised, all identified TCRs from Eno241cit, Vim28cit and Vim415cit cultures stated in Table 5.7 plus the MAGE A3 control TCR were designed as 4th generation constructs. Constructs were designed by Rachael Metheringham (Scancell Ltd).

Table 5.8

TCR ID	FULL LENTI TRANSFER PLASMID NAME	DONOR	TCR	CODON OPTIMISED	TRBC/TRAC CONSTANT REGION	MARKER	PUROMYCIN RESISTANCE	FURIN CLEAVAGE SITE	GENERATION
MAGE A3	LENTI-TCR-Z080718-Z2D MAGE A3 DP4 TCR (Obtained from Creative Biolabs)	N/A	MAGE A3 DP4	No	HUMAN (TRBC2)	N/A	Yes	No	1
E214-41-1	LENTI-BD0041 Eno241-260cit^{253} TCR1 cl.B2	BD41	Eno241-260cit^{253} TCR1	No	HUMAN (TRBC1)	N/A	Yes	No	1
E214-41-2	LENTI-BD0041 Eno241-260cit^{253} TCR2 cl.D2	BD41	Eno241-260cit^{253} TCR2	No	HUMAN (TRBC2)	N/A	Yes	No	1
E241-41-3	LENTI-BD0041 Eno241-260cit^{253} TCR3 cl.3E	BD41	Eno241-260cit^{253} TCR3	No	HUMAN (TRBC2)	N/A	Yes	No	1
E241-41-4	LENTI-BD0041 Eno241-260cit^{253} TCR4 cl.4D	BD41	Eno241-260cit^{253} TCR4	No	HUMAN (TRBC2)	N/A	Yes	No	1
MAGE A3-C	LENTI-CO MAGE A3 DP4 TCR MODC cl.M4	N/A	MAGE A3 DP4	Yes	HUMAN (TRBC2 MODC)	N/A	Yes	No	2
E241-41-C1	LENTI-CO BD0041 Eno241-260cit^{253} TCR1 MODC cl.E7	BD41	Eno241-260cit^{253} TCR1	Yes	HUMAN (TRBC1 MODC)	N/A	Yes	No	2
MAGE A3-Rat	LENTI-CO MAGE A3 DP4 TCR MODC + RAT CD2 cl.M25/30	N/A	MAGE A3 DP4	Yes	HUMAN (TRBC2 MODC)	RAT CD2	No	No	3
E241-41-R1	LENTI-CO BD0041 Eno241-260cit^{253} TCR1 MODC + RAT CD2 cl.E6/E14	BD41	Eno241-260cit^{253} TCR1	Yes	HUMAN (TRBC1 MODC)	RAT CD2	No	No	3
MAGE A3-GFP	LENTI-CO MAGE A3 DP4 TCR MODC + EMGFP	N/A	MAGE A3 DP4	Yes	HUMAN (TRBC2 MODC)	EMGFP	No	No	3
MAGE A3-tCD34	LENTI-CO MAGE A3 DP4 TCR MODC + tCD34	N/A	MAGE A3 DP4	Yes	HUMAN (TRBC2 MODC)	truncated CD34	No	No	3
MAGE A3-Murine	LENTI-CO MAGE A3 DP4 TCR MURINE TRBC2/TRAC	N/A	MAGE A3 DP4	Yes	MURINE (TRBC2/TRAC)	N/A	Yes	No	3
MM1	LENTI-CO MAGE A3 DP4 TCR MURINE TRBC2/TRAC	N/A	MAGE A3 DP4	Yes	MURINE (TRBC2/TRAC)	N/A	No	Yes	4
E241-41-M1	LENTI-CO BD0041 Eno241-260cit^{253} TCR1 FURIN/SG	BD41	Eno241-260cit^{253} TCR1	Yes	MURINE (TRBC1/TRAC)	N/A	No	Yes	4
E241-41-M2	LENTI-CO BD0041 Eno241-260cit^{253} TCR2 FURIN/SG	BD41	Eno241-260cit^{253} TCR2	Yes	MURINE (TRBC2/TRAC)	N/A	No	Yes	4
E241-41-M3	LENTI-CO BD0041 Eno241-260cit^{253} TCR3 FURIN/SG	BD41	Eno241-260cit^{253} TCR3	Yes	MURINE (TRBC2/TRAC)	N/A	No	Yes	4
E241-41-M4	LENTI-CO BD0041 Eno241-260cit^{253} TCR4 FURIN/SG	BD41	Eno241-260cit^{253} TCR4	Yes	MURINE (TRBC2/TRAC)	N/A	No	Yes	4
V28-41-M1	LENTI-CO BD0041 Vim28-49cit^{28,36,45} TCR1 FURIN/SG	BD41	Vim29-49cit^{28,36,45} TCR1	Yes	MURINE (TRBC2/TRAC)	N/A	No	Yes	4
V28-41-M2	LENTI-CO BD0041 Vim28-49cit^{28,36,45} TCR2 FURIN/SG	BD41	Vim29-49cit^{28,36,45} TCR2	Yes	MURINE (TRBC2/TRAC)	N/A	No	Yes	4
V28-41-M3	LENTI-CO BD0041 Vim28-49cit^{28,36,45} TCR3 FURIN/SG	BD41	Vim29-49cit^{28,36,45} TCR3	Yes	MURINE (TRBC2/TRAC)	N/A	No	Yes	4
V28-41-M4	LENTI-CO BD0041 Vim28-49cit^{28,36,45} TCR4 FURIN/SG	BD41	Vim29-49cit^{28,36,45} TCR4	Yes	MURINE (TRBC1/TRAC)	N/A	No	Yes	4
V28-41-M5	LENTI-CO BD0041 Vim28-49cit^{28,36,45} TCR5 FURIN/SG	BD41	Vim29-49cit^{28,36,45} TCR5	Yes	MURINE (TRBC2/TRAC)	N/A	No	Yes	4
V28-41-M6	LENTI-CO BD0041 Vim28-49cit^{28,36,45} TCR6 FURIN/SG	BD41	Vim29-49cit^{28,36,45} TCR6	Yes	MURINE (TRBC1/TRAC)	N/A	No	Yes	4
V28-41-M7	LENTI-CO BD0041 Vim28-49cit^{28,36,45} TCR7 FURIN/SG	BD41	Vim29-49cit^{28,36,45} TCR7	Yes	MURINE (TRBC2/TRAC)	N/A	No	Yes	4
V28-41-M8	LENTI-CO BD0041 Vim28-49cit^{28,36,45} TCR8 FURIN/SG	BD41	Vim29-49cit^{28,36,45} TCR8	Yes	MURINE (TRBC2/TRAC)	N/A	No	Yes	4
V28-41-M9	LENTI-CO BD0041 Vim28-49cit^{28,36,45} TCR9 FURIN/SG	BD41	Vim29-49cit^{28,36,45} TCR9	Yes	MURINE (TRBC2/TRAC)	N/A	No	Yes	4
V28-41-M10	LENTI-CO BD0041 Vim28-49cit^{28,36,45} TCR10 FURIN/SG	BD41	Vim29-49cit^{28,36,45} TCR10	Yes	MURINE (TRBC1/TRAC)	N/A	No	Yes	4
V28-41-M11	LENTI-CO BD0041 Vim28-49cit^{28,36,45} TCR11 FURIN/SG	BD41	Vim29-49cit^{28,36,45} TCR11	Yes	MURINE (TRBC2/TRAC)	N/A	No	Yes	4
V28-41-M12	LENTI-CO BD0041 Vim28-49cit^{28,36,45} TCR12 FURIN/SG	BD41	Vim29-49cit^{28,36,45} TCR12	Yes	MURINE (TRBC2/TRAC)	N/A	No	Yes	4
V28-41-M13	LENTI-CO BD0041 Vim28-49cit^{28,36,45} TCR13 FURIN/SG	BD41	Vim29-49cit^{28,36,45} TCR13	Yes	MURINE (TRBC1/TRAC)	N/A	No	Yes	4
V28-41-M14	LENTI-CO BD0041 Vim28-49cit^{28,36,45} TCR14 FURIN/SG	BD41	Vim29-49cit^{28,36,45} TCR14	Yes	MURINE (TRBC1/TRAC)	N/A	No	Yes	4
V28-41-M15	LENTI-CO BD0041 Vim28-49cit^{28,36,45} TCR15 FURIN/SG	BD41	Vim29-49cit^{28,36,45} TCR15	Yes	MURINE (TRBC2/TRAC)	N/A	No	Yes	4
V28-41-M16	LENTI-CO BD0041 Vim28-49cit^{28,36,45} TCR16 FURIN/SG	BD41	Vim29-49cit^{28,36,45} TCR16	Yes	MURINE (TRBC2/TRAC)	N/A	No	Yes	4
V415-11-M1	LENTI-CO BD0011 Vim415-433cit^{424} TCR1 FURIN/SG	BD11	Vim415-433cit^{424} TCR1	Yes	MURINE (TRBC1/TRAC)	N/A	No	Yes	4
V415-11-M2	LENTI-CO BD0011 Vim415-433cit^{424} TCR2 FURIN/SG	BD11	Vim415-433cit^{424} TCR2	Yes	MURINE (TRBC2/TRAC)	N/A	No	Yes	4
V415-11-M3	LENTI-CO BD0011 Vim415-433cit^{424} TCR3 FURIN/SG	BD11	Vim415-433cit^{424} TCR3	Yes	MURINE (TRBC2/TRAC)	N/A	No	Yes	4
V415-11-M4	LENTI-CO BD0011 Vim415-433cit^{424} TCR4 FURIN/SG	BD11	Vim415-433cit^{424} TCR4	Yes	MURINE (TRBC2/TRAC)	N/A	No	Yes	4
V415-11-M5	LENTI-CO BD0011 Vim415-433cit^{424} TCR5 FURIN/SG	BD11	Vim415-433cit^{424} TCR5	Yes	MURINE (TRBC1/TRAC)	N/A	No	Yes	4
V415-11-M6	LENTI-CO BD0011 Vim415-433cit^{424} TCR6 FURIN/SG	BD11	Vim415-433cit^{424} TCR6	Yes	MURINE (TRBC2/TRAC)	N/A	No	Yes	4
V415-11-M7	LENTI-CO BD0011 Vim415-433cit^{424} TCR7 FURIN/SG	BD11	Vim415-433cit^{424} TCR7	Yes	MURINE (TRBC2/TRAC)	N/A	No	Yes	4
V415-11-M8	LENTI-CO BD0011 Vim415-433cit^{424} TCR8 FURIN/SG	BD11	Vim415-433cit^{424} TCR8	Yes	MURINE (TRBC2/TRAC)	N/A	No	Yes	4

Table 5.8. List of plasmids used in transduction experiments. Divided into 4 generations based on optimisations to improve transduction efficiencies.

Figure 5.14

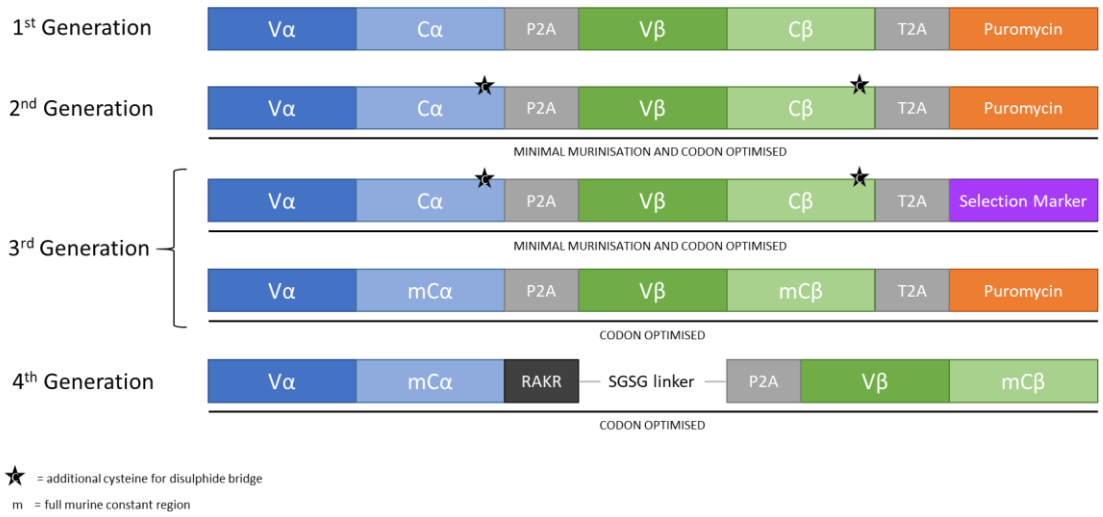


Figure 5.14 Schematic representing the structure of TCR lenti viral constructs in all 4 generations. Selections markers (purple) in 3rd generation constructs include Rat CD2, GFP and truncated CD34.

To identify the optimal cell combination for antigen presentation assays, the reactivity of transduced J76 and T cells were tested against a range of peptide pulsed APCs. T cells and J76 were transduced with either 1st or 2nd generation MAGE A3 TCR and Eno241cit TCR1/2 for 10 days before coculture with BD41 LCLs, dendritic cells or activated B cells at 1:1 effector to target ratio (Figure 5.15). B cells were activated prior to assay by coculture with NIH3T3 cell line expression CD40 ligand (CD40L) for 14 days by Thomas Kirk (Scancell Ltd). CD69 expression was assessed as previously described. Higher expression levels were seen with MAGE A3 (1st and 2nd generation) when cultured with MAGE A3 peptide pulsed cells (~50-80% CD3/CD69) in all cell combinations except in LCL vs T cell cultures (20-30% CD3/CD69), compared to irrelevant peptide or no peptide controls.

The percentage of CD3+ve/CD69+ve activated cells were slightly higher (~70-80%) in conditions with 2nd generation MAGE A3 TCR compared to 50-70% activation seen with the 1st generation equivalent (Figure 5.15b, d, and e). However, the background

signal, CD69 expression in no peptide and irrelevant peptide conditions, were also slightly elevated in 2nd generation MAGE A3 TCR cultures. Lower levels of activation were observed in both T cell and J76 cocultures with activated B cells; a maximum of 15% CD3+ve/CD69+ve cells were detected in MAGE A3 cultures (Figure 5.15c and f). However, the difference between specific and irrelevant peptide pulsed conditions was distinct. Despite good detection with MAGE A3 transduced T cell/J76, no positive responses were observed with Eno241cit TCRs 1 and 2 in any coculture combination (Figure 5.15). Eno241cit TCRs 3 and 4 were not tested in this experiment.

The TCR expression of transduced T cells used in the cell combination experiment discussed above, were very low. Transduced T cells at Day 7 of culture only showed a 4% and 5% increase of MAGE A3 1st and 2nd generation TCRs respectively, compared to untransduced controls (Figure 5.15g). A similar level of increase was seen with 2nd generation Eno241cit TCR1 however there was no difference in transduction efficiency between 1st generation Eno241cit TCR2 and the untransduced control (Figure 5.15g). Despite low MAGE A3 TCR expressions, activation was observed in antigen presentation assays. The lack of response to Eno241cit TCRs could have been due to TCR expression, so increasing the transduction efficiency may increase target recognition in these assays. APC activation markers MHC-II, CD80 and CD86 were assessed on the day of coculture for both dendritic cells and B cells (gated on CD19+ve cells first). Expression of CD80 was similar between the two cell types however the percentage and MFI of MHC-II and CD86 was greater on dendritic cells compared to B cells. This could explain the lower levels of activation seen in coculture with CD40L activated B cells compared to dendritic cells.

Figure 5.15

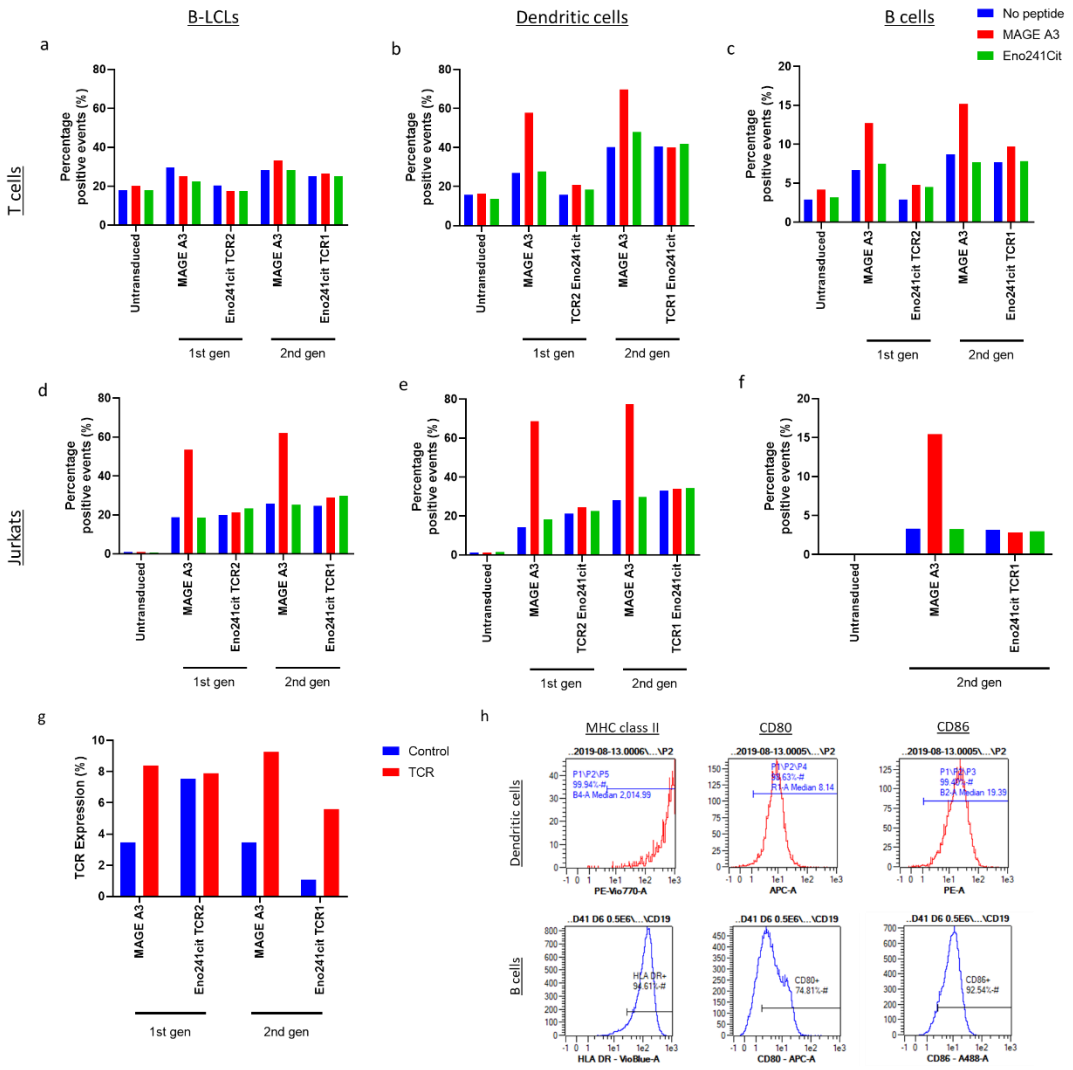


Figure 5.15 T cells and Jurkat 76 cells transduced with MAGE A3 and Eno241cit TCR1/2 1st or 2st generation lentiviral constructs were cultured overnight at 1:1 ratio with specific and irrelevant peptide pulsed BD41 B-LCLs (a, d), dendritic cells (b, e), and B cells (c, f). CD69 activation was assessed the following day via flow cytometry and data was collated for (CD19-ve, B-LCLs and B cells only)/CD3+ve/CD69+ve events. TCR expression of transduced T cells measured using vBeta specific antibodies; vβ22 for MAGE A3, vβ11 for Eno241cit TCR1 and vβ2 for Eno241cit TCR2. Untransduced T cells stained with equivalent antibody used as a control (g). Expression of activation markers MHC class II, CD80 and CD86 checked in dendritic cells and B cells (gated on CD19+ve) on day of assay (h). N=1.

Transduction efficiency was slightly improved with 2nd generation constructs compared to the 1st generation, with a greater difference between untransduced controls and TCR transduced T cells, however the total number of TCR positive cells remained less than 15% (Figure 5.16a). To increase the chance of identifying a TCR specific to a citrullinated epitope in an antigen presentation assay, the transduction efficiency had to be improved. As the vβ specific antibodies were not always reliable and specific antibodies are not available for every vβ chain, the addition of a selection marker was thought to help identify successfully transduced cells that could be sorted or enriched for a desired TCR. Unexpectedly, this selection marker ablated the expression of TCR as similar levels of TCR expression were observed in transduced compared to the untransduced controls; <5%. This was independent of the selection marker and there was minimal increase in TCR expression with all MAGE A3 TCR constructs containing rat CD2, GFP or CD34 (Figure 5.16a). The only 3rd generation construct that showed equal levels of TCR expression (5-10%) as the 2nd generation constructs was MAGE A3 murine which contains a full murine constant region and puromycin resistance (Table 5.8).

To assess whether the lack of TCR expression with the 3rd generation constructs containing a selection marker was due to a problem with the construct or due to poor staining with vβ specific antibodies, J76 were transduced with 2nd and 3rd generation MAGE A3 TCR and stained for TCR using both pan-TCR and specific vβ22 antibodies after 3 days in culture. No antibiotic selection was applied. TCR expression was only slightly higher with the pan-TCR antibody compared to specific vβ22 antibody, however there was a great difference in transduction efficiency between the constructs. J76 cells transduced with 2nd generation MAGE A3 were ~50% for CD3 and TCR however the 3rd generation condition was less than 10% (Figure 5.16b). The level of rat CD2 and TCR double positive events was similar; <10% for 3rd generation MAGE A3, suggesting all TCR positive cells also expressed rat CD2 (Figure 5.16c).

In a separate experiment, the total expression levels of pan-TCR, specific vβ22 and rat CD2 in MAGE A3 3rd generation transduction efficiency was compared between J76 and T cells. Almost all J76 cells were positive for rat CD2 with low expression (~20%) of TCR highlighting cells had successfully been transduced (Figure 5.16d). Expression levels were further reduced in T cells with only 40% rat CD2 and <10% TCR positive (Figure 5.16e). As the rat CD2 molecule is encoded down stream of the TCR alpha and beta chains on the 3rd generation construct, the high expression levels of rat CD2 in J76 cells shows the construct was functional. Taking into consideration that the vβ specific antibody staining was comparable to the pan-TCR antibody, suggests a problem with either TCR translation, assemble or translocation to the cell surface of 3rd generation constructs with a selection marker. In addition, there was still a large difference in transduction efficiency levels between J76 and T cells.

Figure 5.16

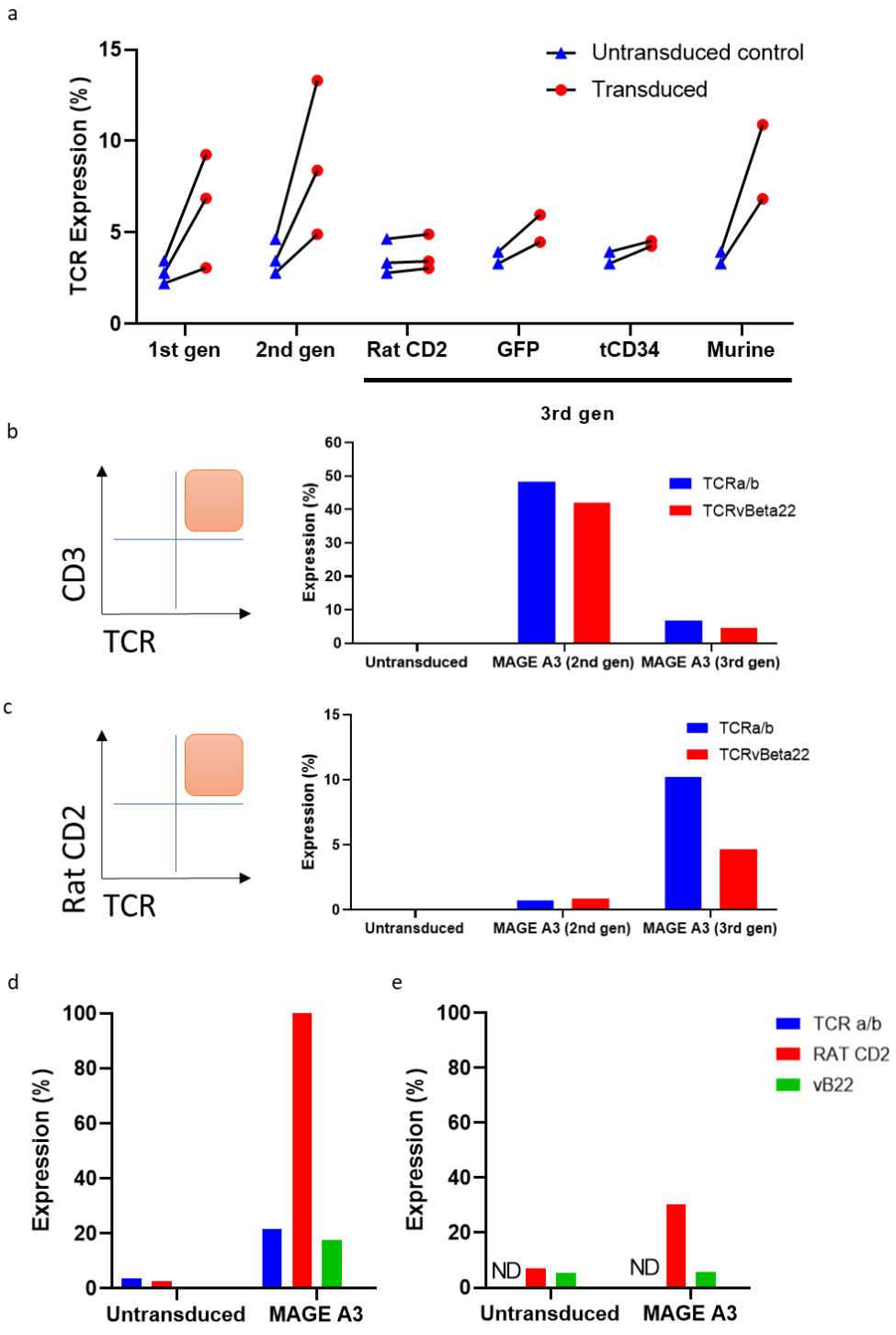


Figure 5.16 TCR transduction efficiencies of MAGE A3/DP4 TCR in T cells at day 7 post transduction using vβ specific antibodies. N≤3 (a). Percentage expression of CD3/TCR double positive cells (b) and Rat CD2/TCR double positive cells (c) in MAGE A3/DP4 TCR 2nd and 3rd generation transduced Jurkat 76 using pan TCR α/β or vβ specific antibodies. Comparison of TCR and Rat CD2 expression in MAGE A3/DP4 TCR 3rd generation transduced Jurkat 76 (d) and T cells (e). N=1.

Various transduction methods have been adopted by research groups and each method aims to increase the chances of interaction between virus and cells. These methods involving techniques such as spinoculation, retronectin coating and polybrene incubation were tested. Increasing the number of virus particles vs target cell, also referred to as the multiplicity of infection (MOI), has also shown to enhance transductions [351]. MAGE A3 2nd generation constructs were transduced at a range of MOIs (5, 10, 20 and 40) in activated T cells from 2 healthy donors. TCR expression in transduced conditions was double, ~11% compared to 5%, than seen in untransduced controls however there was no increase in TCR positive cells with increasing MOI (Figure 5.17a and b). Performing the transduction in rectronectin coated plates also did not improved TCR levels (Figure 5.17b). In addition, there was no increase in vβ22 expression in MAGE A3 3rd generation transduced T cells in any combination transduction method involving at least two of the following; spinoculation, rectronectin coated plates and polybrene, compared to the standard method (adding virus directly to wells) (Figure 5.17c). However, differences in rat CD2 expression were observed. The percentage of rat CD2 positive cells were greater than 30% using the standard transduction method. Similar levels of rat CD2 were found using virus bound rectronectin coated plates. However, methods involving spinoculation (spinning the virus and cell mixture plus 4µg/ml Polybrene at 800g for 45 minutes at 32°C) reduced transduction efficiency as seen by the decrease in rat CD2 expression (Figure 5.16c). These transduced T cells were cocultured overnight with MAGE A3 (specific peptide) and Eno241cit (irrelevant peptide) pulsed CD40L activated B cells at Day 11 and activation was assessed using IFNγ ELISpot. No increase in activation was observed with MAGE A3 peptide pulsed conditions compared to no peptide or irrelevant peptide controls for all transduction conditions (Figure 5.18d). Difference of 30-50 spots between MAGE A3 pulsed and unpulsed conditions, increasing in mean spot count from 125 to 140 to 225 for standard, spin/polybrene and rectronectin/polybrene transduction conditions. Spot counts for irrelevant peptide

pulsed conditions were lower than no peptide conditions for all three transduction methods; 75, 80 and 185 for standard, spin/polybrene and rectronectin/polybrene respectively (Figure 5.17d). The reduced activation in this experiment could be due to the low transduction efficiencies of these T cell cultures. There was also no increased activation levels with T cell cultures transduced via spinoculation or rectronectin coated plates (Figure 5.17d). These findings alongside TCR expression data showed the standard transduction method as the most optimal.

Figure 5.17

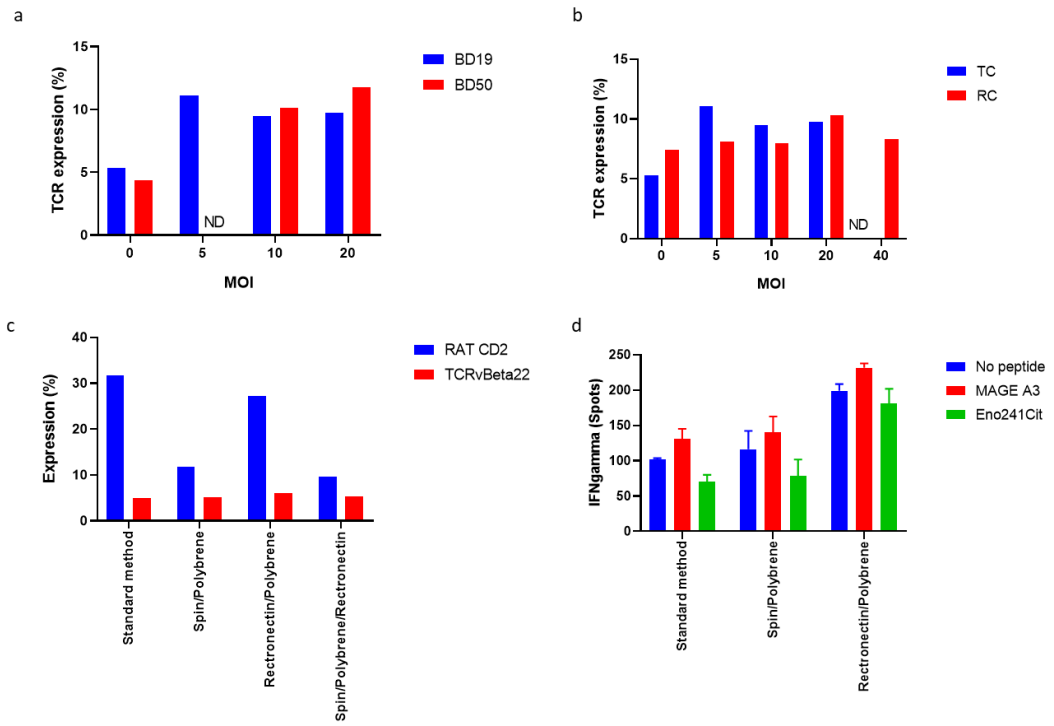


Figure 5.17 TCR expressions of MAGE A3/DP4 TCR 2nd generation transduced T cells at range of multiplicity of infections (MOI) in 2 healthy donors (a) and cultured in either tissue culture treated (TC) or rectronectin coated (RC) plates (b). TCR expressions of T cells transduced with MAGE A3/DP4 TCR Rat CD2 3rd generation at MOI 10 via various methods. Polybrene added at 8µg/ml during spinoculation and at 4µg/ml in rectronectin plate (c). IFNγ ELISpot of T cells transduced with MAGE A3/DP4 TCR Rat CD2 3rd generation at MOI 10 via methods, cocultured with peptide pulsed B cells. Eno241cit used an irrelevant peptide control (d). N=1.

All methods used to boost transduction efficiencies were unsuccessful. Therefore it was hypothesised that improvements to the transfection method for viral production could increase transduction efficiency. A new transfection protocol was established referred to as the 'adapted method'. The original transfection method involved transfection of HEK293T cells with lenti vectors and helper plasmids using Lipofectamine 3000, with viral supernatants harvested at 48 hours and 72 hours post transfection. Supernatants were then incubated with Lenti-X concentrator (Takara) for 2-4 hours before centrifugation to pellet the virus. Viral capsid protein p24 was measured using GoStix (Takara) to estimate viral titre and calculate IFU/mL. The adapted transfection method uses Turbofect for transfection and supernatants were only collect at 48 hours. The viral particles were concentrated by overnight centrifugation. T cells from 3 healthy donors were transduced with Lenti-GFP produced via original and adapted transfection methods. GFP expression ranged between 40-55% in conditions transduced with adapted Lenti-GFP, almost double the levels observed in conditions transduced with original Lenti-GFP (Figure 5.18a). MAGE A3 3rd generation lenti virus produced via both transfection methods were also compared in four healthy donors and 1 buffy coat (BC9). No responses were found with BC9. However, increased transduction efficiencies were seen with all constructs produced by the adapted compared to the original method with TCR expression reaching ~27% for MAGE Murine using an antibody specific to the vβ sequence of the MAGE TCR; vβ22 (Figure 5.18b). T cells transduced with MAGE Murine TCR were also successfully detected using an anti-Mouse TCR beta chain antibody (Ms TCRβ). A more distinct TCR positive population was observed when stained with Ms TCRβ antibody compared to staining with vβ22 (Figure 5.18c). In addition, greater levels of TCR expression were found when stained with a Ms TCR beta antibody, but this was not significant, P=0.0578 (Figure 5.18d). Data from these experiments highlight a fully murinised constant region allows optimal detection of TCR transduced

cells, and a smaller construct, as seen with Lenti-GFP, increased transduction efficiency. This resulted in the formation of 4th generation lenti viral constructs (Figure 5.14 and Table 5.8).

Figure 5.18

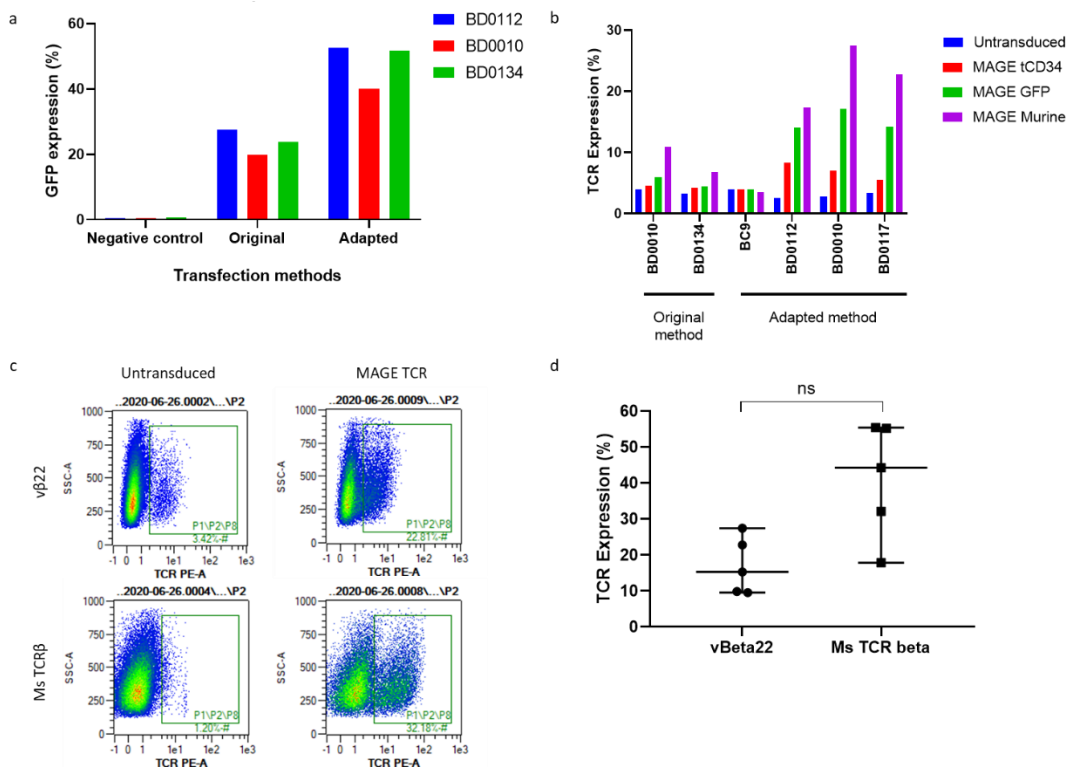


Figure 5.18. Comparison of two different transfection methods for viral production; original and adapted. GFP Lenti virus produced via original and adapted transfection methods and transduced in T cells from 3 healthy donors. Untransduced samples used as negative control. N=3 (a). MAGE A3 2nd and 3rd generation lenti virus produced via original or adapted transfection methods and transduced in T cells derived from either healthy donor (BD) or buffy coat (BC) N≥2 (b). Comparison of TCR expression assessed using vβ specific and Mouse TCRβ chain antibodies in untransduced and MAGE TCR transduced samples (c) and (d). Paired t test significance ns = p≥0.05. N=5.

5.2.6 Production of activated B cells for antigen presentation assays

Optimisation experiments discussed in section 5.2.5 helped to establish a functional model for T cell transductions and recognition of TCR engagement induced activation via IFNγ response. The 4th generation (full murinised constant region) of TCR constructs was selected for all future experiments due to its elevated TCR expression. A suitable source of antigen presenting cells (APCs) were required to keep consistency between experiments when comparing TCR specificities. Activated B cells were selected and used as APCs in coculture assays due to their high expansion capacity and the ability to recover from frozen when required. Prior to testing of all citrullinated TCRs, bulk batches of activated B cells from the healthy donors that the TCRs were identified (Vim28cit and Eno241cit TCRs from BD41 and Vim415cit TCRs from BD11), were required and an expansion protocol needed to be established. Two activated B cell expansion methods were compared; a Miltenyi Biotec expansion kit and coculture with CD40L expressing NIH3T3 cells. CD19+ve B cells were isolated from healthy donor BD19 and buffy coat donor BCG. Cells counts and expression of activation markers (CD19, CD80, CD86 and HLA-DR) were assessed routinely (every 3-4 days) throughout the 14 day culture period (Figure 5.19a and b). Expansion using CD40L expressing NIH3T3 cells resulted in approximately 10 times more cells than with the Miltenyi kit; BD19 B cells expanded from 4 to 40 million cells/mL and BCG B cells expanded from 2 to 30million cells/mL by Day 12 (Figure 5.19a). Final cell counts for BD19 and BCG B cells expanded via the NIH3T3 method were 30 million cells/mL and 50 million cells/mL respectively. These values would have been higher however some cells were removed for use in antigen presentation assays (19.4 million cells from BD19 3T3 at Day 11) or for frozen stocks (all except 12 million cells from BD19 and BCG 3T3 at Day 12).

Differences in activation marker expressions were also seen between the two expansion methods. Cultures were stained for CD19, CD80, CD86 and HLA-DR on days 1, 5, 8,12 and 14 of culture. A more uniform increase in all markers was seen with both BD19 and BCG B cells expanded via the NIH3T3 method, with greater than 80% expression by day 14 (Figure 5.19b). The same donor B cells cultured using the Miltenyi expansion kit did boost CD80 expression to 80% by day 14 (Figure 5.19b(iii)) however CD19 and CD86 levels remained stable at ~60% (Figure 5.19b(i) and (ii)). HLA-DR was used as a marker for MHC-II expression, the molecule required for antigen presentation. The one advantage of the Miltenyi expansion kit was the elevated HLA-DR expression of ~100% from day 1 of culture, which remained constant through to day 14. B cells expanded and activated with CD40L expressing NIH3T3 were 70% positive for HLA-DR expression which increased to >90% by day 14 (Figure 5.19b(iv)).

Due to the high cell numbers obtained and optimum expression of activation markers, the NIH3T3 CD40L expansion method was used for expansion and activation of bulk batches of BD41 and BD11 B cells. HLA typing of these donors shown in Appendix 6. CD80, CD86 and HLA-DR expression of CD19+ve cells of BD41 and BD11 cultures all ranged between 97-100% at day 14 (Figure 5.20a). Cells were frozen down at day 14 for cryo-storage until use in assays. When required, cells were revived and cultured with CD40L expressing NIH3T3 for 3 days prior to use in assay to obtain optimal activation levels. It was also important to routinely check the NIH3T3 cell line for high CD40L (CD154) expression to maintain maximum activation of B cells. Greater than 90% CD40L expression was expected and if levels began to decrease the cell line was sorted for high expressers; top 10% of positive cells (Figure 5.20b).

Figure 5.19

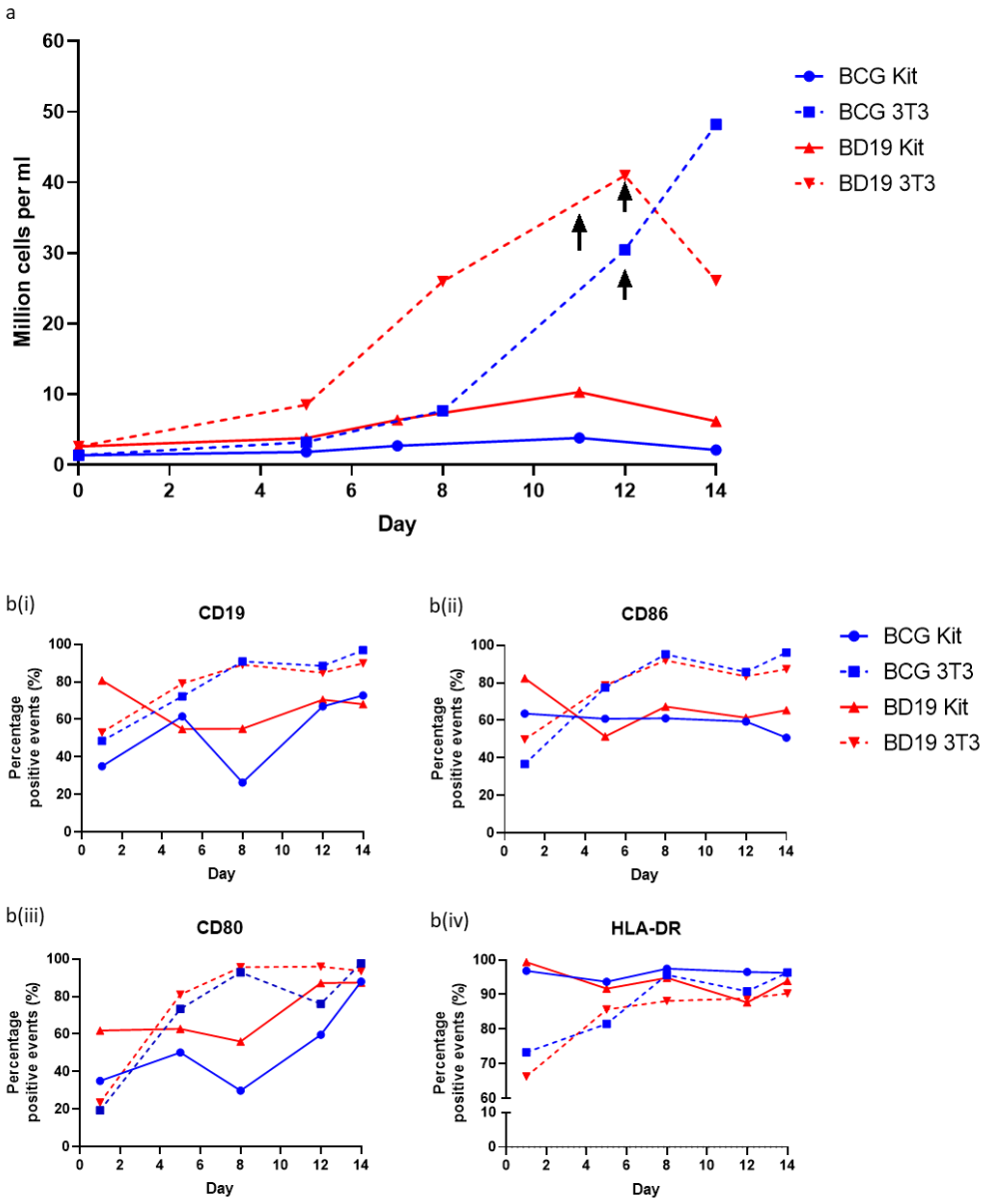


Figure 5.19 B cells isolated from healthy donor (BD19, red lines) or buffy coat (BCG, blue lines) and cultured via two different methods; using the Miltenyi expansion kit (solid lines) or using NIH3T3 CD40-ligand expressing feeder cells (dashed lines). Cell counts collected over 14 day culture period. Black arrows indicate time points where some cells were removed from cultures. 19.4million cells from BD19 3T3 on Day 11. All except, 12 million cells from BCG 3T3 and BD19 3T3 on Day 12 (a). Percentage of B cells expressing activation markers CD19 (b(i)), CD86 (b(ii)), CD80 (b(iii)) and HLA-DR (b(iv)) throughout 14 day culture period. N=2.

Figure 5.20

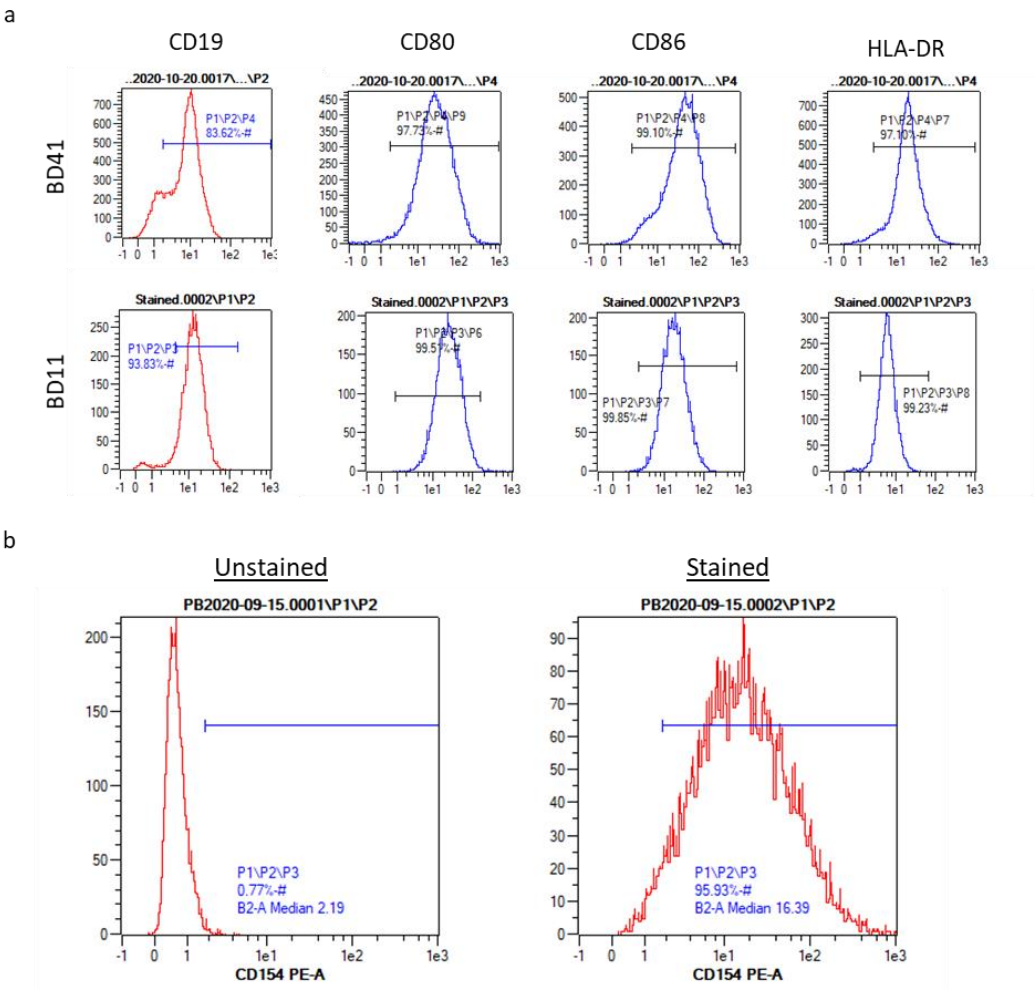


Figure 5.20 Expression of activation markers CD80, CD86 and HLA-DR of CD19+ve B cells from healthy donors BD41 and BD11 at Day 14 of culture. N=2 (a). CD40 ligand (CD154) expression of NIH3T3 feeder cells (b).

5.2.7 Specificity of Transduced T cells

Preliminary experiments to test the transduction efficiency of 4th generation constructs and identify the optimal effector to target ratio were performed with the MAGE A3 TCR, referred to as MM1. Transduced T cells showed between 20-60% TCR expression using the mouse TCRβ chain antibody at Day 7 of culture (Figure 5.21a and b). Approximately 80% of T cells in culture were CD4+ve, two thirds of which expressed the MAGE TCR by Day 7 (Figure 5.21b). In addition, only 50% of positively transduced T cells retained expression of the endogenous TCR, the remainder of which were only positive for the MM1 TCR (Figure 5.21b).

MM1 TCR transduced T cells were cocultured with no peptide, MAGE A3 (specific peptide) or Eno241cit (irrelevant peptide) pulsed BD41 activated B cells at various effector (T cell) to target (activated B cell) ratios. T cell activation was assessed via IFNγ ELISpot and spot counts were analysed (Figure 5.21d). T cell densities were kept constant at 25,000 cells per well and B cell densities were adjusted to obtained desired E:T ratios of 2:1, 1:1 and 0.5:1. Activated B cells did not produce any IFNγ but background levels of up to 80 spots were observed in conditions with untransduced T cells. Background was reduced with decreasing effector to target ratio (Figure 5.21c and d). Good IFNγ responses were seen in MAGE A3 peptide pulsed conditions with spot counts equal to the PHA control with ratios 2:1 and 1:1, however a slight reduction in levels were found at ratio 0.5:1 (Figure 5.21c). Based on these results all following experiments were conducted at a 1:1 E:T ratio.

Originally the expression of activation marker CD69 was used to confirm recognition of specific peptide by TCR transduced T cells. MAGE A3 TCR (2nd generation) transduced T cells previously showed small but distinct activation levels with specific peptide compared to no peptide B cell conditions; increased CD69 percentage from

10% to 15% (Figure 5.15c). IFNγ secretion and CD69 expression levels were compared in 3 donors transduced with MM1. Spot counts were elevated in MM1 cultures with MAGE A3 pulsed B cells compared to no peptide in all donors; ~100-150 spot count increase in donors BCG and BCN2 and 50 spots in donor BCI (Figure 5.21e(i)). However, this did not correlate with CD69 expression as no difference was observed with MM1 transduced T cells cultured with MAGE A3 peptide pulsed B cells compared to unpulsed conditions (Figure 5.21e(ii)). Taken together, IFNγ ELISPOT proved to be a more sensitive assay to analyse T cell recognition of specific peptide.

Figure 5.21

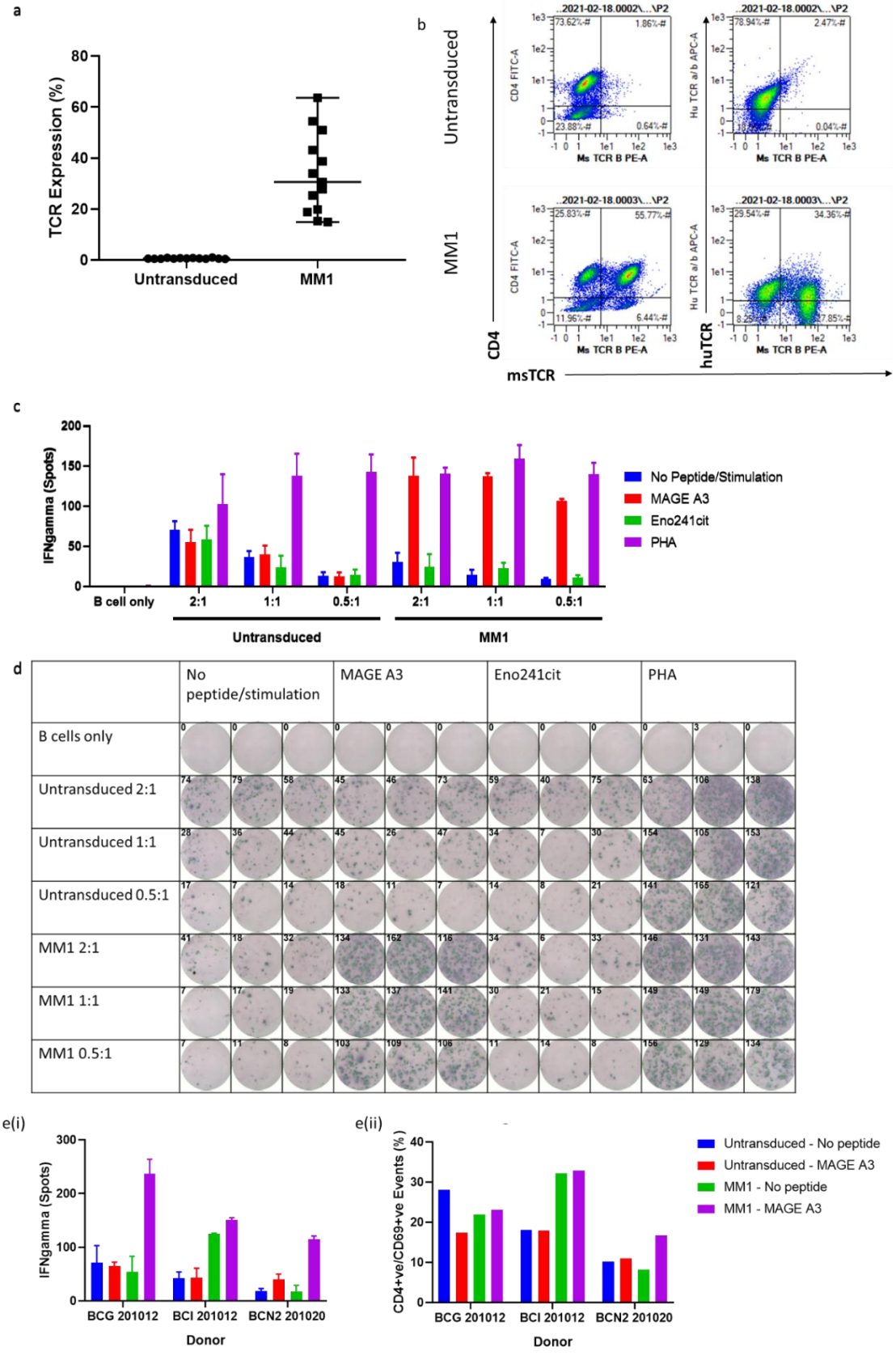

a
TCR Expression (%)
Untransduced
MM1
b
Untransduced
MM1
CD4
msTCR
huTCR
CD4 FITC-A
Ms TCR B PE-A
Hu TCR a/b APC-A
c
IFNgamma (Spots)
B cell only
2:1
1:1
0.5:1
Untransduced
MM1
No Peptide/Stimulation
MAGE A3
Eno241cit
PHA
d
No peptide/stimulation
MAGE A3
Eno241cit
PHA
B cells only
Untransduced 2:1
Untransduced 1:1
Untransduced 0.5:1
MM1 2:1
MM1 1:1
MM1 0.5:1
e(i)
IFNgamma (Spots)
BCG 201012
BCI 201012
BCN2 201020
Donor
e(ii)
CD4+ve/CD69+ve Events (%)
Untransduced - No peptide
Untransduced - MAGE A3
MM1 - No peptide
MM1 - MAGE A3

Figure 5.21 T cells transduced with 4th generation MAGE A3 TCR, referred to as MM1 (full details in table 5.9). Collated TCR expression data of untransduced and MM1 transduced T cells using mouse TCRβ chain antibody. N≤12 (a). Co-staining of MAGE A3 TCR transduced T cells with mouse TCRβ chain antibody, human pan TCR α/β and CD4 antibodies (b). IFNγ ELISpot (c) and plate layout (d) of antigen presentation assay comparing various effector:target (T:B cell) ratios of untransduced and MM1 transduced cultures. Error bars represent triplicate wells. Comparison of IFNγ spots (e(i)) and CD69 (e(ii)) expression from three healthy donors either untransduced or transduced with MAGE A3 TCR and cocultured with unpulsed (no peptide) or MAGE A3 peptide pulsed B cells. N=3.

TCR expression on transduced T cells (and untransduced controls) were checked on day 7 of culture prior to the antigen presentation assay (day 10). This helped to determine the health of the cultures as well as levels of desired TCR. T cells were routinely stained with CD4 and mouse TCRβ chain antibodies as shown in Figure 5.21b. Each TCR was transduced in at least 2 different healthy donors or buffy coat T cells and average expression ranged between 20-60% (Figure 5.22). Untransduced T cells showed less than 1% expression of mouse TCRβ chain. Majority of TCRs specific to citrullinated peptides showed high transduction efficiency (>30%) however expression of V28-41-M8, V415-11-M2, and V415-11-M6 were all <20% in all donors tested with that TCR (Figure 5.22a and b). Low TCR expression could result in low T cell activation and an ablated IFNγ response.

T cells transduced with TCRs specific to citrullinated peptide were cocultured with either BD41 or BD11 activated B cells, at 1:1 E:T ratio, previously pulsed for 2 hours with specific peptides and irrelevant peptides. Transductions and antigen presentation assays for BD41 Eno241cit and BD11 Vim415cit TCRs were performed by Ruhul Choudhury (Scancell Ltd). Un-pulsed (no peptide) and 10µg/ml PHA conditions were used as negative and positive controls respectively. The percentage difference in IFNγ responses from specific peptide pulsed conditions compared to un-pulsed conditions were calculated. There was a significant upregulation in IFNγ responses in MM1 T cell cultures compared to untransduced conditions with up to

700% increase (P=0.0003). Smaller percentage increases in V28-41-M2 and V28-41-M7 transduced cultures were identified however this was not significant (P=0.0959 and P=0.6163 respectively), and there were no responses from the remaining Vim28cit TCRs (Figure 5.23a). In addition, no percentage increases were observed in any Vim415cit or Eno241cit TCR cultures (Figure 5.23b and c). TCR expression in the majority of citrullinated peptide TCR cultures matched those of MM1 cultures therefore variations in TCR expression in unlikely to be the reason for the lack of responses measured.

To eliminate insufficient peptide processing as a possible cause for the absence of positive responses from all citrullinated peptide specific TCRs, shorter versions of each peptide were used in antigen presentation assays. Full length peptides were run alongside to compare IFNγ responses. As seen in previous experiments, MM1 TCR cultures and PHA controls produced high IFNγ levels. High background levels (responses in no peptide controls) were seen for V28-41-M4 and V28-41-M13 cultures, equal to the PHA control. No positive responses were found in any citrullinated peptide TCR transduced T cell cultures (Figure 5.24).

Figure 5.22

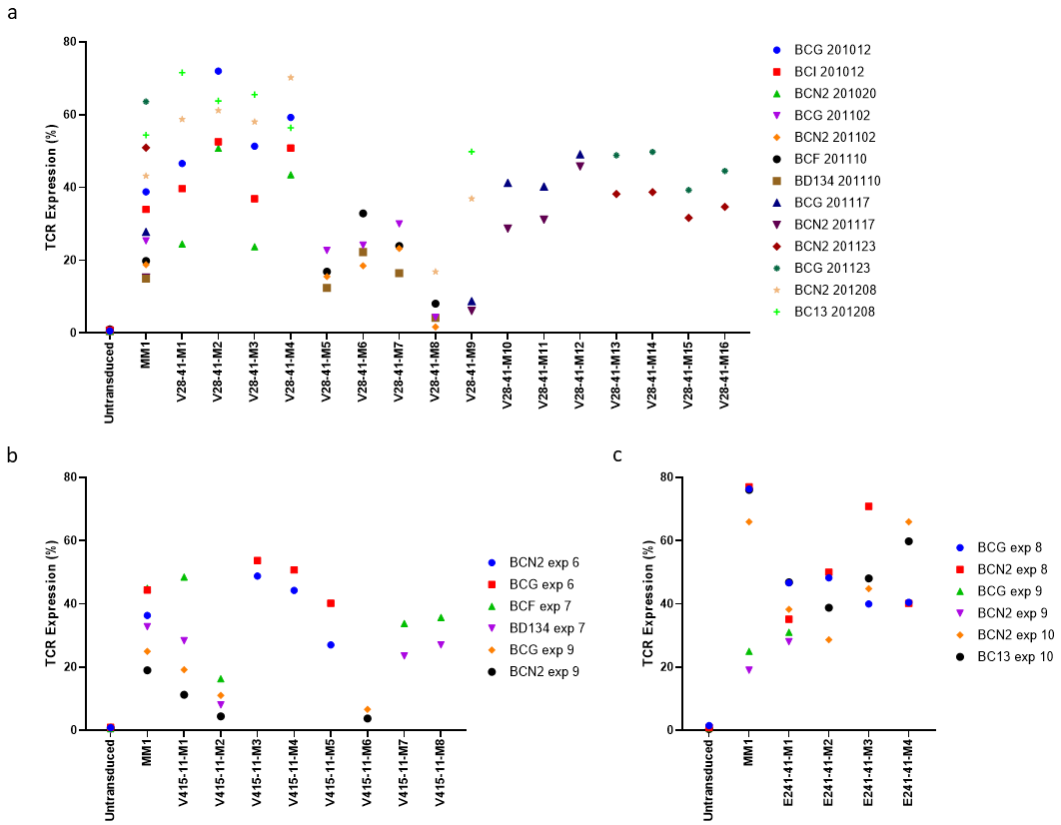


Figure 5.22 TCR expressions using mouse TCRβ chain antibody of T cells transduced with Vim28cit TCRs 1-16 (b), Vim415cit TCRs 1-8 (c) and Eno241cit TCRs 1-4 (d). N>2.

Figure 5.23

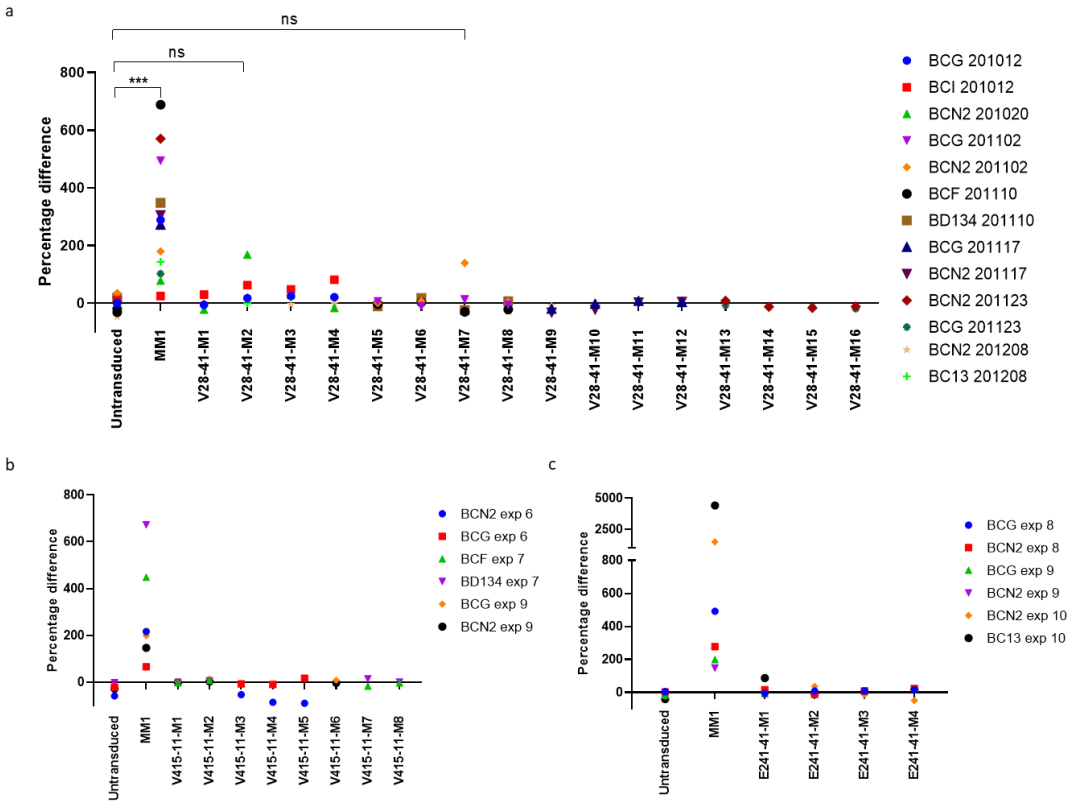


Figure 5.23 Percentage difference of TCR transduced T cell IFNγ responses between specific peptide pulsed conditions compared to unpulsed conditions. Data shown for T cells transduced with Vim28cit TCRs 1-16 (a), Vim415cit TCRs 1-8 (b) and Eno241cit TCRs 1-4 (c). Paired t test analysis ns = P > 0.05, *** = P≤0.001. N>2.

Figure 5.24

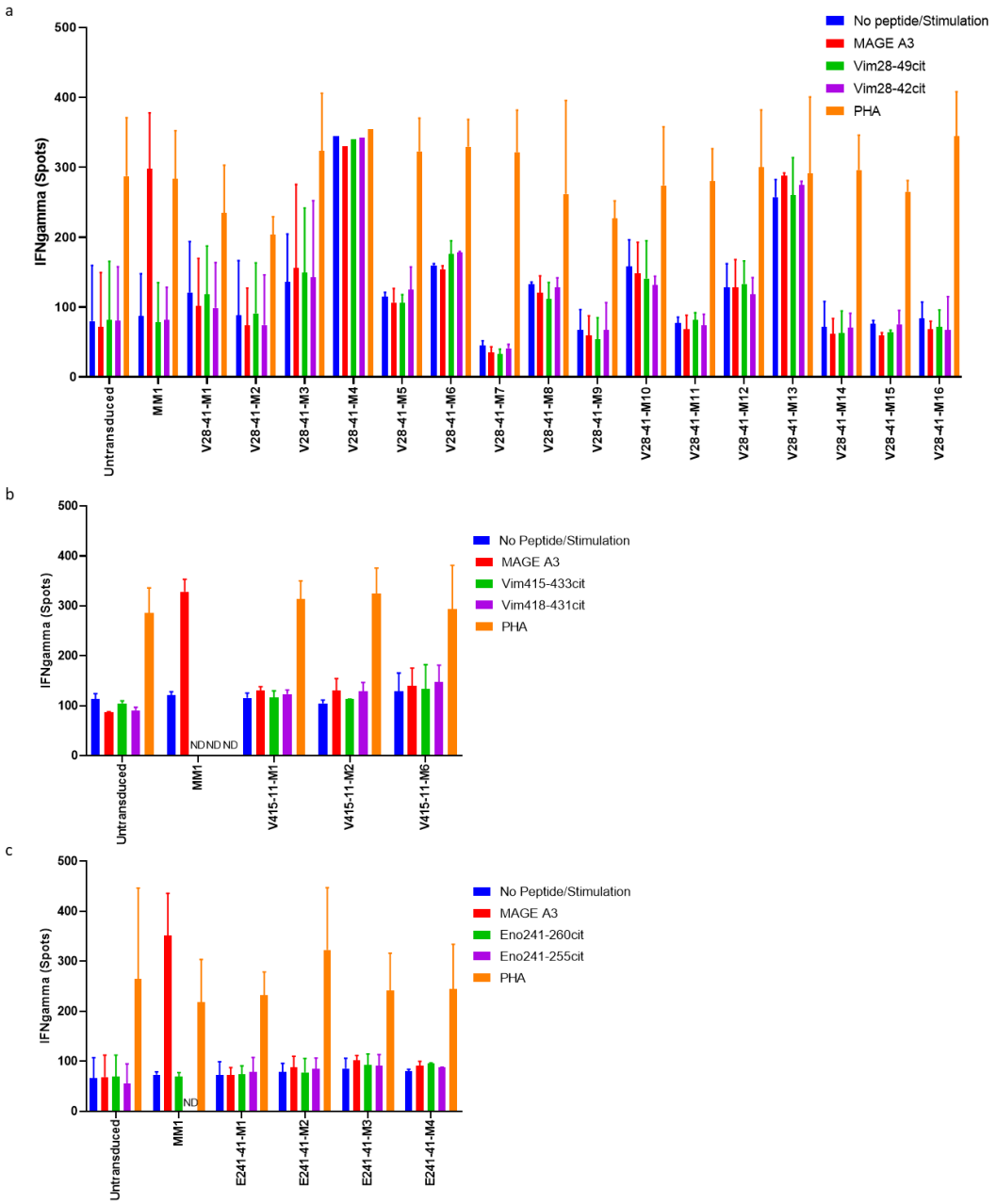


Figure 5.24 Comparison of IFNgamma response of transduced T cells cocultured with B cells peptide pulsed with long and short citrullinated peptides. Data shown for T cells transduced with Vim28cit TCRs 1-16 (a), Vim415cit TCRs 1,2,6 (b) and Eno241cit TCRs 1-4 (c). ND = not done. N>2.

5.2.8 Results summary

We have previously shown that citrullinated peptides from vimentin and α-enolase are presented on HLA-DR4 or DP4 in tumour cells and stimulate strong CD4 mediated anti-tumour responses [1, 2]. The MODI1 peptides, Vim28-49cit, Vim415-433cit and Eno241-260cit were preferentially expressed in B16F1 tumours compared to the equivalent wildtype forms. Analysis of the human CD4 repertoires responding to the MODI1 peptides showed oligoclonal proliferation of mainly T effector memory (TEM) cells but also an increase in the cytotoxic CD45RA expressing TEM population (TEMRA). Bulk RNA sequencing showed some CDR3 sequences found in non-proliferating populations were expanded in proliferating populations however most sequences in responding cultures were unique. There was also some V-J usage bias between the three MODI1 peptide cultures with high percentages of TRBV29-1 in response to all peptides. Single cell RNA sequencing of the alpha and beta TCR chains of proliferating populations identified high frequency TCRs were transduced using lentiviral technology into the immortalised T cell line deficient of endogenous TCR, J76 [352] and or T cells, and tested in antigen presentation assays to confirm their specificity to citrullinated peptides. In total, 16 high frequency TCRs were identified in response to Vim28cit, 4 in response to Eno241cit and 8 in response to Vim415cit. The MAGE $A3^{243-258}$ (MAGE A3) HLA-DP4 restricted TCR was used as a control and for optimisation of transfection and transduction methods [343, 344]. TCR constructs were continuously improved throughout the project and cocultures of J76 and T cells were tested against a range of peptide pulsed antigen presenting cells; B16F1, B-LCLs, activated B cells and dendritic cells. Final experiments involved TCR constructs with a fully murinised constant region, the adapted transfection method and transduction of T cells. Recognition of specific TCR was assessed by upregulation of the activation marker CD69 in J76, and the potent cytokine, IFNγ in T

cells. The MAGE A3 TCR control exhibited great activation levels however confirmation of a citrullinated protein specific TCR is yet to be determined.

5.3 Discussion

T cells can recognise stress induced post-translational modifications (siPTMs) on tumour cells as seen by strong IFNγ production in splenocytes from B16F1 tumour bearing transgenic mice [1, 2, 77, 220]. Mass spectrometry analysis of B16F1 tumours identified citrullinated peptides (MODI1) Vim28cit, Eno241cit and Vim415cit. These were preferentially expressed at higher levels compared to their wildtype equivalents. In addition, MODI1 peptides were shown to induce cytotoxic CD4 T cell responses in mouse models and healthy human individuals, as observed in previous work [1, 2, 77, 220]. Only three other vimentin and enolase citrullinated peptide sequences were identified, and these could also potentially stimulate T cell responses. However, expression of these citrullinated epitopes in human tumours and their ability to induce T cell responses in healthy individuals and mouse models is yet to be verified.

In this chapter we aimed to understand the T cell phenotypes responding to citrullinated peptides and the TCR repertoire in healthy individuals that can recognise these siPTMs. Determining the specificity of the identified TCRs proved challenging. Many techniques were tested to optimise and improve TCR transduction efficiencies and recognition of specific peptide by TCR transduced cells, and three method changes allowed substantial advancements in this project. Optimisation of the transfection method, transduction of T cells instead of the Jurkat 76 cell line (J76) and IFNγ secretion as a readout of T cell responses. The first improvement was largely due to the concentration of lenti virus after transfection into the packaging cell line HEK293T. Literature shows ultracentrifugation reduced viral titre but gave better transduction efficiencies in T cells due to the removal of impurities. This research group also found reducing the centrifuge speed from 90000g to 20000g increased viral titre, but was lower when using slower speeds [353]. The original transfection

protocol involved using a concentrator solution and centrifugation at low speed for 45 minutes. This may have resulted in a lower viral titre and more impurities compared to the adapted protocol that involved overnight centrifugation at 10000g. Colony forming titration needs to be performed with lenti viral cultures produced via both transfection methods to confirm the viral titres produced and the resulting poor transduction efficiencies.

The second major optimisation was using T cells for transductions. The human T cell lymphoma cell line J76, a derivative of Jurkat E6.1, does not express cell surface CD3 or TCR allowing optimum detection of successfully transduced cells, especially using the pan-TCR antibody for all TCR constructs eliminating the need to purchase individual vβ specific antibodies based on the TCR β chain. However, as an immortalised T cell line, many other signalling pathways are also altered reducing activation sensitivity. These abnormalities include reduced ZAP-70 phosphorylation and secretion of limited cytokines, IL-2, IL-8 and MIP-1α/β, as seen in Jurkat E6.1 cells after CD3/CD28 stimulation compared to peripheral blood T cells [347]. The J76 cell line used in our assays also lacked accessory molecule CD226 and had low levels of CD2, which needed to be introduced retrovirally to show TCR recognition responses [345]. In addition, this cell line is commonly transfected with reporter genes such as NFAT to assess activation [345]. Although T cells, as a primary suspension cell, are more difficult to transduce than a cell line, they are better representative of the responses and activation levels found *in vivo*. Optimal transduction efficiencies were initially difficult to obtain, however substantial improvements were made after development of the adapted lenti viral production method. TCR levels were also enhanced when transduced with a smaller construct, as seen by up to 60% transduction efficiency with GFP lenti viral constructs. This is a known phenomenon where cells are more likely to take up and express additional genetic material if smaller in size [354, 355]. Transduction efficiencies with the 3rd generation fully

murine constant region construct was substantially better than 3rd generation constructs containing additional selection markers rat CD2, truncated CD34 or GFP. The smaller size of the construct was predicted to have contributed to this, therefore a final (4th) generation of lenti viral construct was produced, dropping the puromycin selection gene. As transductions were to be performed in T cells and not a cell line, puromycin selection was not required to inhibit growth of untransduced cells and obtain pure cultures. The fully murinised constant region of TCRs in this construct version allowed a clear distinction of successfully transduced cells using an anti-Mouse TCR α/β antibody against expression of the endogenous human TCR. This technique has been successfully utilised by others and has even showed increased expression and IFNγ secretion compared to TCRs containing the equivalent human constant region [344, 356, 357]. In addition, the fully murinised constant region avoids mispairing with the endogenous human TCR and has shown to bind better to CD3 increasing its stability compared to the fully humanised TCR and improving its functional sensitivity [357, 358].

Although, we were able to see good transduction efficiencies, CD69 expression levels of the MAGE A3 peptide by MAGE A3 TCR transduced T cells were low and did not show increased levels compared to no peptide or irrelevant peptide controls, as previously seen with transduced J76 or preliminary experiments with T cells. Effector:Target (E:T) cell ratios were the same, 1:1, for both experiments however double the number of cells were used in preliminary experiments that may have contributed to the slight increase in CD69 activation observed. These levels were still not as high as seen with peptide pulsed dendritic cells (DCs). In addition, as CD69 is considered an early activation marker and can be detected within 4 hours after activation, the peak expression window (18-48 hours) for this marker may differ between donors [359]. Therefore, it was necessary to find a more suitable activation marker. CD69 has been used to determine activation of CD4 T cells however higher

concentrations of peptide were required to stimulate a response [360]. Instead, expression of cytokines, IFNγ, TNF-α, IL-17, IL-2 and chemokine MIP-1β are preferentially used to determine T cell activation via the TCR [33, 349, 358, 361, 362]. IFNγ has also been used as an activation readout in J76 cells when cocultured with T2 (human HLA-A2 TAP deficient lymphoblastoid) and K562-A2 (human chronic myelogenous leukaemia, transduced with HLA-A2) cell lines despite ablated secretions witnessed in the original Jurkat E6.1 line, however this effect was only observed at higher peptide concentrations [353, 363]. Therefore, most studies utilise CD69, IL-2 or NFAT expression to measure Jurkat activation [33, 333, 345, 358, 364-366]. In addition, CD69 showed no difference between various CAR-T cultures and was upregulated without TCR engagement in Jurkat E6.1 but not CD4 T cells [364, 365], highlighting IFNγ as a more specific readout for T cell activation.

LCLs are commonly used as APCs and are able to activate T cells when peptide pulsed and cocultured [33, 362]. But this was not observed in our experiments and responses to LCLs were only found when cocultured with J76. Compared to J76, T cells express more co-stimulatory molecules and their own endogenous TCR some of which may be able to recognise latent EBV antigens. It is possible that peptides generated by the EBV infection are bound with high affinity to the MHC molecules on the LCLs, and the MAGE A3 and citrullinated peptides were not of high enough affinity to dissociate these endogenous peptides from the MHC, resulting in no reactivity. In addition, literature has shown LCLs secrete MHC class II +ve/FasL+ve exosomes that can induce apoptosis in CD4 T cells [367], however low viability was not found in these assays. CD4 T cell responses to citrullinated peptides have been observed in healthy donors expressing a range of MHC-II HLA alleles, not just HLA-DR4 and HLA-DP4 [77]. As the HLA-restrictions of the TCRs identified and tested were unconfirmed, we required APCs from the donors that the TCRs were isolated from, BD41 and BD11. HLA typing of both donors shown in Appendix 6. Peptide pulsed DCs showed

good T cell stimulation but harvesting and culturing the appropriate number of DCs to test all TCRs from the two donors was not feasible. In contrast, B cells (also professional APCs), could be activated, expanded, cultured and thawed from cryo-storage when needed. Culturing B cells on a feeder cell line expressing CD40 ligand (CD40L) gave better overall activation marker (MHC-II, CD80, CD86) expression compared to expansion kits. Preliminary experiments with 4th generation MAGE A3 TCR (MM1) transduced T cells showed elevated IFNγ secretion when cocultured with MAGE A3 pulsed activated B cells, and reduced background signal when cultured at 0.5:1 or 1:1 E:T ratios. CD40L expression on the NIH3T3 cells was routinely monitored and B cell activation markers were assessed at time of use for antigen presentation assays to ensure the best level of peptide presentation and stimulation.

Despite significant improvements to lenti viral production, construct design optimisations to prevent mispairing of α and β chains, APC optimisation, and activation readout, no TCRs specific to citrullinated MODI1 peptides were identified. Initial thoughts were to upgrade the TCR screening assays however the many methods attempted were unsuccessful. As the MAGE A3 control worked well in every scenario, the investigation narrowed down to two questions; are the peptides being sufficiently processed and presented and have the correct TCRs been selected? As the short peptide Vim48-42cit, was abundant in B16F1 tumours analysed by mass spectrometry, it was hypothesised that the full length peptides are cleaved into shorter sequences before being presented. To address the first question, shorter peptides were pulsed in the antigen presentation assays alongside the full length peptides. However, this still did not produce a positive response. Although Sidney et al., (2017) found variable binding affinities of RA citrullinated peptides compared to its wildtype equivalent [368], previous work conducted by Scancell shows increased binding of Vim28cit, Vim415cit and Eno241cit to HLA-DP4 compared to wildtype [77]. However, these peptides had a 3-fold lower binding affinity than a Hepatitis B HLA-DP4

restricted peptide (181-193) [77]. It is possible that MAGE A3 is a high affinity peptide in comparison therefore showed positive responses with low TCR transduction efficiencies. This peptide is known to have a strong affinity for HLA-DPB1*0401 and 5 times more peptide was required to induce similar IFNγ levels when presented by HLA-DPB1*0402 [369]. Donor BD41 expressed this high binding allele HLA-DPB1*0401 and could explain why no decrease in IFNγ levels were seen with 100 times less peptide (Appendix 7). Evidence suggest a threshold of ~8000 stimulated TCRs or ~1500 stimulated TCRs in the presence of CD28-CD80/CD86, is required to produce maximal IFNγ levels [370]. In addition, a higher number of TCR molecules per cell were required when exposed to low antigen concentrations to obtain sufficient IFNγ and IL-2 cytokine release. In conditions with a high abundance of antigen, less TCR molecules per cell were required to induce similar levels of proliferation and cytokine expression [371]. Although citrullinated peptide specific TCR expression in T cells was increased with the various optimisation methods, a higher concentration of peptide may have been needed to see a similar level of response to the MAGE A3 TCR.

Another challenge to address is whether the correct citrullinated specific TCRs have been identified. T cell responses in healthy human individuals to Vim28cit, Vim415cit and Eno241cit looked promising with good CD4 proliferation and expression of activation marker CD134, and functionality markers IFNγ and Granzyme B (data from this report and previous Scancell publications) [77, 220]. These markers are all expressed or released by activated effector T cells promoting further expansion of antigen-specific T cells [372-374]. Further phenotyping of the responding CD4 population found most cells were CD127 (IL-7 receptor) and CD197 (chemokine receptor 7; CCR7) negative suggesting a majority effector memory group, some of which had begun to re-express CD45RA; a marker that can also be found on naïve T cells. This phenotype has also been described for a subset of highly cytotoxic T

effector memory cells re-expressing CD45RA known as TEMRA [79]. Taken together the data indicates that citrullinated epitopes promote cytotoxic T cell responses within 10 days.

TCR sequencing of these responding CD4 cultures showed less diversity in TCR sequences compared to non-proliferating populations suggesting selective expansion of T cells. Not all of the top 10 sequences in proliferating populations were abundant in the non-proliferating population again indicating specific T cell expansion. Some TCRs were found at high frequencies in both populations such as β chain CDR3 (CDR3β) sequences SVWTSVQETQY in Vim28cit responses, ASSDGGVDTEAF in Eno241cit responses and SVRKSGDTQY in Vim415cit responses from the bulk sequencing. This may suggest non-specific expansion of clones carrying this β chain or the presence of a public TCR. These TCRs are often shared between individuals and are clonally dominant (found at a high copy number within the repertoire) compared to private TCRs. Factors such as convergent recombination and recombinational bias, as discussed in section 5.1, contribute to the presence of public TCRs. Recombination events occur in the thymus; rearrangements of both chains occur prior to positive selection with β-chain rearrangement in CD4/CD8 double negative thymocytes, followed by α-chain rearrangement in CD4/CD8 double positive (DP) cells. Analysis of the TCR repertoire in mice with human thymus grafts did not detect an increase in clonality with positive selection (comparing CD69-ve against CD69+ve DP cells) but did see more clonality and an elevated number of shared CDR3βs in single positive (SP) cells compared to CD69-ve DP cells [334]. CDR3β sharing was even greater in peripheral T cells with expression of the same chains found on both CD4 and CD8 cells, indicating the preferential expansion of certain TCRβ chains, unrestricted by MHC class, during negative selection and post-thymic selection [334]. This finding was interesting as it suggested public TCRs shared a common property or feature that was favourable for escaping negative selection. It is

difficult to determine whether the TCR sequences identified by our work are public or private. TCR repertoire responses to MODI1 peptides would need to be determined in multiple individuals to assess whether the sequences found at high frequency in both non-proliferating and proliferating populations are shared between individuals. However, the commonly studied phenomenon of recombination bias, V-J usage, showed dominance of certain domains in responding populations with TRAV26-2 abundant in BD41 Eno241cit and BD11 Vim415cit cultures, and TRBV29-1 at high frequency in all three citrullinated peptide cultures. TRAJ54, TRBJ2-5 and TRBJ2-3 were also greater in BD41 Vim28cit and BD11 Vim415cit cultures. Benati et al (2016) found public GAG293-specific clonotypes exhibited common alpha and beta chain V domain usage that were associated with limit CDR3 peptide motifs [333]. Although the cultures analysed in this work were against different citrullinated peptides, this data suggests a V-J usage preference for citrullinated epitopes. Again, responses in multiple individuals against a single citrullinated peptide is require to confirm the prevalence of these domains. Comparison against the wildtype peptide would also help to distinguish citrullination preferential usage.

Single cell TCR sequencing of the responding cultures allowed pairing of the α and β chains. Only 4 TCRs were detected from BD41 Eno241cit cultures suggesting specific expansion of T cells however many more TCRs were detected (up to 16) with both Vimentin peptides. With regards to Vim28cit, some wells contained multiple α and β chains. Dual α and β chain expression has been reported in literature with mRNA of one chain expressed at higher levels than the other [375, 376]. Therefore, the lower chain reads were discounted and only the high chain reads were considered for pairing. However, as this was a frequent finding with responding TCRs to Vim28cit, it is possible that this peptide is recognised by TCRs containing the second less prevalent β chain, which escaped thymic selection due to interactions of the dominant TCR with self-peptide-MHC.

The MAGE A3$^{243-258}$/HLA-DP4 restricted TCR was identified using a slightly different method. PBMCs were isolated from a melanoma patient previously vaccinated with monocyte derived DCs loaded with MAGE A3$^{243-258}$ peptide. This would induce more specific and higher affinity TCRs. They were stained with the multimers that involved covalent linking of the N terminus of the MAGE A3$^{243-258}$ peptide to the β chain of DPB1*0401. Cells positively labelled with the monomer and CD3 but not CD8 were sorted by FACs and stimulated with specific peptide pulsed B-LCLs. Two re-stimulations were applied and a total of 81 IFNγ secreting CD4 T cells were sorted [377]. T cell clone R12-C9 containing the MAGE A3/HLA-DP4 restricted TCR was later established through sequencing methods [343]. To isolate this high affinity, specific TCR multiple rounds of stimulation was applied to narrow down the responding clones. Only one round of stimulation with peptide was applied in our assay, which were added directly to the PBMCs and not pre-pulsed in APCs which may have improved stimulation. It is possible that the TCRs selected are of low affinity for the citrullinated peptides, and therefore do not show responses to peptide pulsed target cells. Three TRBV2 clonotypes were found to associate with the dominant TRBV24 sequence in GAG293-specific cultures. When the beta chain was paired with each alpha chain and transduced into J76 cells a substantial difference in TCR affinities were observed against HLA-DR alleles [333]. This highlights the sensitivity of the TCR to a specific peptide based on slight differences in CDR3 motifs and suggests all alpha/beta chain combinations identified by single cell sequencing should be tested. Other research groups have also used similar re-stimulation methods. For example, the identification of NY-ESO$^{157-165}$ specific T cell clones by expansion of melanoma patient PBMCs with a panel of NY-ESO peptides which were then restimulated and IFNγ secreting reactive cells were sorted using peptide-MHC tetramers. The selected clones were sequenced using RT-PCR for paired α and β genes and incorporated into a retroviral vector for transductions [358]. Alternatively,

TCR analysis of single stimulation T cell clones from multiple donors may help to identify the citrullinated specific TCRs. Hepatitis B virus (HBV) specific clones were isolated from three individuals previously infected with HBV also using cell sorting, from which 100 clones exhibit cytotoxicity and several clones (including V-J usage) were shared between the patients. By titrating the specific peptide to nano- or picomolar concentrations, they were able to identify the most specific T cell clones [378].

To conclude, citrullinated peptides (MODI1) induced cytotoxic CD4 T cell responses in healthy individuals and were also identified in B16F1 tumours. TCR sequencing of responding CD4 T cell cultures were oligoclonal. Further analysis highlighted common V-J domain usage between the citrullinated peptide cultures. Some TCR chain sequences were also highly abundant in both non-proliferating and proliferating populations suggesting recognition of citrullinated peptides by public TCRs. However, these selected TCRs may be of low affinity due to only one round of stimulation, resulting in the ablated responses in the various assays attempted. Re-stimulation, binding with multimers and testing sensitivity to low peptide concentrations could help to improve identification of high affinity, specific TCRs.

6 General Discussion

6.1 Citrullination in normal vs tumour cells

For a citrullinated protein to stimulate an immune response, multiple conditions need to converge; a stress factor such as lack of cell-to-cell contact, upregulation of autophagy, increased proliferation and inflammation induced MHC-II expression. Cells are subjected to stress on a regular basis and in most cases, they are able to overcome this pressure. The response to this stress can either be protective or destructive depending on the nature and duration of the stress applied. To survive, cells undergo the well characterised process autophagy where damaged or unwanted proteins are degraded and re-distributed and used to build new proteins and membranes. Under normal conditions, selective autophagy occurs where the cargo is dependent on binding to specific ligands e.g p62 in mammals [379]. At the later stages of autophagy, the autophagosome can fuse with MHC class II containing compartments (MIIC) forming multivesicular bodies and this allows the presentation of endogenous, processed self-peptides to be presented on the cell surface [207]. However, MHC-II is not ubiquitously expressed and non-professional APCs will only upregulate this molecule when exposed to inflammatory cytokine IFNγ, as shown by our data in Chapter 4. In normal tissues there is no inflammation unless cells become infected by pathogens and/or are damaged. Therefore, under normal conditions citrullinated peptides would not be expressed on MHC-II and be recognised by CD4 T cells. In addition, results from Chapter 3 showed an association between citrullinated vimentin expression and proliferation. Cell proliferation in normal cells is tightly regulated by cyclins and cyclin-dependent kinases (CDKs), controlling the movement through cell cycle phases G1, S, G2 and M. Many differentiated cells will arrest in the G1 stage or proceed to G0 from G1, entering a state of quiescence where they maintain metabolic activity without dividing [380]. The lower levels of proliferation

in normal cells suggest citrullination would not be a common occurrence. To summarise there should be no expression of citrullinated epitopes on the surface of normal cells.

Tumours naturally express the conditions required for citrullination, a stress factor such as lack of cell-to-cell contact/proliferation and upregulation of autophagy. In the early stages of immunosurveillance they may also have inflammation induced MHC-II expression and be good targets for CD4 T cells. As the tumour progresses and becomes more immunosuppressive, inflammation is controlled and citrullinated epitopes may no longer be presented. This is reversible as it has been shown that citrullinated peptide vaccines can promote survival, tumour regression, and IFNγ responses in mouse models, and the *in vitro* stimulation of cytotoxic CD4 oligoclonal T cells in humans [77, 220].

IFNγ is required to induce the expression of MHC-II on the tumour cell. Data from Chapter 4 showed low levels of MHC-II are found in human cancers and this expression could be elevated in the presence of IFNγ. This pro-inflammatory cytokine is mostly secreted by effector T cells, activated NK cells and M1 macrophages. Therefore, for tumour cell presentation of citrullinated peptides by MHC-II to occur, these cells need to be in the microenvironment and need to express tumour specific pro-inflammatory responses. Vaccinations against TAAs can induce this (as discussed in Chapter 1). Brentville and colleagues have shown immunisation with citrullinated peptides induced *ex vivo* IFNγ responses and significant survival in mice bearing B16F1 tumours expressing IFNγ inducible MHC-II [1, 77, 220]. In Chapter 5 we showed CD4 T cells differentiated into cytotoxic effector cells after culture with citrullinated peptides, expressing lytic granules capable of inducing tumour cell death. The efficacy of peptide vaccines can be low in patients with low tumour infiltration of immune cells, however adoptive transfer of citrullinated peptide antigen specific cells

could boost anti-tumour responses. Identification of a citrullinated peptide specific TCR would have provided us with the ability to proceed with this type of therapy. To conclude, without this inflammation, the tumour microenvironment would remain in an immune suppressive state and stress-induced citrullinated peptides would not be presented on the surface by MHC-II for detection. Vaccination with citrullinated peptides can reverse this effect and induce strong anti-tumour immunity.

The presentation of citrullinated peptides in tumours differs to that in autoimmune diseases such as Rheumatoid arthritis (RA). Firstly, excessive inflammation in this disorder promotes cell death, activation of PADs and hence citrullination in the synovial fluid. Tumour cells remain viable and yet can undergo citrullination. Secondly, RA is more prevalent in individuals expressing a 'shared epitope' (SE) HLA allele such as HLA-DR4. Most SE alleles in RA belong to the DR group [202, 203]. Citrullinated peptides may bind strongly to the HLA-DR allele hence the chronic inflammation and association with RA. However, T cell responses to citrullinated peptides were not restricted to healthy individuals only expressing these SE alleles, and are also found to be presented by DP alleles [77, 220]. As discussed in Chapter 5, HLA-DP does not require DM or invariant chain to bind peptide [308, 309]. Therefore, it is possible for them to bind endogenous peptides more efficiently than the other HLA alleles. This would allow the continuous presentation of peptides with low affinity such as citrullinated peptides in stressed cells.

6.2 Citrullinated epitopes for immunotherapy

As cancer immunotherapy advances, more TAAs are identified. To reduce off-target toxicity effects and be useful in immunotherapy they must adhere to certain criteria; they must only be expressed on tumour cells or at low levels on healthy cells, be able to induce a T cell response and be vital for tumour cell survival. Data from this project

shows citrullinated peptides follow these principles. Unfortunately, most self-antigens that mount a T cell response are recognised by the TCR with low affinity due to the process of negative selection in the thymus. Foreign antigens induce stronger activation due to their higher affinity for TCR [381, 382].

Tumours commonly have increased levels of mutations compared to healthy tissue. These somatic mutations are highly variable but some cancer types show a greater prevalence of mutations than others. For example, melanoma, lung and bladder cancer have a 100-fold mutational average than leukaemia and medulloblastoma [134]. Somatic mutations can give rise to neoepitopes that are recognised by the adaptive immune system when presented on the tumour cell surface by MHC molecules. For this to occur, the mutated amino acid must be positioned within the MHC binding groove at the optimum location for contact with the TCR. A mutation of an anchor residue could also elicit immunogenicity by stabilising the peptide to the MHC. If the mutated residue faces away from the TCR it is unlikely to create an immunogenic epitope [383]. Neoepitopes can also be formed by post-translational modifications such as citrullination, not just somatic mutations. The conversion of an arginine to a citrulline changes the charge of the side chain from positive to neutral. Shifts in charges can cause alterations to protein-protein interactions and therefore structure [384]. In this way a new epitope is created that will have different binding and antigenic properties to the original form. The affinities of citrullinated peptides for MHC-II were found to be greater than their equivalent wildtype peptides suggesting the conversion of the arginine to a citrulline in the peptide sequence induced a confirmational change and resulted in strong binding [77].

A study by Linnemann et al (2015) found mutational neoepitopes that are recognised by CD4 T cells are commonly found in human melanoma tumours. TCR sequencing of alpha and beta chains showed that the CD4 repertoires responding to these

neoepitopes were oligoclonal, similar to the findings in this project [385]. Taking into consideration the vast number of mutational neoepitopes recognised by CD4 T cells, it is unsurprising that citrullinated peptides also follow the same pattern. This was later followed by reports that tumour-specific responses to neoepitopes were CD4 dependent rather than CD8 [298, 299]. The ability of MHC-II to present peptides with a range of lengths was suggested as the reason for the high level of neoepitopes restricted to this molecule. Coupled with CD4 T cell requirement to maintain antigen specific CD8 responses, targeting CD4-restricted neoepitopes for cancer immunotherapy is very beneficial.

Combination therapies involving engineered T cells alongside antibody therapy targeting immune checkpoints and cytokine adjuvants such as IL-2 are still under testing for solid tumours. These are necessary to re-edit tumours, moving the cancer out of the 'escape' phase back to 'equilibrium', and eventually resulting in 'elimination' of the tumour . A successful T-cell based therapy will specifically target TAAs, home to the tumour site, avoid exhaustion and modulate the tumour microenvironment (TME) to promote a proinflammatory state and restrict tumour metastasis. Addressing all these points may seem challenging, but the substantial amount of work ongoing in this field brings us closer to the endpoint. The immune system can be primed to recognise citrullinated epitopes using the MODI 1 peptide vaccines. Citrullinated epitope specific TCR engineered T cells administered alongside the MODI 1 peptide vaccines not only primes the immune system against the tumour antigen, but also provides functionally active T cells to ensure the desired response is initiated. The optimum phenotype, naïve or effector, of engineered T cells needs to be determined to avoid exhaustion before an effective response is established. These therapies coupled with checkpoint inhibitors, adjuvants and immunomodulators could target the TME, suppressing regulatory cells/molecules and stimulating inflammation.

6.3 Importance of findings in other fields

The role of citrullination in RA has been discussed in Chapter 1; immune responses to citrullinated peptides drives inflammation in the synovial fluid of joints in patients, promoting disease. We have reported CD4 responses to citrullinated epitopes in healthy individuals. Determining the CD4 repertoire and TCRs that recognise RA associated citrullinated epitopes could be utilised to suppress the chronic inflammation. Regulatory T cells (Tregs), an immunosuppressive CD4 phenotype, can be modified to express the desired TCR. Many clinical trials are already investigating the use of Tregs for treatment of Graft versus Host Disease (GvHD), Type 1 Diabetes (T1D), Multiples Sclerosis, and Inflammatory Bowel Diseases [386, 387]. Antigen specific Tregs are required to reduce infection susceptibility and anti-tumour activity but the lack of autoantigens in most of these autoimmune diseases is a limiting factor. Citrullinated epitopes expand the antigen pool available and some citrullinated proteins have been identified in autoimmune diseases such as GAD65 and GRP78 in T1D, and MBP and GFAP in multiple sclerosis [388-390].

Citrullination may also be important in viral immunity. In Chapter 1, we have shown citrullination is a stress induced post-translational modification. Viruses are able to persist within mammalian cells utilising it's machinery to replicate and survive. Autophagy is activated by viral infection through virion binding, membrane fusion or through ER stress and the UPR. The main purpose is to deliver viral particles for degradation in lysosomes [391]. However, the increased autophagy may also expose more epitopes for citrullination, allowing their presentation on the cell surface by MHC. Investigation into the citrullinated epitopes in viral infection could propose a novel target antigen.

6.4 Summary

The aim of the project was to determine what cellular stresses induced citrullination of proteins and whether they are good targets for cancer immunotherapy.

1. The hypothesis was that “stress “ induces citrullination in association with autophagy and is a good target for cancer immunotherapy.

In this thesis we have shown that low cell density plated cells were the best produces of citrullinated vimentin, were the most proliferative and had the highest levels of autophagy. This could be related to the requirement of these cells for increased nutrients or could be due to signalling associated with loss of contact inhibition. Citrullinated vimentin was also expressed in human cancers head and neck (58%), sarcoma (80%), osteosarcoma (86%), renal (36%), ovarian (97%), lung (62%) and ER negative breast (90%). High expression significantly correlated with survival in lung (P=0.016) cancers. Additionally, citrullinated vimentin positively correlated with MHC class II, PAD2 and Ambra1 (autophagy) in these cancers. These results confirm that stress induces citrullination in association with autophagy and that it is a good target for cancer immunotherapy.

2. The hypothesis was that citrullinated peptides would only be presented in association with inflammation which up regulates MHC-II.

MHC-II was either expressed or upregulated by IFNγ and expression was associated with expression of the CIITA which is controlled by the pIV promoter. In addition, there a strong correlation between the IFNγ inducible protein, IRF-1 and CIITA mRNA as found in 10 cancers analysed from the TCGA database. IFNγ also increased citrullinated vimentin expression in the murine melanoma cell line B16F1. Of interest was that 27-55 % of tumour expressed MHC-II and this was associated with improved

survival in Breast cancer. In contrast, when Ovarian cancer patients were divided into negative, low and high MHC-II expressing groups, the MHC-II low compared to the MHC-II high expressing group had improved survival suggesting MHC-II low expressing tumours still had active immune surveillance but high expressing tumours had evaded the immune response and chronic inflammation was driving a more aggressive phenotype. In addition, MHC class II positively correlated with citrullinated vimentin, PAD2, IFNγ receptor and autophagy marker Ambra1. This is consistent with the hypothesis that tumour cells can express MHC-II and that it could present citrullinated epitopes via autophagy.

3. The hypothesis is that there is a repertoire of CD4 T cells that recognise siPTMs.

We have previously shown that citrullinated peptides from vimentin and α-enolase are presented on HLA-DR4 or DP4 in tumour cells and stimulate strong CD4 mediated anti-tumour responses [1, 2]. The MODI1 peptides, Vim28-49cit, Vim415-433cit and Eno241-260cit were preferentially expressed in B16F1 tumours compared to the equivalent wildtype forms. Despite analysis of the human CD4 repertoire responding to the MODI1 peptides showing oligoclonal proliferation of mainly T effector memory (TEM) cells but also an increase in the cytotoxic CD45RA expressing TEM population (TEMRA) we could not prove that the isolated TCRs recognised citrullinated epitopes. Experiments with a MAGE A3 specific CD4 TCR showed that a chimeric mouse constant region and human viable TCR construct showed the greatest expression and activation with little mispairing and good recognition of autologous B cell pulsed with cognate peptide. If citrullinated peptide specific TCRs can be identified from vaccine immunised patients then adoptive transfer of citrullinated protein specific TCR expressing T cells would be beneficial for cancer patients to increase tumour infiltration of antigen specific immune cells and could be used in combination with citrullinated peptide vaccines or other immunotherapy

techniques such as checkpoint blockade to regain control of the tumour microenvironment.

6.5 Future work

6.5.1 Improvements to TCR selection process

Results from this project have shown citrullinated peptides are able to activate CD4 T cells, inducing their proliferation and secretion of cytotoxic modulators. The responding populations were also oligoclonal with expansion of selective TCR clones. Unfortunately, we were unable to confirm whether any of these expanded TCR clones were specific for the citrullinated peptide. Many attempts were made to tackle this including techniques to enhance TCR expression and detection post-transduction, and to optimise the assay used to check recognition of specific peptide. As discussed in Chapter 5, it is possible that the TCRs selected in this project were of low affinity due to only one round of stimulation with citrullinated peptide. Other researchers have used multiple rounds of stimulation and have also screened T cell clones shared between individuals against very low concentrations of specific peptide [377, 378]. Both of these methods should be attempted to make advancements in this project. Another method for antigen-specific TCR detection is by isolating TILs or analysis of the responding T cells in cancer patient bloods. Earlier experiments with the group showed promising PBMC responses to citrullinated peptides in healthy donors. However, cancer patients should have an expanded repertoire to exposed citrullinated epitopes in the tumour.

6.5.2 Normal cells checked for citrullination

Selection of high affinity TCRs must come with caution. Disastrous off-target adverse effects were observed in patients treated with engineered T cells expressing a TCR

that recognises a high HLA-A2 binding MAGE-A3 peptide [119, 392]. This enforces the need to confirm expression of the target TAA in all tissues before selecting them for immunotherapy. As discussed at the start of this chapter, normal cells are hypothesised not to express citrullinated proteins. However, this should be confirmed by immunohistochemistry staining of normal tissues for citrullinated vimentin using ECV-1. As mass spectrometry of frozen tumours proved successful, the same analysis of fixed tissue lysates (normal vs tumour) could also be performed. This poses some caveats as tissues must be processed immediately after resection to avoid excessive damage inducing citrullination. Flow cytometry staining of citrullinated vimentin expression in matched fresh normal and cancer cells would also be supportive and may provide cleaner results.

6.5.3 Confirmation of HIPPO pathway and EMT involvement in citrullination

Preliminary experiments in Chapter 3 indicate some involvement of the HIPPO pathway and EMT in citrullination. Unfortunately, due to time constraints, repeated experiments using the TGF-β and MST1/2 inhibitor were not performed. These should be repeated to evaluate whether either of these pathways do contribute to citrullinated protein expression. The next stage would be to check the effect of these inhibitors on autophagy and proliferation in low and high density cells. Identifying the signalling pathways and mechanism involved in citrullination would provide target cells for use in future experiments to assess the specificity and activation of citrullination protein T cells.

6.5.4 Testing in outbred mouse strain

HLA transgenic and C57Bl/6 mice were used in these experiments, both of which are examples of inbred mouse strains. For research, these strains provide confidence in results by minimising genetic and phenotypic variability, allowing for better

reproducibility. However, as humans are not genetically identical, an outbred mouse strain could be a more preferable representative. A study comparing CD8 T cell responses following infection in inbred and outbred mice found outbred populations to vary size of their memory CD8 T cell pool, and were not always protected against re-infection compared to the inbred mice [393]. This suggests immunological responses are more complex than shown in inbred mouse studies and the responses seen in outbred mice better mimic those found in humans. In addition to evaluating responses to MODI1 immunisations, outbred mice implanted with B16F1 tumours could also be analysed for their TCR repertoire and screened for potential antigen-specific TCRs.

7 References

1. Brentville, V.A., et al., *Citrullinated Vimentin Presented on MHC-II in Tumor Cells Is a Target for CD4+ T-Cell-Mediated Antitumor Immunity.* Cancer Res, 2016. **76**(3): p. 548-60.

2. Cook, K., et al., *Citrullinated alpha-enolase is an effective target for anti-cancer immunity.* Oncoimmunology, 2018. **7**(2): p. e1390642.

3. Hanahan, D. and R.A. Weinberg, *The hallmarks of cancer.* Cell, 2000. **100**(1): p. 57-70.

4. Hanahan, D. and R.A. Weinberg, *Hallmarks of cancer: the next generation.* Cell, 2011. **144**(5): p. 646-74.

5. Kaplan, D.H., et al., *Demonstration of an interferon gamma-dependent tumor surveillance system in immunocompetent mice.* Proc Natl Acad Sci U S A, 1998. **95**(13): p. 7556-61.

6. Street, S.E., E. Cretney, and M.J. Smyth, *Perforin and interferon-gamma activities independently control tumor initiation, growth, and metastasis.* Blood, 2001. **97**(1): p. 192-7.

7. Dighe, A.S., et al., *Enhanced in vivo growth and resistance to rejection of tumor cells expressing dominant negative IFN gamma receptors.* Immunity, 1994. **1**(6): p. 447-56.

8. Stanton, S.E. and M.L. Disis, *Clinical significance of tumor-infiltrating lymphocytes in breast cancer.* J Immunother Cancer, 2016. **4**: p. 59.

9. Fu, Q., et al., *Prognostic value of tumor-infiltrating lymphocytes in melanoma: a systematic review and meta-analysis.* Oncoimmunology, 2019. **8**(7): p. 1593806.

10. Idos, G.E., et al., *The Prognostic Implications of Tumor Infiltrating Lymphocytes in Colorectal Cancer: A Systematic Review and Meta-Analysis.* Sci Rep, 2020. **10**(1): p. 3360.

11. Dunn, G.P., L.J. Old, and R.D. Schreiber, *The three Es of cancer immunoediting.* Annu Rev Immunol, 2004. **22**: p. 329-60.

12. Robertson, M.J., *Role of chemokines in the biology of natural killer cells.* J Leukoc Biol, 2002. **71**(2): p. 173-83.

13. Roda, J.M., et al., *Natural killer cells produce T cell-recruiting chemokines in response to antibody-coated tumor cells.* Cancer Res, 2006. **66**(1): p. 517-26.

14. Voskoboinik, I., M.J. Smyth, and J.A. Trapani, *Perforin-mediated target-cell death and immune homeostasis.* Nat Rev Immunol, 2006. **6**(12): p. 940-52.

15. Smyth, M.J., et al., *Tumor necrosis factor-related apoptosis-inducing ligand (TRAIL) contributes to interferon gamma-dependent natural killer cell protection from tumor metastasis.* J Exp Med, 2001. **193**(6): p. 661-70.

16. Motz, G.T. and G. Coukos, *Deciphering and reversing tumor immune suppression.* Immunity, 2013. **39**(1): p. 61-73.

17. Garrido, F., T. Cabrera, and N. Aptsiauri, *"Hard" and "soft" lesions underlying the HLA class I alterations in cancer cells: implications for immunotherapy.* Int J Cancer, 2010. **127**(2): p. 249-56.

18. Murphy, K., et al., *Janeway's Immunobiology*. 9th ed. 2017, New York: Garland Science/ Taylor & Francis Group.

19. van den Broek, T., J.A.M. Borghans, and F. van Wijk, *The full spectrum of human naive T cells.* Nat Rev Immunol, 2018. **18**(6): p. 363-373.

20. Bromley, S.K., et al., *The immunological synapse and CD28-CD80 interactions.* Nat Immunol, 2001. **2**(12): p. 1159-66.

21. Hall, B.M., *T Cells: Soldiers and Spies--The Surveillance and Control of Effector T Cells by Regulatory T Cells.* Clin J Am Soc Nephrol, 2015. **10**(11): p. 2050-64.

22. Howland, K.C., et al., *The roles of CD28 and CD40 ligand in T cell activation and tolerance.* J Immunol, 2000. **164**(9): p. 4465-70.

23. Benichou, G., et al., *Role of Memory T Cells in Allograft Rejection and Tolerance.* Front Immunol, 2017. **8**: p. 170.

24. Buhelt, S., et al., *Relationship between Multiple Sclerosis-Associated IL2RA Risk Allele Variants and Circulating T Cell Phenotypes in Healthy Genotype-Selected Controls.* Cells, 2019. **8**(6).

25. Valujskikh, A. and X.C. Li, *Frontiers in nephrology: T cell memory as a barrier to transplant tolerance.* J Am Soc Nephrol, 2007. **18**(8): p. 2252-61.

26. Wieczorek, M., et al., *Major Histocompatibility Complex (MHC) Class I and MHC Class II Proteins: Conformational Plasticity in Antigen Presentation.* Front Immunol, 2017. **8**: p. 292.

27. van Hateren, A., A. Bailey, and T. Elliott, *Recent advances in Major Histocompatibility Complex (MHC) class I antigen presentation: Plastic MHC molecules and TAPBPR-mediated quality control.* F1000Res, 2017. **6**: p. 158.

28. Blum, J.S., P.A. Wearsch, and P. Cresswell, *Pathways of antigen processing.* Annu Rev Immunol, 2013. **31**: p. 443-73.

29. Koopmann, J.O., et al., *Translocation of long peptides by transporters associated with antigen processing (TAP).* Eur J Immunol, 1996. **26**(8): p. 1720-8.

30. Biochemist, M. *Immunology: Antigen processing and presentation MCQ*. 2019 June 02, 2021]; Available from: https://www.medicalbiochemist.com/2019/01/antigen-processing.html.

31. Medd, P.G. and B.M. Chain, *Protein degradation in MHC class II antigen presentation: opportunities for immunomodulation.* Semin Cell Dev Biol, 2000. **11**(3): p. 203-10.

32. van Ham, S.M., et al., *HLA-DO is a negative modulator of HLA-DM-mediated MHC class II peptide loading.* Curr Biol, 1997. **7**(12): p. 950-7.

33. Legut, M., et al., *CRISPR-mediated TCR replacement generates superior anticancer transgenic T cells.* Blood, 2018. **131**(3): p. 311-322.

34. Therapeutics, G.D., *Unlocking the power of Vdelta1 and gamma-delta T lymphocytes to transform cancer celll therapy.* 2021.

35. Nambiar, M.P., et al., *Reconstitution of deficient T cell receptor zeta chain restores T cell signaling and augments T cell receptor/CD3-induced interleukin-2 production in patients with systemic lupus erythematosus.* Arthritis Rheum, 2003. **48**(7): p. 1948-55.

36. Birnbaum, M.E., et al., *Molecular architecture of the alphabeta T cell receptor-CD3 complex.* Proc Natl Acad Sci U S A, 2014. **111**(49): p. 17576-81.

37. Love, P.E. and S.M. Hayes, *ITAM-mediated signaling by the T-cell antigen receptor.* Cold Spring Harb Perspect Biol, 2010. **2**(6): p. a002485.

38. Laydon, D.J., C.R. Bangham, and B. Asquith, *Estimating T-cell repertoire diversity: limitations of classical estimators and a new approach.* Philos Trans R Soc Lond B Biol Sci, 2015. **370**(1675).

39. Hodges, E., et al., *Diagnostic role of tests for T cell receptor (TCR) genes.* J Clin Pathol, 2003. **56**(1): p. 1-11.

40. Hale, J.S., et al., *Cutting Edge: Rag deletion in peripheral T cells blocks TCR revision.* J Immunol, 2010. **184**(11): p. 5964-8.

41. Morello, G., et al., *T cells expressing receptor recombination/revision machinery are detected in the tumor microenvironment and expanded in genomically over-unstable models.* Cancer Immunol Res, 2021.

42. Venturi, V., et al., *Sharing of T cell receptors in antigen-specific responses is driven by convergent recombination.* Proc Natl Acad Sci U S A, 2006. **103**(49): p. 18691-6.

43. Bio-Rad. *An overview of T cell receptors*. n.d May 5, 2021]; Available from: https://www.bio-rad-antibodies.com/t-cell-receptor-minireview.html.

44. Janeway, C.A., et al., *Immunobiology*, in *The immune system in health and disease*, P. Austin, et al., Editors. 2001, Garland Publishing: New York.

45. Li, X. and H. von Boehmer, *Notch Signaling in T-Cell Development and T-ALL.* ISRN Hematol, 2011. **2011**: p. 921706.

46. Tan, C., et al., *Ten-color flow cytometry reveals distinct patterns of expression of CD124 and CD126 by developing thymocytes.* BMC Immunol, 2011. **12**: p. 36.

47. Taghon, T., et al., *Notch signaling is required for proliferation but not for differentiation at a well-defined beta-selection checkpoint during human T-cell development.* Blood, 2009. **113**(14): p. 3254-63.

48. Klein, L., et al., *Positive and negative selection of the T cell repertoire: what thymocytes see (and don't see).* Nat Rev Immunol, 2014. **14**(6): p. 377-91.

49. Takahama, Y., et al., *Generation of diversity in thymic epithelial cells.* Nat Rev Immunol, 2017. **17**(5): p. 295-305.

50. Ruiz, A.L., et al., *NK1.1+ CD8+ T cells escape TGF-beta control and contribute to early microbial pathogen response.* Nat Commun, 2014. **5**: p. 5150.

51. Ohigashi, I., et al., *Trans-omics Impact of Thymoproteasome in Cortical Thymic Epithelial Cells.* Cell Rep, 2019. **29**(9): p. 2901-2916 e6.

52. Uddin, M.N., et al., *Autophagic activity in thymus and liver during aging.* Age (Dordr), 2012. **34**(1): p. 75-85.

53. Kondo, K., I. Ohigashi, and Y. Takahama, *Thymus machinery for T-cell selection.* Int Immunol, 2019. **31**(3): p. 119-125.

54. Moran, A.E. and K.A. Hogquist, *T-cell receptor affinity in thymic development.* Immunology, 2012. **135**(4): p. 261-7.

55. Kuznetsova, M., et al., *Cytotoxic Activity and Memory T Cell Subset Distribution of in vitro-Stimulated CD8(+) T Cells Specific for HER2/neu Epitopes.* Front Immunol, 2019. **10**: p. 1017.

56. Yap, M., et al., *Expansion of highly differentiated cytotoxic terminally differentiated effector memory CD8+ T cells in a subset of clinically stable*

kidney transplant recipients: a potential marker for late graft dysfunction. J Am Soc Nephrol, 2014. **25**(8): p. 1856-68.

57. Verma, K., et al., *Human CD8+ CD57- TEMRA cells: Too young to be called "old".* PLoS One, 2017. **12**(5): p. e0177405.

58. Topham, D.J. and E.C. Reilly, *Tissue-Resident Memory CD8(+) T Cells: From Phenotype to Function.* Front Immunol, 2018. **9**: p. 515.

59. Artyomov, M.N., et al., *CD4 and CD8 binding to MHC molecules primarily acts to enhance Lck delivery.* Proc Natl Acad Sci U S A, 2010. **107**(39): p. 16916-21.

60. Williams, C.M., et al., *Normalized Synergy Predicts That CD8 Co-Receptor Contribution to T Cell Receptor (TCR) and pMHC Binding Decreases As TCR Affinity Increases in Human Viral-Specific T Cells.* Front Immunol, 2017. **8**: p. 894.

61. Cole, D.K., et al., *The molecular determinants of CD8 co-receptor function.* Immunology, 2012. **137**(2): p. 139-48.

62. Holler, P.D. and D.M. Kranz, *Quantitative analysis of the contribution of TCR/pepMHC affinity and CD8 to T cell activation.* Immunity, 2003. **18**(2): p. 255-64.

63. Davis, S.J., et al., *The nature of molecular recognition by T cells.* Nat Immunol, 2003. **4**(3): p. 217-24.

64. Van Laethem, F., et al., *Deletion of CD4 and CD8 coreceptors permits generation of alphabetaT cells that recognize antigens independently of the MHC.* Immunity, 2007. **27**(5): p. 735-50.

65. Casas, J., et al., *Ligand-engaged TCR is triggered by Lck not associated with CD8 coreceptor.* Nat Commun, 2014. **5**: p. 5624.

66. Horkova, V., et al., *Dynamics of the Coreceptor-LCK Interactions during T Cell Development Shape the Self-Reactivity of Peripheral CD4 and CD8 T Cells.* Cell Rep, 2020. **30**(5): p. 1504-1514 e7.

67. Golubovskaya, V. and L. Wu, *Different Subsets of T Cells, Memory, Effector Functions, and CAR-T Immunotherapy.* Cancers (Basel), 2016. **8**(3).

68. Dobrzanski, M.J., *Expanding roles for CD4 T cells and their subpopulations in tumor immunity and therapy.* Front Oncol, 2013. **3**: p. 63.

69. DuPage, M. and J.A. Bluestone, *Harnessing the plasticity of CD4(+) T cells to treat immune-mediated disease.* Nat Rev Immunol, 2016. **16**(3): p. 149-63.

70. Luckheeram, R.V., et al., *CD4(+)T cells: differentiation and functions.* Clin Dev Immunol, 2012. **2012**: p. 925135.

71. Haabeth, O.A., et al., *Inflammation driven by tumour-specific Th1 cells protects against B-cell cancer.* Nat Commun, 2011. **2**: p. 240.

72. Sredni, B., et al., *Predominance of TH1 response in tumor-bearing mice and cancer patients treated with AS101.* J Natl Cancer Inst, 1996. **88**(18): p. 1276-84.

73. Huang, H., et al., *CD4+ Th1 cells promote CD8+ Tc1 cell survival, memory response, tumor localization and therapy by targeted delivery of interleukin 2 via acquired pMHC I complexes.* Immunology, 2007. **120**(2): p. 148-59.

74. Bogen, B., et al., *CD4(+) T cells indirectly kill tumor cells via induction of cytotoxic macrophages in mouse models.* Cancer Immunol Immunother, 2019. **68**(11): p. 1865-1873.

75. Chen, X., et al., *Artesunate promotes Th1 differentiation from CD4+ T cells to enhance cell apoptosis in ovarian cancer via miR-142.* Braz J Med Biol Res, 2019. **52**(5): p. e7992.

76. Ekkens, M.J., et al., *Th1 and Th2 cells help CD8 T-cell responses.* Infect Immun, 2007. **75**(5): p. 2291-6.

77. Brentville, V.A., et al., *T cell repertoire to citrullinated self-peptides in healthy humans is not confined to the HLA-DR SE alleles; Targeting of citrullinated self-peptides presented by HLA-DP4 for tumour therapy.* OncoImmunology, 2019: p. 1-14.

78. Mucida, D., et al., *Transcriptional reprogramming of mature CD4(+) helper T cells generates distinct MHC class II-restricted cytotoxic T lymphocytes.* Nat Immunol, 2013. **14**(3): p. 281-9.

79. Tian, Y., et al., *Unique phenotypes and clonal expansions of human CD4 effector memory T cells re-expressing CD45RA.* Nat Commun, 2017. **8**(1): p. 1473.

80. Quezada, S.A., et al., *Tumor-reactive CD4(+) T cells develop cytotoxic activity and eradicate large established melanoma after transfer into lymphopenic hosts.* J Exp Med, 2010. **207**(3): p. 637-50.

81. Konomi, Y., et al., *Cytotoxic activity of CD4+ T cells against autologous tumor cells.* Jpn J Cancer Res, 1995. **86**(9): p. 854-60.

82. Oh, D.Y., et al., *Intratumoral CD4(+) T Cells Mediate Anti-tumor Cytotoxicity in Human Bladder Cancer.* Cell, 2020. **181**(7): p. 1612-1625 e13.

83. Merlo, A., et al., *Virus-specific cytotoxic CD4+ T cells for the treatment of EBV-related tumors.* J Immunol, 2010. **184**(10): p. 5895-902.

84. Bozzacco, L., et al., *Mass spectrometry analysis and quantitation of peptides presented on the MHC II molecules of mouse spleen dendritic cells.* J Proteome Res, 2011. **10**(11): p. 5016-30.

85. Sakihama, T., A. Smolyar, and E.L. Reinherz, *Oligomerization of CD4 is required for stable binding to class II major histocompatibility complex proteins but not for interaction with human immunodeficiency virus gp120.* Proc Natl Acad Sci U S A, 1995. **92**(14): p. 6444-8.

86. Foti, M., et al., *p56Lck anchors CD4 to distinct microdomains on microvilli.* Proc Natl Acad Sci U S A, 2002. **99**(4): p. 2008-13.

87. Mellman, I., G. Coukos, and G. Dranoff, *Cancer immunotherapy comes of age.* Nature, 2011. **480**(7378): p. 480-9.

88. Vandenborre, K., et al., *Interaction of CTLA-4 (CD152) with CD80 or CD86 inhibits human T-cell activation.* Immunology, 1999. **98**(3): p. 413-21.

89. Savoia, P., C. Astrua, and P. Fava, *Ipilimumab (Anti-Ctla-4 Mab) in the treatment of metastatic melanoma: Effectiveness and toxicity management.* Hum Vaccin Immunother, 2016. **12**(5): p. 1092-101.

90. Formenti, S.C., et al., *Radiotherapy induces responses of lung cancer to CTLA-4 blockade.* Nat Med, 2018. **24**(12): p. 1845-1851.

91. Rudqvist, N.P., et al., *Radiotherapy and CTLA-4 Blockade Shape the TCR Repertoire of Tumor-Infiltrating T Cells.* Cancer Immunol Res, 2018. **6**(2): p. 139-150.

92. Parry, R.V., et al., *CTLA-4 and PD-1 receptors inhibit T-cell activation by distinct mechanisms.* Mol Cell Biol, 2005. **25**(21): p. 9543-53.

93. Day, C.L., et al., *PD-1 expression on HIV-specific T cells is associated with T-cell exhaustion and disease progression.* Nature, 2006. **443**(7109): p. 350-4.

94. Ahmadzadeh, M., et al., *Tumor antigen-specific CD8 T cells infiltrating the tumor express high levels of PD-1 and are functionally impaired.* Blood, 2009. **114**(8): p. 1537-44.

95. Kumagai, S., et al., *The PD-1 expression balance between effector and regulatory T cells predicts the clinical efficacy of PD-1 blockade therapies.* Nat Immunol, 2020. **21**(11): p. 1346-1358.

96. Rotte, A., *Combination of CTLA-4 and PD-1 blockers for treatment of cancer.* J Exp Clin Cancer Res, 2019. **38**(1): p. 255.

97. Gu, L., et al., *The safety and tolerability of combined immune checkpoint inhibitors (anti-PD-1/PD-L1 plus anti-CTLA-4): a systematic review and meta-analysis.* BMC Cancer, 2019. **19**(1): p. 559.

98. Mougel, A., M. Terme, and C. Tanchot, *Therapeutic Cancer Vaccine and Combinations With Antiangiogenic Therapies and Immune Checkpoint Blockade.* Front Immunol, 2019. **10**: p. 467.

99. Santos, P.M., et al., *Impact of checkpoint blockade on cancer vaccine-activated CD8+ T cell responses.* J Exp Med, 2020. **217**(7).

100. Lopes, A., et al., *Combination of immune checkpoint blockade with DNA cancer vaccine induces potent antitumor immunity against P815 mastocytoma.* Sci Rep, 2018. **8**(1): p. 15732.

101. Rosenberg, S.A., et al., *Treatment of patients with metastatic melanoma with autologous tumor-infiltrating lymphocytes and interleukin 2.* J Natl Cancer Inst, 1994. **86**(15): p. 1159-66.

102. Nguyen, L.T., et al., *Phase II clinical trial of adoptive cell therapy for patients with metastatic melanoma with autologous tumor-infiltrating lymphocytes and low-dose interleukin-2.* Cancer Immunol Immunother, 2019. **68**(5): p. 773-785.

103. Dudley, M.E., et al., *Adoptive cell transfer therapy following non-myeloablative but lymphodepleting chemotherapy for the treatment of patients with refractory metastatic melanoma.* J Clin Oncol, 2005. **23**(10): p. 2346-57.

104. Besser, M.J., et al., *Minimally cultured or selected autologous tumor-infiltrating lymphocytes after a lympho-depleting chemotherapy regimen in metastatic melanoma patients.* J Immunother, 2009. **32**(4): p. 415-23.

105. Dudley, M.E., et al., *Generation of tumor-infiltrating lymphocyte cultures for use in adoptive transfer therapy for melanoma patients.* J Immunother, 2003. **26**(4): p. 332-42.

106. Dudley, M.E., et al., *Cancer regression and autoimmunity in patients after clonal repopulation with antitumor lymphocytes.* Science, 2002. **298**(5594): p. 850-4.

107. Tran, K.Q., et al., *Minimally cultured tumor-infiltrating lymphocytes display optimal characteristics for adoptive cell therapy.* J Immunother, 2008. **31**(8): p. 742-51.

108. Donia, M., et al., *Characterization and comparison of 'standard' and 'young' tumour-infiltrating lymphocytes for adoptive cell therapy at a Danish translational research institution.* Scand J Immunol, 2012. **75**(2): p. 157-67.

109. Besser, M.J., et al., *Clinical responses in a phase II study using adoptive transfer of short-term cultured tumor infiltration lymphocytes in metastatic melanoma patients.* Clin Cancer Res, 2010. **16**(9): p. 2646-55.

110. van den Berg, J.H., et al., *Tumor infiltrating lymphocytes (TIL) therapy in metastatic melanoma: boosting of neoantigen-specific T cell reactivity and long-term follow-up.* J Immunother Cancer, 2020. **8**(2).

111. Krishna, S., et al., *Stem-like CD8 T cells mediate response of adoptive cell immunotherapy against human cancer.* Science, 2020. **370**(6522): p. 1328-1334.

112. Thistlethwaite, F.C., et al., *The clinical efficacy of first-generation carcinoembryonic antigen (CEACAM5)-specific CAR T cells is limited by poor persistence and transient pre-conditioning-dependent respiratory toxicity.* Cancer Immunol Immunother, 2017. **66**(11): p. 1425-1436.

113. Guedan, S., et al., *Enhancing CAR T cell persistence through ICOS and 4-1BB costimulation.* JCI Insight, 2018. **3**(1).

114. Enblad, G., et al., *A Phase I/IIa Trial Using CD19-Targeted Third-Generation CAR T Cells for Lymphoma and Leukemia.* Clin Cancer Res, 2018. **24**(24): p. 6185-6194.

115. Zhang, C., et al., *Engineering CAR-T cells.* Biomark Res, 2017. **5**: p. 22.

116. Chmielewski, M., et al., *IL-12 release by engineered T cells expressing chimeric antigen receptors can effectively Muster an antigen-independent macrophage response on tumor cells that have shut down tumor antigen expression.* Cancer Res, 2011. **71**(17): p. 5697-706.

117. Mei, Z., et al., *MUC1 as a target for CAR-T therapy in head and neck squamous cell carinoma.* Cancer Med, 2020. **9**(2): p. 640-652.

118. Morgan, R.A., et al., *Cancer regression and neurological toxicity following anti-MAGE-A3 TCR gene therapy.* J Immunother, 2013. **36**(2): p. 133-51.

119. Linette, G.P., et al., *Cardiovascular toxicity and titin cross-reactivity of affinity-enhanced T cells in myeloma and melanoma.* Blood, 2013. **122**(6): p. 863-71.

120. Robbins, P.F., et al., *A pilot trial using lymphocytes genetically engineered with an NY-ESO-1-reactive T-cell receptor: long-term follow-up and correlates with response.* Clin Cancer Res, 2015. **21**(5): p. 1019-27.

121. Sanderson, J.P., et al., *Preclinical evaluation of an affinity-enhanced MAGE-A4-specific T-cell receptor for adoptive T-cell therapy.* Oncoimmunology, 2020. **9**(1): p. 1682381.

122. Hong, D.S., et al., *Phase I dose escalation and expansion trial to assess the safety and efficacy of ADP-A2M4 SPEAR T cells in advanced solid tumors.* Journal of Clinical Oncology, 2020. **38**(15_suppl): p. 102-102.

123. Rath, J.A. and C. Arber, *Engineering Strategies to Enhance TCR-Based Adoptive T Cell Therapy.* Cells, 2020. **9**(6).

124. Lu, Y.C., et al., *Treatment of Patients With Metastatic Cancer Using a Major Histocompatibility Complex Class II-Restricted T-Cell Receptor Targeting the Cancer Germline Antigen MAGE-A3.* J Clin Oncol, 2017. **35**(29): p. 3322-3329.

125. Xie, Y., et al., *Naive tumor-specific CD4(+) T cells differentiated in vivo eradicate established melanoma.* J Exp Med, 2010. **207**(3): p. 651-67.

126. Lin, Y., et al., *HLA-DPB1*05: 01-restricted WT1332-specific TCR-transduced CD4+ T lymphocytes display a helper activity for WT1-specific CTL induction and a cytotoxicity against leukemia cells.* J Immunother, 2013. **36**(3): p. 159-70.

127. Veatch, J.R., et al., *Tumor-infiltrating BRAFV600E-specific CD4+ T cells correlated with complete clinical response in melanoma.* J Clin Invest, 2018. **128**(4): p. 1563-1568.

128. Schober, S.J., et al., *MHC Class I-Restricted TCR-Transgenic CD4(+) T Cells Against STEAP1 Mediate Local Tumor Control of Ewing Sarcoma In Vivo.* Cells, 2020. **9**(7).

129. Soto, C.M., et al., *MHC-class I-restricted CD4 T cells: a nanomolar affinity TCR has improved anti-tumor efficacy in vivo compared to the micromolar wild-type TCR.* Cancer Immunol Immunother, 2013. **62**(2): p. 359-69.

130. Oh, J., et al., *Phase II study of Vigil(R) DNA engineered immunotherapy as maintenance in advanced stage ovarian cancer.* Gynecol Oncol, 2016. **143**(3): p. 504-510.

131. Vermorken, J.B., et al., *Active specific immunotherapy for stage II and stage III human colon cancer: a randomised trial.* Lancet, 1999. **353**(9150): p. 345-50.

132. Godoy-Calderon, M.J., et al., *Autologous tumor cells/bacillus Calmette-Guerin/formalin-based novel breast cancer vaccine induces an immune antitumor response.* Oncotarget, 2018. **9**(29): p. 20222-20238.

133. Derre, L., et al., *Intravesical Bacillus Calmette Guerin Combined with a Cancer Vaccine Increases Local T-Cell Responses in Non-muscle-Invasive Bladder Cancer Patients.* Clin Cancer Res, 2017. **23**(3): p. 717-725.

134. Alexandrov, L.B., et al., *Signatures of mutational processes in human cancer.* Nature, 2013. **500**(7463): p. 415-21.

135. Macri, C., et al., *Dendritic cell subsets.* Semin Cell Dev Biol, 2018. **84**: p. 11-21.

136. Nestle, F.O., et al., *Vaccination of melanoma patients with peptide- or tumor lysate-pulsed dendritic cells.* Nat Med, 1998. **4**(3): p. 328-32.

137. Van Tendeloo, V.F., et al., *Induction of complete and molecular remissions in acute myeloid leukemia by Wilms' tumor 1 antigen-targeted dendritic cell vaccination.* Proc Natl Acad Sci U S A, 2010. **107**(31): p. 13824-9.

138. Rosenblatt, J., et al., *Vaccination with dendritic cell/tumor fusions following autologous stem cell transplant induces immunologic and clinical responses in multiple myeloma patients.* Clin Cancer Res, 2013. **19**(13): p. 3640-8.

139. Butterfield, L.H., et al., *Determinant spreading associated with clinical response in dendritic cell-based immunotherapy for malignant melanoma.* Clin Cancer Res, 2003. **9**(3): p. 998-1008.

140. Charles, J., et al., *An innovative plasmacytoid dendritic cell line-based cancer vaccine primes and expands antitumor T-cells in melanoma patients in a first-in-human trial.* Oncoimmunology, 2020. **9**(1): p. 1738812.

141. van de Loosdrecht, A.A., et al., *A novel allogeneic off-the-shelf dendritic cell vaccine for post-remission treatment of elderly patients with acute myeloid leukemia.* Cancer Immunol Immunother, 2018. **67**(10): p. 1505-1518.

142. Leaf, R.K., et al., *DCOne as an Allogeneic Cell-based Vaccine for Multiple Myeloma.* J Immunother, 2017. **40**(9): p. 315-322.

143. Westdorp, H., et al., *Blood-derived dendritic cell vaccinations induce immune responses that correlate with clinical outcome in patients with chemo-naive castration-resistant prostate cancer.* J Immunother Cancer, 2019. **7**(1): p. 302.

144. Hodge, J.W., et al., *Admixture of a recombinant vaccinia virus containing the gene for the costimulatory molecule B7 and a recombinant vaccinia virus containing a tumor-associated antigen gene results in enhanced specific T-cell responses and antitumor immunity.* Cancer Res, 1995. **55**(16): p. 3598-603.

145. Eisenberger, A., B.M. Elliott, and H.L. Kaufman, *Viral vaccines for cancer immunotherapy.* Hematol Oncol Clin North Am, 2006. **20**(3): p. 661-87.

146. Hemminki, O., J.M. Dos Santos, and A. Hemminki, *Oncolytic viruses for cancer immunotherapy.* J Hematol Oncol, 2020. **13**(1): p. 84.

147. Andtbacka, R.H., et al., *Patterns of Clinical Response with Talimogene Laherparepvec (T-VEC) in Patients with Melanoma Treated in the OPTiM Phase III Clinical Trial.* Ann Surg Oncol, 2016. **23**(13): p. 4169-4177.

148. Kaufman, H.L., et al., *Local and distant immunity induced by intralesional vaccination with an oncolytic herpes virus encoding GM-CSF in patients with stage IIIc and IV melanoma.* Ann Surg Oncol, 2010. **17**(3): p. 718-30.

149. Gupta, S., et al., *A multi-trimeric fusion of CD40L and gp100 tumor antigen activates dendritic cells and enhances survival in a B16-F10 melanoma DNA vaccine model.* Vaccine, 2015. **33**(38): p. 4798-806.

150. Pan, Y.R., et al., *Comprehensive Evaluation of Immune-Checkpoint DNA Cancer Vaccines in a Rat Cholangiocarcinoma Model.* Vaccines (Basel), 2020. **8**(4).

151. Jorritsma, S.H.T., et al., *Delivery methods to increase cellular uptake and immunogenicity of DNA vaccines.* Vaccine, 2016. **34**(46): p. 5488-5494.

152. Xue, W., et al., *SCIB1, a huIgG1 antibody DNA vaccination, combined with PD-1 blockade induced efficient therapy of poorly immunogenic tumors.* Oncotarget, 2016. **7**(50): p. 83088-83100.

153. Xue, W., et al., *SCIB2, an antibody DNA vaccine encoding NY-ESO-1 epitopes, induces potent antitumor immunity which is further enhanced by checkpoint blockade.* Oncoimmunology, 2016. **5**(6): p. e1169353.

154. Lopes, A., G. Vandermeulen, and V. Preat, *Cancer DNA vaccines: current preclinical and clinical developments and future perspectives.* J Exp Clin Cancer Res, 2019. **38**(1): p. 146.

155. McNeel, D.G., et al., *Phase II Trial of a DNA Vaccine Encoding Prostatic Acid Phosphatase (pTVG-HP [MVI-816]) in Patients With Progressive, Nonmetastatic, Castration-Sensitive Prostate Cancer.* J Clin Oncol, 2019. **37**(36): p. 3507-3517.

156. Wargowski, E., et al., *Prime-boost vaccination targeting prostatic acid phosphatase (PAP) in patients with metastatic castration-resistant prostate cancer (mCRPC) using Sipuleucel-T and a DNA vaccine.* J Immunother Cancer, 2018. **6**(1): p. 21.

157. Patel, P.M., et al., *Targeting gp100 and TRP-2 with a DNA vaccine: Incorporating T cell epitopes with a human IgG1 antibody induces potent T cell responses that are associated with favourable clinical outcome in a phase I/II trial.* Oncoimmunology, 2018. **7**(6): p. e1433516.

158. Fredriksen, A.B. *Update from Vaccibody's clinical trial with the personalised cancer neoantigen vaccine, VB10.NEO*. 2020 July 8, 2021]; Available from: https://www.vaccibody.com/wp-content/uploads/2020/03/200304-World-Immunotherapy-Congress-San-Diego-Agnete_cf.pdf.

159. Cafri, G., et al., *mRNA vaccine-induced neoantigen-specific T cell immunity in patients with gastrointestinal cancer.* J Clin Invest, 2020. **130**(11): p. 5976-5988.

160. Sahin, U., et al., *Personalized RNA mutanome vaccines mobilize poly-specific therapeutic immunity against cancer.* Nature, 2017. **547**(7662): p. 222-226.

161. Disis, M.L., et al., *Generation of T-cell immunity to the HER-2/neu protein after active immunization with HER-2/neu peptide-based vaccines.* J Clin Oncol, 2002. **20**(11): p. 2624-32.

162. Disis, M.L., et al., *Humoral epitope-spreading following immunization with a HER-2/neu peptide based vaccine in cancer patients.* J Clin Immunol, 2004. **24**(5): p. 571-8.

163. Gritzapis, A.D., et al., *Vaccination with human HER-2/neu (435-443) CTL peptide induces effective antitumor immunity against HER-2/neu-expressing tumor cells in vivo.* Cancer Res, 2006. **66**(10): p. 5452-60.

164. Gritzapis, A.D., et al., *HER-2/neu (657-665) represents an immunogenic epitope of HER-2/neu oncoprotein with potent antitumor properties.* Vaccine, 2009. **28**(1): p. 162-70.

165. Lekka, E., et al., *Identification and characterization of a HER-2/neu epitope as a potential target for cancer immunotherapy.* Cancer Immunol Immunother, 2010. **59**(5): p. 715-27.

166. Khong, H. and W.W. Overwijk, *Adjuvants for peptide-based cancer vaccines.* J Immunother Cancer, 2016. **4**: p. 56.

167. Zom, G.G., et al., *Two in one: improving synthetic long peptide vaccines by combining antigen and adjuvant in one molecule.* Oncoimmunology, 2014. **3**(7): p. e947892.

168. Guo, C., J.R. Subjeck, and X.Y. Wang, *Creation of Recombinant Chaperone Vaccine Using Large Heat Shock Protein for Antigen-Targeted Cancer Immunotherapy.* Methods Mol Biol, 2018. **1709**: p. 345-357.

169. Tornesello, A.L., et al., *Nanoparticles to Improve the Efficacy of Peptide-Based Cancer Vaccines.* Cancers (Basel), 2020. **12**(4).

170. Hodi, F.S., et al., *Improved survival with ipilimumab in patients with metastatic melanoma.* N Engl J Med, 2010. **363**(8): p. 711-23.

171. Ulloa-Montoya, F., et al., *Predictive gene signature in MAGE-A3 antigen-specific cancer immunotherapy.* J Clin Oncol, 2013. **31**(19): p. 2388-95.

172. Kitagawa, K., et al., *Development of oral cancer vaccine using recombinant Bifidobacterium displaying Wilms' tumor 1 protein.* Cancer Immunol Immunother, 2017. **66**(6): p. 787-798.

173. Shirakawa, T. and K. Kitagawa, *Antitumor effect of oral cancer vaccine with Bifidobacterium delivering WT1 protein to gut immune system is superior to WT1 peptide vaccine.* Hum Vaccin Immunother, 2018. **14**(1): p. 159-162.

174. Engelhard, V.H., et al., *MHC-restricted phosphopeptide antigens: preclinical validation and first-in-humans clinical trial in participants with high-risk melanoma.* J Immunother Cancer, 2020. **8**(1).

175. Cytoskeleton Inc. *Citrullination: Taking the Charge out of Arg*. 2018 [cited 2018 30 Nov]; Available from: https://www.cytoskeleton.com/blog/citrullination-news-detailed/.

176. Bicker, K.L. and P.R. Thompson, *The protein arginine deiminases: Structure, function, inhibition, and disease.* Biopolymers, 2013. **99**(2): p. 155-63.

177. Gyorgy, B., et al., *Citrullination: a posttranslational modification in health and disease.* Int J Biochem Cell Biol, 2006. **38**(10): p. 1662-77.

178. Taki, H., et al., *Purification of enzymatically inactive peptidylarginine deiminase type 6 from mouse ovary that reveals hexameric structure different from other dimeric isoforms.* Advances in Bioscience and Biotechnology, 2011. **Vol.02No.04**: p. 7.

179. Witalison, E.E., P.R. Thompson, and L.J. Hofseth, *Protein Arginine Deiminases and Associated Citrullination: Physiological Functions and Diseases Associated with Dysregulation.* Curr Drug Targets, 2015. **16**(7): p. 700-10.

180. Chang, X. and J. Han, *Expression of peptidylarginine deiminase type 4 (PAD4) in various tumors.* Mol Carcinog, 2006. **45**(3): p. 183-96.

181. Horibata, S., et al., *Role of peptidylarginine deiminase 2 (PAD2) in mammary carcinoma cell migration.* BMC Cancer, 2017. **17**(1): p. 378.

182. Guo, W., et al., *Investigating the expression, effect and tumorigenic pathway of PADI2 in tumors.* Onco Targets Ther, 2017. **10**: p. 1475-1485.

183. Chung, J.H., et al., *Myofilament Calcium Sensitivity: Role in Regulation of In vivo Cardiac Contraction and Relaxation.* Front Physiol, 2016. **7**: p. 562.

184. Klec, C., et al., *Calcium Signaling in ss-cell Physiology and Pathology: A Revisit.* Int J Mol Sci, 2019. **20**(24).

185. Eno, C.O., et al., *Distinct roles of mitochondria- and ER-localized Bcl-xL in apoptosis resistance and Ca2+ homeostasis.* Mol Biol Cell, 2012. **23**(13): p. 2605-18.

186. Pinton, P., et al., *Reduced loading of intracellular Ca(2+) stores and downregulation of capacitative Ca(2+) influx in Bcl-2-overexpressing cells.* J Cell Biol, 2000. **148**(5): p. 857-62.

187. Palmer, A.E., et al., *Bcl-2-mediated alterations in endoplasmic reticulum Ca2+ analyzed with an improved genetically encoded fluorescent sensor.* Proc Natl Acad Sci U S A, 2004. **101**(50): p. 17404-9.

188. Ott, M., et al., *Cytochrome c release from mitochondria proceeds by a two-step process.* Proc Natl Acad Sci U S A, 2002. **99**(3): p. 1259-63.

189. Yavorskyy, A., et al., *Determination of calcium in synovial fluid samples as an aid to diagnosing osteoarthritis.* Bioanalysis, 2010. **2**(2): p. 189-95.

190. Sabchyshyn, V., et al., *Concurrence of rheumatoid arthritis and calcium pyrophosphate deposition disease: A case collection and review of the literature.* Semin Arthritis Rheum, 2018. **48**(1): p. 9-11.

191. Ea, H.K., et al., *Pathogenic role of basic calcium phosphate crystals in destructive arthropathies.* PLoS One, 2013. **8**(2): p. e57352.

192. Ishigami, A., et al., *Abnormal accumulation of citrullinated proteins catalyzed by peptidylarginine deiminase in hippocampal extracts from patients with Alzheimer's disease.* J Neurosci Res, 2005. **80**(1): p. 120-8.

193. Moscarello, M.A., F.G. Mastronardi, and D.D. Wood, *The role of citrullinated proteins suggests a novel mechanism in the pathogenesis of multiple sclerosis.* Neurochem Res, 2007. **32**(2): p. 251-6.

194. Vomero, M., et al., *Autophagy and Rheumatoid Arthritis: Current Knowledges and Future Perspectives.* Front Immunol, 2018. **9**: p. 1577.

195. Song, Y.W. and E.H. Kang, *Autoantibodies in rheumatoid arthritis: rheumatoid factors and anticitrullinated protein antibodies.* QJM, 2010. **103**(3): p. 139-46.

196. Tilleman, K., et al., *Synovial detection and autoantibody reactivity of processed citrullinated isoforms of vimentin in inflammatory arthritides.* Rheumatology (Oxford), 2008. **47**(5): p. 597-604.

197. Matsuo, K., et al., *Identification of novel citrullinated autoantigens of synovium in rheumatoid arthritis using a proteomic approach.* Arthritis Res Ther, 2006. **8**(6): p. R175.

198. Van Steendam, K., et al., *Citrullinated vimentin as an important antigen in immune complexes from synovial fluid of rheumatoid arthritis patients with antibodies against citrullinated proteins.* Arthritis Res Ther, 2010. **12**(4): p. R132.

199. Janssen, K.M.J., et al., *Autoantibodies against citrullinated histone H3 in rheumatoid arthritis and periodontitis patients.* J Clin Periodontol, 2017. **44**(6): p. 577-584.

200. Damgaard, D., et al., *Relative efficiencies of peptidylarginine deiminase 2 and 4 in generating target sites for anti-citrullinated protein antibodies in fibrinogen, alpha-enolase and histone H3.* PLoS One, 2018. **13**(8): p. e0203214.

201. van Venrooij, W.J. and G.J. Pruijn, *How citrullination invaded rheumatoid arthritis research.* Arthritis Res Ther, 2014. **16**(1): p. 103.

202. van Drongelen, V. and J. Holoshitz, *Human Leukocyte Antigen-Disease Associations in Rheumatoid Arthritis.* Rheum Dis Clin North Am, 2017. **43**(3): p. 363-376.

203. Sandoughi, M., et al., *Frequency of HLA-DRB1 alleles in rheumatoid arthritis patients in Zahedan, southeast Iran.* Ann Saudi Med, 2011. **31**(2): p. 171-3.

204. Ireland, J.M. and E.R. Unanue, *Autophagy in antigen-presenting cells results in presentation of citrullinated peptides to CD4 T cells.* J Exp Med, 2011. **208**(13): p. 2625-32.

205. Glick, D., S. Barth, and K.F. Macleod, *Autophagy: cellular and molecular mechanisms.* J Pathol, 2010. **221**(1): p. 3-12.

206. Munz, C., *Antigen processing by macroautophagy for MHC presentation.* Front Immunol, 2011. **2**: p. 42.

207. Munz, C., *Antigen Processing for MHC Class II Presentation via Autophagy.* Front Immunol, 2012. **3**: p. 9.

208. Fimia, G.M., et al., *Ambra1 at the crossroad between autophagy and cell death.* Oncogene, 2013. **32**(28): p. 3311-8.

209. Lin, Y., et al., *Cancer and ER stress: Mutual crosstalk between autophagy, oxidative stress and inflammatory response.* Biomed Pharmacother, 2019. **118**: p. 109249.

210. Shen, J., et al., *ER stress regulation of ATF6 localization by dissociation of BiP/GRP78 binding and unmasking of Golgi localization signals.* Dev Cell, 2002. **3**(1): p. 99-111.

211. Matsumoto, H., et al., *Selection of autophagy or apoptosis in cells exposed to ER-stress depends on ATF4 expression pattern with or without CHOP expression.* Biol Open, 2013. **2**(10): p. 1084-90.

212. Rouschop, K.M., et al., *The unfolded protein response protects human tumor cells during hypoxia through regulation of the autophagy genes MAP1LC3B and ATG5.* J Clin Invest, 2010. **120**(1): p. 127-41.

213. Marino, M.L., et al., *Autophagy is a protective mechanism for human melanoma cells under acidic stress.* J Biol Chem, 2012. **287**(36): p. 30664-76.

214. Gong, C., et al., *Beclin 1 and autophagy are required for the tumorigenicity of breast cancer stem-like/progenitor cells.* Oncogene, 2013. **32**(18): p. 2261-72, 2272e 1-11.

215. Ouyang, D.Y., et al., *Autophagy is differentially induced in prostate cancer LNCaP, DU145 and PC-3 cells via distinct splicing profiles of ATG5.* Autophagy, 2013. **9**(1): p. 20-32.

216. Yang, A., et al., *Autophagy is critical for pancreatic tumor growth and progression in tumors with p53 alterations.* Cancer Discov, 2014. **4**(8): p. 905-13.

217. Brech, A., et al., *Autophagy in tumour suppression and promotion.* Mol Oncol, 2009. **3**(4): p. 366-75.

218. Ngabire, D. and G.D. Kim, *Autophagy and Inflammatory Response in the Tumor Microenvironment.* Int J Mol Sci, 2017. **18**(9).

219. Green, D.R. and B. Levine, *To be or not to be? How selective autophagy and cell death govern cell fate.* Cell, 2014. **157**(1): p. 65-75.

220. Brentville, V.A., et al., *Combination vaccine based on citrullinated vimentin and enolase peptides induces potent CD4-mediated anti-tumor responses.* J Immunother Cancer, 2020. **8**(1).

221. Brentville, V.A., et al., *T cell repertoire to citrullinated self-peptides in healthy humans is not confined to the HLA-DR SE alleles; Targeting of citrullinated self-peptides presented by HLA-DP4 for tumour therapy.* Oncoimmunology, 2019. **8**(5): p. e1576490.

222. Nieminen, M., et al., *Vimentin function in lymphocyte adhesion and transcellular migration.* Nat Cell Biol, 2006. **8**(2): p. 156-62.

223. Helfand, B.T., et al., *Vimentin organization modulates the formation of lamellipodia.* Mol Biol Cell, 2011. **22**(8): p. 1274-89.

224. Roche, J., *The Epithelial-to-Mesenchymal Transition in Cancer.* Cancers (Basel), 2018. **10**(2).

225. Wu, S., et al., *Upregulation of the EMT marker vimentin is associated with poor clinical outcome in acute myeloid leukemia.* J Transl Med, 2018. **16**(1): p. 170.

226. Du, L., et al., *High Vimentin Expression Predicts a Poor Prognosis and Progression in Colorectal Cancer: A Study with Meta-Analysis and TCGA Database.* Biomed Res Int, 2018. **2018**: p. 6387810.

227. Yin, S., F.F. Chen, and G.F. Yang, *Vimentin immunohistochemical expression as a prognostic factor in gastric cancer: A meta-analysis.* Pathol Res Pract, 2018. **214**(9): p. 1376-1380.

228. Tadokoro, A., et al., *Vimentin Regulates Invasiveness and Is a Poor Prognostic Marker in Non-small Cell Lung Cancer.* Anticancer Res, 2016. **36**(4): p. 1545-51.

229. Schmidt, G., et al., *Is vimentin a potential prognostic factor for patients with triple-negative breast cancer?* J Cancer Res Clin Oncol, 2020. **146**(8): p. 2109-2116.

230. Tarbet, H.J., et al., *Site-specific glycosylation regulates the form and function of the intermediate filament cytoskeleton.* Elife, 2018. **7**.

231. Ulirsch, J., et al., *Vimentin DNA methylation predicts survival in breast cancer.* Breast Cancer Res Treat, 2013. **137**(2): p. 383-96.

232. Gibbons, D.L. and C.J. Creighton, *Pan-cancer survey of epithelial-mesenchymal transition markers across the Cancer Genome Atlas.* Dev Dyn, 2018. **247**(3): p. 555-564.

233. Grelet, S., et al., *Pleiotropic Roles of Non-Coding RNAs in TGF-beta-Mediated Epithelial-Mesenchymal Transition and Their Functions in Tumor Progression.* Cancers (Basel), 2017. **9**(7).

234. Jolly, M.K., et al., *Implications of the Hybrid Epithelial/Mesenchymal Phenotype in Metastasis.* Front Oncol, 2015. **5**: p. 155.

235. Gasior, K., et al., *The role of cellular contact and TGF-beta signaling in the activation of the epithelial mesenchymal transition (EMT).* Cell Adh Migr, 2018: p. 1-13.

236. Imai, D., et al., *IFN-gamma Promotes Epithelial-Mesenchymal Transition and the Expression of PD-L1 in Pancreatic Cancer.* J Surg Res, 2019. **240**: p. 115-123.

237. Goules, J.D., A.V. Goules, and A.G. Tzioufas, *Fine specificity of anti-citrullinated peptide antibodies discloses a heterogeneous antibody population in rheumatoid arthritis.* Clin Exp Immunol, 2013. **174**(1): p. 10-7.

238. Zhang, B., et al., *In vitro elimination of autoreactive B cells from rheumatoid arthritis patients by universal chimeric antigen receptor T cells.* Ann Rheum Dis, 2021. **80**(2): p. 176-184.

239. Ganley, I.G., et al., *Distinct autophagosomal-lysosomal fusion mechanism revealed by thapsigargin-induced autophagy arrest.* Mol Cell, 2011. **42**(6): p. 731-43.

240. Engedal, N., et al., *Modulation of intracellular calcium homeostasis blocks autophagosome formation.* Autophagy, 2013. **9**(10): p. 1475-90.

241. Dobrokhotov, O., et al., *Mechanoregulation and pathology of YAP/TAZ via Hippo and non-Hippo mechanisms.* Clin Transl Med, 2018. **7**(1): p. 23.

242. Zhao, B., et al., *Inactivation of YAP oncoprotein by the Hippo pathway is involved in cell contact inhibition and tissue growth control.* Genes Dev, 2007. **21**(21): p. 2747-61.

243. Pavel, M., et al., *Contact inhibition controls cell survival and proliferation via YAP/TAZ-autophagy axis.* Nat Commun, 2018. **9**(1): p. 2961.

244. Fan, F., et al., *Pharmacological targeting of kinases MST1 and MST2 augments tissue repair and regeneration.* Sci Transl Med, 2016. **8**(352): p. 352ra108.

245. Oliver-De La Cruz, J., et al., *Substrate mechanics controls adipogenesis through YAP phosphorylation by dictating cell spreading.* Biomaterials, 2019. **205**: p. 64-80.

246. Huang, R.Y., et al., *An EMT spectrum defines an anoikis-resistant and spheroidogenic intermediate mesenchymal state that is sensitive to e-cadherin restoration by a src-kinase inhibitor, saracatinib (AZD0530).* Cell Death Dis, 2013. **4**: p. e915.

247. Wang, L., et al., *PADI2-Mediated Citrullination Promotes Prostate Cancer Progression.* Cancer Res, 2017. **77**(21): p. 5755-5768.

248. Yuzhalin, A.E., et al., *Colorectal cancer liver metastatic growth depends on PAD4-driven citrullination of the extracellular matrix.* Nat Commun, 2018. **9**(1): p. 4783.

249. Li, N., C. Xie, and N. Lu, *Crosstalk between Hippo signalling and miRNAs in tumour progression.* FEBS J, 2017. **284**(7): p. 1045-1055.

250. Song, Q., et al., *YAP enhances autophagic flux to promote breast cancer cell survival in response to nutrient deprivation.* PLoS One, 2015. **10**(3): p. e0120790.

251. Lin, Z., et al., *Acetylation of VGLL4 Regulates Hippo-YAP Signaling and Postnatal Cardiac Growth.* Dev Cell, 2016. **39**(4): p. 466-479.

252. Zhang, Y., et al., *VGLL4 Selectively Represses YAP-Dependent Gene Induction and Tumorigenic Phenotypes in Breast Cancer.* Sci Rep, 2017. **7**(1): p. 6190.

253. Zhang, B., et al., *Identification of a novel YAP-14-3-3zeta negative feedback loop in gastric cancer.* Oncotarget, 2017. **8**(42): p. 71894-71910.

254. Song, S., et al., *A Novel YAP1 Inhibitor Targets CSC-Enriched Radiation-Resistant Cells and Exerts Strong Antitumor Activity in Esophageal Adenocarcinoma.* Mol Cancer Ther, 2018. **17**(2): p. 443-454.

255. Kim, J.Y., et al., *VGLL4 with low YAP expression is associated with favorable prognosis in colorectal cancer.* APMIS, 2020. **128**(10): p. 543-551.

256. Jiao, S., et al., *A peptide mimicking VGLL4 function acts as a YAP antagonist therapy against gastric cancer.* Cancer Cell, 2014. **25**(2): p. 166-80.

257. Scholzen, T. and J. Gerdes, *The Ki-67 protein: from the known and the unknown.* J Cell Physiol, 2000. **182**(3): p. 311-22.

258. Tasdemir, E., et al., *Cell cycle-dependent induction of autophagy, mitophagy and reticulophagy.* Cell Cycle, 2007. **6**(18): p. 2263-7.

259. Sorice, M., et al., *Autophagy generates citrullinated peptides in human synoviocytes: a possible trigger for anti-citrullinated peptide antibodies.* Rheumatology (Oxford), 2016. **55**(8): p. 1374-85.

260. Dengjel, J., et al., *Autophagy promotes MHC class II presentation of peptides from intracellular source proteins.* Proc Natl Acad Sci U S A, 2005. **102**(22): p. 7922-7.

261. Chen, R., et al., *The general amino acid control pathway regulates mTOR and autophagy during serum/glutamine starvation.* J Cell Biol, 2014. **206**(2): p. 173-82.

262. Schutte, B., et al., *Annexin V binding assay as a tool to measure apoptosis in differentiated neuronal cells.* J Neurosci Methods, 1998. **86**(1): p. 63-9.

263. Sa-Nongdej, W., S. Chongthammakun, and C. Songthaveesin, *Nutrient starvation induces apoptosis and autophagy in C6 glioma stem-like cells.* Heliyon, 2021. **7**(2): p. e06352.

264. Trier, N.H., et al., *Specificity of Anti-Citrullinated Protein Antibodies in Rheumatoid Arthritis.* Antibodies (Basel), 2019. **8**(2).

265. Ioan-Facsinay, A., et al., *Anti-cyclic citrullinated peptide antibodies are a collection of anti-citrullinated protein antibodies and contain overlapping and non-overlapping reactivities.* Ann Rheum Dis, 2011. **70**(1): p. 188-93.

266. Kissel, T., et al., *Antibodies and B cells recognising citrullinated proteins display a broad cross-reactivity towards other post-translational modifications.* Ann Rheum Dis, 2020. **79**(4): p. 472-480.

267. Ge, C., et al., *Structural Basis of Cross-Reactivity of Anti-Citrullinated Protein Antibodies.* Arthritis Rheumatol, 2019. **71**(2): p. 210-221.

268. Landskron, G., et al., *Chronic inflammation and cytokines in the tumor microenvironment.* J Immunol Res, 2014. **2014**: p. 149185.

269. Lamar, J.M., et al., *The Hippo pathway target, YAP, promotes metastasis through its TEAD-interaction domain.* Proc Natl Acad Sci U S A, 2012. **109**(37): p. E2441-50.

270. Lei, Q.Y., et al., *TAZ promotes cell proliferation and epithelial-mesenchymal transition and is inhibited by the hippo pathway.* Mol Cell Biol, 2008. **28**(7): p. 2426-36.

271. Ricciardi, M., et al., *Epithelial-to-mesenchymal transition (EMT) induced by inflammatory priming elicits mesenchymal stromal cell-like immune-modulatory properties in cancer cells.* Br J Cancer, 2015. **112**(6): p. 1067-75.

272. Rodon, L., et al., *Active CREB1 promotes a malignant TGFbeta2 autocrine loop in glioblastoma.* Cancer Discov, 2014. **4**(10): p. 1230-41.

273. Ahmadzadeh, M. and S.A. Rosenberg, *TGF-beta 1 attenuates the acquisition and expression of effector function by tumor antigen-specific human memory CD8 T cells.* J Immunol, 2005. **174**(9): p. 5215-23.

274. Baka, Z., et al., *Specific expression of PAD4 and citrullinated proteins in lung cancer is not associated with anti-CCP antibody production.* Int Immunol, 2011. **23**(6): p. 405-14.

275. Bidkar, M., et al., *Cigarette Smoke Induces Immune Responses to Vimentin in both, Arthritis-Susceptible and -Resistant Humanized Mice.* PLoS One, 2016. **11**(9): p. e0162341.

276. Qin, H., et al., *PAD1 promotes epithelial-mesenchymal transition and metastasis in triple-negative breast cancer cells by regulating MEK1-ERK1/2-MMP2 signaling.* Cancer Lett, 2017. **409**: p. 30-41.

277. Ye, L., et al., *Tumor-Infiltrating Immune Cells Act as a Marker for Prognosis in Colorectal Cancer.* Front Immunol, 2019. **10**: p. 2368.

278. Sato, E., et al., *Intraepithelial CD8+ tumor-infiltrating lymphocytes and a high CD8+/regulatory T cell ratio are associated with favorable prognosis in ovarian cancer.* Proc Natl Acad Sci U S A, 2005. **102**(51): p. 18538-43.

279. Lee, H.E., et al., *Prognostic implications of type and density of tumour-infiltrating lymphocytes in gastric cancer.* Br J Cancer, 2008. **99**(10): p. 1704-11.

280. Singh, N., et al., *Inflammation and cancer.* Ann Afr Med, 2019. **18**(3): p. 121-126.

281. Nagarajan, U.M., A. Bushey, and J.M. Boss, *Modulation of gene expression by the MHC class II transactivator.* J Immunol, 2002. **169**(9): p. 5078-88.

282. Reith, W., S. LeibundGut-Landmann, and J.M. Waldburger, *Regulation of MHC class II gene expression by the class II transactivator.* Nat Rev Immunol, 2005. **5**(10): p. 793-806.

283. Martin, B.K., et al., *Induction of MHC class I expression by the MHC class II transactivator CIITA.* Immunity, 1997. **6**(5): p. 591-600.

284. Muhlethaler-Mottet, A., et al., *Expression of MHC class II molecules in different cellular and functional compartments is controlled by differential usage of multiple promoters of the transactivator CIITA.* EMBO J, 1997. **16**(10): p. 2851-60.

285. LeibundGut-Landmann, S., et al., *Mini-review: Specificity and expression of CIITA, the master regulator of MHC class II genes.* Eur J Immunol, 2004. **34**(6): p. 1513-25.

286. Piskurich, J.F., et al., *Expression of the MHC class II transactivator (CIITA) type IV promoter in B lymphocytes and regulation by IFN-gamma.* Mol Immunol, 2006. **43**(6): p. 519-28.

287. Muhlethaler-Mottet, A., et al., *Activation of the MHC class II transactivator CIITA by interferon-gamma requires cooperative interaction between Stat1 and USF-1.* Immunity, 1998. **8**(2): p. 157-66.

288. Krause, C.D., et al., *Modulation of the activation of Stat1 by the interferon-gamma receptor complex.* Cell Res, 2006. **16**(1): p. 113-23.

289. Kumatori, A., et al., *Cooperation of STAT-1 and IRF-1 in interferon-gamma-induced transcription of the gp91(phox) gene.* J Biol Chem, 2002. **277**(11): p. 9103-11.

290. Murtas, D., et al., *IRF-1 responsiveness to IFN-gamma predicts different cancer immune phenotypes.* Br J Cancer, 2013. **109**(1): p. 76-82.

291. Lee, S.J., H. Qin, and E.N. Benveniste, *The IFN-gamma-induced transcriptional program of the CIITA gene is inhibited by statins.* Eur J Immunol, 2008. **38**(8): p. 2325-36.

292. Bou Nasser Eddine, F., et al., *CIITA-driven MHC class II expressing tumor cells can efficiently prime naive CD4(+) TH cells in vivo and vaccinate the host against parental MHC-II-negative tumor cells.* Oncoimmunology, 2017. **6**(1): p. e1261777.

293. Naves, R., et al., *MHC class II-deficient tumor cell lines with a defective expression of the class II transactivator.* Int Immunol, 2002. **14**(5): p. 481-91.

294. Duncan, T.J., et al., *Loss of IFN gamma receptor is an independent prognostic factor in ovarian cancer.* Clin Cancer Res, 2007. **13**(14): p. 4139-45.

295. Gao, F.G., et al., *Antigen-specific CD4+ T-cell help is required to activate a memory CD8+ T cell to a fully functional tumor killer cell.* Cancer Res, 2002. **62**(22): p. 6438-41.

296. Novy, P., et al., *CD4 T cells are required for CD8 T cell survival during both primary and memory recall responses.* J Immunol, 2007. **179**(12): p. 8243-51.

297. Ahrends, T., et al., *CD4(+) T cell help creates memory CD8(+) T cells with innate and help-independent recall capacities.* Nat Commun, 2019. **10**(1): p. 5531.

298. Kreiter, S., et al., *Mutant MHC class II epitopes drive therapeutic immune responses to cancer.* Nature, 2015. **520**(7549): p. 692-6.

299. Ott, P.A., et al., *An immunogenic personal neoantigen vaccine for patients with melanoma.* Nature, 2017. **547**(7662): p. 217-221.

300. Warabi, M., M. Kitagawa, and K. Hirokawa, *Loss of MHC class II expression is associated with a decrease of tumor-infiltrating T cells and an increase of metastatic potential of colorectal cancer: immunohistological and histopathological analyses as compared with normal colonic mucosa and adenomas.* Pathol Res Pract, 2000. **196**(12): p. 807-15.

301. Shi, B., et al., *Differential expression of MHC class II molecules in highly metastatic breast cancer cells is mediated by the regulation of the CIITA transcription Implication of CIITA in tumor and metastasis development.* Int J Biochem Cell Biol, 2006. **38**(4): p. 544-62.

302. Forero, A., et al., *Expression of the MHC Class II Pathway in Triple-Negative Breast Cancer Tumor Cells Is Associated with a Good Prognosis and Infiltrating Lymphocytes.* Cancer Immunol Res, 2016. **4**(5): p. 390-9.

303. He, Y., et al., *MHC class II expression in lung cancer.* Lung Cancer, 2017. **112**: p. 75-80.

304. Park, I.A., et al., *Expression of the MHC class II in triple-negative breast cancer is associated with tumor-infiltrating lymphocytes and interferon signaling.* PLoS One, 2017. **12**(8): p. e0182786.

305. Sollie, S., et al., *Chronic inflammation markers are associated with risk of pancreatic cancer in the Swedish AMORIS cohort study.* BMC Cancer, 2019. **19**(1): p. 858.

306. Balachandran, V.P., et al., *Identification of unique neoantigen qualities in long-term survivors of pancreatic cancer.* Nature, 2017. **551**(7681): p. 512-516.

307. Castelli, F.A., et al., *HLA-DP4, the most frequent HLA II molecule, defines a new supertype of peptide-binding specificity.* J Immunol, 2002. **169**(12): p. 6928-34.

308. van Lith, M., R.M. McEwen-Smith, and A.M. Benham, *HLA-DP, HLA-DQ, and HLA-DR have different requirements for invariant chain and HLA-DM.* J Biol Chem, 2010. **285**(52): p. 40800-8.

309. Anczurowski, M. and N. Hirano, *Mechanisms of HLA-DP Antigen Processing and Presentation Revisited.* Trends Immunol, 2018. **39**(12): p. 960-964.

310. van der Stoep, N., et al., *Lack of IFN-gamma-mediated induction of the class II transactivator (CIITA) through promoter methylation is predominantly found in developmental tumor cell lines.* Int J Cancer, 2002. **97**(4): p. 501-7.

311. Chen, C., et al., *Modulation of IFN-gamma receptor 1 expression by AP-2alpha influences IFN-gamma sensitivity of cancer cells.* Am J Pathol, 2012. **180**(2): p. 661-71.

312. Lasfar, A., et al., *Critical role of the endogenous interferon ligand-receptors in type I and type II interferons response.* Immunology, 2014. **142**(3): p. 442-52.

313. Shen, T., et al., *Genetic defects of the IRF1-mediated major histocompatibility complex class I antigen presentation pathway occur prevalently in the JAK2 gene in non-small cell lung cancer.* Oncotarget, 2017. **8**(37): p. 60975-60986.

314. Zaretsky, J.M., et al., *Mutations Associated with Acquired Resistance to PD-1 Blockade in Melanoma.* N Engl J Med, 2016. **375**(9): p. 819-29.

315. Johnson, D.B., et al., *Melanoma-specific MHC-II expression represents a tumour-autonomous phenotype and predicts response to anti-PD-1/PD-L1 therapy.* Nat Commun, 2016. **7**: p. 10582.

316. Takamura, Y., et al., *Regulation of MHC class II expression in glioma cells by class II transactivator (CIITA).* Glia, 2004. **45**(4): p. 392-405.

317. Bobinet, M., et al., *Overexpression of meloe gene in melanomas is controlled both by specific transcription factors and hypomethylation.* PLoS One, 2013. **8**(9): p. e75421.

318. Weon, J.L. and P.R. Potts, *The MAGE protein family and cancer.* Curr Opin Cell Biol, 2015. **37**: p. 1-8.

319. von Witzleben, A., et al., *HNSCC: Tumour Antigens and Their Targeting by Immunotherapy.* Cells, 2020. **9**(9).

320. Turner, T.B., et al., *Epigenetic modifiers upregulate MHC II and impede ovarian cancer tumor growth.* Oncotarget, 2017. **8**(27): p. 44159-44170.

321. Gao, J., et al., *Loss of IFN-gamma Pathway Genes in Tumor Cells as a Mechanism of Resistance to Anti-CTLA-4 Therapy.* Cell, 2016. **167**(2): p. 397-404 e9.

322. Neuwelt, A.J., et al., *Cancer cell-intrinsic expression of MHC II in lung cancer cell lines is actively restricted by MEK/ERK signaling and epigenetic mechanisms.* J Immunother Cancer, 2020. **8**(1).

323. Song, M., et al., *Low-Dose IFNgamma Induces Tumor Cell Stemness in Tumor Microenvironment of Non-Small Cell Lung Cancer.* Cancer Res, 2019. **79**(14): p. 3737-3748.

324. Gu, W., et al., *Ambra1 is an essential regulator of autophagy and apoptosis in SW620 cells: pro-survival role of Ambra1.* PLoS One, 2014. **9**(2): p. e90151.

325. Cianfanelli, V., et al., *AMBRA1 links autophagy to cell proliferation and tumorigenesis by promoting c-Myc dephosphorylation and degradation.* Nat Cell Biol, 2015. **17**(5): p. 706.

326. Fricke, I., et al., *Mycobacteria induce IFN-gamma production in human dendritic cells via triggering of TLR2.* J Immunol, 2006. **176**(9): p. 5173-82.

327. Darwich, L., et al., *Secretion of interferon-gamma by human macrophages demonstrated at the single-cell level after costimulation with interleukin (IL)-12 plus IL-18.* Immunology, 2009. **126**(3): p. 386-93.

328. Wang, R., et al., *Natural killer cell-produced IFN-gamma and TNF-alpha induce target cell cytolysis through up-regulation of ICAM-1.* J Leukoc Biol, 2012. **91**(2): p. 299-309.

329. Opata, M.M., et al., *Early effector cells survive the contraction phase in malaria infection and generate both central and effector memory T cells.* J Immunol, 2015. **194**(11): p. 5346-54.

330. Li, X., et al., *IFNgamma and TNFalpha synergistically induce apoptosis of mesenchymal stem/stromal cells via the induction of nitric oxide.* Stem Cell Res Ther, 2019. **10**(1): p. 18.

331. Demine, S., et al., *Pro-inflammatory cytokines induce cell death, inflammatory responses, and endoplasmic reticulum stress in human iPSC-derived beta cells.* Stem Cell Res Ther, 2020. **11**(1): p. 7.

332. Attaf, M., et al., *Major TCR Repertoire Perturbation by Immunodominant HLA-B(*)44:03-Restricted CMV-Specific T Cells.* Front Immunol, 2018. **9**: p. 2539.

333. Benati, D., et al., *Public T cell receptors confer high-avidity CD4 responses to HIV controllers.* J Clin Invest, 2016. **126**(6): p. 2093-108.

334. Khosravi-Maharlooei, M., et al., *Crossreactive public TCR sequences undergo positive selection in the human thymic repertoire.* J Clin Invest, 2019. **129**(6): p. 2446-2462.

335. Gil, A., et al., *Epstein-Barr Virus Epitope-Major Histocompatibility Complex Interaction Combined with Convergent Recombination Drives Selection of Diverse T Cell Receptor alpha and beta Repertoires.* mBio, 2020. **11**(2).

336. Venturi, V., et al., *The molecular basis for public T-cell responses?* Nat Rev Immunol, 2008. **8**(3): p. 231-8.

337. Li, H., et al., *Recombinatorial biases and convergent recombination determine interindividual TCRbeta sharing in murine thymocytes.* J Immunol, 2012. **189**(5): p. 2404-13.

338. Munson, D.J., et al., *Identification of shared TCR sequences from T cells in human breast cancer using emulsion RT-PCR.* Proc Natl Acad Sci U S A, 2016. **113**(29): p. 8272-7.

339. Cui, C., et al., *T cell receptor beta-chain repertoire analysis of tumor-infiltrating lymphocytes in pancreatic cancer.* Cancer Sci, 2019. **110**(1): p. 61-71.

340. Zhang, C., et al., *TCR repertoire intratumor heterogeneity of CD4(+) and CD8(+) T cells in centers and margins of localized lung adenocarcinomas.* Int J Cancer, 2019. **144**(4): p. 818-827.

341. Jiang, X., et al., *Comprehensive TCR repertoire analysis of CD4(+) T-cell subsets in rheumatoid arthritis.* J Autoimmun, 2020. **109**: p. 102432.

342. Kiazyk, S.A. and K.R. Fowke, *Loss of CD127 expression links immune activation and CD4(+) T cell loss in HIV infection.* Trends Microbiol, 2008. **16**(12): p. 567-73.

343. Straetemans, T., et al., *TCR gene transfer: MAGE-C2/HLA-A2 and MAGE-A3/HLA-DP4 epitopes as melanoma-specific immune targets.* Clin Dev Immunol, 2012. **2012**: p. 586314.

344. Yao, X., et al., *Isolation and Characterization of an HLA-DPB1*04: 01-restricted MAGE-A3 T-Cell Receptor for Cancer Immunotherapy.* J Immunother, 2016. **39**(5): p. 191-201.

345. Rosskopf, S., et al., *A Jurkat 76 based triple parameter reporter system to evaluate TCR functions and adoptive T cell strategies.* Oncotarget, 2018. **9**(25): p. 17608-17619.

346. Cibrian, D. and F. Sanchez-Madrid, *CD69: from activation marker to metabolic gatekeeper.* Eur J Immunol, 2017. **47**(6): p. 946-953.

347. Bartelt, R.R., et al., *Comparison of T cell receptor-induced proximal signaling and downstream functions in immortalized and primary T cells.* PLoS One, 2009. **4**(5): p. e5430.

348. Kuball, J., et al., *Facilitating matched pairing and expression of TCR chains introduced into human T cells.* Blood, 2007. **109**(6): p. 2331-8.

349. Sommermeyer, D. and W. Uckert, *Minimal amino acid exchange in human TCR constant regions fosters improved function of TCR gene-modified T cells.* J Immunol, 2010. **184**(11): p. 6223-31.

350. Scholten, K.B., et al., *Codon modification of T cell receptors allows enhanced functional expression in transgenic human T cells.* Clin Immunol, 2006. **119**(2): p. 135-45.

351. Millington, M., et al., *Towards a clinically relevant lentiviral transduction protocol for primary human CD34 hematopoietic stem/progenitor cells.* PLoS One, 2009. **4**(7): p. e6461.

352. Heemskerk, M.H., et al., *Redirection of antileukemic reactivity of peripheral T lymphocytes using gene transfer of minor histocompatibility antigen HA-2-specific T-cell receptor complexes expressing a conserved alpha joining region.* Blood, 2003. **102**(10): p. 3530-40.

353. Cribbs, A.P., et al., *Simplified production and concentration of lentiviral vectors to achieve high transduction in primary human T cells.* BMC Biotechnol, 2013. **13**: p. 98.

354. Bos, T.J., et al., *Large double copy vectors are functional but show a size-dependent decline in transduction efficiency.* J Biotechnol, 2010. **150**(1): p. 37-40.

355. Wu, Z., H. Yang, and P. Colosi, *Effect of genome size on AAV vector packaging.* Mol Ther, 2010. **18**(1): p. 80-6.

356. Goff, S.L., et al., *Enhanced receptor expression and in vitro effector function of a murine-human hybrid MART-1-reactive T cell receptor following a rapid expansion.* Cancer Immunol Immunother, 2010. **59**(10): p. 1551-60.

357. Cohen, C.J., et al., *Enhanced antitumor activity of murine-human hybrid T-cell receptor (TCR) in human lymphocytes is associated with improved pairing and TCR/CD3 stability.* Cancer Res, 2006. **66**(17): p. 8878-86.

358. Bethune, M.T., et al., *Isolation and characterization of NY-ESO-1-specific T cell receptors restricted on various MHC molecules.* Proc Natl Acad Sci U S A, 2018. **115**(45): p. E10702-E10711.

359. Simms, P.E. and T.M. Ellis, *Utility of flow cytometric detection of CD69 expression as a rapid method for determining poly- and oligoclonal lymphocyte activation.* Clin Diagn Lab Immunol, 1996. **3**(3): p. 301-4.

360. Allison, K.A., et al., *Affinity and dose of TCR engagement yield proportional enhancer and gene activity in CD4+ T cells.* Elife, 2016. **5**.

361. Katsuhara, A., et al., *Transduction of a novel HLA-DRB1*04:05-restricted, WT1-specific TCR gene into human CD4+ T cells confers killing activity against human leukemia cells.* Anticancer Res, 2015. **35**(3): p. 1251-61.

362. Kitano, S., et al., *Enhancement of tumor-reactive cytotoxic CD4+ T cell responses after ipilimumab treatment in four advanced melanoma patients.* Cancer Immunol Res, 2013. **1**(4): p. 235-44.

363. Knies, D., et al., *An optimized single chain TCR scaffold relying on the assembly with the native CD3-complex prevents residual mispairing with endogenous TCRs in human T-cells.* Oncotarget, 2016. **7**(16): p. 21199-221.

364. Bloemberg, D., et al., *A High-Throughput Method for Characterizing Novel Chimeric Antigen Receptors in Jurkat Cells.* Mol Ther Methods Clin Dev, 2020. **16**: p. 238-254.

365. Cimo, A.M., et al., *CD25 and CD69 induction by alpha4beta1 outside-in signalling requires TCR early signalling complex proteins.* Biochem J, 2013. **454**(1): p. 109-21.

366. Li, Z., et al., *Thrombospondin-1 inhibits TCR-mediated T lymphocyte early activation.* J Immunol, 2001. **166**(4): p. 2427-36.

367. Klinker, M.W., et al., *Human B Cell-Derived Lymphoblastoid Cell Lines Constitutively Produce Fas Ligand and Secrete MHCII(+)FasL(+) Killer Exosomes.* Front Immunol, 2014. **5**: p. 144.

368. Sidney, J., et al., *Citrullination only infrequently impacts peptide binding to HLA class II MHC.* PLoS One, 2017. **12**(5): p. e0177140.

369. Schultz, E.S., et al., *A MAGE-A3 peptide presented by HLA-DP4 is recognized on tumor cells by CD4+ cytolytic T lymphocytes.* Cancer Res, 2000. **60**(22): p. 6272-5.

370. Viola, A. and A. Lanzavecchia, *T cell activation determined by T cell receptor number and tunable thresholds.* Science, 1996. **273**(5271): p. 104-6.

371. Labrecque, N., et al., *How much TCR does a T cell need?* Immunity, 2001. **15**(1): p. 71-82.

372. Gramaglia, I., et al., *The OX40 costimulatory receptor determines the development of CD4 memory by regulating primary clonal expansion.* J Immunol, 2000. **165**(6): p. 3043-50.

373. Lin, L., et al., *Granzyme B secretion by human memory CD4 T cells is less strictly regulated compared to memory CD8 T cells.* BMC Immunol, 2014. **15**: p. 36.

374. Opata, M.M., et al., *Protection by and maintenance of CD4 effector memory and effector T cell subsets in persistent malaria infection.* PLoS Pathog, 2018. **14**(4): p. e1006960.

375. Padovan, E., et al., *Expression of two T cell receptor alpha chains: dual receptor T cells.* Science, 1993. **262**(5132): p. 422-4.

376. Padovan, E., et al., *Normal T lymphocytes can express two different T cell receptor beta chains: implications for the mechanism of allelic exclusion.* J Exp Med, 1995. **181**(4): p. 1587-91.

377. Zhang, Y., et al., *A polyclonal anti-vaccine CD4 T cell response detected with HLA-DP4 multimers in a melanoma patient vaccinated with MAGE-3.DP4-peptide-pulsed dendritic cells.* Eur J Immunol, 2005. **35**(4): p. 1066-75.

378. Wisskirchen, K., et al., *Isolation and functional characterization of hepatitis B virus-specific T-cell receptors as new tools for experimental and clinical use.* PLoS One, 2017. **12**(8): p. e0182936.

379. Gatica, D., V. Lahiri, and D.J. Klionsky, *Cargo recognition and degradation by selective autophagy.* Nat Cell Biol, 2018. **20**(3): p. 233-242.

380. Duronio, R.J. and Y. Xiong, *Signaling pathways that control cell proliferation.* Cold Spring Harb Perspect Biol, 2013. **5**(3): p. a008904.

381. Holler, P.D., L.K. Chlewicki, and D.M. Kranz, *TCRs with high affinity for foreign pMHC show self-reactivity.* Nat Immunol, 2003. **4**(1): p. 55-62.

382. Ober, B.T., et al., *Affinity of thymic self-peptides for the TCR determines the selection of CD8(+) T lymphocytes in the thymus.* Int Immunol, 2000. **12**(9): p. 1353-63.

383. Chen, D.S. and I. Mellman, *Elements of cancer immunity and the cancer-immune set point.* Nature, 2017. **541**(7637): p. 321-330.

384. Tarcsa, E., et al., *Protein unfolding by peptidylarginine deiminase. Substrate specificity and structural relationships of the natural substrates trichohyalin and filaggrin.* J Biol Chem, 1996. **271**(48): p. 30709-16.

385. Linnemann, C., et al., *High-throughput epitope discovery reveals frequent recognition of neo-antigens by CD4+ T cells in human melanoma.* Nat Med, 2015. **21**(1): p. 81-5.

386. Rana, J. and M. Biswas, *Regulatory T cell therapy: Current and future design perspectives.* Cell Immunol, 2020. **356**: p. 104193.

387. Sadeqi Nezhad, M., et al., *Chimeric Antigen Receptor Based Therapy as a Potential Approach in Autoimmune Diseases: How Close Are We to the Treatment?* Front Immunol, 2020. **11**: p. 603237.

388. McGinty, J.W., et al., *Recognition of posttranslationally modified GAD65 epitopes in subjects with type 1 diabetes.* Diabetes, 2014. **63**(9): p. 3033-40.

389. Buitinga, M., et al., *Inflammation-Induced Citrullinated Glucose-Regulated Protein 78 Elicits Immune Responses in Human Type 1 Diabetes.* Diabetes, 2018. **67**(11): p. 2337-2348.

390. Bradford, C.M., et al., *Localisation of citrullinated proteins in normal appearing white matter and lesions in the central nervous system in multiple sclerosis.* J Neuroimmunol, 2014. **273**(1-2): p. 85-95.

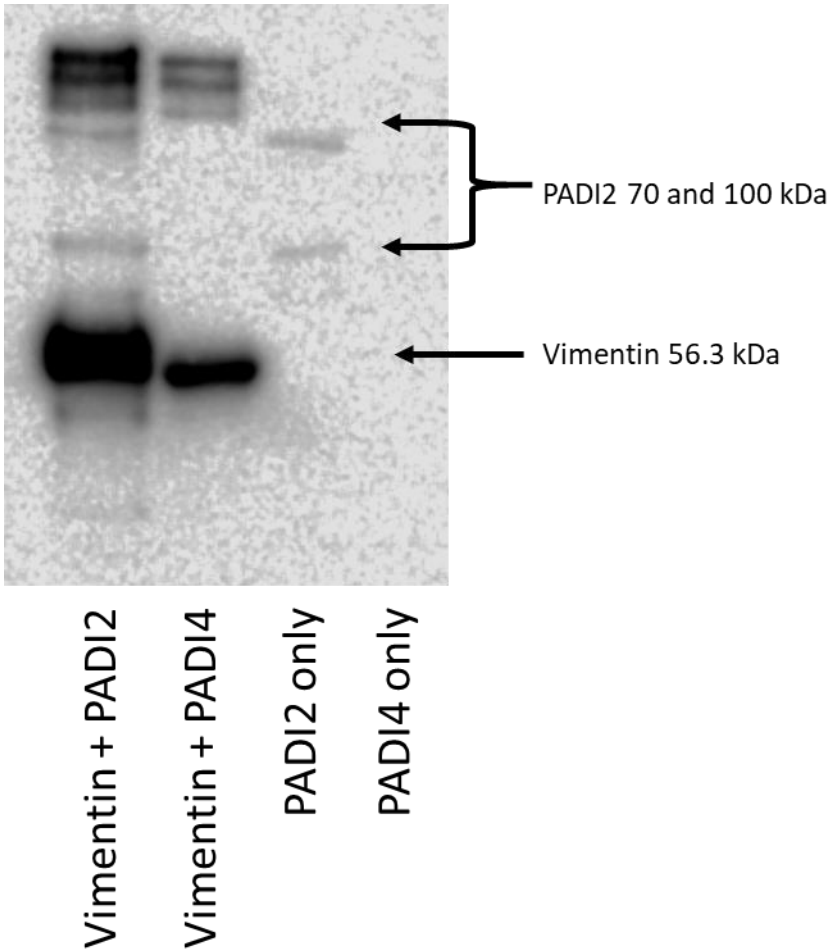
391. Deretic, V., T. Saitoh, and S. Akira, *Autophagy in infection, inflammation and immunity.* Nat Rev Immunol, 2013. **13**(10): p. 722-37.

392. van der Bruggen, P., et al., *A peptide encoded by human gene MAGE-3 and presented by HLA-A2 induces cytolytic T lymphocytes that recognize tumor cells expressing MAGE-3.* Eur J Immunol, 1994. **24**(12): p. 3038-43.

393. Martin, M.D., et al., *Revealing the Complexity in CD8 T Cell Responses to Infection in Inbred C57B/6 versus Outbred Swiss Mice.* Front Immunol, 2017. **8**: p. 1527.

8 Appendix

Appendix 1



Appendix 2

Epitope Content PEPperCHIP® Conformational Citrullinated Peptide Microarray

The PEPperCHIP® Conformational Citrullinated Peptide Microarray covers 337 citrullinated peptides (highlighted in light blue) including the corresponding arginine variants.

Epitope ID	Linear Sequence	CITR Modified Residues	Source Molecule Accession	Source Molecule Name	Source Organism ID	Source Organism Name	Length
19700	GGDNHGRGRGRGRGZGG	R15	82703982	EBNA-1	10376	Human herpesvirus 4	15
19700	RGZGGGRPGAPG	R15	82703982	EBNA-1	10376	Human herpesvirus 4	14
19700	RGRGRGRGZGGGRPGAP	R15	82703982	EBNA-1	10376	Human herpesvirus 4	14
19701	GGDNHGRGRGRGZGZGG	R13,R15	82703982	EBNA-1	10376	Human herpesvirus 4	17
19701	ZGZGGGRPGAPG	R13,R15	82703982	EBNA-1	10376	Human herpesvirus 4	17
19701	RGRGRGZGZGGGRPGAP	R13,R15	82703982	EBNA-1	10376	Human herpesvirus 4	17
19702	GGDNHGRGRGZGRGZGG	R11, R15	82703982	EBNA-1	10376	Human herpesvirus 4	17
19702	RGRGZGRGZGGGRPGAP	R11, R15	82703982	EBNA-1	10376	Human herpesvirus 4	17
19703	GGDNHGZGZGZGZGZGG	R7, R9, R11, R13, R15, R19	82703982	EBNA-1	10376	Human herpesvirus 4	13
19703	ZGZGGGZPGAPG	R7, R9, R11, R13, R15, R19	82703982	EBNA-1	10376	Human herpesvirus 4	13
19703	ZGZGZGZGZGGGZPGAP	R7, R9, R11, R13, R15, R19	82703982	EBNA-1	10376	Human herpesvirus 4	13
19704	GGDNHGRGRGRGRGRGG		139424506	EBNA-1	10376	Human herpesvirus 4	17
19704	RGRGGGRPGAPG		139424506	EBNA-1	10376	Human herpesvirus 4	12
19704	RGRGRGRGRGGGRPGAP		139424506	EBNA-1	10376	Human herpesvirus 4	17
30661	KEVPALTAVETGAT		217315555	VP1	270338	Human poliovirus 3 strain Sabin	17
106990	VYATZSSAVZLZSSV	R5, R10, R12	55977767	Vimentin	9606	Homo sapiens	17
106990	VYATZSSAVZLZSSVP	R5, R10, R12	55977767	Vimentin	9606	Homo sapiens	17
107788	DHEGTHSTKZGHAKSZP	R10, R16, R19	13591823	Fibrinogen alpha chain preproprotein, isoform alpha	9606	Homo sapiens	17
107788	DHEGTHSTKRGHAKSRP		13591823	Fibrinogen alpha chain preproprotein, isoform alpha	9606	Homo sapiens	17
107788	GHAKSZPVZG	R10, R16, R19	13591823	Fibrinogen alpha chain preproprotein, isoform alpha	9606	Homo sapiens	17
107788	GTHSTKZGHAKSZPVZG	R10, R16, R19	13591823	Fibrinogen alpha chain preproprotein, isoform alpha	9606	Homo sapiens	17
107788	GTHSTKRGHAKSRPVRG		13591823	Fibrinogen alpha chain preproprotein, isoform alpha	9606	Homo sapiens	17
107788	HSTKZGHAKSZPVZG	R10, R16, R19	13591823	Fibrinogen alpha chain preproprotein, isoform alpha	9606	Homo sapiens	17
107788	THSTKZGHAKSZPVZ	R10, R16, R19	13591823	Fibrinogen alpha chain preproprotein, isoform alpha	9606	Homo sapiens	17
107799	DSGHZGYSGSQASDNEG	R5	182605	Filaggrin	9606	Homo sapiens	17
107799	DSGHRGYSGSQASDNEG		182605	Filaggrin	9606	Homo sapiens	17
107799	SGHZGYSGSQASDNEGH	R5	182605	Filaggrin	9606	Homo sapiens	17
107799	SGHRGYSGSQASDNEGH		182605	Filaggrin	9606	Homo sapiens	17
107856	GGQGSZHQQAZ	R6	PT10004292	Filaggrin	9606	Homo sapiens	17
107856	GGQGSRHQQAR		PT10004292	Filaggrin	9606	Homo sapiens	17
107859	GHZPLDKKZEEAPSLZP	R3, R9, R16	119625338	Fibrinogen beta chain, isoform CRA_d	9606	Homo sapiens	17
107859	HZPLDKKZEEAPSLZPA	R3, R9, R16	119625338	Fibrinogen beta chain, isoform CRA_d	9606	Homo sapiens	14
107889	HQCHQESTZGRSRGRCG	R9	PT10004292	Filaggrin	9606	Homo sapiens	17
107889	HQCHQESTRGRSRGRCG		PT10004292	Filaggrin	9606	Homo sapiens	17
107889	QESTZGRSRGRCGRSGS	R9	PT10004292	Filaggrin	9606	Homo sapiens	17
107889	QESTRGRSRGRCGRSGS		PT10004292	Filaggrin	9606	Homo sapiens	17
107892	HSASQDGQDTIZGHPGS	R12	182605	Filaggrin	9606	Homo sapiens	17
107892	HSASQDGQDTIRGHPGS		182605	Filaggrin	9606	Homo sapiens	17
107892	SASQDGQDTIZGHPGSS	R12	182605	Filaggrin	9606	Homo sapiens	17
107892	SASQDGQDTIRGHPGSS		182605	Filaggrin	9606	Homo sapiens	14
107893	HGQASSAVRDSGHZGYS	R19	182605	Filaggrin	9606	Homo sapiens	17
107893	HGQASSAVRDSGHRGYS		182605	Filaggrin	9606	Homo sapiens	17
107896	HSTSQEGQDTIHGHZGS	R15	182605	Filaggrin	9606	Homo sapiens	17
107896	HSTSQEGQDTIHGHRGS		182605	Filaggrin	9606	Homo sapiens	17
108050	NZDNTYNZVSEDLZSZI	R2, R8, R14, R16	13591823	Fibrinogen alpha chain preproprotein, isoform alpha	9606	Homo sapiens	17
108050	NRDNTYNRVSEDLRSRI		13591823	Fibrinogen alpha chain preproprotein, isoform alpha	9606	Homo sapiens	17
108363	FLAEGGGVZGPRVVERH	R9	1706799	Fibrinogen alpha chain precursor	9606	Homo sapiens	17
108363	FLAEGGGVRGPRVVERH		1706799	Fibrinogen alpha chain precursor	9606	Homo sapiens	17
108623	QESTRGRSRGRSGZSGS	R16	190404	Profilaggrin	9606	Homo sapiens	15
108623	SHQESTRGRSRGRS		190404	Profilaggrin	9606	Homo sapiens	15
108623	SHQESTRGRSRGRSGZS	R16	190404	Profilaggrin	9606	Homo sapiens	15
108624	QESTRGRSRGZSGRSGS	R13	190404	Profilaggrin	9606	Homo sapiens	13
108624	SHQESTRGRSRGZSGRS	R13	190404	Profilaggrin	9606	Homo sapiens	17
108625	QESTRGRSZGRSGRSGS	R11	190404	Profilaggrin	9606	Homo sapiens	17
108625	SHQESTRGRSZGRSGRS	R11	190404	Profilaggrin	9606	Homo sapiens	17
108627	QESTZGRSRGRSGZSGS	R7, R16	190404	Profilaggrin	9606	Homo sapiens	16
108627	SHQESTZGRSRGRSGZS	R7, R16	190404	Profilaggrin	9606	Homo sapiens	16
108627	SHQESTZGRSRGRS	R7, R16	190404	Profilaggrin	9606	Homo sapiens	15
108628	QESTZGRSRGZSGRSGS	R7, R13	190404	Profilaggrin	9606	Homo sapiens	10
108628	SHQESTZGRSRGZSGRS	R7, R13	190404	Profilaggrin	9606	Homo sapiens	10
108629	QESTZGRSZGRSGRSGS	R7, R11	190404	Profilaggrin	9606	Homo sapiens	11
108629	SHQESTZGRSZGRSGRS	R7, R11	190404	Profilaggrin	9606	Homo sapiens	11
108630	QESTZGZSZGRSGRSGS	R7, R9, R11	190404	Profilaggrin	9606	Homo sapiens	11
108630	SHQESTZGZSZGRSGRS	R7, R9, R11	190404	Profilaggrin	9606	Homo sapiens	13
108631	QESTRGRSRGRSGRSGS		190404	Profilaggrin	9606	Homo sapiens	12
108631	SHQESTRGRSRGRSGRS		190404	Profilaggrin	9606	Homo sapiens	17
108631	SHQESTRGRSRGRSGR		190404	Profilaggrin	9606	Homo sapiens	17
108631	ESTRGRSRGRSGRSGS		190404	Profilaggrin	9606	Homo sapiens	17
108645	STZSVSSSSYZZMFGG	R3, R11, R12	55977767	Vimentin	9606	Homo sapiens	16
108652	TGPSTRGRQSZHE	R12	182605	Filaggrin	9606	Homo sapiens	17
108652	TGPSTRGRQSRHE		182605	Filaggrin	9606	Homo sapiens	17
108652	TGPSTRGRQSZHEQAQ	R12	182605	Filaggrin	9606	Homo sapiens	17
108653	TGPSTZGRQSRHEQAQ	R6	182605	Filaggrin	9606	Homo sapiens	17
108653	TGPSTRGRQSRHEQAQ		182605	Filaggrin	9606	Homo sapiens	17
109917	QESTRGZSRGRSGRSGS	R9	190404	Profilaggrin	9606	Homo sapiens	17
109917	SHQESTRGZSRGRSGRS	R9	190404	Profilaggrin	9606	Homo sapiens	17
110770	ARGHRPLDKKREEAPSL		117938823	FGB protein	9606	Homo sapiens	15
110770	HRPLDKKREEAPSLZPA	R18	117938823	FGB protein	9606	Homo sapiens	15
110771	ARGHRPLDKKZEEAPSL	R11	117938823	FGB protein	9606	Homo sapiens	17
110771	HRPLDKKZEEAPSLRPA	R11	117938823	FGB protein	9606	Homo sapiens	17
110772	HRPLDKKZEEAPSLZPA	R11, R18	117938823	FGB protein	9606	Homo sapiens	17
110773	ARGHZPLDKKREEAPSL	R5	117938823	FGB protein	9606	Homo sapiens	17
110773	HZPLDKKREEAPSLRPA	R5	117938823	FGB protein	9606	Homo sapiens	17
110775	ARGHZPLDKKZEEAPSL	R5, R11	117938823	FGB protein	9606	Homo sapiens	17
110775	HZPLDKKZEEAPSLRPA	R5, R11	117938823	FGB protein	9606	Homo sapiens	17
110777	AZGHRPLDKKREEAPSL	R2	117938823	FGB protein	9606	Homo sapiens	14
110777	GHRPLDKKREEAPSLRP		117938823	FGB protein	9606	Homo sapiens	17
110777	HRPLDKKREEAPSLRPA		117938823	FGB protein	9606	Homo sapiens	17
110779	AZGHRPLDKKZEEAPSL	R2, R11	117938823	FGB protein	9606	Homo sapiens	17
110781	AZGHZPLDKKREEAPSL	R2, R5	117938823	FGB protein	9606	Homo sapiens	17
110782	HZPLDKKREEAPSLZPA	R2, R5, R18	117938823	FGB protein	9606	Homo sapiens	17
110783	AZGHZPLDKKZEEAPSL	R2, R5, R11	117938823	FGB protein	9606	Homo sapiens	12
110786	ZPLDKKREEAPSLZPAD	R5, R18	117938823	FGB protein	9606	Homo sapiens	17
110786	RPLDKKREEAPSLRPAD		117938823	FGB protein	9606	Homo sapiens	17
110787	EAPSLZPAGGGHSTKZG	R5, R18, R28, R37	117938823	FGB protein	9606	Homo sapiens	17

110787	EAPSLRPAGGGHSTKRG		117938823	FGB protein	9606	Homo sapiens	17
110787	HSTKZGHAKSRPVZG	R5, R18, R28, R37	117938823	FGB protein	9606	Homo sapiens	17
110787	LDKKREEAPSLZPAGGG	R5, R18, R28, R37	117938823	FGB protein	9606	Homo sapiens	17
110787	LDKKREEAPSLRPAGGG		117938823	FGB protein	9606	Homo sapiens	17
110787	PAGGGHSTKZGHAKSRP	R5, R18, R28, R37	117938823	FGB protein	9606	Homo sapiens	17
110787	PAGGGHSTKRGHAKSRP		117938823	FGB protein	9606	Homo sapiens	17
110787	STKZGHAKSRPVZG	R5, R18, R28, R37	117938823	FGB protein	9606	Homo sapiens	17
110847	FFSARGHRPLDKKZEEA	R14	117938823	FGB protein	9606	Homo sapiens	17
110847	FSARGHRPLDKKZEEAP	R14	117938823	FGB protein	9606	Homo sapiens	17
110848	FFSARGHZPLDKKREEA	R8	117938823	FGB protein	9606	Homo sapiens	13
110848	FSARGHZPLDKKREEAP	R8	117938823	FGB protein	9606	Homo sapiens	13
110849	FFSARGHZPLDKKZEEA	R8, R14	117938823	FGB protein	9606	Homo sapiens	17
110849	FSARGHZPLDKKZEEAP	R8, R14	117938823	FGB protein	9606	Homo sapiens	17
110850	FFSAZGHRPLDKKREEA	R5	117938823	FGB protein	9606	Homo sapiens	17
110850	FSAZGHRPLDKKREEAP	R5	117938823	FGB protein	9606	Homo sapiens	17
110851	FFSAZGHRPLDKKZEEA	R5, R14	117938823	FGB protein	9606	Homo sapiens	17
110851	FSAZGHRPLDKKZEEAP	R5, R14	117938823	FGB protein	9606	Homo sapiens	17
110852	FFSAZGHZPLDKKREEA	R5, R8	117938823	FGB protein	9606	Homo sapiens	17
110852	FSAZGHZPLDKKREEAP	R5, R8	117938823	FGB protein	9606	Homo sapiens	17
110853	FFSAZGHZPLDKKZEEA	R5, R8, R14	117938823	FGB protein	9606	Homo sapiens	17
110853	FSAZGHZPLDKKZEEAP	R5, R8, R14	117938823	FGB protein	9606	Homo sapiens	17
110854	FFSARGHRPLDKKREEA		117938823	FGB protein	9606	Homo sapiens	17
110854	FSARGHRPLDKKREEAP		117938823	FGB protein	9606	Homo sapiens	12
110866	GNVSPGTRZEYHTEKLV	R9	13591823	Fibrinogen alpha chain preproprotein, isoform alpha	9606	Homo sapiens	17
110866	NVSPGTRZEYHTEKLVT	R9	13591823	Fibrinogen alpha chain preproprotein, isoform alpha	9606	Homo sapiens	17
110867	GNVSPGTZZEYHTEKLV	R8, R9	13591823	Fibrinogen alpha chain preproprotein, isoform alpha	9606	Homo sapiens	17
110867	NVSPGTZZEYHTEKLVT	R8, R9	13591823	Fibrinogen alpha chain preproprotein, isoform alpha	9606	Homo sapiens	17
110868	GNVSPGTRREYHTEKLV		13591823	Fibrinogen alpha chain preproprotein, isoform alpha	9606	Homo sapiens	17
110868	NVSPGTRREYHTEKLVT		13591823	Fibrinogen alpha chain preproprotein, isoform alpha	9606	Homo sapiens	17
110882	HCTKZGHAKSZPVZGIH	R5, R11, R14	13591823	Fibrinogen alpha chain preproprotein, isoform alpha	9606	Homo sapiens	17
110882	HCTKRGHAKSRPVRGIH	R5, R11, R14	13591823	Fibrinogen alpha chain preproprotein, isoform alpha	9606	Homo sapiens	17
110882	ZGHAKSZPVZGIHTCPL	R5, R11, R14	13591823	Fibrinogen alpha chain preproprotein, isoform alpha	9606	Homo sapiens	17
110882	RGHAKSRPVRGIHTCPL		13591823	Fibrinogen alpha chain preproprotein, isoform alpha	9606	Homo sapiens	17
110886	HSTKRGHAKSRPVZG	R14	13591823	Fibrinogen alpha chain preproprotein, isoform alpha	9606	Homo sapiens	17
110887	HSTKRGHAKSZPVRG	R11	13591823	Fibrinogen alpha chain preproprotein, isoform alpha	9606	Homo sapiens	17
110888	HSTKRGHAKSZPVZG	R11, R14	13591823	Fibrinogen alpha chain preproprotein, isoform alpha	9606	Homo sapiens	17
110889	GHAKSRPVRG		13591823	Fibrinogen alpha chain preproprotein, isoform alpha	9606	Homo sapiens	17
110889	HSTKZGHAKSRPVRG	R5	13591823	Fibrinogen alpha chain preproprotein, isoform alpha	9606	Homo sapiens	17
110891	HSTKZGHAKSZPVRG	R5, R11	13591823	Fibrinogen alpha chain preproprotein, isoform alpha	9606	Homo sapiens	17
110893	HSTKRGHAKSRPVRG		13591823	Fibrinogen alpha chain preproprotein, isoform alpha	9606	Homo sapiens	12
110893	STKRGHAKSRPVRG		13591823	Fibrinogen alpha chain preproprotein, isoform alpha	9606	Homo sapiens	17
110899	AKDLLPSRDZQHLPLIK	R11	13591823	Fibrinogen alpha chain preproprotein, isoform alpha	9606	Homo sapiens	17
110899	IAKDLLPSRDZQHLPLI	R11	13591823	Fibrinogen alpha chain preproprotein, isoform alpha	9606	Homo sapiens	17
110899	KDLLPSRDZQHLPLI	R11	13591823	Fibrinogen alpha chain preproprotein, isoform alpha	9606	Homo sapiens	17
110900	AKDLLPSZDRQHLPLIK	R9	13591823	Fibrinogen alpha chain preproprotein, isoform alpha	9606	Homo sapiens	17
110900	IAKDLLPSZDRQHLPLI	R9	13591823	Fibrinogen alpha chain preproprotein, isoform alpha	9606	Homo sapiens	17
110901	AKDLLPSZDZQHLPLIK	R9, R11	13591823	Fibrinogen alpha chain preproprotein, isoform alpha	9606	Homo sapiens	17
110901	IAKDLLPSZDZQHLPLI	R9, R11	13591823	Fibrinogen alpha chain preproprotein, isoform alpha	9606	Homo sapiens	17
110901	KDLLPSZDZQHLPLI	R9, R11	13591823	Fibrinogen alpha chain preproprotein, isoform alpha	9606	Homo sapiens	17
110901	DLLPSZDZQHLPLIK	R9, R11	13591823	Fibrinogen alpha chain preproprotein, isoform alpha	9606	Homo sapiens	17
110902	AKDLLPSRDRQHLPLIK		13591823	Fibrinogen alpha chain preproprotein, isoform alpha	9606	Homo sapiens	14
110902	IAKDLLPSRDRQHLPLI		13591823	Fibrinogen alpha chain preproprotein, isoform alpha	9606	Homo sapiens	15
110902	DLLPSRDRQHLPLIK		13591823	Fibrinogen alpha chain preproprotein, isoform alpha	9606	Homo sapiens	16
110990	ARPAKAAATQKKVEZKA	R16	117938823	FGB protein	9606	Homo sapiens	15
110990	RARPAKAAATQKKVEZK	R16	117938823	FGB protein	9606	Homo sapiens	15
110991	AZPAKAAATQKKVERKA	R3	117938823	FGB protein	9606	Homo sapiens	17
110991	RAZPAKAAATQKKVERK	R3	117938823	FGB protein	9606	Homo sapiens	17
110993	AZPAKAAATQKKVEZKA	R3, R16	117938823	FGB protein	9606	Homo sapiens	16
110993	RAZPAKAAATQKKVEZK	R3, R16	117938823	FGB protein	9606	Homo sapiens	16
110994	ZAZPAKAAATQKKVERK	R1, R3	117938823	FGB protein	9606	Homo sapiens	14
110995	ZAZPAKAAATQKKVEZK	R1, R3, R16	117938823	FGB protein	9606	Homo sapiens	17
110996	ARPAKAAATQKKVERKA		117938823	FGB protein	9606	Homo sapiens	17
110996	RARPAKAAATQKKVERK		117938823	FGB protein	9606	Homo sapiens	17
111022	SGIGTLDGFRHRHPD		13591823	Fibrinogen alpha chain preproprotein, isoform alpha	9606	Homo sapiens	10
111026	RALAZEVDLKDYEDQQK	R5	47124990	FGA protein	9606	Homo sapiens	17
111026	SRALAZEVDLKDYEDQQ	R5	47124990	FGA protein	9606	Homo sapiens	17
111027	ZALAREVDLKDYEDQQK	R2	47124990	FGA protein	9606	Homo sapiens	17
111027	SZALAREVDLKDYEDQQ	R2	47124990	FGA protein	9606	Homo sapiens	17
111028	ZALAZEVDLKDYEDQQK	R2, R5	47124990	FGA protein	9606	Homo sapiens	15
111028	RALAREVDLKDYEDQQK		47124990	FGA protein	9606	Homo sapiens	15
111028	SZALAZEVDLKDYEDQQ	R2, R5	47124990	FGA protein	9606	Homo sapiens	17
111028			47124990	FGA protein	9606	Homo sapiens	12
112037			127795659	MBP protein	9606	Homo sapiens	17
112037			127795659	MBP protein	9606	Homo sapiens	17
113744			1706799	Fibrinogen alpha chain precursor	9606	Homo sapiens	17
113744	QDFTNZINKLKNS	R6	1706799	Fibrinogen alpha chain precursor	9606	Homo sapiens	17
115056	GLSLSRFSWGAEGQZPG	R15	127795659	MBP protein	9606	Homo sapiens	15
115056	SLSRFSWGAEGQZPGFG	R15	127795659	MBP protein	9606	Homo sapiens	15
115109	FKLGGZDSRSGSPMARZ	R9, R20	127795659	MBP protein	9606	Homo sapiens	16
115109	SKIFKLGGZDSRSGSPM	R9, R20	127795659	MBP protein	9606	Homo sapiens	16
116458	GLSLSRFSWGAEGQRPG		127795659	MBP protein	9606	Homo sapiens	15
116458	SLSRFSWGAEGQRPGFG		127795659	MBP protein	9606	Homo sapiens	15
117381	RNGWSHKDLLRLSHLKP		177783	Ro ribonucleoprotein	9606	Homo sapiens	17
117381	TKYKQRNGWSHKDLLRL		177783	Ro ribonucleoprotein	9606	Homo sapiens	17
117651	ZNGWSHKDLLZLSHLKP	R6, R16	177783	Ro ribonucleoprotein	9606	Homo sapiens	17
117651	TKYKQZNGWSHKDLLZL	R6, R16	177783	Ro ribonucleoprotein	9606	Homo sapiens	17
136126	AKYNQLLZIEEELGSKA	R9	62897945	Enolase 1 variant	9606	Homo sapiens	17
136126	AKYNQLLRIEEELGSKA		62897945	Enolase 1 variant	9606	Homo sapiens	17
136134	ANGWGVMVSHZSGETED	R12	62897945	Enolase 1 variant	9606	Homo sapiens	17
136134	ANGWGVMVSHRSGETED		62897945	Enolase 1 variant	9606	Homo sapiens	17
136134	NGWGVMVSHZSGETEDT	R12	62897945	Enolase 1 variant	9606	Homo sapiens	17
136134	NGWGVMVSHRSGETEDT		62897945	Enolase 1 variant	9606	Homo sapiens	13
136197	EKGVPLYZHIADLAGNS	R9	62897945	Enolase 1 variant	9606	Homo sapiens	15
136197	EKGVPLYRHIADLAGNS		62897945	Enolase 1 variant	9606	Homo sapiens	16
136197	KGVPLYZHIADLAGNSE	R9	62897945	Enolase 1 variant	9606	Homo sapiens	17
136197	KGVPLYRHIADLAGNSE		62897945	Enolase 1 variant	9606	Homo sapiens	17
136237	FZSGKYDLDFKSPDDPS	R3, R19	62897945	Enolase 1 variant	9606	Homo sapiens	16
136237	FRSGKYDLDFKSPDDPS		62897945	Enolase 1 variant	9606	Homo sapiens	17
136237	SGKYDLDFKSPDDPSZY	R3, R19	62897945	Enolase 1 variant	9606	Homo sapiens	17
136237	SGKYDLDFKSPDDPSRY		62897945	Enolase 1 variant	9606	Homo sapiens	17

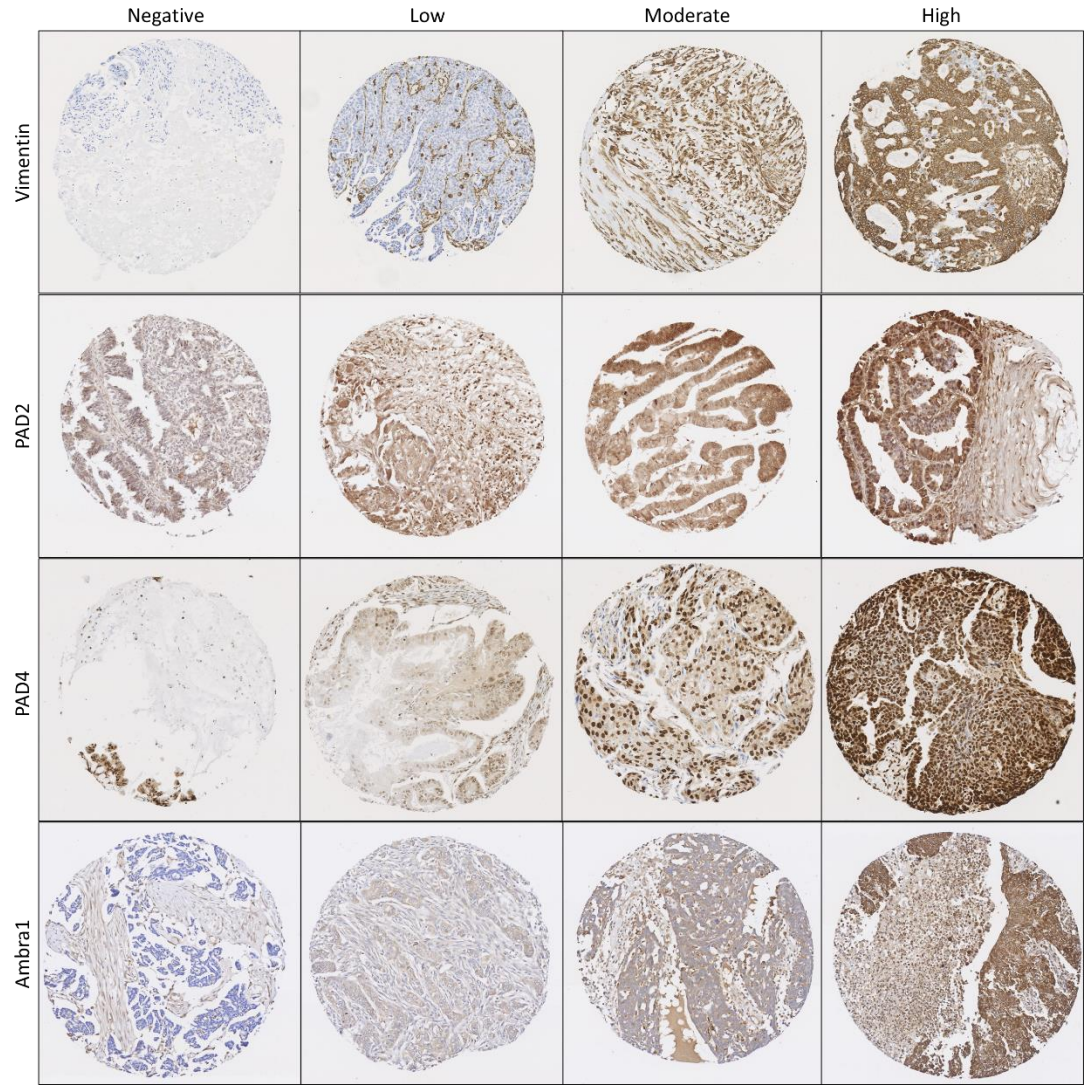
136304	GAZGLTGZPGDA	R3, R8	124056489	Collagen alpha-1(II) chain	9606	Homo sapiens	17
136304	GARGLTGRPGDA		124056489	Collagen alpha-1(II) chain	9606	Homo sapiens	17
136397	IQVVGDDLTVTNPKZIA	R16	62897945	Enolase 1 variant	9606	Homo sapiens	15
136397	IQVVGDDLTVTNPKRIA		62897945	Enolase 1 variant	9606	Homo sapiens	15
136397	VVGDDLTVTNPKZIAKA	R16	62897945	Enolase 1 variant	9606	Homo sapiens	15
136397	VVGDDLTVTNPKRIAKA		62897945	Enolase 1 variant	9606	Homo sapiens	15
136415	KFAGZNFZNPLAK	R6, R9	62897945	Enolase 1 variant	9606	Homo sapiens	17
136415	KFAGRNFRNPLAK		62897945	Enolase 1 variant	9606	Homo sapiens	17
136418	KIHAREIFDSZGNPTVE	R12	62897945	Enolase 1 variant	9606	Homo sapiens	13
136419	KIHAZEIFDSRGNPTVE	R6	62897945	Enolase 1 variant	9606	Homo sapiens	17
136421	KIHAREIFDSRGNPTV		119339	Alpha-enolase	9606	Homo sapiens	17
136421	KIHAREIFDSRGNPTVE		119339	Alpha-enolase	9606	Homo sapiens	17
136422	KIIGZEILDSZGNPTVE	R6, R12	34397760	Enolase	242619	Porphyromonas gingivalis W83	17
136422	KIIGREILDSRGNPTVE		34397760	Enolase	242619	Porphyromonas gingivalis W83	17
136524	FZEAMZIGAEVYHNLKN	R4, R8	62897945	Enolase 1 variant	9606	Homo sapiens	13
136524	FREAMRIGAEVYHNLKN		62897945	Enolase 1 variant	9606	Homo sapiens	13
136524	NFZEAMZIGAEVYHNLK	R4, R8	62897945	Enolase 1 variant	9606	Homo sapiens	13
136524	NFREAMRIGAEVYHNLK		62897945	Enolase 1 variant	9606	Homo sapiens	13
136533	NPKZIAKAVNEKSCNCL	R5	62897945	Enolase 1 variant	9606	Homo sapiens	17
136533	NPKRIAKAVNEKSCNCL		62897945	Enolase 1 variant	9606	Homo sapiens	17
136533	PKZIAKAVNEKSCNCLL	R5	62897945	Enolase 1 variant	9606	Homo sapiens	17
136533	PKRIAKAVNEKSCNCLL		62897945	Enolase 1 variant	9606	Homo sapiens	17
136703	VDLFTSKGLFZAAVPSG	R12	62897945	Enolase 1 variant	9606	Homo sapiens	17
136703	VDLFTSKGLFRAAVPSG		62897945	Enolase 1 variant	9606	Homo sapiens	17
136752	ELZDNDKTZYMGKGVSK	R8, R14	62897945	Enolase 1 variant	9606	Homo sapiens	17
136752	ELRDNDKTRYMGKGVSK		62897945	Enolase 1 variant	9606	Homo sapiens	17
136752	YEALELZDNDKTZYMGK	R8, R14	62897945	Enolase 1 variant	9606	Homo sapiens	17
136752	YEALELRDNDKTRYMGK		62897945	Enolase 1 variant	9606	Homo sapiens	17
137756	HQCHQESTZGKSKGKCG	K9	PT10007238	PREDICTED: similar to filaggrin	10090	Mus musculus	17
137756	HQCHQESTRGKSKGKCG		PT10007238	PREDICTED: similar to filaggrin	10090	Mus musculus	17
137756	QESTZGKSKGKCGKSGS	K9	PT10007238	PREDICTED: similar to filaggrin	10090	Mus musculus	16
137756	QESTRGKSKGKCGKSGS		PT10007238	PREDICTED: similar to filaggrin	10090	Mus musculus	16
139482	DSPGSGNAZPNNPDW	R9	11761629	Fibrinogen alpha chain isoform alpha preproprotein	9606	Homo sapiens	16
139482	DSPGSGNARPNNPDW		11761629	Fibrinogen alpha chain isoform alpha preproprotein	9606	Homo sapiens	16
139493	EQSADSSZHSGSGH	R8	PT10004292	Filaggrin	9606	Homo sapiens	17
139493	EQSADSSRHSGSGH		PT10004292	Filaggrin	9606	Homo sapiens	17
139494	EZGSAGHWTSESSVS	R2	11761629	Fibrinogen alpha chain isoform alpha preproprotein	9606	Homo sapiens	15
139494	ERGSAGHWTSESSVS		11761629	Fibrinogen alpha chain isoform alpha preproprotein	9606	Homo sapiens	15
139496	ESSRDGSZHPRSHD	R8	PT10004292	Filaggrin	9606	Homo sapiens	17
139496	ESSRDGSRHPRSHD		PT10004292	Filaggrin	9606	Homo sapiens	17
139512	GPZVVEZHQSACKDS	R3, R7	182424	Alpha-fibrinogen precursor	9606	Homo sapiens	17
139512	GPRVVERHQSACKDS		182424	Alpha-fibrinogen precursor	9606	Homo sapiens	17
139515	GTFEEVSGNVSPGTZ	R15	11761629	Fibrinogen alpha chain isoform alpha preproprotein	9606	Homo sapiens	14
139515	GTFEEVSGNVSPGTR		11761629	Fibrinogen alpha chain isoform alpha preproprotein	9606	Homo sapiens	14
139554	MELEZPGGNEITZGG	R5, R13	11761629	Fibrinogen alpha chain isoform alpha preproprotein	9606	Homo sapiens	17
139554	MELERPGGNEITRGG		11761629	Fibrinogen alpha chain isoform alpha preproprotein	9606	Homo sapiens	17
139565	PEWKALTDMPQMZME	R13	11761629	Fibrinogen alpha chain isoform alpha preproprotein	9606	Homo sapiens	17
139565	PEWKALTDMPQMRME		11761629	Fibrinogen alpha chain isoform alpha preproprotein	9606	Homo sapiens	16
139569	PZKQCSKEDGGGWWY	R2	7924018	Fibrinogen beta chain	9606	Homo sapiens	15
139569	PRKQCSKEDGGGWWY		7924018	Fibrinogen beta chain	9606	Homo sapiens	15
139571	QKLESDVSAQMEYCZ	R15	7924018	Fibrinogen beta chain	9606	Homo sapiens	15
139571	QKLESDVSAQMEYCR		7924018	Fibrinogen beta chain	9606	Homo sapiens	15
139597	ZGHAKSZPVZGIHTS	R1, R7, R10	11761629	Fibrinogen alpha chain isoform alpha preproprotein	9606	Homo sapiens	17
139597	RGHAKSRPVRGIHTS		11761629	Fibrinogen alpha chain isoform alpha preproprotein	9606	Homo sapiens	17
139598	ZPAPPPISGGGYZAZ	R1, R13, R15	117938823	FGB protein	9606	Homo sapiens	16
139598	RPAPPPISGGGYRAR		117938823	FGB protein	9606	Homo sapiens	14
139601	SCSZALAZEVDLKDY	R4, R8	11761629	Fibrinogen alpha chain isoform alpha preproprotein	9606	Homo sapiens	13
139601	SCSRALAREVDLKDY		11761629	Fibrinogen alpha chain isoform alpha preproprotein	9606	Homo sapiens	13
139612	SZGSESGIFTNTKES	R2	11761629	Fibrinogen alpha chain isoform alpha preproprotein	9606	Homo sapiens	15
139612	SRGSESGIFTNTKES		11761629	Fibrinogen alpha chain isoform alpha preproprotein	9606	Homo sapiens	15
139614	SSHHPGIAEFPSZGK	R13	11761629	Fibrinogen alpha chain isoform alpha preproprotein	9606	Homo sapiens	17
139614	SSHHPGIAEFPSRGK		11761629	Fibrinogen alpha chain isoform alpha preproprotein	9606	Homo sapiens	17
139616	SYNZGDSTFESKSYK	R4	11761629	Fibrinogen alpha chain isoform alpha preproprotein	9606	Homo sapiens	17
139616	SYNRGDSTFESKSYK		11761629	Fibrinogen alpha chain isoform alpha preproprotein	9606	Homo sapiens	13
139619	TGSSTGGZQGSHHE	R8	PT10004292	Filaggrin	9606	Homo sapiens	17
139619	TGSSTGGRQGSHHE		PT10004292	Filaggrin	9606	Homo sapiens	17
139621	IHAHPGSZZGGRHGYHH	R9, R10	190396	Profilaggrin	9606	Homo sapiens	16
139621	IHAHPGSRRGGRHGYHH		190396	Profilaggrin	9606	Homo sapiens	16
139621	TIHAHPGSZZGGRHGYH	R9, R10	190396	Profilaggrin	9606	Homo sapiens	17
139621	TIHAHPGSRRGGRHGYH		190396	Profilaggrin	9606	Homo sapiens	17
139630	VDIDIKIZSCZGSCS	R8, R11	11761629	Fibrinogen alpha chain isoform alpha preproprotein	9606	Homo sapiens	17
139630	VDIDIKIRSCRGSCS		11761629	Fibrinogen alpha chain isoform alpha preproprotein	9606	Homo sapiens	17
139631	VIQNZQDGSVDFGZK	R5, R14	7924018	Fibrinogen beta chain	9606	Homo sapiens	17
139631	VIQNRQDGSVDFGRK		7924018	Fibrinogen beta chain	9606	Homo sapiens	17
139640	WYNZCHAANPNGZYY	R4, R13	7924018	Fibrinogen beta chain	9606	Homo sapiens	17
139640	WYNRCHAANPNGRYY		7924018	Fibrinogen beta chain	9606	Homo sapiens	16
142386	ANKYQISVNKYZGTAGN	R12	223002	Fibrin beta	9606	Homo sapiens	17
142386	ANKYQISVNKYRGTAGN		223002	Fibrin beta	9606	Homo sapiens	17
142386	KYQISVNKYZGTAGNAL	R12	223002	Fibrin beta	9606	Homo sapiens	17
142437	KYQISVNKYRGTAGNAL		223002	Fibrin beta	9606	Homo sapiens	17
142437	KYRGTAGNALMDGASQL		223002	Fibrin beta	9606	Homo sapiens	12
142437	NKYRGTAGNALMDGASQ		223002	Fibrin beta	9606	Homo sapiens	12
142438	KYZGTAGNALMDGASQL	R10, R29	223002	Fibrin beta	9606	Homo sapiens	17
142438	NKYZGTAGNALMDGASQ	R10, R29	223002	Fibrin beta	9606	Homo sapiens	17
144899	GQSZGQSZGZGZGZGZG	R4, R8, R10, R12, R14, R16, R18	330444	Nuclear protein EBNA2	10376	Human herpesvirus 4	16
144899	GQSRGQSRGRGRGRGRG		330444	Nuclear protein EBNA2	10376	Human herpesvirus 4	16
144899	GQSZGZGZGZGZGZGKG	R4, R8, R10, R12, R14, R16, R18	330444	Nuclear protein EBNA2	10376	Human herpesvirus 4	15
144899	GQSRGRGRGRGRGRGKG		330444	Nuclear protein EBNA2	10376	Human herpesvirus 4	15
144901	GZGZGZGZGRGGGZG	R2, R4, R6, R8, R14	PT10002293	EBNA-1	10376	Human herpesvirus 4	17
144901	GRGRGRGRGRGGGRG		PT10002293	EBNA-1	10376	Human herpesvirus 4	17
145157	EEAPSLRPAPPPISGGG		119625343	Fibrinogen beta chain, isoform CRA_i	9606	Homo sapiens	15
145157	ISGGGYZAZPAK	R19, R21	119625343	Fibrinogen beta chain, isoform CRA_i	9606	Homo sapiens	15
145157	ISGGGYRARPAK		119625343	Fibrinogen beta chain, isoform CRA_i	9606	Homo sapiens	15
145157	LRPAPPPISGGGYZAZP	R19, R21	119625343	Fibrinogen beta chain, isoform CRA_i	9606	Homo sapiens	15
145157	LRPAPPPISGGGYRARP		119625343	Fibrinogen beta chain, isoform CRA_i	9606	Homo sapiens	15
145157	PISGGGYZAZPA	R19, R21	119625343	Fibrinogen beta chain, isoform CRA_i	9606	Homo sapiens	15
145157	PISGGGYRARPA		119625343	Fibrinogen beta chain, isoform CRA_i	9606	Homo sapiens	15
145157	RPAPPPISGGGYZAZPA	R19, R21	119625343	Fibrinogen beta chain, isoform CRA_i	9606	Homo sapiens	14
145158	EEAPSLZPAPPPISGGG	R7, R19, R21	119625343	Fibrinogen beta chain, isoform CRA_i	9606	Homo sapiens	15
145158	ZPAPPPISGGGYZAZPA	R7, R19, R21	119625343	Fibrinogen beta chain, isoform CRA_i	9606	Homo sapiens	17

145158	RPAPPPISGGGYRARPA		119625343	Fibrinogen beta chain, isoform CRA_i	9606	Homo sapiens	17
145158	LZPAPPPISGGGYZAZ	R7, R19, R21	119625343	Fibrinogen beta chain, isoform CRA_i	9606	Homo sapiens	17
145158	LRPAPPPISGGGYRAR		119625343	Fibrinogen beta chain, isoform CRA_i	9606	Homo sapiens	17
145158	LZPAPPPISGGGYRAR	R7, R19, R21	119625343	Fibrinogen beta chain, isoform CRA_i	9606	Homo sapiens	14
145158	LRPAPPPISGGGYZAR	R7, R19, R21	119625343	Fibrinogen beta chain, isoform CRA_i	9606	Homo sapiens	14
145158	LRPAPPPISGGGYRAZ	R7, R19, R21	119625343	Fibrinogen beta chain, isoform CRA_i	9606	Homo sapiens	17
145179	ESSSHHPGIAEFPSZGK	R15	11761629	Fibrinogen alpha chain isoform alpha preproprotein	9606	Homo sapiens	15
145179	ESSSHHPGIAEFPSRGK		11761629	Fibrinogen alpha chain isoform alpha preproprotein	9606	Homo sapiens	15
145274	KESSSHHPGIAEFPSZG	R16	11761629	Fibrinogen alpha chain isoform alpha preproprotein	9606	Homo sapiens	15
145274	KESSSHHPGIAEFPSRG		11761629	Fibrinogen alpha chain isoform alpha preproprotein	9606	Homo sapiens	15
145283	KQFTSSTSYNZGDSTFE	R11	11761629	Fibrinogen alpha chain isoform alpha preproprotein	9606	Homo sapiens	17
145283	KQFTSSTSYNRGDSTFE		11761629	Fibrinogen alpha chain isoform alpha preproprotein	9606	Homo sapiens	17
145283	QFTSSTSYNZGDSTFES	R11	11761629	Fibrinogen alpha chain isoform alpha preproprotein	9606	Homo sapiens	17
145283	QFTSSTSYNRGDSTFES		11761629	Fibrinogen alpha chain isoform alpha preproprotein	9606	Homo sapiens	17
145283	TSSTSYNZGDSTF	R11	11761629	Fibrinogen alpha chain isoform alpha preproprotein	9606	Homo sapiens	17
145283	TSSTSYNRGDSTF		11761629	Fibrinogen alpha chain isoform alpha preproprotein	9606	Homo sapiens	15
145287	KZEEAPSLRPAP	R2, R21, R23	119625343	Fibrinogen beta chain, isoform CRA_i	9606	Homo sapiens	17
145287	KREEAPSLRPAP		119625343	Fibrinogen beta chain, isoform CRA_i	9606	Homo sapiens	17
145287	ZEEAPSLRPAPPPISGG	R2, R21, R23	119625343	Fibrinogen beta chain, isoform CRA_i	9606	Homo sapiens	17
145287	REEAPSLRPAPPPISGG		119625343	Fibrinogen beta chain, isoform CRA_i	9606	Homo sapiens	17
145287	KZEEAPSLZPAPPPIS	R2, R21, R23	119625343	Fibrinogen beta chain, isoform CRA_i	9606	Homo sapiens	17
145287	KZEEAPSLRPAPPPIS	R2, R21, R23	119625343	Fibrinogen beta chain, isoform CRA_i	9606	Homo sapiens	17
145287	KREEAPSLZPAPPPIS	R2, R21, R23	119625343	Fibrinogen beta chain, isoform CRA_i	9606	Homo sapiens	17
145287	KREEAPSLRPAPPPIS		119625343	Fibrinogen beta chain, isoform CRA_i	9606	Homo sapiens	17
145447	FTSSTSYNZGDSTFESK	R10	11761629	Fibrinogen alpha chain isoform alpha preproprotein	9606	Homo sapiens	17
145447	FTSSTSYNRGDSTFESK		11761629	Fibrinogen alpha chain isoform alpha preproprotein	9606	Homo sapiens	17
146298	GVYATRSSAVRLRSSV		55977767	Vimentin	9606	Homo sapiens	17
146298	TRSSAVRLRSSVPGVR		55977767	Vimentin	9606	Homo sapiens	17
146298	GVYATZSSAVZLZSSV	R6, R11, R13	55977767	Vimentin	9606	Homo sapiens	17
146298	TZSSAVZLZSSVPGVR	R6, R11, R13	55977767	Vimentin	9606	Homo sapiens	17
146298	GVYATRSSAVRLR		55977767	Vimentin	9606	Homo sapiens	17
146298	GVYATRSSAVZLR	R6, R11, R13	55977767	Vimentin	9606	Homo sapiens	17
146298	GVYATZSSAVRLR	R6, R11, R13	55977767	Vimentin	9606	Homo sapiens	17
146298	GVYATRSSAVRLZ	R6, R11, R13	55977767	Vimentin	9606	Homo sapiens	17
146298	GVYATZSSAVZLZ	R6, R11, R13	55977767	Vimentin	9606	Homo sapiens	17
146298	SAVRLRSSVPGVR		55977767	Vimentin	9606	Homo sapiens	17
146298	SAVZLZSSVPGVR	R6, R11, R13	55977767	Vimentin	9606	Homo sapiens	17
146463	MSTZSVSSSSYZZMFG	R4, R12, R13	55977767	Vimentin	9606	Homo sapiens	16
146463	MSTRSVSSSSYRRMFG		55977767	Vimentin	9606	Homo sapiens	17
156675	GPZVVERHQSACKDS	R3	182424	Alpha-fibrinogen precursor	9606	Homo sapiens	17
156956	SGIGTLDGFZHZHPD	R10,12	11761629	Fibrinogen alpha chain isoform alpha preproprotein	9606	Homo sapiens	17
167200	AAAIAYGLDKZEGEKNI	R11	1143492	BiP	9606	Homo sapiens	17
167200	AAAIAYGLDKREGEKNI		1143492	BiP	9606	Homo sapiens	17
167200	IAYGLDKZEGEKNILVF	R11	1143492	BiP	9606	Homo sapiens	17
167200	IAYGLDKREGEKNILVF		1143492	BiP	9606	Homo sapiens	17
167206	AGTIAGLNVMZIINEPT	R11	1143492	BiP	9606	Homo sapiens	14
167206	AGTIAGLNVMRIINEPT		1143492	BiP	9606	Homo sapiens	17
167206	IAGLNVMZIINEPTAAA	R11	1143492	BiP	9606	Homo sapiens	17
167206	IAGLNVMRIINEPTAAA		1143492	BiP	9606	Homo sapiens	17
167208	AKFEELNMDLFZSTMKP	R12	14916999	78 kDa glucose-regulated protein	9606	Homo sapiens	17
167208	AKFEELNMDLFRSTMKP		14916999	78 kDa glucose-regulated protein	9606	Homo sapiens	17
167208	EELNMDLFZSTMKPVQK	R12	14916999	78 kDa glucose-regulated protein	9606	Homo sapiens	17
167208	EELNMDLFRSTMKPVQK		14916999	78 kDa glucose-regulated protein	9606	Homo sapiens	17
167209	AKRALSSQHQAZIEIES	R12	14916999	78 kDa glucose-regulated protein	9606	Homo sapiens	17
167209	ALSSQHQAZIEIESFYE	R12	14916999	78 kDa glucose-regulated protein	9606	Homo sapiens	17
167210	AKRALSSQHQARIEIES		14916999	78 kDa glucose-regulated protein	9606	Homo sapiens	11
167210	ALSSQHQARIEIESFYE		14916999	78 kDa glucose-regulated protein	9606	Homo sapiens	11
167236	EDKKLKERIDTZNELES	R12	14916999	78 kDa glucose-regulated protein	9606	Homo sapiens	17
167236	EDKKLKERIDTRNELES		14916999	78 kDa glucose-regulated protein	9606	Homo sapiens	17
167236	LKERIDTZNELESYAYS	R12	14916999	78 kDa glucose-regulated protein	9606	Homo sapiens	17
167236	LKERIDTRNELESYAYS		14916999	78 kDa glucose-regulated protein	9606	Homo sapiens	17
167252	EDKKLKEZIDTRNELES	R11	1143492	BiP	9606	Homo sapiens	17
167252	FAEEDKKLKEZIDTRNE	R11	1143492	BiP	9606	Homo sapiens	17
167252	FAEEDKKLKERIDTRNE		1143492	BiP	9606	Homo sapiens	17
167282	IDEIVLVGGSTZIPKIQ	R12	14916999	78 kDa glucose-regulated protein	9606	Homo sapiens	17
167282	IDEIVLVGGSTRIPKIQ		14916999	78 kDa glucose-regulated protein	9606	Homo sapiens	17
167282	IVLVGGSTZIPKIQQLV	R12	14916999	78 kDa glucose-regulated protein	9606	Homo sapiens	17
167282	IVLVGGSTRIPKIQQLV		14916999	78 kDa glucose-regulated protein	9606	Homo sapiens	17
167294	KDNRAVQKLRZEVEKAK	R11	14916999	78 kDa glucose-regulated protein	9606	Homo sapiens	17
167294	RAVQKLRZEVEKAKRAL	R11	14916999	78 kDa glucose-regulated protein	9606	Homo sapiens	17
167294	RAVQKLRREVEKAKRAL		14916999	78 kDa glucose-regulated protein	9606	Homo sapiens	17
167300	KIHAZEIFDSZGNPTV	R5,R11	119339	Alpha-enolase	9606	Homo sapiens	17
167301	KLRREVEKAKZALSSQH	R11	14916999	78 kDa glucose-regulated protein	9606	Homo sapiens	17
167301	KLRREVEKAKRALSSQH		14916999	78 kDa glucose-regulated protein	9606	Homo sapiens	17
167301	REVEKAKZALSSQHQAR	R11	14916999	78 kDa glucose-regulated protein	9606	Homo sapiens	17
167301	REVEKAKRALSSQHQAR		14916999	78 kDa glucose-regulated protein	9606	Homo sapiens	17
167304	KDVRKDNZAVQKLRREV	R11	1143492	BiP	9606	Homo sapiens	17
167304	KTGKDVRKDNZAVQKLR	R11	1143492	BiP	9606	Homo sapiens	17
167305	KDVRKDNRAVQKLRREV		1143492	BiP	9606	Homo sapiens	17
167305	KTGKDVRKDNRAVQKLR		1143492	BiP	9606	Homo sapiens	17
167333	KKTGKDVZKDNRAVQKL	R11	1143492	BiP	9606	Homo sapiens	17
167333	KKTGKDVRKDNRAVQKL		1143492	BiP	9606	Homo sapiens	17
167333	LYKKKTGKDVZKDNRAV	R11	1143492	BiP	9606	Homo sapiens	17
167333	LYKKKTGKDVRKDNRAV		1143492	BiP	9606	Homo sapiens	17
167342	NKITITNDQNZLTPEEI	R11	14916999	78 kDa glucose-regulated protein	9606	Homo sapiens	17
167342	NKITITNDQNRLTPEEI		14916999	78 kDa glucose-regulated protein	9606	Homo sapiens	17
167342	TITNDQNZLTPEEIERM	R11	14916999	78 kDa glucose-regulated protein	9606	Homo sapiens	17
167342	TITNDQNRLTPEEIERM		14916999	78 kDa glucose-regulated protein	9606	Homo sapiens	17
167347	NPENTVFDAKZLIGRTW	R11	1143492	BiP	9606	Homo sapiens	17
167347	NPENTVFDAKRLIGRTW		1143492	BiP	9606	Homo sapiens	17
167347	NTVFDAKZLIGRTWNDP	R11	1143492	BiP	9606	Homo sapiens	17
167347	NTVFDAKRLIGRTWNDP		1143492	BiP	9606	Homo sapiens	15
167372	LTPEEIEZMVNDAEKFA	R11	1143492	BiP	9606	Homo sapiens	15
167372	LTPEEIERMVNDAEKFA		1143492	BiP	9606	Homo sapiens	15
167372	QNRLTPEEIEZMVNDAE	R11	1143492	BiP	9606	Homo sapiens	10
167372	QNRLTPEEIERMVNDAE		1143492	BiP	9606	Homo sapiens	15
167388	NRAVQKLZREVEKAKRA	R11	14916999	78 kDa glucose-regulated protein	9606	Homo sapiens	15
167388	RKDNRAVQKLZREVEKA	R11	14916999	78 kDa glucose-regulated protein	9606	Homo sapiens	15
167389	KDNRAVQKLRREVEKAK		14916999	78 kDa glucose-regulated protein	9606	Homo sapiens	17
167389	NRAVQKLRREVEKAKRA		14916999	78 kDa glucose-regulated protein	9606	Homo sapiens	17

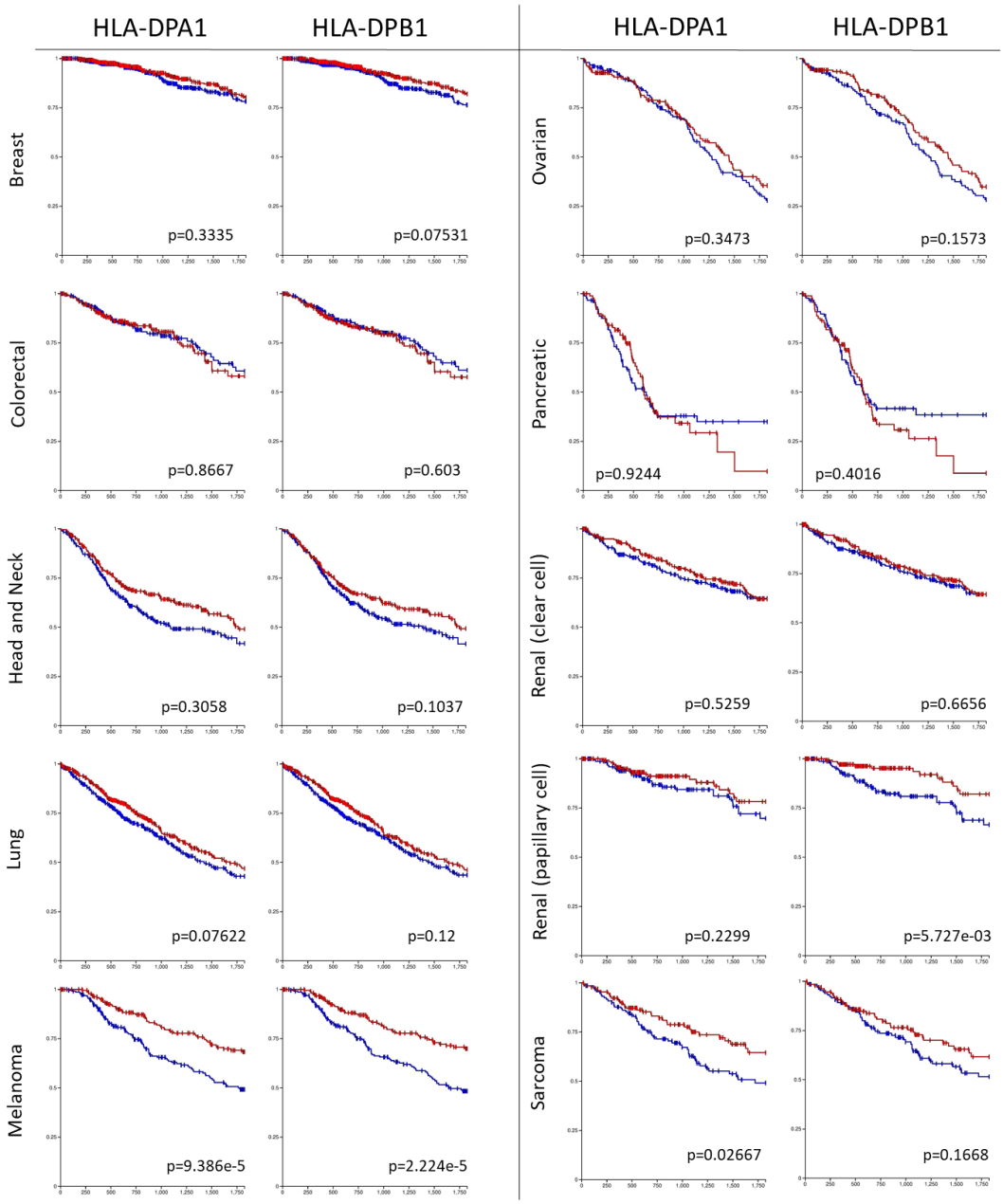
167389	RKDNRAVQKLRREVEKA		14916999	78 kDa glucose-regulated protein	9606	Homo sapiens	17
167412	AFTPEGEZLIGDAAKNQ	R11	1143492	BiP	9606	Homo sapiens	14
167412	AFTPEGERLIGDAAKNQ		1143492	BiP	9606	Homo sapiens	17
167412	SYVAFTPEGEZLIGDAA	R11	1143492	BiP	9606	Homo sapiens	17
167412	SYVAFTPEGERLIGDAA		1143492	BiP	9606	Homo sapiens	15
167416	IDVNGILZVTAEDKGTG	R11	14916999	78 kDa glucose-regulated protein	9606	Homo sapiens	17
167416	TFEIDVNGILZVTAEDK	R11	14916999	78 kDa glucose-regulated protein	9606	Homo sapiens	17
167417	IDVNGILRVTAEDKGTG		14916999	78 kDa glucose-regulated protein	9606	Homo sapiens	17
167417	TFEIDVNGILRVTAEDK		14916999	78 kDa glucose-regulated protein	9606	Homo sapiens	17
167431	GVMTKLIPZNTVVPTKK	R12	14916999	78 kDa glucose-regulated protein	9606	Homo sapiens	17
167431	GVMTKLIPRNTVVPTKK		14916999	78 kDa glucose-regulated protein	9606	Homo sapiens	17
167431	TVGGVMTKLIPZNTVVP	R12	14916999	78 kDa glucose-regulated protein	9606	Homo sapiens	17
167431	TVGGVMTKLIPRNTVVP		14916999	78 kDa glucose-regulated protein	9606	Homo sapiens	17
167433	AYFNDAQZQATKDAGTI	R11	1143492	BiP	9606	Homo sapiens	17
167433	AYFNDAQRQATKDAGTI		1143492	BiP	9606	Homo sapiens	17
167433	TVPAYFNDAQZQATKDA	R11	1143492	BiP	9606	Homo sapiens	15
167433	TVPAYFNDAQRQATKDA		1143492	BiP	9606	Homo sapiens	15
167435	IKVYEGERZLTKDNHLL	R11	14916999	78 kDa glucose-regulated protein	9606	Homo sapiens	17
167435	IKVYEGERRLTKDNHLL		14916999	78 kDa glucose-regulated protein	9606	Homo sapiens	17
167435	TVTIKVYEGERZLTKDN	R11	14916999	78 kDa glucose-regulated protein	9606	Homo sapiens	15
167435	TVTIKVYEGERRLTKDN		14916999	78 kDa glucose-regulated protein	9606	Homo sapiens	17
167440	IANDQGNZITPSYVAFT	R11	1143492	BiP	9606	Homo sapiens	17
167440	IANDQGNRITPSYVAFT		1143492	BiP	9606	Homo sapiens	17
167440	VEIIANDQGNZITPSYV	R11	1143492	BiP	9606	Homo sapiens	17
167440	VEIIANDQGNRITPSYV		1143492	BiP	9606	Homo sapiens	17
167444	FFNGKEPSZGINPDEAV	R12	14916999	78 kDa glucose-regulated protein	9606	Homo sapiens	17
167444	FFNGKEPSRGINPDEAV		14916999	78 kDa glucose-regulated protein	9606	Homo sapiens	12
167444	VKEFFNGKEPSZGINPD	R12	14916999	78 kDa glucose-regulated protein	9606	Homo sapiens	12
167444	VKEFFNGKEPSRGINPD		14916999	78 kDa glucose-regulated protein	9606	Homo sapiens	17
167459	EDFSETLTZAKFEELNM	R12	14916999	78 kDa glucose-regulated protein	9606	Homo sapiens	17
167459	EDFSETLTRAKFEELNM		14916999	78 kDa glucose-regulated protein	9606	Homo sapiens	17
167459	YEGEDFSETLTZAKFEE	R12	14916999	78 kDa glucose-regulated protein	9606	Homo sapiens	17
167459	YEGEDFSETLTRAKFEE		14916999	78 kDa glucose-regulated protein	9606	Homo sapiens	13
178121	APAPTAZNKLTSE	R7	730038	Myeloid cell nuclear differentiation antigen	9606	Homo sapiens	17
178121	APAPTARNKLTSE		730038	Myeloid cell nuclear differentiation antigen	9606	Homo sapiens	17
178122	AVFPSIVGZPRHQGVMV	R4, R13	46397333	Actin, cytoplasmic 1	9606	Homo sapiens	16
178122	AVFPSIVGRPRHQGVMV		46397333	Actin, cytoplasmic 1	9606	Homo sapiens	16
178122	DAPZAVFPSIVGZPRHQ	R4, R13	46397333	Actin, cytoplasmic 1	9606	Homo sapiens	16
178122	DAPRAVFPSIVGRPRHQ		46397333	Actin, cytoplasmic 1	9606	Homo sapiens	13
178125	EAQSKZGILTLK	R6	46397333	Actin, cytoplasmic 1	9606	Homo sapiens	17
178125	EAQSKRGILTLK		46397333	Actin, cytoplasmic 1	9606	Homo sapiens	17
178128	EZLGPLVEQGR	R3	114039	Apolipoprotein E	9606	Homo sapiens	17
178128	ERLGPLVEQGR		114039	Apolipoprotein E	9606	Homo sapiens	16
178137	GPSIVHZKCF	R7	46397333	Actin, cytoplasmic 1	9606	Homo sapiens	17
178137	GPSIVHRKCF		46397333	Actin, cytoplasmic 1	9606	Homo sapiens	17
178140	IWHHTFYNELZVAPEE	R11	46397333	Actin, cytoplasmic 1	9606	Homo sapiens	17
178140	IWHHTFYNELRVAPEE		46397333	Actin, cytoplasmic 1	9606	Homo sapiens	17
178141	KLTSEAZGZIPVAQK	R7, R9	730038	Myeloid cell nuclear differentiation antigen	9606	Homo sapiens	17
178141	KLTSEARGRIPVAQK		730038	Myeloid cell nuclear differentiation antigen	9606	Homo sapiens	16
178143	LAVYQAGAZEGAEZGLS	R9, R14	114039	Apolipoprotein E	9606	Homo sapiens	17
178143	LAVYQAGAREGAERGLS		114039	Apolipoprotein E	9606	Homo sapiens	17
178143	YQAGAZEGAEZGLSAIR	R9, R14	114039	Apolipoprotein E	9606	Homo sapiens	17
178143	YQAGAREGAERGLSAIR		114039	Apolipoprotein E	9606	Homo sapiens	17
178144	LDLAGZDLTDYLMK	R6	46397333	Actin, cytoplasmic 1	9606	Homo sapiens	17
178144	LDLAGRDLTDYLMK		46397333	Actin, cytoplasmic 1	9606	Homo sapiens	17
178148	EZGYSFTTTAEREIVRD	R7	46397333	Actin, cytoplasmic 1	9606	Homo sapiens	17
178148	ERGYSFTTTAEREIVRD		46397333	Actin, cytoplasmic 1	9606	Homo sapiens	17
178148	MKILTEZGYSFTTTAE	R7	46397333	Actin, cytoplasmic 1	9606	Homo sapiens	13
178148	MKILTERGYSFTTTAE		46397333	Actin, cytoplasmic 1	9606	Homo sapiens	13
178151	PGIADZMQKEI	R6	46397333	Actin, cytoplasmic 1	9606	Homo sapiens	17
178151	PGIADRMQKEI		46397333	Actin, cytoplasmic 1	9606	Homo sapiens	17
178156	RQVDARZNVPQND	R7	730038	Myeloid cell nuclear differentiation antigen	9606	Homo sapiens	17
178156	RQVDARRNVPQND		730038	Myeloid cell nuclear differentiation antigen	9606	Homo sapiens	17
180071	QYMRADQAAGGLR		111118976	Collagen, type II, alpha 1 isoform 1 precursor	9606	Homo sapiens	13
180071	QYMRADQAAGGLZ	R4	111118976	Collagen, type II, alpha 1 isoform 1 precursor	9606	Homo sapiens	12
180071	QYMZADQAAGGLZ	R4	111118976	Collagen, type II, alpha 1 isoform 1 precursor	9606	Homo sapiens	12
180071	QYMZADQAAGGLR	R4	111118976	Collagen, type II, alpha 1 isoform 1 precursor	9606	Homo sapiens	17
180366	ALMZGKSTEEAZKELQA	R4, R12	18201905	Glucose-6-phosphate isomerase isoform 2	9606	Homo sapiens	17
180366	ALMRGKSTEEARKELQA		18201905	Glucose-6-phosphate isomerase isoform 2	9606	Homo sapiens	16
180366	MZGKSTEEAZKELQAAG	R4, R12	18201905	Glucose-6-phosphate isomerase isoform 2	9606	Homo sapiens	16
180366	MRGKSTEEARKELQAAG		18201905	Glucose-6-phosphate isomerase isoform 2	9606	Homo sapiens	16
180368	AMLPYDQYLHZFAAYFQ	R11	18201905	Glucose-6-phosphate isomerase isoform 2	9606	Homo sapiens	17
180368	AMLPYDQYLHRFAAYFQ		18201905	Glucose-6-phosphate isomerase isoform 2	9606	Homo sapiens	17
180368	LPYDQYLHZFAAYFQQG	R11	18201905	Glucose-6-phosphate isomerase isoform 2	9606	Homo sapiens	17
180368	LPYDQYLHRFAAYFQQG		18201905	Glucose-6-phosphate isomerase isoform 2	9606	Homo sapiens	15
180378	ASTNGLINFIKQQZEAZ	R14, R17	18201905	Glucose-6-phosphate isomerase isoform 2	9606	Homo sapiens	17
180378	ASTNGLINFIKQQREAR		18201905	Glucose-6-phosphate isomerase isoform 2	9606	Homo sapiens	17
180378	TNGLINFIKQQZEAZVQ	R14, R17	18201905	Glucose-6-phosphate isomerase isoform 2	9606	Homo sapiens	17
180378	TNGLINFIKQQREARVQ		18201905	Glucose-6-phosphate isomerase isoform 2	9606	Homo sapiens	17
180401	AKSZGVEAAZEZMFNGE	R6, R12, R14	18201905	Glucose-6-phosphate isomerase isoform 2	9606	Homo sapiens	17
180401	AKSRGVEAARERMFNGE		18201905	Glucose-6-phosphate isomerase isoform 2	9606	Homo sapiens	17
180401	DLAKSZGVEAAZEZMFN	R6, R12, R14	18201905	Glucose-6-phosphate isomerase isoform 2	9606	Homo sapiens	17
180401	DLAKSRGVEAARERMFN		18201905	Glucose-6-phosphate isomerase isoform 2	9606	Homo sapiens	17
180418	EDLEZLLPHKVFEGNZP	R5, R16	18201905	Glucose-6-phosphate isomerase isoform 2	9606	Homo sapiens	17
180418	EDLERLLPHKVFEGNRP		18201905	Glucose-6-phosphate isomerase isoform 2	9606	Homo sapiens	17
180418	LEZLLPHKVFEGNZPTN	R5, R16	18201905	Glucose-6-phosphate isomerase isoform 2	9606	Homo sapiens	17
180418	LERLLPHKVFEGNRPTN		18201905	Glucose-6-phosphate isomerase isoform 2	9606	Homo sapiens	16
180452	FEFWDWVGGZYSLWSAI	R10	18201905	Glucose-6-phosphate isomerase isoform 2	9606	Homo sapiens	17
180452	FEFWDWVGGRYSLWSAI		18201905	Glucose-6-phosphate isomerase isoform 2	9606	Homo sapiens	17
180452	FWDWVGGZYSLWSAIGL	R10	18201905	Glucose-6-phosphate isomerase isoform 2	9606	Homo sapiens	17
180452	FWDWVGGRYSLWSAIGL		18201905	Glucose-6-phosphate isomerase isoform 2	9606	Homo sapiens	17
180565	KLQQWYZEHZSELNLZZ	R7, R10, R16, R17	18201905	Glucose-6-phosphate isomerase isoform 2	9606	Homo sapiens	17
180565	KLQQWYREHRSELNLRR		18201905	Glucose-6-phosphate isomerase isoform 2	9606	Homo sapiens	17
180565	QQWYZEHZSELNLZZLF	R7, R10, R16, R17	18201905	Glucose-6-phosphate isomerase isoform 2	9606	Homo sapiens	12
180565	QQWYREHRSELNLRRLF		18201905	Glucose-6-phosphate isomerase isoform 2	9606	Homo sapiens	12
180690	NYTEGZAVLHVALZNZS	R6, R14, R16	18201905	Glucose-6-phosphate isomerase isoform 2	9606	Homo sapiens	17
180690	NYTEGRAVLHVALRNRS		18201905	Glucose-6-phosphate isomerase isoform 2	9606	Homo sapiens	17
180690	TEGZAVLHVALZNZSNT	R6, R14, R16	18201905	Glucose-6-phosphate isomerase isoform 2	9606	Homo sapiens	17
180690	TEGRAVLHVALRNRSNT		18201905	Glucose-6-phosphate isomerase isoform 2	9606	Homo sapiens	17
180742	CQZVZSGDWKGYTGKTI	R5, R7	18201905	Glucose-6-phosphate isomerase isoform 2	9606	Homo sapiens	17

180742	CQRVRSGDWKGYTGKTI		18201905	Glucose-6-phosphate isomerase isoform 2	9606	Homo sapiens	17
180742	SFCQZVZSGDWKGYTGK	R5, R7	18201905	Glucose-6-phosphate isomerase isoform 2	9606	Homo sapiens	17
180742	SFCQRVRSGDWKGYTGK		18201905	Glucose-6-phosphate isomerase isoform 2	9606	Homo sapiens	17
181040	VYATRSSAVRLRSSV		340219	Vimentin	9606	Homo sapiens	17
181040	VYATRSSAVRLRSSVP		340219	Vimentin	9606	Homo sapiens	17
181132	NEEGFFSAZGHRPLDKK	R8	532595	Beta-fibrinogen	9606	Homo sapiens	17
181132	NEEGFFSARGHRPLDKK		532595	Beta-fibrinogen	9606	Homo sapiens	17
181132	NEEGFFSARGHRPLDK		532595	Beta-fibrinogen	9606	Homo sapiens	17
181132	EEGFFSARGHRPLDKK		532595	Beta-fibrinogen	9606	Homo sapiens	17
181132	NEEGFFSAZGHRPLDK	R8	532595	Beta-fibrinogen	9606	Homo sapiens	17
181132	EEGFFSAZGHRPLDKK	R8	532595	Beta-fibrinogen	9606	Homo sapiens	17
185642	QESTZGZSRGRSGRSGS	R7, R9	190404	Profilaggrin	9606	Homo sapiens	16
185642	SHQESTZGZSRGRSGRS	R7, R9	190404	Profilaggrin	9606	Homo sapiens	11
186855	GHQSHQESTZGRSRGRS	R14, R24	7924018	Fibrinogen beta chain	9606	Homo sapiens	17
186855	GHQSHQESTRGRSRGRS		7924018	Fibrinogen beta chain	9606	Homo sapiens	17
186855	KSRPVZGHQSHQESTZG	R14, R24	7924018	Fibrinogen beta chain	9606	Homo sapiens	17
186855	KSRPVRGHQSHQESTRG		7924018	Fibrinogen beta chain	9606	Homo sapiens	17
186855	QESTZGRSRGRSGRSGS	R14, R24	7924018	Fibrinogen beta chain	9606	Homo sapiens	17
186855	SHQESTZGRSRGRSGRS	R14, R24	7924018	Fibrinogen beta chain	9606	Homo sapiens	17
186855	TKRGHAKSRPVZGHQSH	R14, R24	7924018	Fibrinogen beta chain	9606	Homo sapiens	17
186855	TKRGHAKSRPVRGHQSH		7924018	Fibrinogen beta chain	9606	Homo sapiens	17
186855	SHQESTZGRSRGRSGR	R14, R24	7924018	Fibrinogen beta chain	9606	Homo sapiens	17
186855	ESTZGRSRGRSGRSGS	R14, R24	7924018	Fibrinogen beta chain	9606	Homo sapiens	15
192690	STRSVSSSSYRRMFGG		340219	Vimentin	9606	Homo sapiens	16
P02649	WFEPLVEDMQRQWAG		P02649	Apolipoprotein E	9606	Homo sapiens	15
P02649	LKSWFEPLVEDMQRQ		P02649	Apolipoprotein E	9606	Homo sapiens	15
P02649	WFEPLVEDMQZQWAG	R11	P02649	Apolipoprotein E	9606	Homo sapiens	15
P02649	LKSWFEPLVEDMQZQ	R14	P02649	Apolipoprotein E	9606	Homo sapiens	15
P02671	THSTKRGHAKSRPVR		P02671	Fibrinogen alpha chain	9606	Homo sapiens	15
P02671	ERHQSASKDSDWPFS		P02671	Fibrinogen alpha chain	9606	Homo sapiens	15
P02671	RGHAKSRPVRDSDDV		P02671	Fibrinogen alpha chain	9606	Homo sapiens	15
P02671	RDRQHLPLIKMKPVP		P02671	Fibrinogen alpha chain	9606	Homo sapiens	15
P02671	STKRGHAKSRPVRDS		P02671	Fibrinogen alpha chain	9606	Homo sapiens	15
P02671	LPSRDRQHLPLIKMK		P02671	Fibrinogen alpha chain	9606	Homo sapiens	15
P02671	EZHQSASKDSDWPFS	R2	P02671	Fibrinogen alpha chain	9606	Homo sapiens	15
P02671	ZGHAKSZPVZDSDDV	R1, R7, R10	P02671	Fibrinogen alpha chain	9606	Homo sapiens	15
P02671	ZDZQHLPLIKMKPVP	R1, R3	P02671	Fibrinogen alpha chain	9606	Homo sapiens	15
P02671	STKZGHAKSZPVZDS	R4, R10, R13	P02671	Fibrinogen alpha chain	9606	Homo sapiens	15
P02671	LPSZDZQHLPLIKMK	R4, R6	P02671	Fibrinogen alpha chain	9606	Homo sapiens	15
P06733	CKIHAREIFDSRGNPT		P06733	Alpha-enolase	9606	Homo sapiens	16
P06734	HAREIFDSRGNPTVEC		P06734	Alpha-enolase	9606	Homo sapiens	16
P06735	CKIHAREIFDSZGNPT	R12	P06735	Alpha-enolase	9606	Homo sapiens	16
P06736	HAREIFDSZGNPTVEC	R9	P06736	Alpha-enolase	9606	Homo sapiens	16
P06737	CKIHAZEIFDSRGNPT	R6	P06737	Alpha-enolase	9606	Homo sapiens	16
P06738	HAZEIFDSRGNPTVEC	R3	P06738	Alpha-enolase	9606	Homo sapiens	16
P06739	CKIHAZEIFDSZGNPT	R6, R12	P06739	Alpha-enolase	9606	Homo sapiens	16
P06740	HAZEIFDSZGNPTVEC	R3, R9	P06740	Alpha-enolase	9606	Homo sapiens	16
P06741	CKIIGREILDSRGNPT		P06741	Alpha-enolase	9606	Homo sapiens	16
P06742	IGREILDSRGNPTVEC		P06742	Alpha-enolase	9606	Homo sapiens	16
P06743	CKIIGZEILDSZGNPT	R6, R12	P06743	Alpha-enolase	9606	Homo sapiens	16
P06744	IGZEILDSZGNPTVEC	R3, R9	P06744	Alpha-enolase	9606	Homo sapiens	16
P10909	HFSRASSIIDELFQD		P10909	Clusterin	9606	Homo sapiens	15
P10909	SSIIDELFQDRFFTR		P10909	Clusterin	9606	Homo sapiens	15
P10909	DVMQDHFSRASSIID		P10909	Clusterin	9606	Homo sapiens	15
P10909	SRASSIIDELFQDRF		P10909	Clusterin	9606	Homo sapiens	15
P10909	HMLDVMQDHFSRASS		P10909	Clusterin	9606	Homo sapiens	15
P10909	HFSZASSIIDELFQD	R4	P10909	Clusterin	9606	Homo sapiens	15
P10909	SSIIDELFQDZFFTZ	R11, R15	P10909	Clusterin	9606	Homo sapiens	15
P10909	DVMQDHFSZASSIID	R9	P10909	Clusterin	9606	Homo sapiens	15
P10909	SZASSIIDELFQDZF	R2, R14	P10909	Clusterin	9606	Homo sapiens	15
P10909	HMLDVMQDHFSZASS	R12	P10909	Clusterin	9606	Homo sapiens	15
P16112	VVLLVATEGRVRVNSA		P16112	Aggrecan	9606	Homo sapiens	16
P16112	VATEGRVRVNSAYQDK		P16112	Aggrecan	9606	Homo sapiens	16
P16112	VVLLVATEGZVZVNSA	R10, R12	P16112	Aggrecan	9606	Homo sapiens	16
P16112	VATEGZVZVNSAYQDK	R6, R8	P16112	Aggrecan	9606	Homo sapiens	16
P16112	VVLLVATEGRVZVNSA	R12	P16112	Aggrecan	9606	Homo sapiens	16
P16112	VATEGRVZVNSAYQDK	R8	P16112	Aggrecan	9606	Homo sapiens	16
P16112	VVLLVATEGZVRVNSA	R10	P16112	Aggrecan	9606	Homo sapiens	16
P16112	VATEGZVRVNSAYQDK	R6	P16112	Aggrecan	9606	Homo sapiens	16
P21810	YSKLYRLGLGHNQIR		P21810	Biglycan	9606	Homo sapiens	15
P21810	LLRYSKLYRLGLGHN		P21810	Biglycan	9606	Homo sapiens	15
P21810	YSKLYZLGLGHNQIZ	R6, R15	P21810	Biglycan	9606	Homo sapiens	15
P21810	LLZYSKLYZLGLGHN	R3, R9	P21810	Biglycan	9606	Homo sapiens	15
Q99878	MSGRGKQGGKARAKA		Q99878	Histone H2A	9606	Homo sapiens	15
Q99878	KQGGKARAKAKTRSS		Q99878	Histone H2A	9606	Homo sapiens	15
Q99878	GRGKQGGKARAKAKT		Q99878	Histone H2A	9606	Homo sapiens	15
Q99878	MSGZGKQGGKAZAKA	R4, R12	Q99878	Histone H2A	9606	Homo sapiens	15
Q99878	KQGGKAZAKAKTZSS	R7, R13	Q99878	Histone H2A	9606	Homo sapiens	15
Q99878	GZGKQGGKAZAKAKT	R2, R10	Q99878	Histone H2A	9606	Homo sapiens	15
Q99880	FVTDIFERIASEASR		Q99880	Histone H2B	9606	Homo sapiens	15
Q99880	MNSFVTDIFERIASE		Q99880	Histone H2B	9606	Homo sapiens	15
Q99880	FVTDIFEZIASEASZ	R8, R15	Q99880	Histone H2B	9606	Homo sapiens	15
Q99880	MNSFVTDIFEZIASE	R11	Q99880	Histone H2B	9606	Homo sapiens	15

Appendix 3

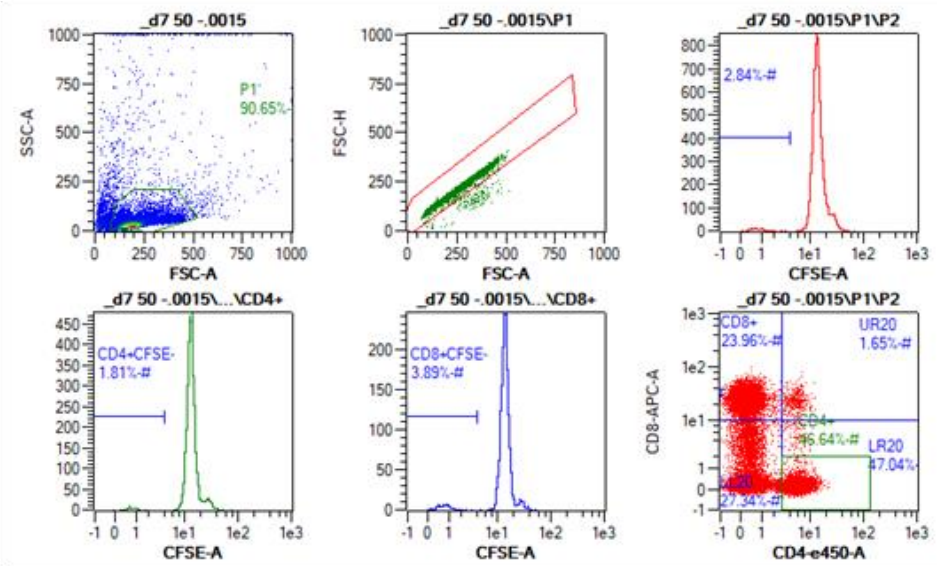


Appendix 4

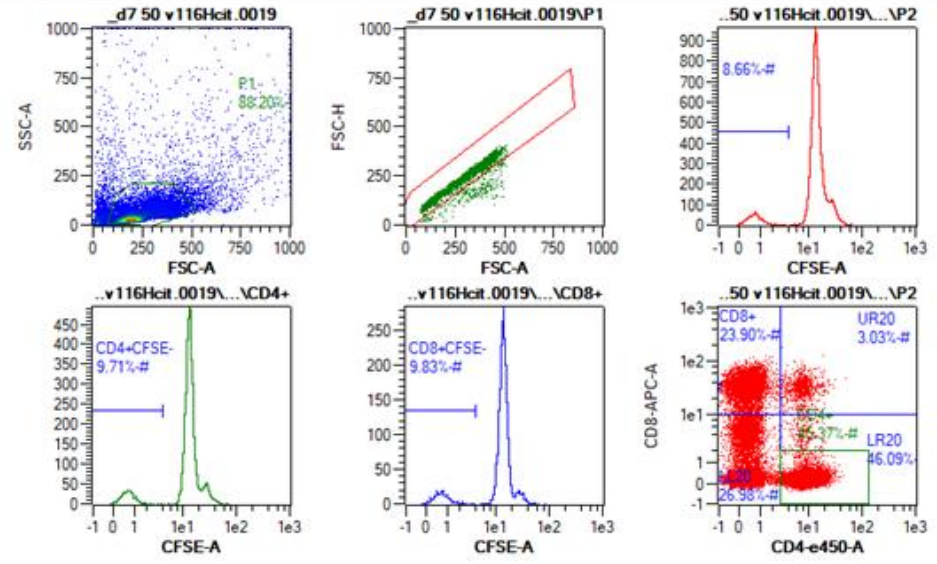

HLA-DPA1
HLA-DPB1
HLA-DPA1
HLA-DPB1
Breast
p=0.3335
p=0.07531
Ovarian
p=0.3473
p=0.1573
Colorectal
p=0.8667
p=0.603
Pancreatic
p=0.9244
p=0.4016
Head and Neck
p=0.3058
p=0.1037
Renal (clear cell)
p=0.5259
p=0.6656
Lung
p=0.07622
p=0.12
Renal (papillary cell)
p=0.2299
p=5.727e-03
Melanoma
p=9.386e-5
p=2.224e-5
Sarcoma
p=0.02667
p=0.1668

Appendix 5

BD0050 media



BD0050 Vim116Hcit



Appendix 6

Donor	HLA-A	HLA-B	HLA-C	HLA-DR	HLA-DQ	HLA-DP
BD41	01 24	07 40	03 07	B1*04 B1*11	B1*03 B1*03	B1*02:01 B1*04:01
BD11	33:03 74:01	18:01 49:01	07:01 07:04	B1*13:01 B1*15:03	A1*01 B1*05:01 B1*06:02	A1*01:03 A1*02:01 B1*17:01 B1*18:01

Appendix 7

